Load Ratio Effects in the Fatigue Crack Propagation of Composite Laminates and Bonded Joints

A thesis submitted in fulfilment of the requirements for the degree of

Doctor of Philosophy (Aerospace Engineering)

Matthew Joseph Donough

Bachelor of Engineering (Hons)

School of Aerospace, Mechanical and Manufacturing Engineering

College of Science, Engineering and Health

RMIT University

6 November 2014

Declaration

I certify that except where due acknowledgement has been made, the work is that of the author alone; the work has not been submitted previously, in whole or in part, to qualify for any other academic award; the contend of the thesis is the result of work which has been carried out since the official commencement date of the approved research program; and, any editorial work, paid or unpaid, carried out by a third party is acknowledged.

Matthew Joseph Donough

6 November 2014

Acknowledgements

Firstly, I will like to thank my supervisors at RMIT University, Professor Chun Wang, Dr Andrew Gunnion and Dr Adrian Orifici. The support, guidance, expertise and insight that they have provided to this PhD project have been invaluable. Also I will like to thank the CRC-ACS for the opportunity of undertaking this PhD project on bonded composite repairs. I will also like to acknowledge the financial support provided by the APA scholarship and CRC-ACS scholarship during the duration of the PhD.

Next, I will like to acknowledge the technical support team especially Peter Tkatchky and Julian Bradler for their guidance and support in the area of material testing. I will also thank RMIT Microscopy and Microanalysis Facility for the use of their equipment. Special thanks are reserved to my colleagues at the Sir Lawrence Wackett Centre, namely Dr Khomkrit Pingkarawat, Dr Lei Peng, Shuai He, Ethan Goh, Mildred Lee and Eugene Chan. Although the journey of completing this PhD is often stressful and filled with difficulties, the constant discussion about work and non-related topics has made the workplace a more enjoyable to be in. I will miss these times when we eventually go our separate ways after completion.

Finally, I dedicate this thesis to my family especially my wife, Clarice, and our children, Luke and Emily. The constant encouragement you have given me gave the strength to push on and finish this PhD at times when the problems seem too huge. To Luke and Emily, I hope that you will be proud of what I have achieved when you get to read my thesis later on in your life.

Abstract

Fatigue cracks, if left uncheck, can lead to the catastrophic failure of the structure. Hence fatigue is an important design consideration. The development of a validated fatigue design methodology for bonded composite repairs is impeded by a lack of design criterion that is independent of load ratios, geometry and mode mixity. Consequently design methodology is largely empirical and involves large safety factors despite the recent research effort in this area.

A critical review of the literature reveals that existing parameters correlating to the crack growths rates are proposed as a means of curve fitting and do not correctly account for the effects of mean loads. Therefore the objective of this Thesis is to develop a mechanistic fatigue model for bonded joints and composite laminates that is capable of quantifying load ratio effects. Firstly, by considering the theoretical similitude requirements in fatigue, a correlating parameter ΔG_{eq} has been proposed. By maintaining similitude condition, this scaling parameter will be independent of specimen size. However the effects of load ratio can still be observed in the Mode I fatigue behaviour for both bonded joints and composite laminates. Therefore a new correlating parameter is needed to quantify these effects. In order to identify the mechanisms responsible for this behaviour, experimental tests and numerical simulations have been carried on two crack propagation mechanisms; cohesive debonding of bonded structures and delamination crack of composite laminates, under two crack propagation modes, Mode I and II.

Plasticity induced crack closure is identified as the primary cause of load ratio effects in the Mode I fatigue behaviour of bonded joints. Elastic-plastic analysis is performed on the bonded double cantilever beam model. The bonded joints are shown to experience significant level of crack closure and this phenomenon is quantified. On the other hand, ΔG_{eq} is able to correlate the Mode II data and numerical investigation confirms the absence plasticity induced crack closure. Therefore a new correlating parameter, based on the crack closure model, is proposed and successfully eliminates the influence of mean loads.

Load ratio also has a strong influence on the delamination growth along 0°//0° interface. Experimental evidence showed extensive fibre bridging in the wake of the crack. Hence this fatigue behaviour is hypothesised to be attributed to plasticity induced crack closure and/or fibre bridging. The Hill's plastic potential is used to simulate the

anisotropic yielding of the lamina. The numerical results eliminate plasticity induced crack closure to be the cause of the observed load ratio effects in the experimental data. However it is also found that crack closure can occur in delamination along 45º//0º and 90º//0º interfaces. Therefore this leaves fibre bridging as the only possible source for the strong influence of load ratio. The parameters of the bridging zone are measured experimentally. Consequently a new correlating parameter is proposed to account for the crack tip shielding by fibre bridging.

In some of the experimental data analysed, G_{max} can affect the fatigue behaviour especially in the case of composite laminates. It is hypothesised that G_{max} introduces damage in the matrix ahead of the crack tip, reducing the matrix resistance to crack growth. The Forman equation is modified for bonded joints and composite and a significant improvement of the crack growth rates can be observed.

Finally mixed mode crack propagation is investigated with the cracked lap-shear specimen of three doubler substrate thicknesses. Mode I is found to be the dominant driving force. Therefore, by using the crack closure and fibre bridging model, a new correlating parameter is proposed that is able to unify the crack growth rates of varying load ratios and mixed mode ratios.

Rather than proposing new empirical relation to describe the observed fatigue behaviour, this Thesis develops a fundamental understanding of the effects of mean load and its mechanisms in bonded joints and composites. A scaling parameter is proposed which describes the crack tip conditions by considering the physical process. This will provide engineers a fatigue criterion which can be used to design a bonded composite repair for an arbitrary load ratio and mixed mode ratio.

Table of Contents

List of Figures

List of Tables

List of Abbreviations

Term	Definition
2D, 3D	Two-dimensional, Three-dimensional
ASTM	American Society for Testing and Materials
CA	Constant amplitude
CLS	Cracked lap-shear
CRC-ACS	Cooperative Research Centre for Advanced Composite Structures
COD	Crack opening displacement
CT	Compact tension
CZM	Cohesive zone model
DCB	Doubler cantilever beam
DOF	Degree of freedom
DOFS	Doubler overlap fatigue specimen
ENF	End notched flexure
FAA	Federal Aviation Administration
FCGR	Fatigue crack growth rate
FE	Finite element
LEFM	Linear elastic fracture mechanics
MT	Middle tension
PICC	Plasticity induced crack closure
SEM	Scanning electron microscope
SERR	Strain energy release rate
SIF	Stress intensity factor
VA	Variable amplitude
VCCT	Virtual Crack Closure Technique
UD	Uni-directional

Nomenclature

Term	Unit	Definition
a	mm	Crack length
a_0	mm	Initial crack length
b	mm	Specimen width
C	mm/N	Compliance of specimen
D, m		Paris law material constants
da/dN	mm/cycle	Rate of fatigue crack growth
E	MPa	Young's modulus (with subscripts 1, 2, 3)
G	MPa	Shear modulus (with subscripts 1, 2,3)
G	J/m^2	Strain energy release rate (with subscripts I, II, III)
h	mm	Thickness of the substrate
l_e	mm	Crack tip element length
K		Stress intensity factor
N	cycle	Number of cycles
P	N	Applied load
r_p	mm	Forward plastic zone length
R		Load ratio
t_A	mm	Bondline thickness
u	mm	Nodal displacement in finite element analysis
U		Effective load range due to crack closure
α		Constraint factor (1 for plane stress and 3 for plane strain)
$\delta_{applied}$	mm	Applied displacement at the crosshead
Δ	mm	Traction separation displacement
σ	MPa	Elemental stress in finite element analysis
v		Poisson ratio

Subscripts

Term	Definition
I, II, III, m	Crack opening modes; I. Peeling; II. Shearing; III. Tearing; m: mixed mode
1, 2, 3	In ply coordinate system; fibre, matrix and through-thickness direction
A	Adhesive
c	Critical
min, max	Minimum, Maximum
T	Total, used with strain energy release rate G
th	Threshold
x, y, z	Global coordinate system in finite element analysis

Chapter 1

Introduction & Motivation

1.1. Motivation

Fibre-reinforced composite materials continue to revolutionise the aerospace and other industry where lightweight is a key enabler to reduce fuel consumption. Key factors influencing the increased usage of composites in aerospace application are structural performance, weight and multi-functional design. Complex, large components can be manufactured as a fully integrated structure to reduce the need for joints and obtain a structure with more continuous fibres. The application of advanced composite materials is gradually increasing year on year in civil aircraft structures, as shown in Figure 1-1 and the trend is likely to continue. As evident in the two largest aircraft manufacturers, Boeing 787 Dreamliner and Airbus A350 XWB will have more than 50% of their structural weight manufactured from advanced composite materials. More importantly, composite technology has been progressively introduced to primary structures due to better understanding of the material behaviour under loading. For example, the wingbox and fuselage of the 787 and A350 are manufactured from advanced composite materials.

Not only limited to aerospace applications, composites today are also used in wind energy, marine, construction, defence, automotive and sporting goods. The widespread application of composite materials will continually increase as the material becomes more affordable. In 2011, the global composite materials market represented USD$19.6 billion in terms of shipment value as shown in Figure 1-2. This is projected to reach an estimated USD$29.9 billion, driven by the growing demands in the aerospace, military, transportation and wind energy markets.

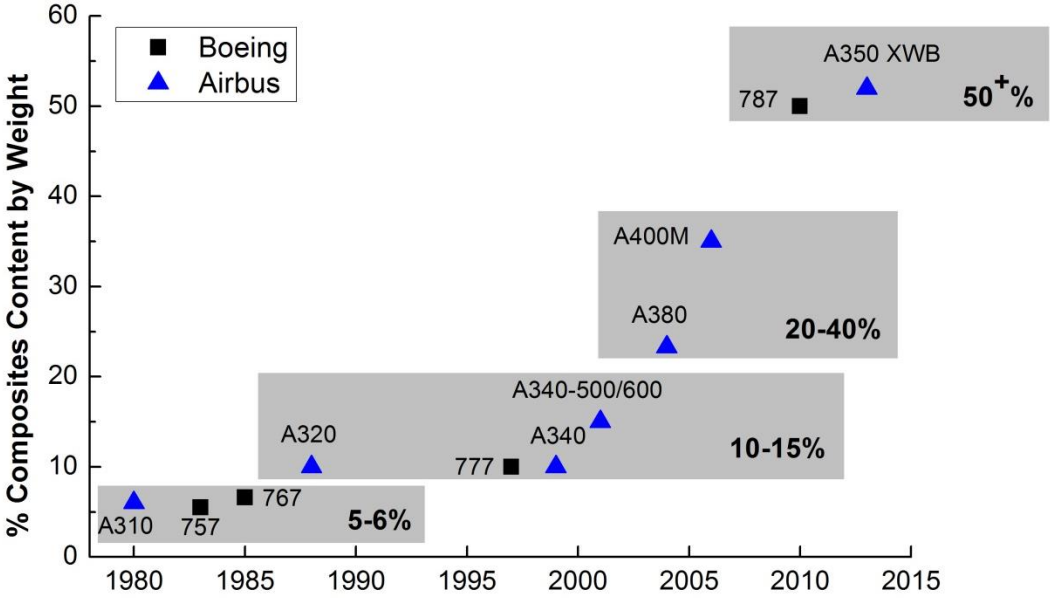

Figure 1-1: Composites material usage in aircraft over the years [1]

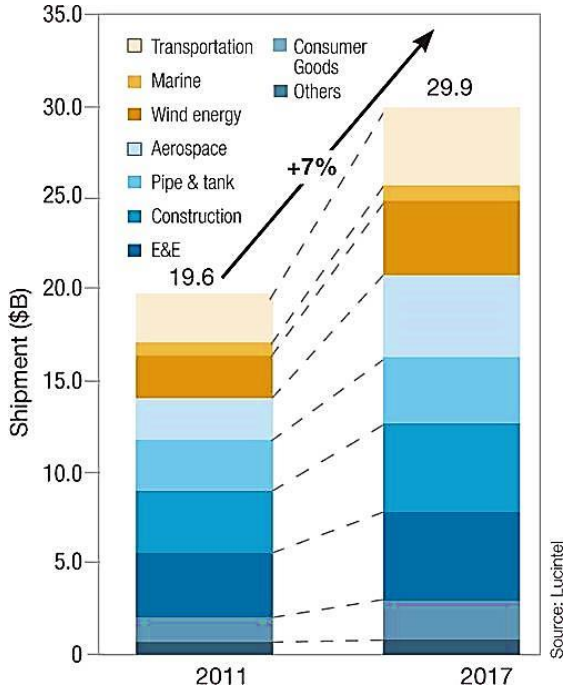

Figure 1-2: Projected global composite material shipments [2]

Composite structures are inherently susceptible to delamination damage due to their low through-thickness strength and fracture toughness. Delamination is the primary mode of damage during the aircraft service life. As the usage of composite materials increases, repairs on in-service damage are essential to prevent disposal of costly

aerospace components. The purpose of the repairs is to restore the structure's capacity to sustain design loads and original functionality without adversely affecting its form. Adhesive bonding is the preferred method of joining or repairing two composite structural components. One of the benefits of bonded joints is that the stresses are more continuous and uniformly distributed. Mechanical joining, on the contrary, introduces additional stress concentration to the pristine structure such as hole drilling required for rivets and bolts. Also the brittle nature of the matrix resin makes it highly susceptible to delamination when the rivet or bolts experience high mechanical loads.

Hence adhesive bonded repairs are an attractive technique for aircraft operators to extend the service life and maintain structural integrity of expensive composite structures. Although bonded repairs are now widely accepted in tertiary and secondary structures, the certification of a bonded repair patch for ensuring airworthiness presents a challenge due to: -

- a lack of non-destructive means of detecting weak interfaces of the adhesive and composite;
- a lack of a validated failure criteria for the design of bonded composite repair and;
- concerns for the long term durability and fatigue performance of the adhesive joint.

It is widely acknowledged that non-destructive inspection technology that can reliably detect weak bonds do not yet to exist. Therefore the limit load capacity of bonded repair must be substantiated by proof-testing and/or by design features which allowed the parent structure to withstand limit loads in the event of complete disbond of the repair. A schematic of the damage threat assessment for a bonded structure, which may occur at any point in its service life, is given in Figure 1-3. In the presence of a detectable disbond, the bonded repair should be able to sustain the ultimate loads. FAA Advisory Circular 20-107B mandates that composites and bonded structures must be designed for no-growth or slow-growth crack growth to ensure continuous airworthiness during its service life [3]. The disbond is assumed to be inherently present in the bonded repair due to an allowable manufacturing damage or a low energy impact event during service. The disbond must not grow to critical length until the next inspection interval where the damage can be detected and corrective measures can be taken. In the event of complete disbond of the repair patch, the parent structure must be capable of sustaining design limit loads. The strength prediction of bonded structures has been extensively studied over the years and prediction can be done with a degree of confidence.

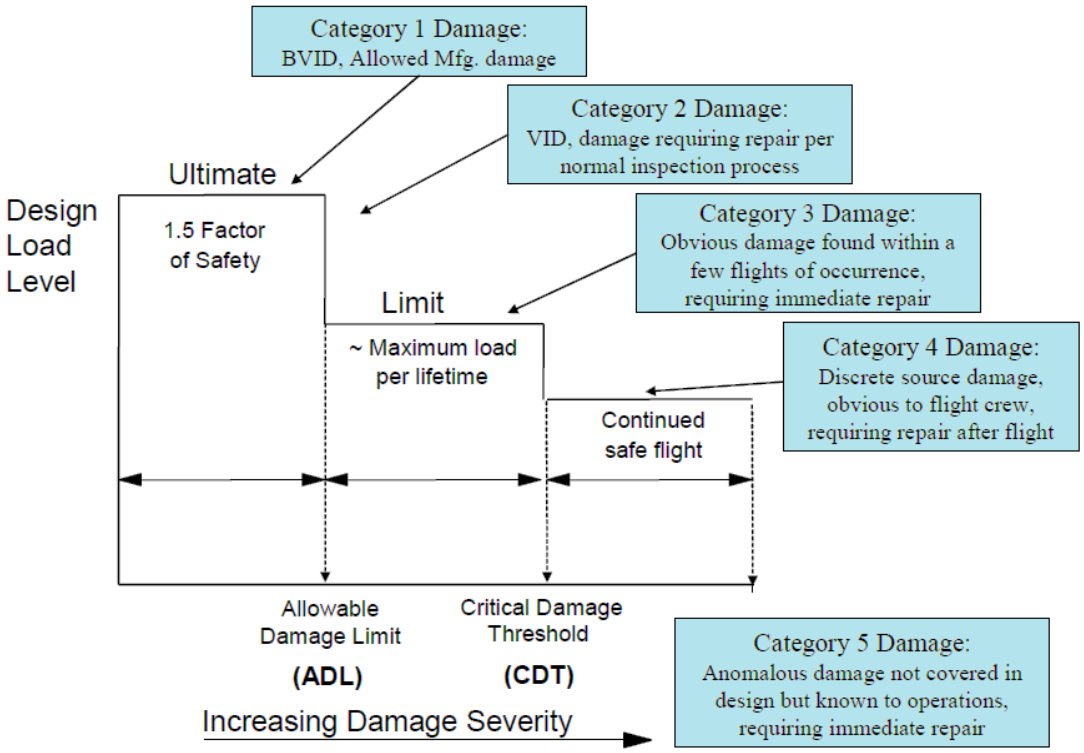

Figure 1-3: Schematic diagram of design load levels versus categories of damage severity [3]

In order to satisfy the durability and fatigue requirements, the bonded repair must demonstrate *"an acceptably low probability of patch disbonding during the remaining life of the structure"* [4]. This will require a good understanding of the behaviour of the adhesive bondline under different environmental conditions and cyclic loads. Unfortunately knowledge in both areas is lacking. There is no accepted design parameter in the characterisation process obtained at coupon level that can be readily applied at component level. At present, low allowable strains or large safety factors based on static design are used in order to avoid structural failure under cyclic loading and environmental degradation. This approach places a very high cost burden on the use of bonded composite structures and/or repairs. For example, during the certification of Airbus A320 vertical fins, no damage was found under static loads but excessive delamination growth was detected under fatigue loading [5]. This demonstrates that fatigue design approach based on strength criteria and knockdown factors is insufficient and requires extensive experimental validations. This will be impractical for large bonded repairs to primary structure as such repairs will likely be done once-off. Furthermore an impasse may be reached in the design of scarf repairs. The additional conservatism can be problematic on a few counts. As the scarf angle decreases, 1) the repair design approaches the limit of what can realistically be machined, 2) the amount of pristine material removed can

effectively reduce the structure's residual strength below limit loads and 3) the available area which can be machined off is limited by the surrounding structural components without affecting their load carrying capability.

1.2. Durability of Bonded Structures

Fatigue relates to the failure of materials under repeated loadings at levels that are much lower than the quasi-static failure loads. Under cyclic loading, bonded components may fail much earlier despite the operational loads being much lower than the limit loads. Fatigue cracks can be initiated or accelerated by accidental impact, environmental ageing etc... Catastrophic failure may occur after years of service if these cracks are left unchecked. Hence the engineer must design against fatigue failure where cyclic loading is significant. The stochastic nature of fatigue makes it difficult to predict accurately. Furthermore, accurate measurements of the in-service loads and environments are rarely known. This difficulty is escalated owing to fatigue crack propagation in an adhesive being sensitive to small changes in loading conditions. Therefore a "*safe life*" design approach is taken for bonded structures where an existing crack must not attain critical length within three service lifetimes.

1.2.1. Fatigue Loads Definitions

A time variable is included when considering fatigue. A typical cyclic load spectrum is characterised by peaks and troughs and is expressed in terms of either applied stress/load or displacement. In more complex structures, it is more useful to correlate the applied cyclic stresses to parameters which relates to the stress-strain field in the vicinity of the crack tip such as the stress intensity factor. Under laboratory conditions, fatigue loads are commonly generated as a constant amplitude (CA) sinusoidal waveform, as illustrated in Figure 1-4. A waveform is defined by the frequency (Hz), stress range ($\Delta\sigma$) and mean stress (σ_m). The mean stress is also typically characterised by the stress or load ratio, R, given as,

$$R = \frac{\sigma_{min}}{\sigma_{max}} \tag{1-1}$$

In engineering applications, such waveform is seldom replicated and it is very likely that the frequency, amplitude and mean stress will vary with time. This is termed as variable amplitude (VA) fatigue.

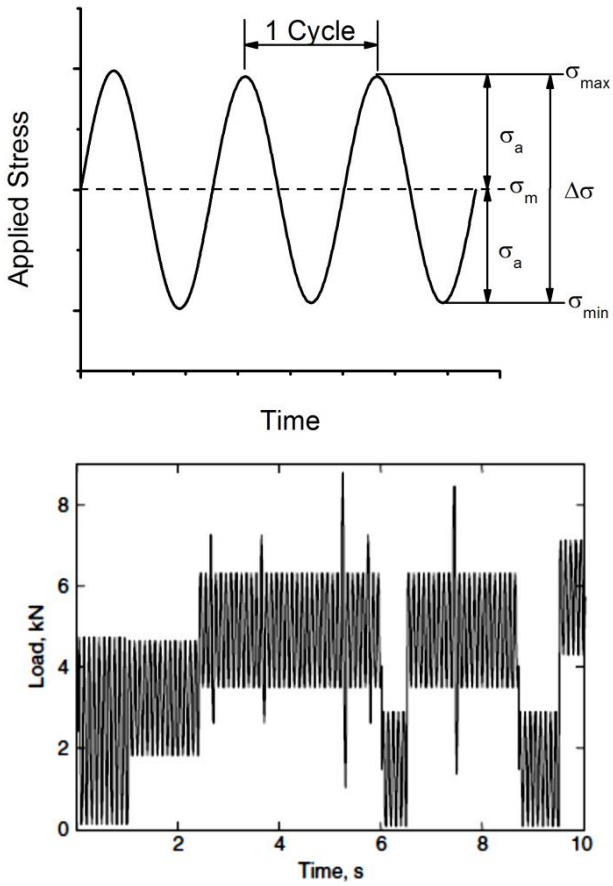

Figure 1-4: Constant and variable amplitude fatigue waveform [6, 7]

The mechanical performance of an adhesive and epoxy composite laminate can be affected by the loading rate and thermal stresses [8-11]. The following effects include a decrease resistance to creep-fatigue, stiffness and failure stress which are greatly amplified as the temperature approaches the glass transition temperature (T_g). The fatigue spectrum frequency can induce significant amount of thermal stresses within the adhesive and composite. Hence it may be important to account for thermal stresses especially if the adhesive mechanical properties are sensitive to elevation in temperature. Degradation of the adhesive and composite, after extended exposure to a particular environment (i.e. hot/wet or cold/dry), is also a major concern for the durability aspect of bonded repairs. The absorption of moisture can potentially affect the chemical bonds between the adhesive and substrate, particularly when the substrate is metallic. This increases the complexity of the analysis when combined with fatigue loading through the introduction of coupled time-dependent parameters. However the environmental effects on the fatigue performance of the bonded repairs will not be covered within the scope of this Thesis.

Fatigue life of a bonded structure is often divided into crack initiation and propagation phases. However fatigue crack initiation in adhesive is a complex and little understood process. Structural adhesives are often multi-component material with filler particles, carrier mats and toughening particles. The crack initiation process may comprise of many failure mechanisms occurring at the same time. Detection through non-destructive means is difficult due to the limitations of current technology. Consequently the characterisation of the crack initiation phase mechanistically is not yet possible and often a more pragmatic approach is taken to differentiate the two phases. From an analysis point of view, it is useful to differentiate the initiation phase as fatigue damage of a sufficient crack length which further growth can be predicted by the fracture mechanics approach. In terms of in-service inspection, crack initiation is related to the threshold of detectability of flaws.

1.2.2. Fatigue Life Prediction Methodologies

The ability to predict the behaviour of bonded joints or repairs is critical in supporting its design to minimise fatigue failure to below an acceptable level in service. This will aid engineers to design an efficient fatigue resistant bonded structure, resulting in safer, cheaper and higher performance structures. The main goal in modelling fatigue is to predict the time (number of cycles) to failure, crack initiation or the critical crack length which unstable crack growth will occur. Fatigue behaviour of a bonded composite joint is represented either as 1) a relation of the applied stress and the time elapse to fracture, known as the total-life approach or; 2) fracture mechanics based model which deals with the crack propagation phase.

In the total-life approach, the number of cycles to failure is plotted as a function of a load related variable such as stress or strain amplitude, termed an S-N curve or Wöhler plot. The Wöhler curve can be expressed as,

$$N = f(\sigma, S_c, R) \tag{1-2}$$

The constants in the curve fitted equations depend on many factors, including material, geometry, surface condition, environment and mean stress. An endurance limit exists for an adhesive where no crack initiation or growth occurs. It has been suggested that this limit coincides when the cyclic stress does not exceed the adhesive's elastic limit [12]. However, due to the S-N curve dependence on different factors, the endurance limit cannot be considered as a material property. This means that the S-N data may not be easily transferable to other bonded joint configuration and conditions that may experience

different level of stress concentration or contain varying size of initial flaws. Therefore there is no unique relation between the stresses in the adhesive layer and applied stress of two bonded joint geometries (for example, single lap joint and scarf joint) [13]. Moreover the standard stress-life method gives no information of the progression of damage and the residual joint strength. Although, in some cases of the S-N curve, the number of cycles is used to determine the onset of crack initiation and allows the propagation phase to be differentiated. The above factors mean that the S-N curve is of rather limited value in terms of predicting fatigue behaviour. However it is still used, due to the lack of better tools, in fatigue modelling as a source of validation data.

The S-N curve is directly applicable to constant amplitude fatigue. Under variable amplitude fatigue, the Palmgren-Miner (P-M) rule can be used to predict the life using S-N data and is represented by

$$\sum \frac{n_i}{N_{fi}} = M \tag{1-3}$$

where n_i is the number of cycles in a block of constant amplitude loads and N_{fi} is the number of cycles to failure at the stress amplitude for that particular block from the S-N curve. The parameter M is the Miner's sum and is generally assumed to be one. The limitations to this simple method are that it assumes (1) damage accumulation is linear, (2) no damage below the fatigue threshold and (3) there are no load history effects. Erpolat *et al.* used the P-M rule to predict failure of a bonded CFRP double lap joint under variable amplitude cyclic loading [7]. The experimental failure cycles was significantly less than the predicted failure cycle by P-M rule with M = 1. This indicates that load sequencing is accelerating the rate of crack growth. Hence, in this case, the P-M rule is not conservative.

In the fracture mechanics approach, the rate of fatigue crack growth is correlated with an appropriate fracture mechanics parameter. The crack initiation phase is ignored and an initial crack is assumed to exist. The strain energy release rate, G, is typically used as the governing correlating parameter for bonded and composite structures due to increased complexity in calculating the stress intensity factor, K, in a heterogeneous system. The disbond growth rates are related to the strain energy release rate via a relationship similar to the Paris law [14],

$$\frac{da}{dN} = D[f(\mathrm{G})]^m \tag{1-4}$$

where D and *m* are material constants, dependent on a number of factors.

A plot of fatigue crack growth rates against the maximum strain energy release rate, G_{max} or other definitions usually consists of three regions as illustrated in Figure 1-5. Region I is defined by the threshold strain energy release rate, G_{th}, where crack growth is slow enough to be considered negligible. Region II is the steady crack growth regime as described by the Equation 1-4. Finally, the fatigue crack growth rate rises to an asymptote in Region III. This is characterised by unstable crack growth. The number of cycles to failure can be determined by integrating Equation (1-4),

$$N_f = \int_{a_0}^{a_F} \frac{da}{D[f(G\}]^m} \tag{1-5}$$

where a_0 is the initial crack length and a_F is the final critical crack length.

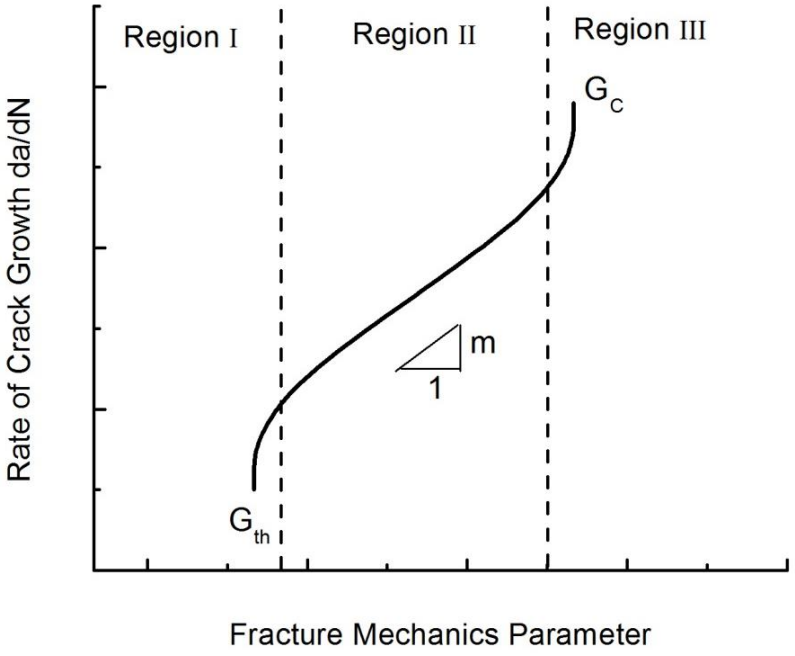

Figure 1-5: Typical fatigue crack growth rate behaviour. Three distinct region of crack growth can be observed; Very slow crack growth (Region I), Stable crack growth (Region II) and Fast crack growth (Region III) [15]

A simple method of predicting VA fatigue from the CA Paris law relation is to perform numerical crack growth integration. The crack size and corresponding fracture parameter are assumed to be constant throughout a CA stage. The crack growth can be obtained from Equation (1-5) and gives the overall crack growth during the stage. This is

used to determine the crack size for the subsequent stage ($a_{i+1} = a_i + \Delta a_i$) and the procedure is repeated until critical damage is attained or the crack is arrested.

$$a_{i+1} = a_i + n_i \frac{da}{dN} \tag{1-6}$$

Repeat until

$G_{max,i+1} \geq G_C$ (critical damage is attained with increasing a)

Or $G_{max,i+1} \leq G_{th}$ (crack is arrested with increasing a)

The fracture mechanics methods have the limitation that the crack initiation phase is not accounted for. Quaresmin and Ricotta attempt to model the crack imitation and propagation phases of pristine conditioned single lap joints [16-18]. The initiation phase, which is defined by the user, is characterised by stress intensity factor, *K*, generated at the corner geometry of the bi-material interface in a K-N_i curve. The propagation life is then characterised using the fracture mechanics approach.

Damage mechanics approach, using the cohesive zone model (CZM) approach, attempts to address some of these problems by modelling progressing degradation and failure, thus accounting for both initiation and propagation phases. The CZM approach is based on the cohesive zone formulation developed by Dugdale [19] and Barenblatt [20] and has enjoyed some success in predicting the static strength of bonded joints. The CZM approach for fatigue crack growth prediction is relatively new and rigorous validation of the methodology is still needed. Early pioneers in using the damage mechanics to simulate the fatigue degradation and crack progress include Robinson et al. [21], Turon *et al.* [22], Khoramishad *et al.* [23] and Harper *et al.* [24]. Fatigue behaviour is simulated by numerically applying a constant load equal to the maximum cyclic load. The fatigue damage parameter and displacement is dependent on pseudo-time, representing the number of cycles elapsed. The mathematical model requires calibration which may not be trivial. Turon et al. attempt to link the CZM and fracture mechanics model [22]. Khoramishad et al. link the CZM to the strain value and degradation over number of cycles [23]. However the CZM fatigue model still lacks a basis in the underlying physics of the fatigue process in composites. This can be seen in the cohesive relation itself and in the damage parameter formulations. Firstly the model assumes damage within the CZM is correlated to an equivalent crack length within the process zone. This can be contentious as damage conventionally refers to the reduction in stiffness of the material. Secondly the fatigue crack growth correlating parameter used is based on the definition of $\Delta G = G_{max} - G_{min}$. This definition violates the similitude principle in fatigue and will be

discussed in Chapter 2. However the potential advantage in the CZM is that it can model both the initiation and propagation phases of fatigue crack growth.

1.3. Research Gaps & Objectives

1.3.1. Problem Statement

The premise of a damage tolerant design philosophy is to ensure the structure is capable of carrying design loads before cracks can be detected and before they become critical to cause failure of the structure. An existing flaw within a bonded composite repair can propagate either cohesively (i.e. within the bondline) or as delamination (i.e. between two composite plies) as shown in Figure 1-6 [25-27].

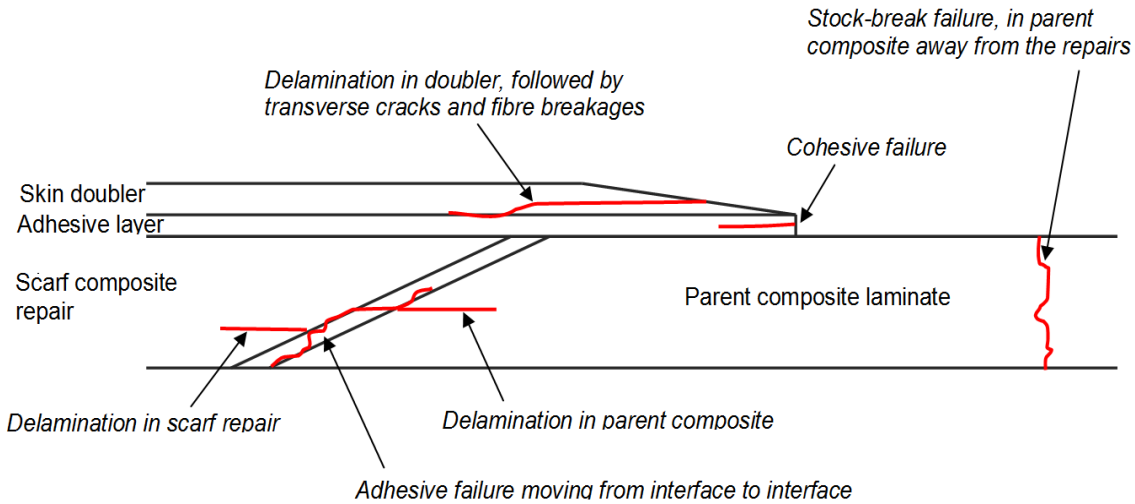

Figure 1-6: Number of possible failure modes in a typically bonded composite repair

In this work, we focussed on the bonded repair's durability subjected to mechanical loadings only. The main failure mechanisms considered are cohesive and delamination. Although not without its limitations, the fracture mechanics approach is a more flexible design tool than the stress-life approach in modelling the progression of cracks to failure and can potentially transfer to different geometries.

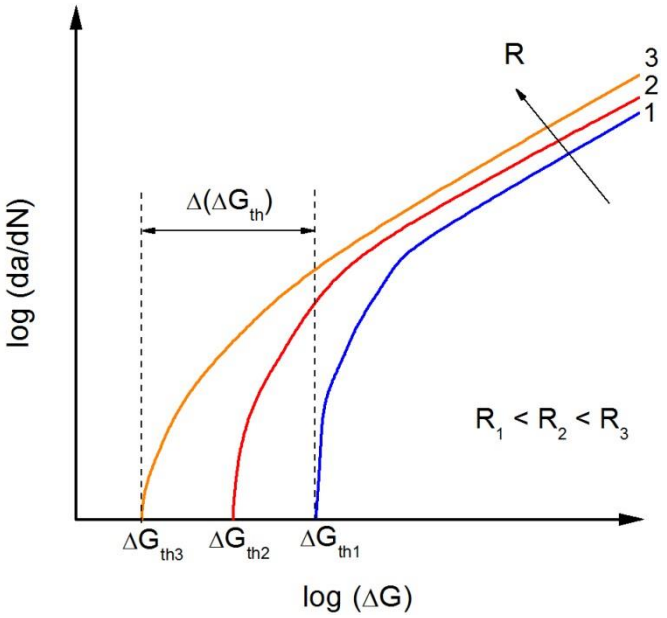

Figure 1-7: Schematic of the threshold value dependence on the load ratio

One of the main reasons for a lack of a fatigue design parameter is the load ratio effect within the threshold crack growth behaviour of bonded joints and composites, shown in Figure 1-7, which will be discussed in Chapter 2. The load ratio effect complicates damage tolerant design. For example in Figure 1-8, the threshold load ΔG_{th1} and ΔG_{th2} occurs at load ratios R_1 and R_2 respectively. ΔG represents a general function of the maximum and minimum strain energy release rate. Due to the dependency on mean loads, the upper bound of ΔG_{th} is a function of G_{max}. Although depicted as a linear function, it is by no means implying any specific function between ΔG_{th} and G_{max}. If ΔG_{th1} is used as the conservative design parameter, crack growth may occur under service loads with G_{max} exceeding the upper bound of the safe region (i.e. > G_{max1}). A safe design can be attained by selecting a ΔG_{th} that is in the safe region for all range of G_{max}. However this safe limit is not known without experimental testing.

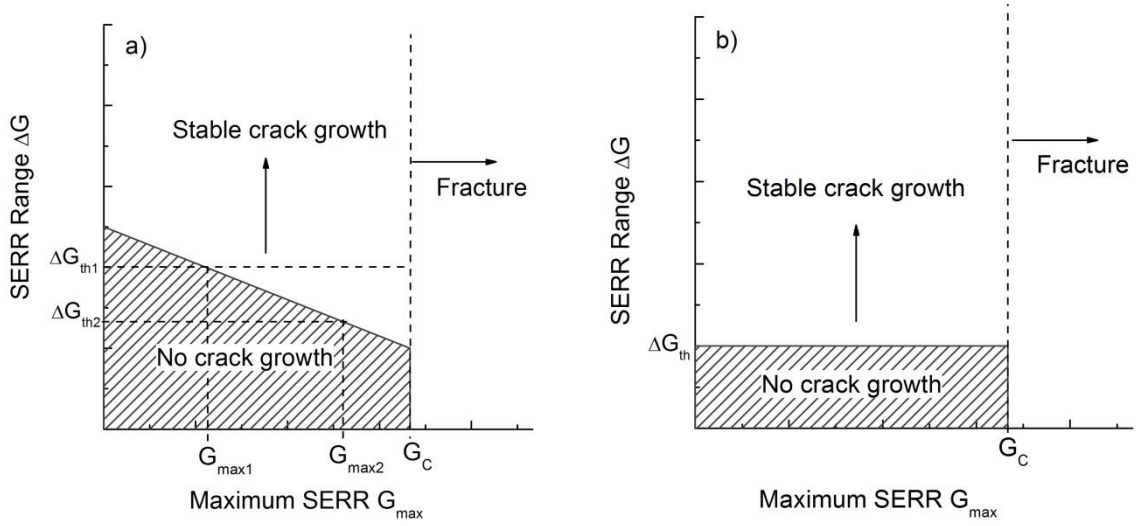

Figure 1-8: Schematic of ΔG versus G_{max} used to demonstrate damage tolerant philosophy; a) non-ideal case of ΔG_{th} being dependent on G_{max} or load ratio and b) idealised case of a unique ΔG_{th} for all load ratios

A lack of understanding of the fatigue behaviour of under different load ratios limits the confidence of the repair design to meet safety and cost requirements. Therefore a better understanding of the load ratio behaviour of bonded and composite structures is needed, which in turn will provide critical input to the development of a quantitative model account for this effect on fatigue crack growth life. If a definition of the threshold ΔG_{th} parameter can be determined that is independent on G_{max} or load ratio, improvement in the design process can be achieved.

1.3.2. Objectives

The overall research objective of this PhD project is to develop a methodology for quantifying the load ratio effects on the fatigue growth behaviour of adhesively bonded repair, including cohesive cracking and interlaminar disbond. In order to achieve this objective, this project addresses the following research questions:

- Which of the current correlating parameters are suitable for characterising fatigue behaviour of composite laminates and bonded joints and what are the limitations?
- What are the mechanisms responsible for the load ratio effects on the fatigue crack growth rates in composite laminates and bonded joints?

- What is the relationship between the threshold load under mixed mode loading and its individual mode components derived from coupon testings?

The new models will improve the design analysis to demonstrate compliance of bonded repair under fatigue loading with current airworthiness requirements.

1.3.3. Thesis Structure

This thesis is structured in seven chapters including the introduction chapter. Chapter 2 presents a critical review of existing correlating parameters used for characterising the fatigue behaviour of composites and bonded joints. A summary of the limitations of current definitions of correlating parameters is provided. The experimental study of Mode I and II fatigue crack growth in a joint is described in Chapter 3, with the results showing the strong influence of mean loads on crack growth rates. This confirms the limitations of existing correlating parameters highlighted in Chapter 2. Possible mechanisms were identified for the load ratio dependency behaviour as part of the experimental investigations. Chapter 4 investigates the load ratio effects in bonded joints using the crack closure model. Plasticity was introduced into the adhesive layer to simulate crack closure and the new correlating parameter was capable of unifying the mode I and II fatigue debonding data. The role of fibre bridging on fatigue delamination is presented Chapter 5. Chapter 6 presents the results of mixed mode crack propagation in a cracked lap shear specimen. A correlating parameter was proposed that eliminates the influence of both load ratios and mixed mode ratios.

This page intentionally left blank

Chapter 2

Review of Fatigue Crack Growth Correlating Parameter for Bonded and Composite Structures

2.1 Fatigue in Bonded Composite Repairs

Bonded repairs or joints in aircraft structures can be expected to operate under fatigue of sinusoidal loads of near constant amplitude (i.e. fuselage) or variable amplitude (i.e. wing). Hence validated design methodologies are needed to predict the crack growth behaviour under different loading conditions and to reduce the need for extensive experimental testing programme.

Cyclic loading parameters (maximum and minimum loads) can significantly affect the fatigue lives of both bonded joint and composite structures. Conventionally the key fatigue controlling parameters are the amplitude and the mean load. It has been experimentally observed that the fatigue life of most materials decreases with an increase in load amplitude or mean loads [7, 13, 28]. The actual value of the maximum load relative to the yield strength of the material is also an important factor: if the adhesive yields under maximum applied load, crack initiation is likely to occur more quickly [29]. Laboratory fatigue tests of bonded joints or composites are typically carried out on coupons or representative joints. Figure 2-1 shows the type of specimens typically used to generate fatigue test data. The most basic specimen configurations are coupon type specimens which are designed to characterise the behaviour of the material system. Experimental testings are also carried out on simple joint configuration to represent the loading conditions in the structure. Fatigue tests are considerably more resource consuming than static tests. By developing an understanding of the physical process and the observed macroscopic behaviour, designing bonded composite repairs for fatigue can then be carried out with confidence and reducing the amount of experimental validations.

a) Coupon type specimens

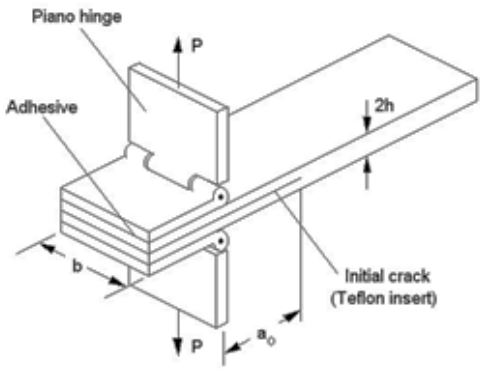

a-1) Double beam cantilever

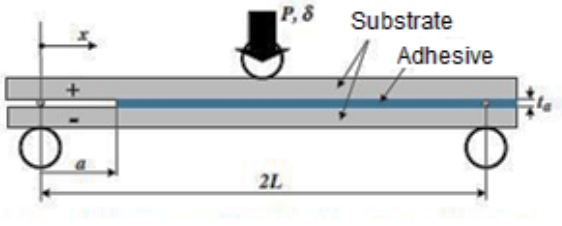

a-2) 3 point End notched flexure

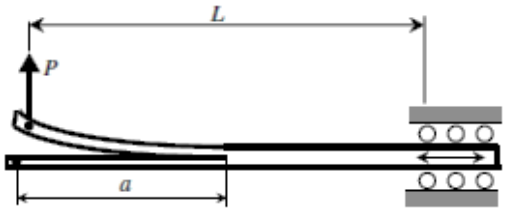

a-3) End load split

b) Representative joint type specimens

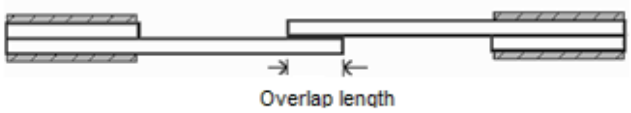

b-1) Single lap joint

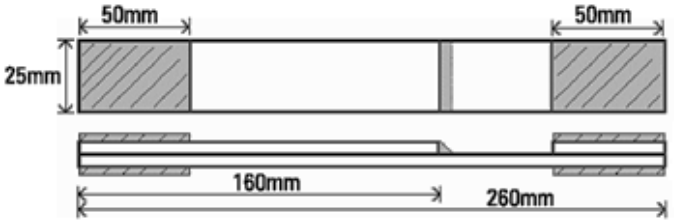

b-2) Lap-shear joint

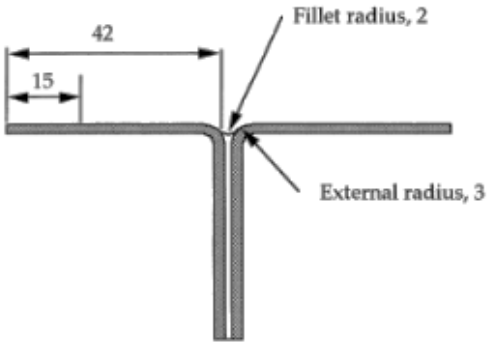

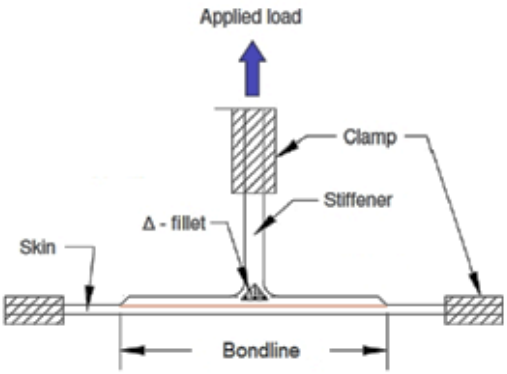

b-3) T-Joints

Figure 2-1: Examples of coupon level specimens and joint type specimens used in fatigue experiments

Fatigue crack growth in bonded structures and composites is conventionally characterised by the strain energy release rate (SERR). However there is no consensus regarding the definition of the correlating parameter under varying load ratios. The most prevalent definition found in the literature is the maximum SERR and cyclic SERR, given as G_{max} and $\Delta G = G_{max} - G_{min}$. However the ΔG definition may give rise to the misconception that ΔG shares the same similitude as ΔK and leads to erroneous conclusions about fatigue crack growth behaviour of bonded and composite structures. In recent years, a definition of the SERR range, consistent with the similitude principle for ΔK for metals fatigue, has been proposed for delamination growth in composite structures [30], which will be described in Section 2.2.

Fatigue modelling of delamination and debonding can be generally categorised in two areas: either explicit expressions for the Paris law parameters (i.e. G_{max}) as function of R [31, 32] or an effective controlling parameter (i.e. ΔG) that merges fatigue crack growth rates of different load ratios into a master curve [33-36]. At present, all correlating parameters used require some form of empirical calibration to account for the influence of mean loads on the fatigue crack growth behaviour of bonded joints and composite laminates. Under variable amplitude (VA) loading, the interactions between load cycles are observed to either accelerate or slow the fatigue crack growth rate. Farrow, first, termed the *"cycle mix"* effect as he found the fatigue life of composite laminates to be shorter for a loading block with higher mean stress [37]. Similarly, Erpolat *et al.* found the Palmgren-Miner severely over-predicts the life of bonded composites joints subjected to a block-loading of VA spectrum due to high load interaction [7]. They had shown that variations in mean loads were far more damaging than overloads as the joint's life was only 20% of the predicted life. Consequently, they proposed a simple predictive model to account for the *"cycle mix"* effect. However the *"cycle mix"* parameters in their model do not have a physical meaning to explain the interaction between load cycles. Therefore the parameters are curve-fitted into variety of loading histories. The first step to developing a predictive methodology of damage evolution in bonded joints and composites under VA spectrum is to develop an understanding of the physical mechanisms accountable for the effects of mean loads. Once that can be achieved, the interaction between load cycles can be accounted for in a mechanistic manner. Consequently a method, similar to the approach taken in metal's fatigue, can be used to predict crack growth under VA spectrum, overcoming the limitations of existing methods.

Since its discovery by Elber [38] of plasticity-induced crack closure in metallic materials, the crack closure concept is now a widely accepted to explain and account for the effects of mean loads on the cyclic crack growth behaviour. Essentially crack closure

reduces fatigue crack growth rates by lowering the effective stress range experienced at the crack tip. This concept has enabled the development of practical life prediction methods of metallic structures under variable spectrum loading. FASTRAN [39], which is widely used in aircraft industry, uses the crack closure concepts to account for load-interaction and predicting the life of metallic structures under variable amplitude loading. By contrast, very little research has been reported in the literature on the crack closure phenomenon in adhesively bonded structures.

The definition of the fracture mechanics parameter should uniquely describe the crack tip conditions and is independent of size and geometry. In short, this parameter should be a material constant. With the appropriate correlating parameter, a variety of joint geometry can then be designed against fatigue failure. A repair's operational life is then only limited by the chemical stability of the polymer to resist environmental degradation. This will also possibly enable structural designers to use higher allowable stress or strain (thus reduce weight) whilst maintaining the benefits inherent of a no-growth criterion. This can be achieved by knowing the precise boundary of the no growth design envelope. Given the different definitions used in characterising crack growth under different load ratios, a literature survey was conducted on the fatigue characterisation for composite laminates and bonded joints. This work considers two major fatigue failure mechanisms: delamination and debonding. The term fatigue delamination refers to crack propagation within composite laminates and the term fatigue debonding refers to crack propagation within the adhesive bondline. The implication and underlying assumptions of each definition are discussed, utilising experimental data taken from literature.

2.2 Definition of Crack Growth Correlating Parameter

In the stress analysis of cracked bodies, there are three basic modes of crack extension as shown in Figure 2-2; opening (Mode I), in-plane shear (Mode II) and out-of-plane tearing (Mode III). Mode I corresponds to the normal dislocation of the crack flanges under the action of tensile stresses. Mode II and III is the shearing action normal and parallel to the crack front respectively in the plane of the crack. A cracked body can experience any one of the three primary fracture modes, or a combination of these three modes.

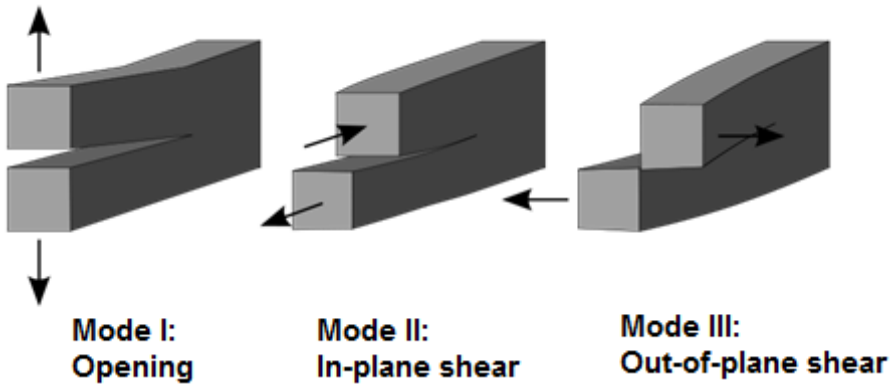

Figure 2-2: Crack propagation modes [40]

Under a single mode of loading, the definition of the correlating parameter is conventionally given as either G_{max} or ΔG. The importance of G_{max} stems from the static crack propagation under monotonic loading. The formation and coalescence of micro-cracks occurs when the crack tip conditions exceed a certain threshold stress. The maximum strain energy release rate, G_{max}, is calculated using the Irwin-Kies relation [40],

$$G_{max} = \frac{P_{max}^2}{2b}\frac{\partial C}{\partial a} \tag{2-1}$$

where b is the specimen width and C is the compliance of the specimen, given as displacement divided by applied load.

Under fatigue loading, the minimum load experienced at the crack tip must be accounted for as the rate of crack propagation depends primarily on the range of stresses in the fatigue cycle. The cyclic SERR ΔG has been defined as,

$$\Delta G = G_{max} - G_{min} = \frac{P_{max}^2 - P_{min}^2}{2b}\frac{\partial C}{\partial a} \tag{2-2}$$

However it must be noted that ΔG is inconsistent with the similitude basis as ΔK. This may lead to misconception of the fatigue behaviour by treating ΔG as a parameter represented purely by the cyclic loading fracture process. Before proceeding further, the concept of similitude must be understood as it provides the basis for applying fracture mechanics to fatigue crack growth. The fundamental principle of similitude is that the size of the object is relative and the physical phenomena can be described by a size independent relation [40]. For example, material constant parameters such as stress,

strain and elastic modulus can be derived from the Hooke's law relation. In fatigue crack growth, similitude implies the crack tip deformation and, hence, crack increment per cycle is uniquely controlled by a single loading parameter such as stress intensity factor, *K,* as in the case of metals. Consider a growing crack under constant amplitude loading, a cyclic plastic zone forms at the crack tip. If the plastic zone is sufficiently small and within the elastic singularity zone, the crack tip conditions then can be said to be uniquely characterised by the stress intensity factor. Hence the crack driving force for growth of a crack is related to the stress-strain field at the crack tip. Thus similar crack growth behaviour will be observed for similar crack tip stresses (regardless of crack length and geometry) since the similitude condition prevails.

Based on the theory of LEFM, the stress at the crack tip is singular and can be described as [40]:

$$\sigma_{ij} = \frac{K}{\sqrt{2r}} f_{ij}(\theta) + \cdots \tag{2-3}$$

where the term *r* and *θ* are the cylindrical co-ordinates of a point with respect to the crack tip and $f_{ij}(\theta)$ is the geometrical factor of the specimen. Hence *K* provides a convenient means of quantifying the magnitude of the crack tip stress field. The fracture process under a cyclic load defined by *ΔK* is then given as,

$$\begin{aligned} \Delta K &= K_{max} - K_{min} \\ &= \frac{\sigma_{max}\sqrt{2r}}{f_{ij}(\theta)} - \frac{\sigma_{min}\sqrt{2r}}{f_{ij}(\theta)} \\ &= \Delta\sigma \frac{\sqrt{2r}}{f_{ij}(\theta)} \end{aligned} \tag{2-4}$$

The geometrical factor for *K* at a bi-material interface is very difficult to determine due to the mismatch in stiffness. The stress fields near the crack tip often oscillate at the interface [41-43] which can possibly introduce crack closure. Hence the SERR is used to characterise the fracture behaviour of composite structures and bonded joints. Since *G* and *K* are related LEFM parameters $(G = K^2/E)$, the ΔG can be expressed in terms of *K* as follows,

$$\Delta G = G_{max} - G_{min} \equiv \frac{K_{max}^2 - K_{min}^2}{E} = \frac{2K_{mean}\Delta K}{E} \quad (2\text{-}5)$$

Therefore,

$$\Delta G \neq \frac{(\Delta K)^2}{E} \quad (2\text{-}6)$$

Equation (2-6) highlights the inconsistency of ΔG with the similitude requirements of ΔK used in metals. In the absence of crack closure or fibre bridging, the use of ΔG for bonded joints or composite structures is incorrect, as it violates the similitude requirement. Hence the ΔG definition is viewed as a curve fitting parameter, manipulated to best fit the experimental data for different load ratios. The lack of physical meaning in ΔG had been noted by some researchers and, in some instances, G_{max} was used to characterise fatigue behaviour to avoid confusion [30].

In keeping consistent with the Irwin relationship, the cyclic SERR range ΔG_{eq} should be defined such that $\Delta G_{eq} = (\Delta K)^2/E$ to conform to the similitude requirement. Consequently the mathematical definition of ΔG_{eq} is given as,

$$\Delta G_{eq} \equiv \frac{(\Delta K)^2}{E} = \left(\sqrt{G_{max}} - \sqrt{G_{min}}\right)^2 = G_{max}(1-R)^2 \quad (2\text{-}7)$$

Therefore ΔG_{eq} establishes a definition in terms of G that is truly analogous to ΔK as a similitude parameter. The use of ΔG_{eq} had been promoted by Rans *et al.* [30] for composite delamination as a means of avoiding potential misinterpretations of delamination growth behaviour. Hojo *et al.* adopted ΔK to describe fatigue delamination growth behaviour in several composite laminates [35, 36]. Jabalonski used a variation of ΔG_{eq} to collapse the crack growth trends of two bondline thickness into a master curve [44]. Matsubara *et al.* [45] used this definition for fatigue delamination under Mode II loading, recognising the lack of physical meaning of ΔG. They proposed that this definition is analogous to the cyclic J-integral range ΔJ used in elastic-plastic fracture mechanics on metals [45, 46]. ΔJ can be divided into elastic and plastic components. Under small scale yielding conditions, K prevails and J is precisely equivalent to G. The elastic component of ΔJ is proportional to ΔP^2 (or $(\Delta K)^2$) for the same crack body configuration.

Although the Paris law itself is an empirical relation, the selection of the correlating parameter should not be arbitrary. A correctly formulated correlating parameter can reduce the number of curve-fitting parameters. By providing a mechanistic basis to the correlating parameter, it will be possible to develop a cycle-by-cycle crack growth model suitable for spectrum loading. To this end, it is important to develop a correlating parameter that can unify crack growth rates under variable load ratio in both composites and bonded joints. In the following Section, the experimental data of composites and bonded joints reported in the literature will be re-analysed with G_{max}, ΔG and ΔG_{eq} to examine their suitability as a unifying correlating parameter under varying load ratios.

As a general comment, these analyses are typically idealised into either plane stress or plane strain conditions. Plane stress assumes the plate is infinitely thin and the out-of-plane stress equals to zero. On the opposite end of the spectrum, plane strain assumes the plate is infinitely thick and the out-of-plane strain is zero. In practice, the joint or repair has finite thickness and the out-of-plane constraint is strongly dependent on the ratio of plate thickness to the notch radius [47]. Therefore the singular stress states is in fact 3-D and coupled fracture modes can be induced [48-51]

2.3 Mode I Fatigue Crack Propagation

In this Section, Mode I experimental data taken from the literature are used to examine the implications of using different definitions of the correlating parameter to interpret the fatigue behaviour. The experimental data are typically generated from a double cantilever beam (DCB) or compact tension (CT) specimens. The crack growth rates are obtained under a load-shedding scheme: the load is gradually reduced until the crack is arrested. Mode I is the most critical as the material's resistance to crack propagation under opening loads is usually the lowest. For this reason, it is widely studied and analysed. It must be noted that fatigue properties are highly material specific. The purpose of this section is not make specific statements about the behaviour of all materials. Rather it is to examine how the definition of the correlating parameter can help improve analysis of the observed trends and detect irregularity from theoretical behaviour.

2.3.1 Debond of Bonded Structure

The data taken from the literature are for cohesive fatigue cracking (within the adhesive) under cyclic loading. The experimental results of four epoxy adhesives are plotted in Figure 2-3 in terms of G_{max}. The variation in fatigue disbond growth rates is perhaps not

surprising, given that G_{max} does not differentiate the minimum load experienced by different load ratios. It is observed that the higher the load ratio the slower is the disbond growth. This is because the cyclic load range experienced at higher load ratio is much smaller. Consequently this leads to a slower disbond growth rate. This behaviour is well recognised when crack growth is correlated with G_{max}. Hence this will not be discussed in later examples.

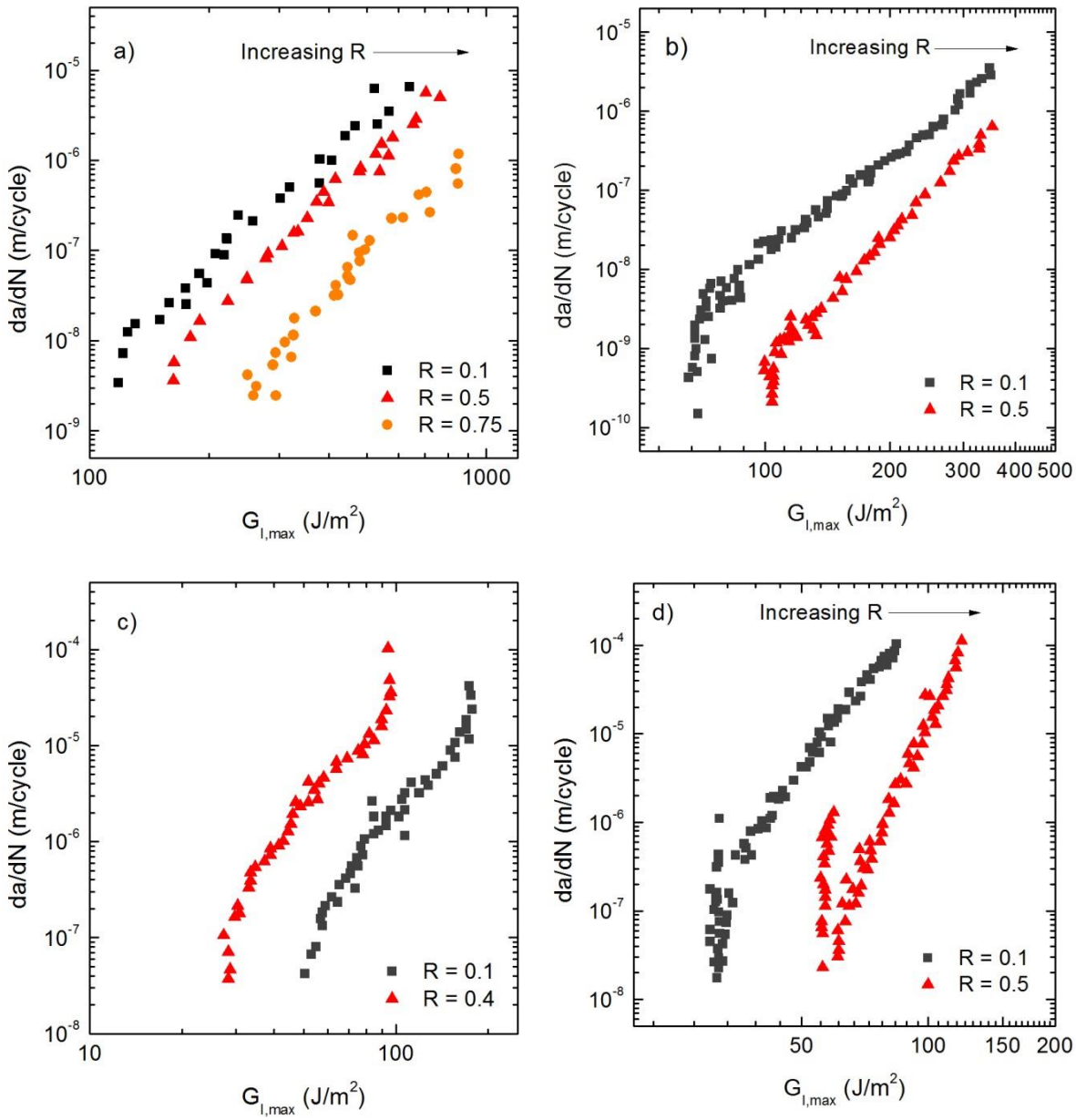

Figure 2-3: Experimental results of Mode I fatigue debonding of a) EC-3445 [52], b) Cytec 4535A [28], c) Multibond 330 [53] and d) Toho 111 interleaved [54] adhesives versus $G_{I,max}$

The same set of experimental data is plotted in Figure 2-4 in terms of the conventional definition of ΔG. It can be seen in Figure 2-4(a) that the load ratio has negligible effects on the disbond growth rates for EC-3445 reported in [52]. However the disbond growth rates and threshold values for three other adhesives reported in [28, 53, 54], as shown in Figure 2-4 (b-d), exhibit strong dependency on the load ratio. Moreover, the load ratio dependency in Figure 2-4(b) and Figure 2-4(d) appears to be counter-intuitive: higher mean load appears to reduce debonding rates under the same ΔG. These results contradict completely with the experimental observations that higher mean stress would lead to shorter fatigue lives [13, 28]. Therefore ΔG does not provide a unique correlating parameter for different load ratios.

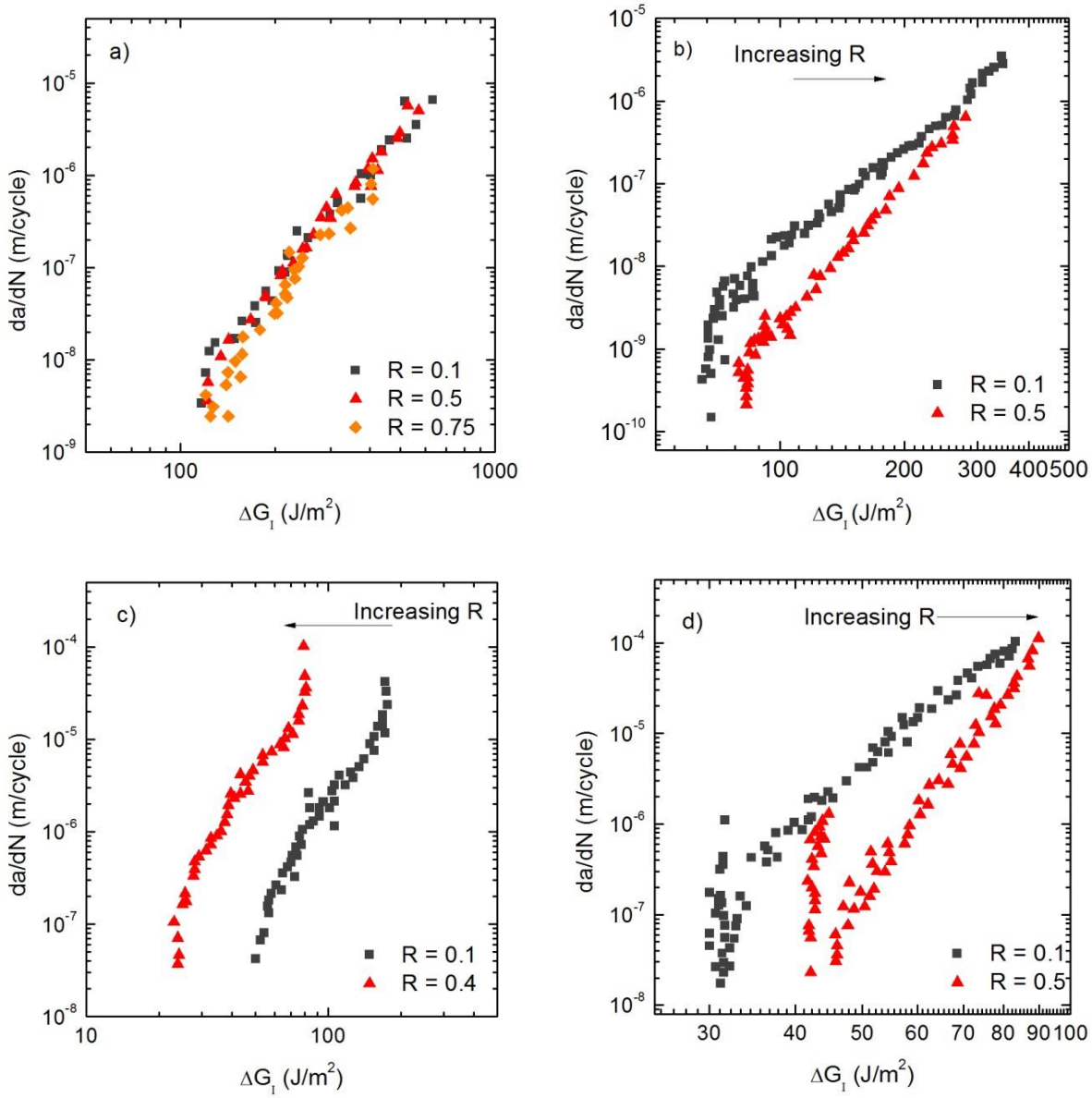

Figure 2-4: Experimental results of Mode I fatigue debonding of a) EC-3445 [52], b) Cytec 4535A [28], c) Multibond 330 [53] and d) Toho 111 interleaved [54] adhesives versus ΔG_I

Re-analysing the experimental data presented in Figure 2-4 using the $\Delta G_{I,eq}$ defined in Equation (2-6), the debonding rates, presented in Figure 2-5, show that a lower load ratio yields higher threshold and lower debonding rates, similar to the observations in metals' fatigue behaviour. Therefore, the equivalent SERR definition corrects the counter-intuitive behaviour of ΔG.

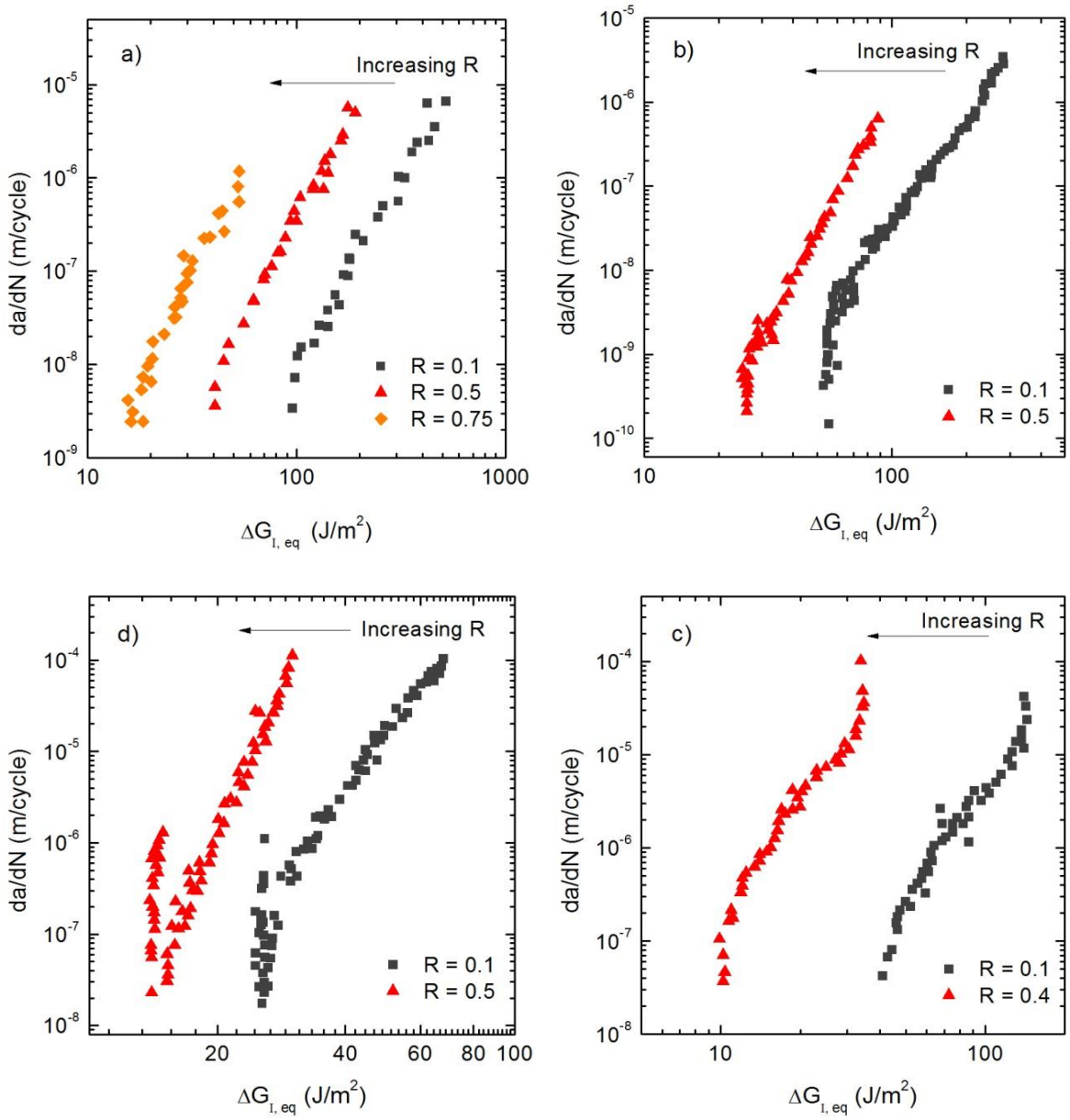

Figure 2-5: Mode I disbond growth rates versus equivalent SERR $\Delta G_{I,eq}$ for (a) EC-3445 [52], b) Cytec 4535A [28], c) Multibond 330 [53] and d) Toho 111 interleaved [54] adhesives.

Since the slope of the disbond growth rates are relatively high as indicated in the Paris law, the fatigue disbond growth is possibly sensitive to G_{max} as the applied load

approaches its critical fracture value. To this end, the Forman model offers a simple correction to account for the influence of fracture toughness on the fatigue crack growth curve. Extending the Forman model in terms of SERR yields

$$\frac{da}{dN} = \frac{C_F\left(\Delta G_{I,eq}\right)^{m_F}}{(1-R)\left(\sqrt{G_C} - \sqrt{G_{max}}\right)} \tag{2-8}$$

where G_C is the fracture toughness of the adhesive and C_F and m_F are the material constants from the Forman model.

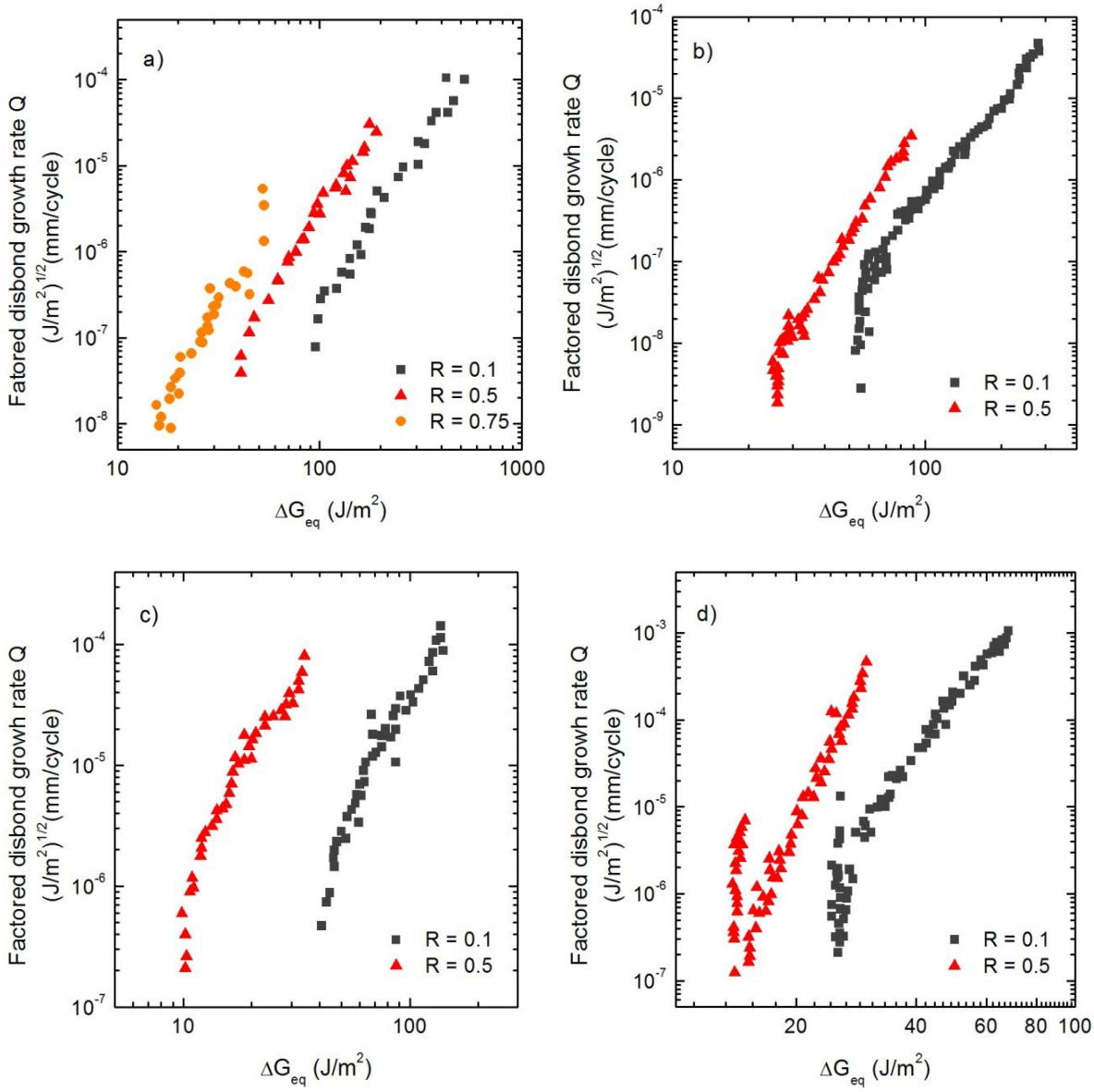

Figure 2-6: Mode I disbond growth rates plotted using Forman model for (a) EC-3445 [52], b) Cytec 4535A [28], c) Multibond 330 [53] and d) Toho 111 interleaved [54] adhesives.

For each experimental data set, the modified Forman equation represents data at various load ratios by computing the factored rate of disbond growth, as shown in Equation (2-9),

$$\mathrm{Q} = (1-R)\left(\sqrt{G_C} - \sqrt{G_{max}}\right)\frac{da}{dN} = C_F\left(\Delta G_{I,eq}\right)^{m_F} \tag{2-9}$$

The Forman material constants can then be obtained from the experimental data by curve fitting. The results of using the Forman model to characterise the fatigue crack growth for the experimental data of the adhesives are shown in Figure 2-6. A unique solution of C_F and m_F cannot be obtained as the results are still dependent on load ratio. Therefore the Forman model is insufficient to completely account for the load ratio effects.

As noted earlier, the dependence of disbond growth rates on load ratio is similar to what is observed in the fatigue behaviour of ductile metals. Plasticity-induced crack closure is now a widely accepted explanation and model to account for mean load effects in metal fatigue behaviour. Figure 2-7 shows the schematic of the crack closure process. As the crack is cyclically loaded, the material at the crack tip is plastically deformed. When the crack advances, it leaves behind a residual wedge on the crack flanks. This causes the crack to prematurely contact prior to when minimum load is attained. Once the crack closes, the stress singularity is no longer present and the cyclic load range experienced at the crack tip is reduced. Hence the crack growth rate is reduced.

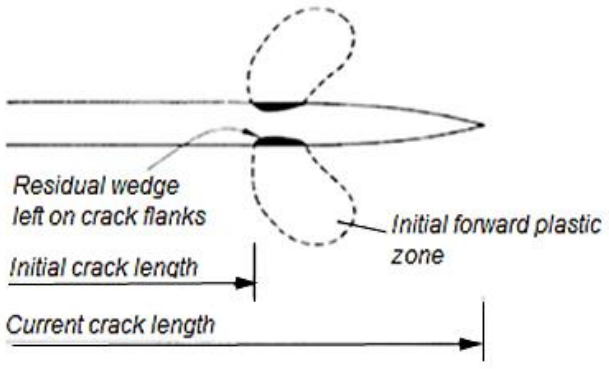

Figure 2-7: Schematic showing the crack closure phenomenon during cyclic loading [55]

Jablonski managed to quantify the bondline thickness influence on the disbond growth rates with the crack closure model [44]. In the experiment study on fatigue behaviour of a tapered DCB bonded with a film adhesive of 10 and 20 mil thickness, the

fatigue crack growth rates for the adhesive of 20 mil thickness was an order of magnitude higher than those of 10 mil thickness. Deviation from linearity in the compliance measurements, taken from the crack mouth and locally behind the crack tip with strain gauges schematically shown in Figure 2-8, showed the presence of premature crack closure prior to minimum load.

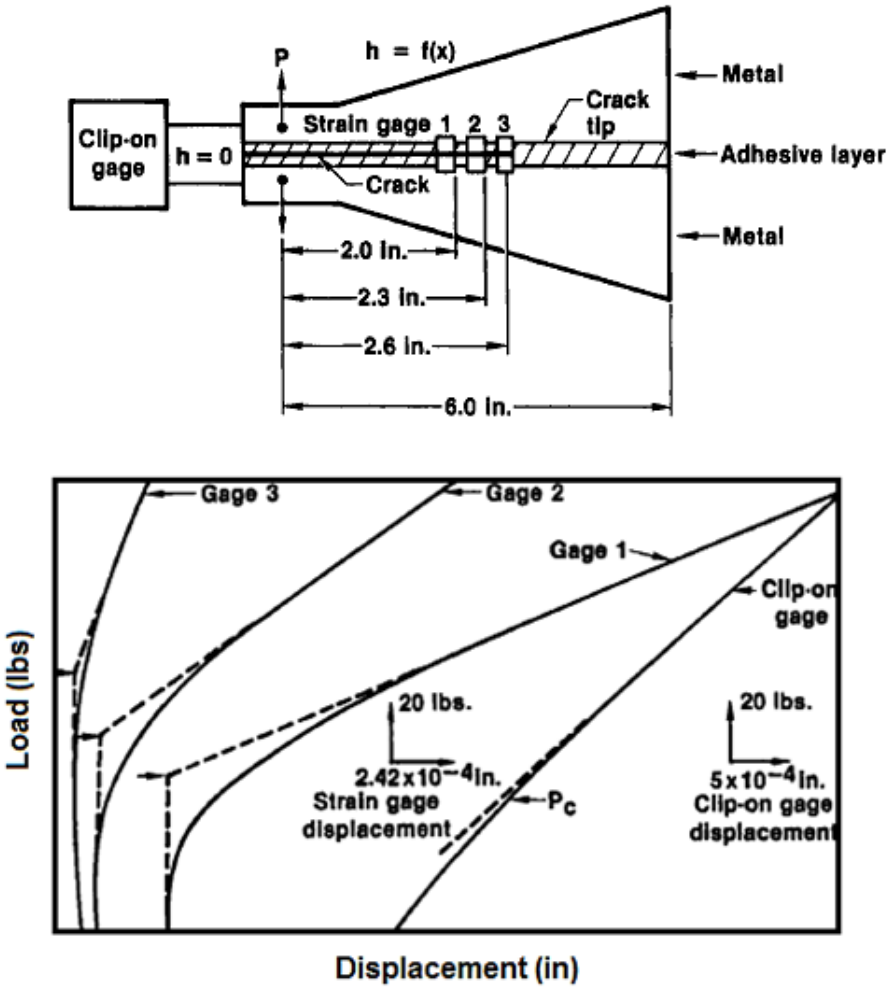

Figure 2-8: Placement of strain gauges and fatigue crack closure measurements in AF-1633 with 10 mil bondline [44]

This confirms the presence of crack closure in the fatigue process in this case. Hence an effective SERR range was defined by substituting an effective load range where the crack is fully open. The expression for the effective SERR range is shown in Equation (2-10). Using this definition, the fatigue behaviour for the two bondline thicknesses could be collapsed into a narrow band, shown in Figure 2-9.

$$\Delta G_{eff} = \frac{\Delta P_{eff}^2}{2B}\frac{\delta C}{\delta a} = \left(\frac{\Delta P_{eff}}{P_{max}}\right)^2 G_{max} \quad (2\text{-}10)$$

Where $\Delta P_{eff} = P_{max} - P_{closure}$ if $P_{closure} > P_{min}$

$\Delta P_{eff} = P_{max} - P_{min}$ if $P_{closure} < P_{min}$

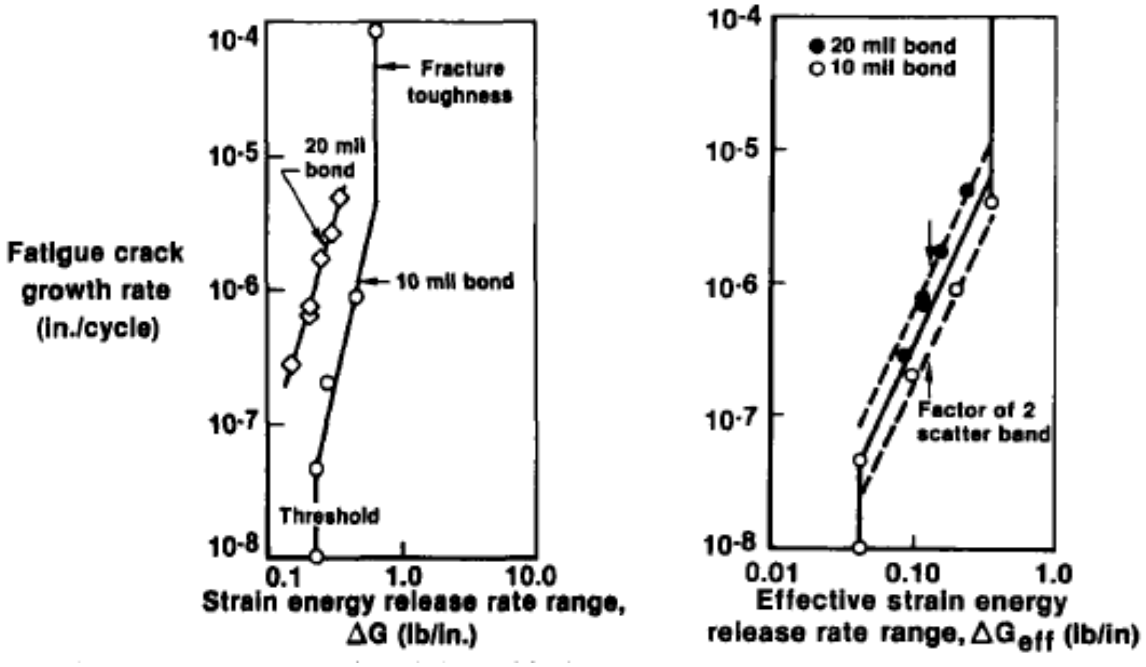

Figure 2-9: Fatigue crack growth rate for EA-9649 with 10 and 20 mil bondline thickness [44]

In another study, Mall *et al.* performed Mode I fatigue tests on the EC-3445 adhesive of 0.102 mm, 0.254 mm and 0.508 mm thickness and reported a FCGR dependency on bondline thickness [56]. A thicker bondline exhibited an improvement in fatigue crack growth resistance. This dependency was initially not surprising, given the results reported by Jablonski. However Mall *et al.* did not attempt to quantify this behaviour. Since the work done by Jablonski, plasticity induced crack closure is presumed to be absent in the fatigue of bonded joints in majority of the work done in the area of bonded joints fatigue.

It is worth noting that the adhesive bondline can be assumed to be a state of plane strain as the joint width is much larger that the bondline thickness. There had been debates as to whether crack closure can occur in plane strain conditions. Since the material cannot deform in the thickness direction, the question is how the additional

material appears on the crack flanks for crack closure to occur. Experimentally, Fleck monitored crack closure under plane strain conditions by measuring the compliance in the middle of a thick steel CT specimens through drilled holes [57]. The closure area behind the crack tip at minimal load was found to be small (0.5 mm). This is in agreement the numerical analysis of plane strain crack closure by Mclung *et al.* [58]. Since the adhesive material is a fairly ductile material, it is highly probable that a plastic zone is developed when the crack is loaded. As the closure area under plane strain is very small, the question of lack of crack closure in Mode I debonding reported in literature can be attributed to the scarcity of data.

2.3.2. Delamination of Composite Structures

Continuous fibre reinforced composite structures are particularly susceptible to delamination. If left unchecked, the delamination damage can grow to a critical size in a short number of cycles leading to failure. Past experimental work has shown that the load ratio has considerable effect on the delamination growth rates in composite materials under Mode I loading. Hojo *et al.* did an extensive experimental study on the Mode I fatigue delamination in unidirectional composite laminates, focusing particularly on different matrices and load ratios [35, 36]. The definitions of correlating parameters, ΔK, ΔG and G_{max} were employed to correlate fatigue delamination growth rates. Their experimental data are plotted against ΔG in Figure 2-10. Experimental data from Erpolat *et al.* [28] are also included. The delamination growth rates of 914C and P305 laminates (Figure 2-10b and Figure 2-10d respectively) are relative independent of mean load effects. However the scatter of the delamination growth rates is more prominent closer to the threshold region. The delamination growth rates at higher loads displayed similar counter-intuitive fatigue behaviour of lower rates under higher mean loads, as previously observed in the fatigue debonding of bonded joints.

The fatigue delamination results are re-analysed using the ΔG_{eq} parameter in Figure 2-11. Again, the mean loads have a significant impact on the delamination growth rates in all the laminates. Similar to fatigue debonding, the counter-intuitive behaviour previously observed is now eliminated.

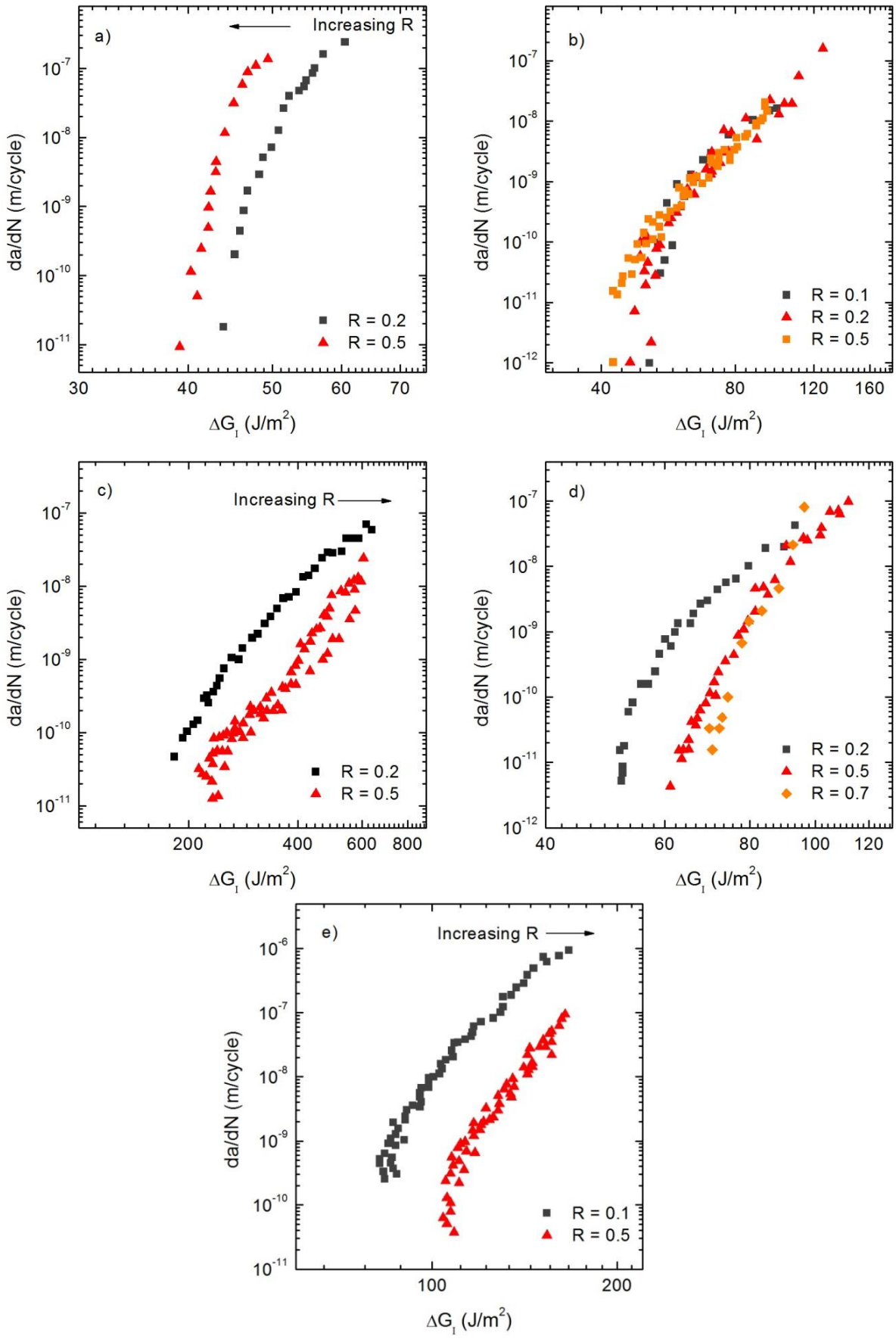

Figure 2-10: Fatigue delamination growth rates versus ΔG for laminates with the resin system; a) 3601 [36], b) 914C [35], c) PEEK [36], d) P305 [35] and e) 8552 [28]

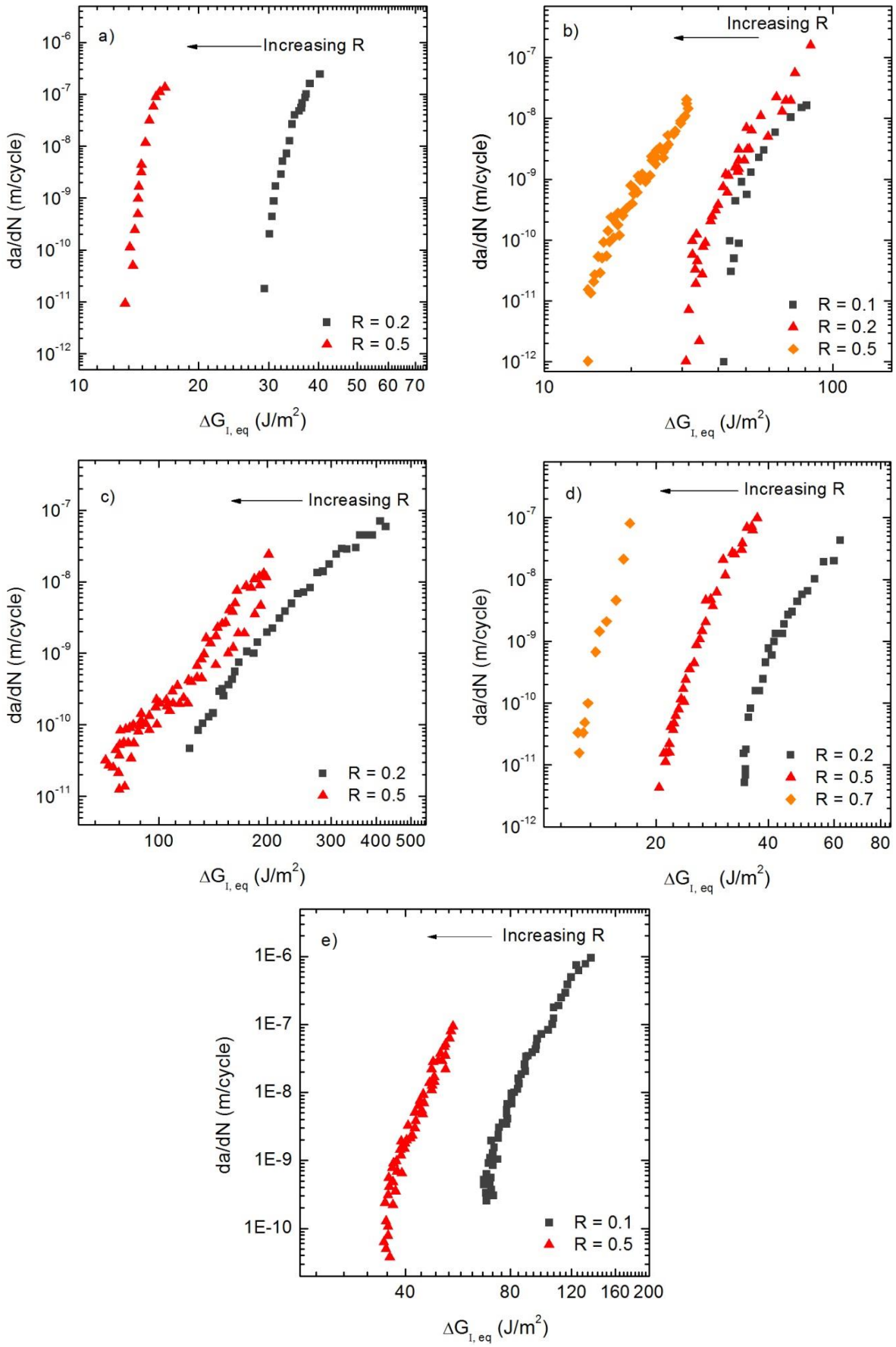

Figure 2-11: Fatigue delamination growth rates versus ΔG_{eq} for laminates with the resin system; a) 3601 [36], b) 914C [35], c) PEEK [36], d) P305 [35] and e) 8552 [28]

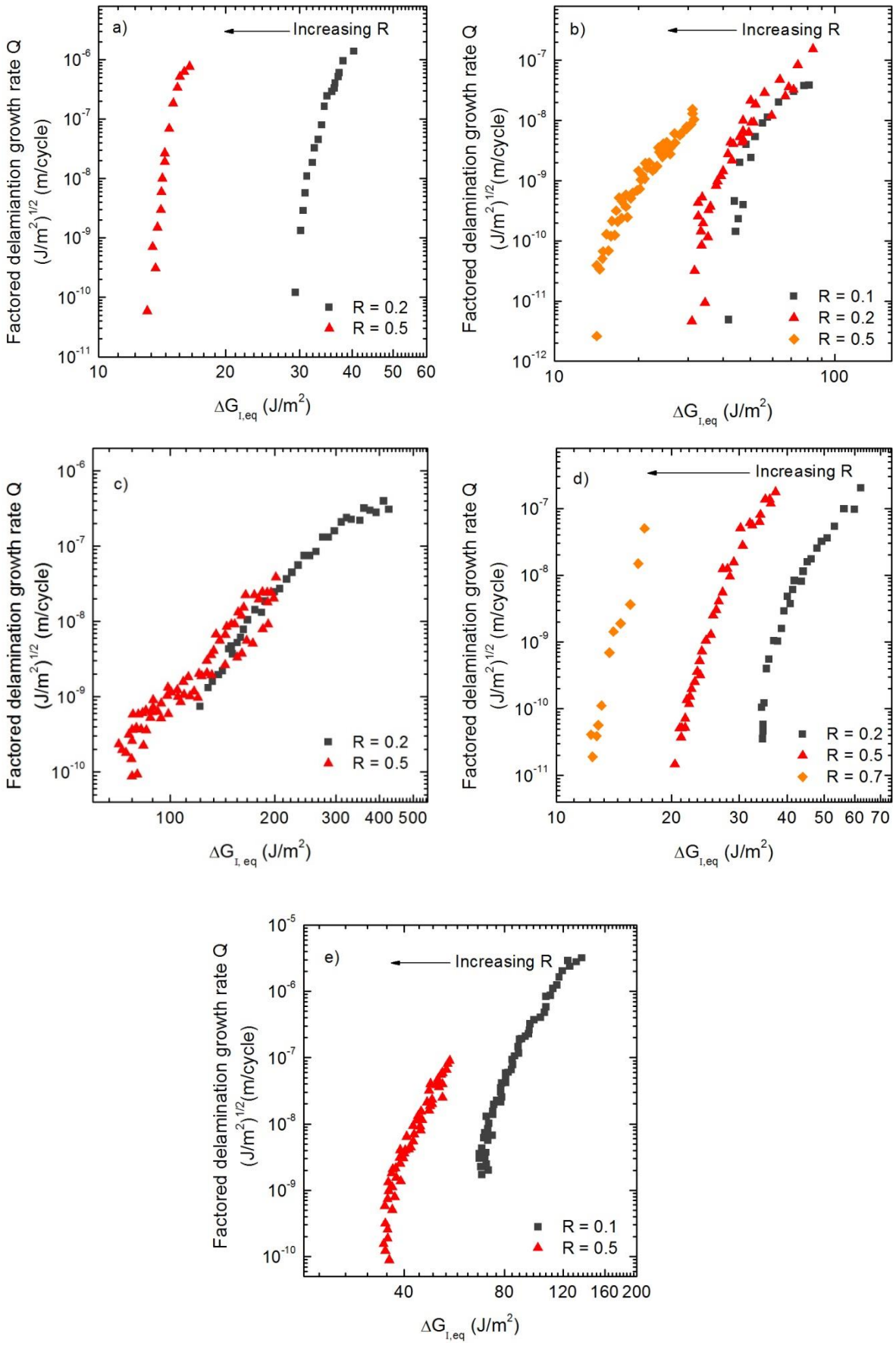

Figure 2-12: Fatigue delamination growth rates using the Forman model for laminates with the resin; a) 3601 [36], b) 914C [35], c) PEEK [36], d) P305 [35] and e) 8552 [28]

The Forman model is employed to characterise the fatigue delamination growth behaviour versus the ΔG_{eq} parameter as shown in Figure 2-12. All four laminates except for the AS4/PEEK laminate display fatigue behaviour dependency on the mean load. A unique solution of the Forman parameters C_F and m_F can be determined for the AS4/PEEK laminates across different load ratios. Consequently for this specific material the fatigue behaviour under varying load ratios may be represented by the Forman model.

Regardless of the correlating parameters used (ΔG or ΔG_{eq}), the fatigue load ratio has a considerable influence on the rates of delamination growth under Mode I loading. Such behaviour is also observed in the crack growth in an adhesive bondline and in metals. Plasticity in the matrix system is generally assumed to be negligible due to high level of constraints provided by the fibres. Hojo *et al.* hypothesised that the rate of delamination growth is driven by static damage associated with monotonic loads, ahead of the crack tip, schematically shown in Figure 2-13 [36]. The formation of the micro-fracture mechanisms (i.e. voids, crazing, micro-cracks and shear yielding) effectively reduces the resistance of the material to cyclically driven fatigue crack growth.

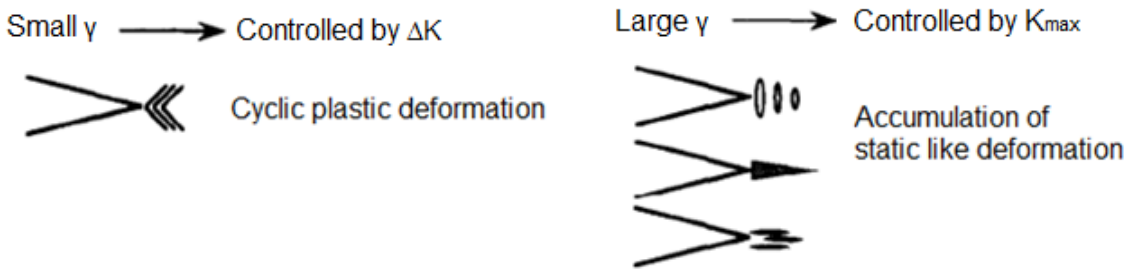

Figure 2-13: Schematic explanation of the mechanism of fatigue delamination crack growth [36]

Hence they proposed a phenomenological two-parameter correlating term that is a power function of ΔK and K_{max}. Based on the above hypothesis, Equation (2-11) assumes that crack propagation is driven by an interaction of two types of process zones at the crack tip, a monotonic process zone defined by K_{max} and a cyclic process zone driven by ΔK.

$$\Delta K_{eff} = \Delta K^{1-\gamma} K_{max}^{\gamma} = \Delta K (1-R)^{-\gamma} \quad (2\text{-}11)$$

While some researchers advocate the use of the two parameters to characterise fatigue crack growth in metals fatigue [59-61], it should be noted that efforts towards explaining this approach in a mechanistic manner is different for metals and polymers as the fatigue fracture is different at the micro-scale. Experimentally, it is difficult to detect (if present) and separate the damage caused by the monotonic and cyclic process zone.

Another plausible explanation for the mean load effects in fatigue delamination is the presence of fibre bridging. Fibre bridging is attributed to “nesting” of fibres and to weak fibre-matrix interfaces [62]. Nesting is common in unidirectional layups where fibres migrate during the pressure/temperature cure cycle as shown in Figure 2-14. This results in meandering of delamination cracks. By offsetting the interfacial plies by 1.5 to 3 degrees may mitigate, but not completely eliminate, the presence of fibre bridging in Mode I crack propagation. As the bridging zone develops under static and fatigue loading, it acts as tension springs behind the crack tip, preventing the crack from fully open or closure. Hence the SERR experienced at the crack tip is much less than the applied SERR. Khan *et al.* also postulated the R-ratio effects observed in ΔG_{eqv} was due to roughness induced crack closure, presence of broken fibres and fibre pull-outs at the delamination front observed in SEM images [63]. However more quantitative evidence is required to support these statements.

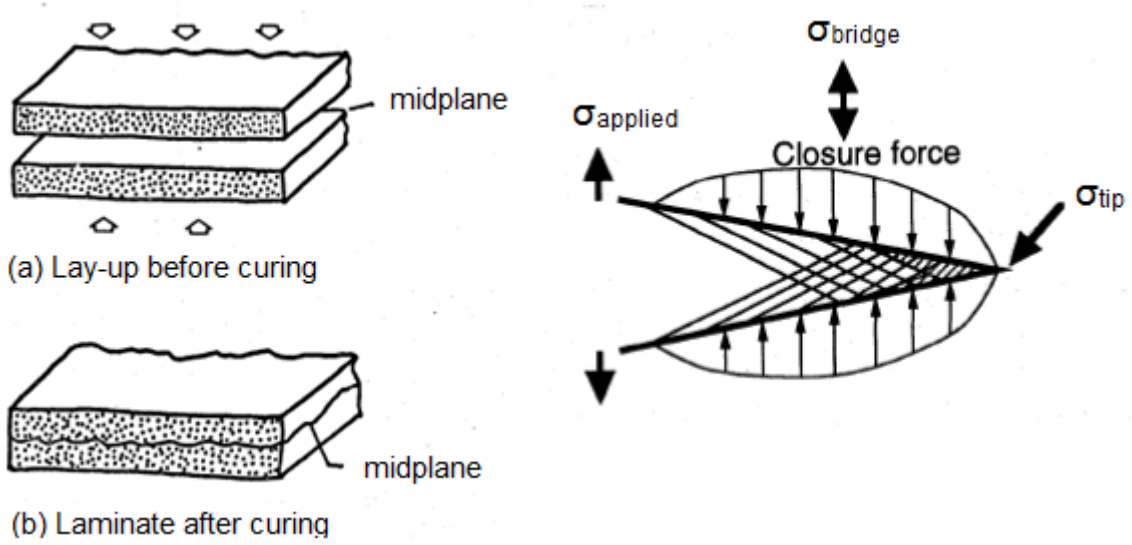

Figure 2-14: Schematic of fibre nesting and increased delamination growth resistance introduced by fibre bridging

In metals, a mechanistic understanding for mean load effects exists in the form of crack closure theories. Such mechanistic understanding, however, does not exist for

composites, let alone prediction models. Therefore the current design process against fatigue failure relies heavily on extensive empirical studies without an adequate knowledge of the damage evolution under cyclic loads. This current lack of suitable correlating parameter provides the motivation for this project to develop a fundamental understanding of the load ratio effects on fatigue crack growth in composite laminates and bonded joints, and predictive model of the damage evolution in bonded composite structures.

2.4 Mode II Fatigue Crack Propagation

Unlike in isotropic materials, cracks in bonded joints or composite laminates can propagate purely under Mode II. Moreover the primary design function of an adhesive bondline is to transfer the load from one substrate to another by shear forces. The ENF specimen is commonly used to carry out Mode II static characterisation tests. Due to its simplicity and known behaviour under static loading, this test configuration is also use to perform fatigue characterisation.

2.4.1 Disbond in Bonded Structures

Unlike Mode I, crack propagation under Mode II loading can occur under fully shear reversal. However the definition of ΔG presents a dilemma under negative load ratio (i.e. $\Delta G = 0$ when $R = -1$). Therefore Mall and Kochhar used the following definition of ΔG to correctly account for fatigue crack growth under full shear reversals [64], because $G_{II,min}$ is always positive even for negative load ratio.

$$\Delta G_{II} = \begin{cases} G_{II,max} - G_{II,min} & R \geq 0 \\ G_{II,max} & R < 0 \end{cases} \quad \text{(2-12)}$$

Significant load ratio dependency under Mode II loading can be seen in Figure 2-15 when the experimental results are plotted against ΔG_{II} for both positive and negative load ratios. Mall and Kochhar [64] argued that the higher crack growth rates for negative load ratios than the results pertinent to zero load ratio are due to the crack tip experiencing $G_{II,max}$ twice, which was not accounted for in ΔG_{II} in Equation (2-12). However, the contradictory mean load behaviour under Mode II is still present for positive load ratios as shown in Figure 2-15(b). This provides further evidence that ΔG is not an

appropriate correlating parameter for characterising Mode II disbond growth under varying load ratios.

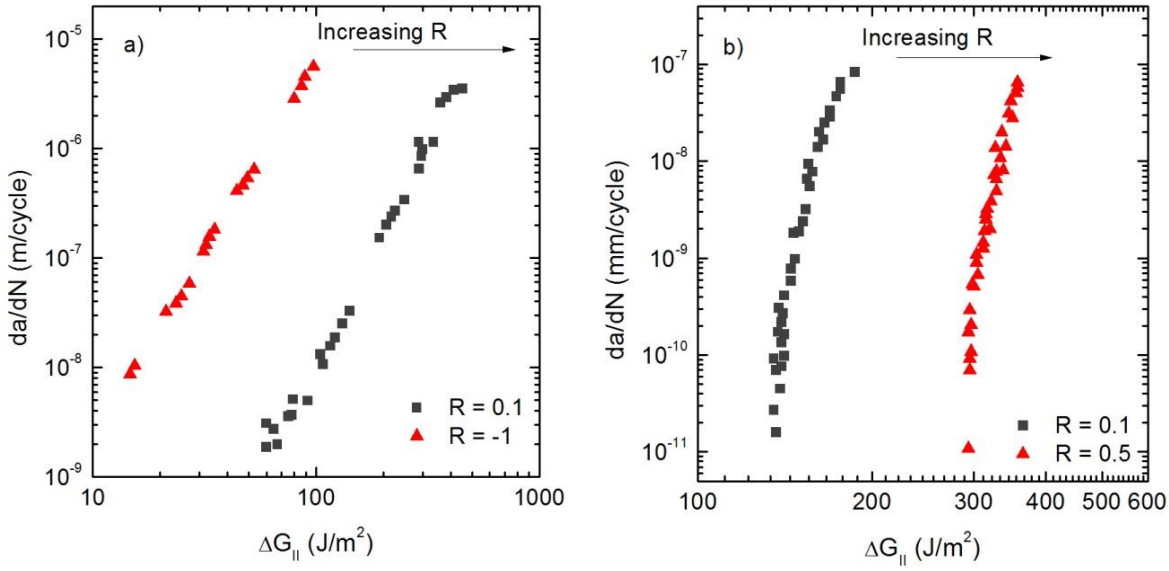

Figure 2-15: Mode II fatigue debonding growth rates of (a) EC-3445 adhesive under shear reversal [64] and (b) Toho 111 interleaved epoxy [54] versus ΔG_{II}

Similar to the Mode I loading, an equivalent SERR range for Mode II can be defined as: -

$$\Delta G_{II,eq} = \left(\sqrt{G_{II,max}} - \sqrt{G_{II,min}}\right)^2 = G_{II,max}(1-R)^2 \qquad (2\text{-}13)$$

which will satisfy the relationship between $\Delta G_{II,eq}$ and ΔK_{II} (i.e. $\Delta G_{II,eq} = \Delta K_{II}^2 / E_A$).

By re-analysing the experimental data presented in Figure 2-16 using the equivalent SERR range $\Delta G_{II,eq}$ given by Equation (2-13), the load ratio dependency of Mode II fatigue crack behaviour of bonded joints is eliminated, as shown in Figure 2-16. Nakagaki and Alturi conducted numerical crack growth analysis of mixed mode fatigue crack growth in isotropic materials [65] and reported that, under pure Mode II loading, cracks did not experience any closure. The absence of load ratio effects in Mode II can be attributed to that cyclic deformation occurs parallel to the fracture plane rather than perpendicular to it. Hence there is no residual plastic stretch in the wake to cause closure under Mode II loading. It can be argued that closure due to roughness of the fracture surfaces can still occur but its contribution to non-linear effects is expected to be minimal [64].

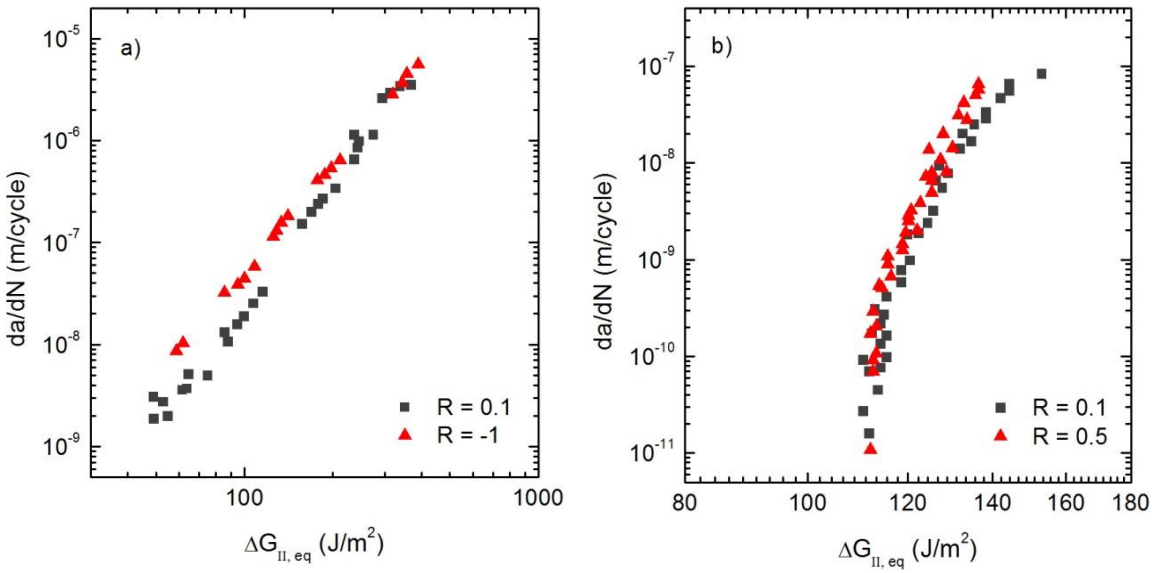

Figure 2-16: Mode II fatigue debonding growth rates of (a) EC-3445 adhesive under shear reversal and (b) Toho 111 interleaved epoxy versus $\Delta G_{II,\,eq}$

In an another study, Chester *et al.* used the doubler overlap fatigue specimen (DOFS) to generate fatigue debonding data of a bonded repair [66]. The DOFS is meant to be representative of the middle of the repair patch where bending moment is minimal. The peel stresses at the crack tip will be under compression and therefore the crack will propagate under Mode II loading. When considering the influence of temperature, they reported that the shear strain range is able to normalise the FCGR into a single curve as shown in Figure 2-17. It should be noted that the SERR is calculated based on the global response of the specimen. A suitable SERR parameter may be derived by determining the local SERR experienced at the crack tip, taking into account the reduction in the adhesive stiffness due to the environmental degradation.

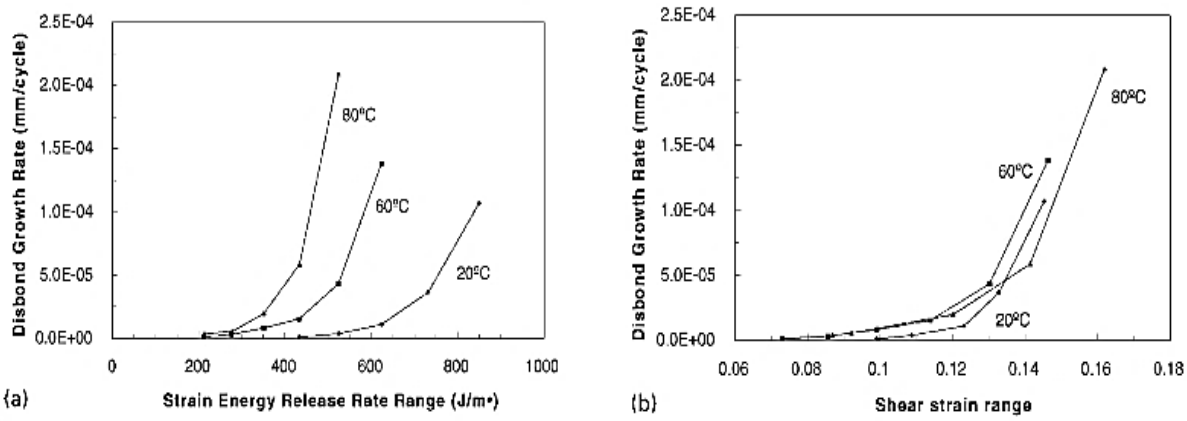

Figure 2-17: Disbond growth rate under different temperature versus ΔG and Δγ [66]

2.4.2 Delamination of Composite Structures

The fatigue behaviour of delamination under Mode II loading is comparable to the observed behaviour in fatigue debonding. Figure 2-18 shows the Mode II fatigue behaviour of various epoxy systems from Matsubara *et al.* [45], Hojo *et al*. [54] and Kawashita *et al.* [67]. The counter-intuitive mean load behaviour can be observed for all experimental data. Therefore the same conclusion can be drawn as for Mode II fatigue debonding; ΔG is not an appropriate correlating parameter for characterising Mode II fatigue behaviour.

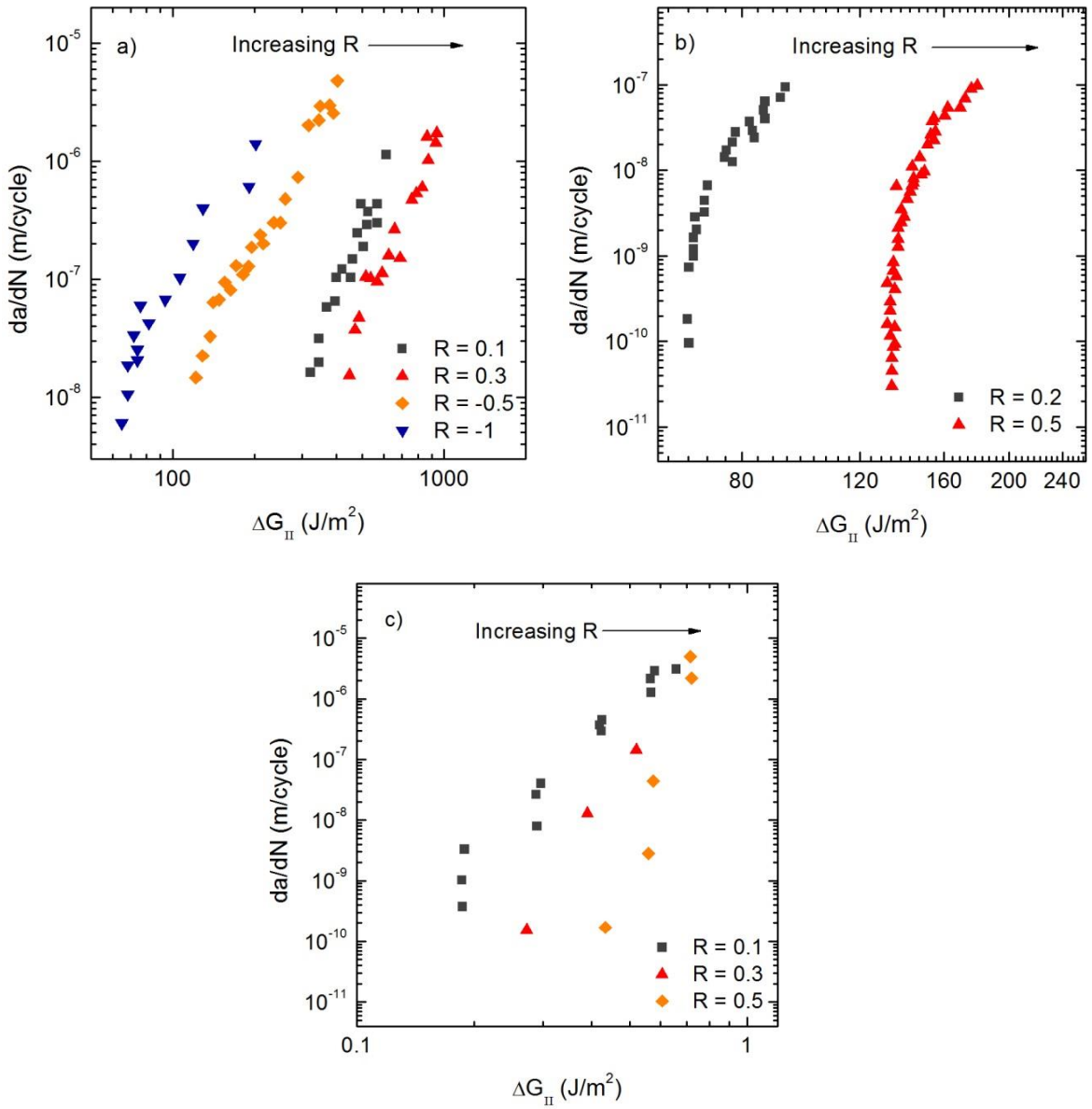

Figure 2-18: Mode II fatigue delamination growth rates versus *ΔG* for laminates with the resin system; a) 3651 [45], b) 111 [54] and c) 8552 [67]

The same experimental data, re-plotted against ΔG_{eq}, are shown in Figure 2-19. Using this correlating parameter, the Mode II delamination growth rates are collapse into a narrow band for all load ratios. In Figure 2-19(c), the exception being two data points at *R = 0.5*, as the applied maximum G_{II} at these points is almost equal to the critical SERR. Hence the subsequent delamination growth rate is possibly an outcome of a combination of stable and unstable crack growth.

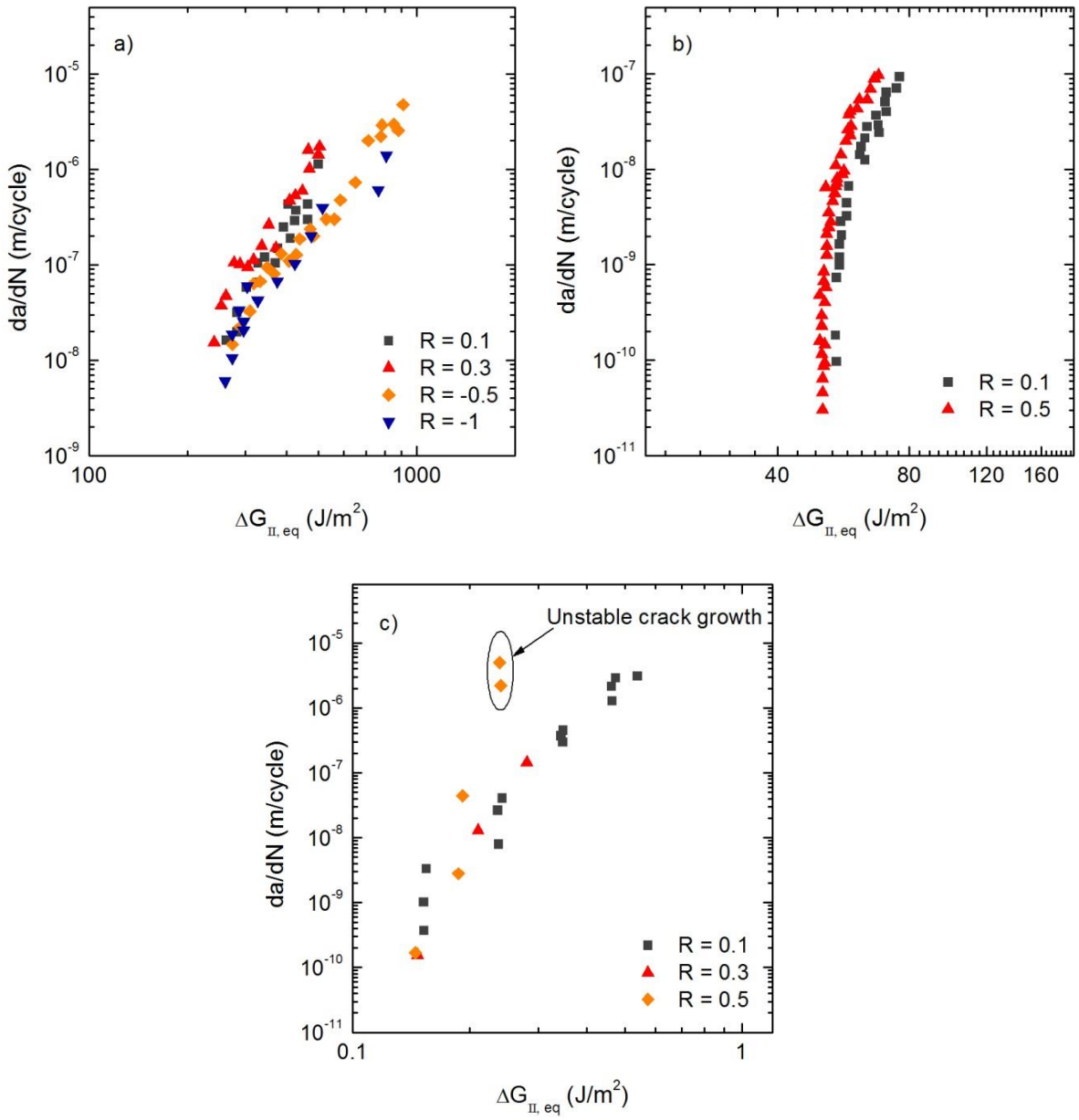

Figure 2-19: Mode II fatigue delamination growth rates versus ΔG for laminates with the resin system; a) 3651 [45], b) 111 [54] and c) 8552 [67]

In order to validate the absence of fiber bridging under Mode II loading, Matsubara *et al.* [45] conducted a separate test using a decreasing load (i.e. decreasing SERR) and constant load (i.e. increasing SERR) scheme at $R = -1$. If non-linear mechanisms are present, the results of the decreasing load test will disagree with that of constant load test. However the results of both tests were nearly indistinguishable to suggest otherwise and ΔG_{eq} is the controlling parameter for Mode II fatigue delamination growth. Figure 2-20 shows the SEM views of the fracture surface of the UD laminates at loads close to the threshold region. The arrow at the lower right corner indicates the crack growth direction. The fibre surfaces show traces of resin on the fibre surfaces and the distance between each striation corresponds well to the crack grown of one load cycle and load range.

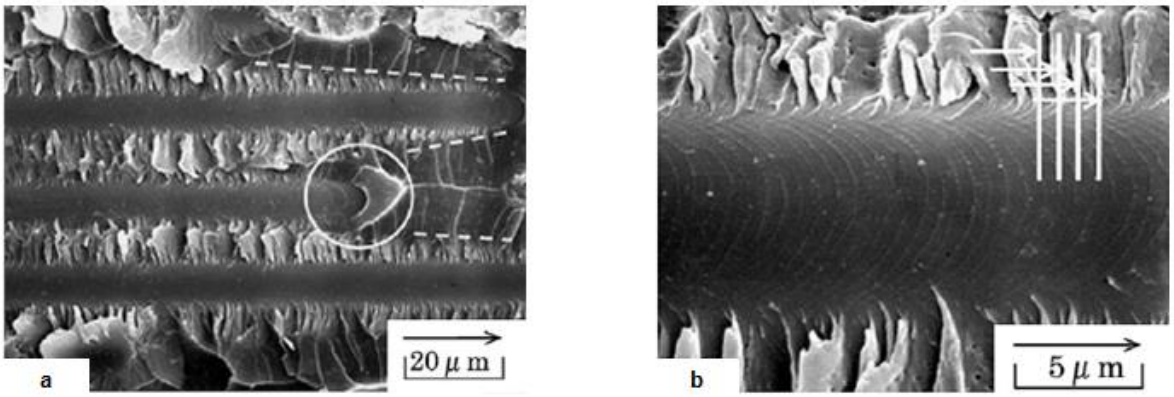

Figure 2-20: SEM fractographs of Mode II fatigue fracture surface (a) *R = 0.1, da/dN = 8 x 10^{-7} mm/cycle* and (b) close up view of the fibre-matrix interface [45]

2.5 Mixed Mode (I + II) Fatigue Crack Propagation

Many practical bonded joint or repair involves the use of a lap, scarf or step joint geometry. Moreover repairs are not restricted to flat panels and can be carried out on curved shapes, tapered thickness or plies with different orientations. The resultant crack formation and propagation within the repair will be under a combination of in-plane tension and shear loading i.e. Mode I, II and III loads. Research focussed mainly on the effects of combination of Mode I and II loading conditions. Mode III is usually not considered as it is typically small for composite structures due to the constraints of adjacent plies. Mode III fracture mechanism will not be discussed in this thesis.

Table 2-1: Definition of correlating parameter for mixed mode delamination and disbond fatigue growth

Reference	Expression of correlating parameter	Eqn
Johnson and Mall [68]	$\frac{da}{dN} = D_m[\Delta G_I + \Delta G_{II}]^m$	(2-14)
Cheuk *et al.* [69]	$\frac{da}{dN} = D_m\left[\Delta G_{I,eq} + \frac{G_{IC}}{G_{IIC}}\Delta G_{II,eq}\right]^{m_m}$	(2-15)
Quaresimin and Ricotta [18]	$\frac{da}{dN} = D_m\left[\triangle G_I + \frac{G_{II}}{G_I + G_{II}} \triangle G_{II}\right]^{m_m}$	(2-16)
Russell and Street [70]	$\frac{da}{dN} = \left(\frac{G_I}{G_I + G_{II}}C_I + \frac{G_{II}}{G_I + G_{II}}C_{II}\right)\left(\frac{\Delta G_I}{G_{IC}} + \frac{\Delta G_{II}}{G_{IIC}}\right)^{\frac{G_I}{G_I+G_{II}}m_I + \frac{G_{II}}{G_I+G_{II}}m_{II}}$	(2-17)
Kenane and Benzeggagh *et al.* [71-73]	$\frac{da}{dN} = D_m[\Delta G_T]^{m_m}$ where $\Delta G_T = \Delta G_I + (\Delta G_{II} - \Delta G_I)\left(\frac{G_{II}}{G_I + G_{II}}\right)^{\eta}$ $log D_m = \log D_{II} + (\log D_I - \log D_{II})\left(1 - \frac{G_{II}}{G_I + G_{II}}\right)^{\alpha}$ $m_m = m_I + (m_{II} - m_I)\left(\frac{G_{II}}{G_I + G_{II}}\right)^{\beta}$	(2-18)
Blanco *et al.* [74]	$\frac{da}{dN} = D_m[\Delta G]^{m_m}$ where $\log D_m = \log D_I + \left(\frac{G_{II}}{G_T}\right)\log D_{I+II} + \left(\frac{G_{II}}{G_T}\right)^2 \log\left(\frac{D_{II}}{D_{I+II}D_I}\right)$ $m_m = m_I + m_{I+II}\left(\frac{G_{II}}{G_T}\right) + (m_{II} - m_I - m_{I+II})\left(\frac{G_{II}}{G_T}\right)^2$ * C_{I+II} and m_{I+II} are the extra mixed-mode parameters determined experimentally	(2-19)
Gustafson and Hojo [75]	$\frac{da}{dN} = D_I(\Delta G_I)^{m_I} + D_{II}(\Delta G_{II})^{m_{II}}$	(2-20)
Rans *et al.* [30]	$\frac{da}{dN} = D_I\left(\Delta G_{I,eq}\right)^{m_I} + D_{II}\left(\Delta G_{II,eq}\right)^{m_{II}}$	(2-21)

For bonded joints experiencing only Mode I or II loadings, the fatigue crack growth rate is correlated to individual mode of $G_{max,}$ ΔG or ΔG_{eq} parameter by means of the Paris law relation. A common approach taken to characterise mixed mode behaviour is to determine the mixed mode SERR and defined in terms of $\Delta G_m = G_{m,max} - G_{m,min}$ where the subscript *m* represents mixed mode loading conditions. The resultant Paris law parameters are then determined by curve fitting the experimental results. This approach does not provide much insight into the interaction (if any) of the various loading modes. Perhaps, a more rigorous method is to characterise the fatigue crack growth behaviour of individual propagation modes from coupon level tests. Then a predictive model which defines the interaction between loading modes can be applied to determine the respective effective SERR and Paris law parameters. Therefore the fatigue crack growth at an arbitrary mode mixity can be predicted without the need of extensive experimental testing. In Table 2-1, a summary of predictive models for crack propagation under mixed mode loading conditions is presented.

Some researchers believed that fatigue crack growth under mixed mode loading is predominately controlled by the mode I component and mode II crack propagation can be classified as the nucleation of micro-cracks initiated under mode I loading. Hart-Smith highlighted the importance of peel stresses in the crack initiation and propagation under static and fatigue loading [76, 77]. Everett applied clamping forces to generate mixed mode in crack lap shear (CLS) specimens [78]. The fatigue crack growth rate was reduced drastically when the crack approached the clamped region where G_I decreased. Hence it was proposed that G_I is the principal loading component causing fatigue crack growth. Xu *et al.* found the Mode I component correlates best for fatigue crack growth rates under mixed mode loading conditions [79]. However Liechti and Lin ruled out using only G_I as the controlling parameter by showing that the crack growth rates do not approach zero as G_I approaches zero. The Mode II component also contributes towards crack growth under mixed mode loading conditions.

Johnson and Mall proposed that the crack driving force under mixed mode is obtained by the superposition of the SERR components in Mode I and in Mode II [68], as presented in Equation (2-14). They reported that the $\Delta G_T = \Delta G_I + \Delta G_{II}$ definition was able to correlate the crack propagation rates with experimental data of a composite cracked lap-shear joint bonded with EC-3445 adhesive [52]. Cheuk *et al.* suggest greater emphasis should be placed on Mode I loading as it is the main driving force for initiating new cracks [69] and, therefore, the effective SERR under mixed mode was proposed in Equation (2-15). In a similar approach, Quaresimin and Ricotta proposed another correlating parameter (Equation (2-16)) [18]. The main difference between the two

approaches is that the ΔG_{eq} definition was used in Cheuk *et al.* model whereas ΔG definition was used in Quaresimin model. Any characterising parameter proposed should apply to Mode I, II and all ranges of mode ratios for the specified material.

The correlating parameter used by Russell and Street is the same as Johnson and Mall, normalised by the critical SERR [70]. In addition to defining the correlating parameter, they observed a dependence of the Paris law parameters between mode ratios. The mixed mode Paris law parameters were determined by a linear rule of mixtures of the individual propagation rates. In their investigation of unidirectional GFRP composites, Kenane and Benzeggah proposed an empirical formulation of the correlating parameter under mixed mode loading which is capable of correlating the majority of the fracture behaviour of composite laminates under mixed mode loading [71, 72]. A non-linear relation of mixed mode and the relative Mode I and II Paris law parameters had also been suggested [73]. Blanco et al. found that a mode mixity dependence of the Paris law parameters in non-monotonic manner from experimental data in literature. Hence they proposed a phenomenological model to capture this behaviour in a manner similar to that of Kenane and Benzeggah. [74]. They suggested that the dependency of the Paris law parameters is due to a complex interaction of fibre bridging, matrix cracking and brittle fracture through fractography analysis. Allegri *et al.* proposed an empirical equation which they report is capable of unifying the effects of load ratio and mode mixity [80].

Gustafasson and Hojo found a large spread in the experimental data for the CLS specimen using Equation (2-20). Using a different modelling approach, they attempted to predict the crack propagation growth rates under combined mode I and II. Hence they proposed that the resultant mixed mode crack growth is the sum of the delamination growth rate induced by Mode I and Mode II components [75]. However the Paris law parameters of the mode II component were fitted from the CLS specimen rather than deriving them from Mode II loading. Similar mixed mode expression is proposed by Rans et al., shown in Equation (2-21). The key difference with Equation (2-20) is that the ΔG_{eq} parameter instead of ΔG was used to characterise the load ratio [30]. In both Equation (2-20) and (2-21), it was assumed that there is no interactions effects between the two loading modes.

Different definitions of the Paris law have been proposed to characterise the fatigue delamination and disbond growth of bonded composite joints. There is no accepted universal solution and is continued to be an area of research interest. Since a bonded composite repair is more than likely to experience a combination of Mode I and II

crack propagation driving forces, it is important to determine an appropriate mixed mode Paris law relation.

2.6 Summary of Key Issues

This chapter has presented a critical review of disbond growth in bonded structures and delamination growth in composite structures. The results highlight the deficiencies of current scaling parameters based on strain energy release rates, both in terms of correlation with experimental results and consistency with the theoretical requirement of similitude. When experimental data of disbond growth rates are plotted against the equivalent strain energy release rates, a strong load-ratio effect is clearly evident for Mode I loading (referring to Fig.2), but absent under Mode II loading. Therefore, maintaining the similitude requirement is sufficient to capture the load ratio effect on Mode II disbond growth behaviour in bonded joint. However, a new scaling parameter is required to correlate Mode I disbond growth data.

Different mechanisms had been hypothesised as the causes for the mean load dependency behaviour and interaction between load cycles in spectrum loading. In light of the success of the crack closure concept in explain and unifying the load ratio dependence of Mode I fatigue crack growth in metals [39], it is contended that the load-ratio effects in bonded joints are also likely caused by the plasticity-induced crack closure phenomenon. The crack density in the damage/plastic zone and fibre bridging has also been suggested as possible reasons. However, little mechanistical modelling exists to account load ratio effects and correlate the fatigue behaviour for bonded joints and composite structures.

The following two Chapters describe an experimental investigation of a suitable correlating parameter and load ratio effects in bonded joint and delamination fatigue behaviour under Mode I and II. Finite element analysis is then used to provide a more quantitative analysis of the load ratio mechanisms. The results are then employed to formulate a new correlating parameter to account for the mean load effects in bonded joints and composite delamination.

This page intentionally left blank

Chapter 3

Experimental Investigation of Mode I and II Fatigue Behaviour

3.1 Preamble

This Chapter presents an experimental investigation of the fatigue crack growth behaviour in (a) adhesively bonded joints and (b) composite laminates. Tests under mode I loading were carried out with double cantilever beam (DCB) specimens. For mode II loading tests, three point end notch flexure (3-ENF) specimens were used. The reasons for selecting these test configurations were simplicity in the manufacturing process of the specimen and the availability of test standards. In the previous Chapter, the fatigue behaviour of different adhesives and composite laminates was analysed using different definitions of correlating parameter. It was found that no scaling parameter is able to satisfactorily correlate the fatigue crack growths under different load ratios and mode I and mode II. It may be argued that the fatigue behaviour may be material-specific. Therefore an experimental investigation with a consistent material system was conducted to determine if similar behaviour was observed. Mechanisms influencing the mean load dependency (if any) in the fatigue crack growth behaviour could then be investigated.

The mechanisms, inducing mean load dependency, can be classified into two groups: extrinsic and intrinsic, schematically shown in Figure 3-1. Intrinsic mechanisms are inherent properties of the material and are present irrespective of the crack length. Examples are the formation of micro-cracks and crazing when under load. As the damage in the material ahead of the crack tip increases, the resistance to crack growth decreases. Extrinsic mechanisms conversely act in the crack wake and are dependent on the crack length. Its influence on the local crack tip stress increases as the crack wake develops and thereby increases the crack growth resistance. Examples of these are roughness, oxide, plasticity induced crack closure and fibre bridging in the case of delamination.

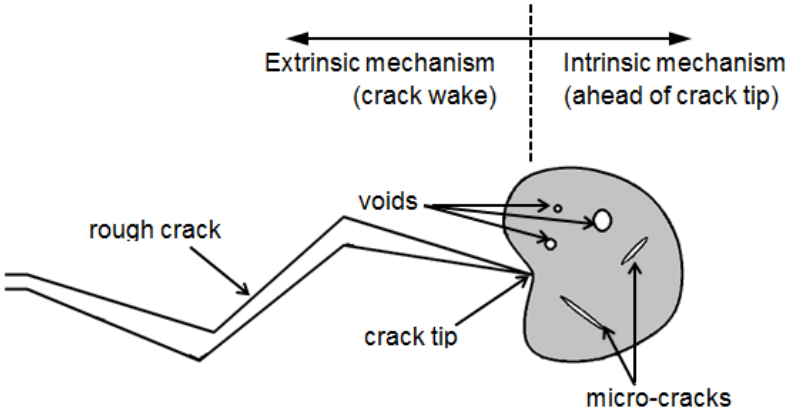

Figure 3-1: Schematic of a generic crack tip and definition extrinsic and intrinsic load ratio effects

3.2 Experimental Setup

3.2.1 Materials and Specimen Design

The composite DCB specimens were fabricated from unidirectional composite laminates with a nominal thickness of 3.38 mm (base laminates: $(0)_{24}$). The composite material used was carbon fibre/epoxy prepregs of IM7/977-3 which is an aerospace grade fibre-resin system. A poly-tetrafluoroethylene (PTFE) film of 13 μm in thickness was inserted at the mid-plane as initial cracks. The composite panels were cured in an autoclave at 177 ºC under a sustained applied pressure of 0.538 MPa for 6 hours, according to the manufacturer's recommended cure cycle.

The film adhesive used in the bonded DCB specimens was Cyctec FM3000-2K. The FM300-2K adhesive is an epoxy film adhesive supported with a carrier fabric and nominal bondline thickness of 0.2 mm. The bonded joints (0_{12}/FM300-2K/0_{12}) were manufactured using the following process in order to replicate the bonding process taken during repairs. The upper and lower substrates, consisting of 12 layers of unidirectional plies, were first cured under the normal curing temperature and pressure. After curing, the bonding surfaces were then sanded, lightly grit-blasted and cleaned to guarantee good chemical bonds at the interface of the adhesive and composite substrates. The adhesive was then placed between the bonding surfaces, along with a PTFE film of 13 μm as initial cracks. The adhesive was cured at 120ºC for 90 mins under vacuum (~ 1 atm) in an oven.

Both composite and bonded DCB specimens had the following dimensions: width b = 20 mm, length L =170 mm, and nominal thickness 2h = 3.38 mm for composite DCB and 3.58 mm for bonded DCB. Figure 3-2 illustrates the bonded DCB specimen specifications and piano hinges for load introductions. The specifications for the composites DCB were the same, minus the adhesive bondline. The side surfaces of the specimens were polished with abrasive papers. The specimen sides were coated with a thin layer of water-based correction fluid to aid the visual observation of the crack tip. A sharp crack was introduced by fatigue pre-cracking under relatively high loads. The initial crack was then measured visually with a traveling microscope. The effective crack length is the measured distance from the loading point of the hinge to the crack tip.

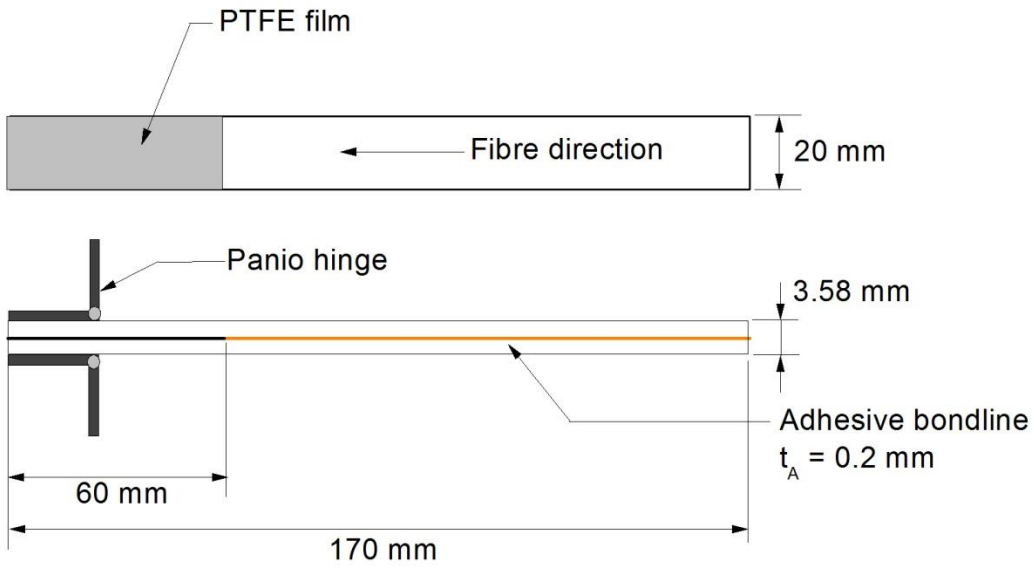

Figure 3-2: Bonded DCB specimen specification with piano hinges

Mode II fatigue loading was achieved through testing specimens in the 3-ENF configuration. Specimen of width b = 20 mm, length between supports 2L = 100 mm and total length = 170 mm were used. Figure 3-3 shows the design of 3-ENF specimens. The initial crack position of 25 mm is placed above the left roller support. The procedure of embedding a sharp crack and initial crack length measurement is the same as Mode I fatigue experiment. The initial crack position was placed at a_o = 0.5L to provide sufficient length for self-similar crack growth to occur without the external influences of the central loading point [81-83]. The central loading point may introduce additional compressive stresses within the neighbouring region of the ENF specimen. As a result of the compressive stresses acting on the crack flanks or tip, it will result in an artificial increase in fracture resistance. This phenomenon was observed experimentally for static tests,

resulting in an increase of the R-curve [84]. This feature should be avoided as it may lead to erroneous conclusions regarding the material behaviour.

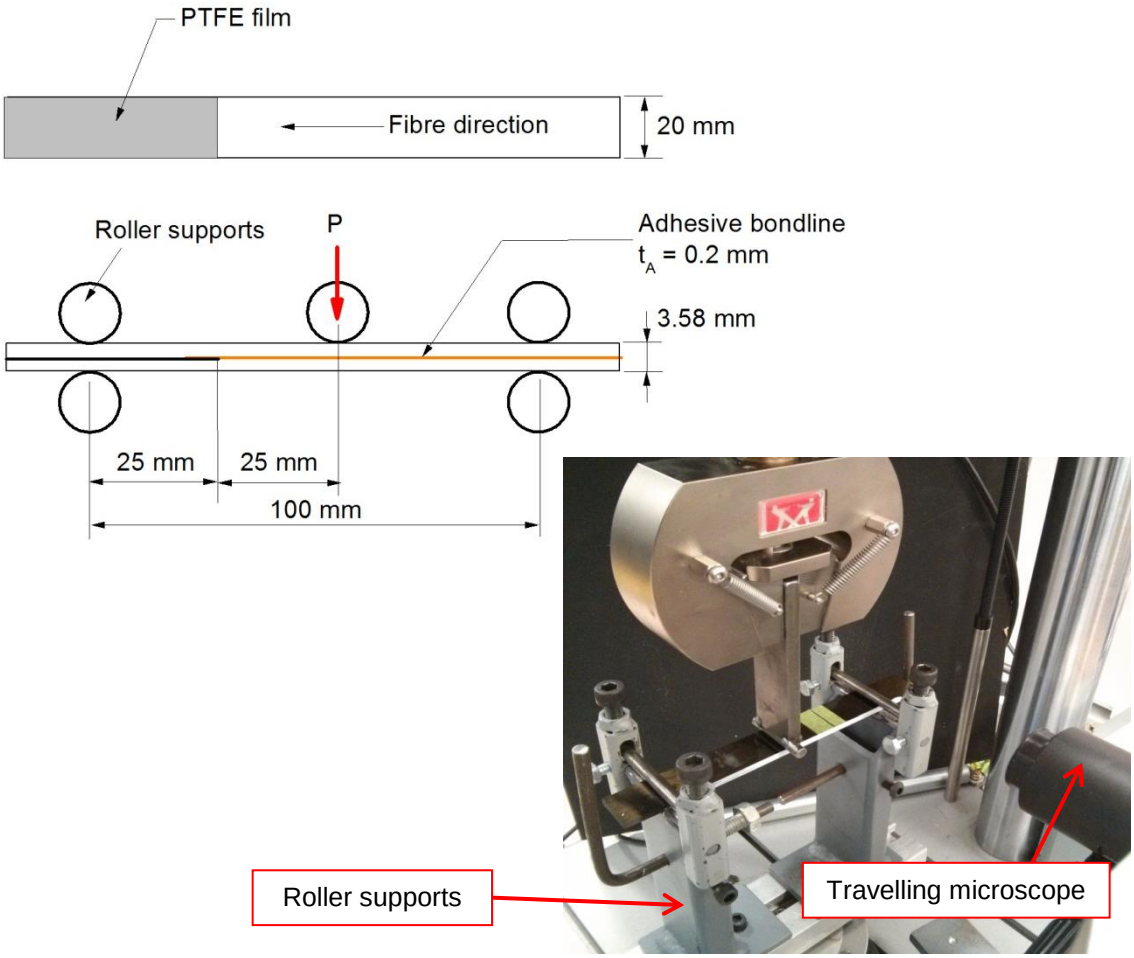

Figure 3-3: Three-point ENF specimen specifications and test configuration for mode II tests

3.2.2 Fracture Mechanics Parameter

The strain energy release rate G_i was used to characterise the fatigue crack growth where i represents the fracture mode. The methodology of calculating the Mode I strain energy release rate G_I is prescribed in ASTM D5528 [85]. Equation (3-1) is derived from the modified beam theory method.

$$G_I = \frac{P^2}{2b}\frac{\partial C}{\partial a} = \frac{3P\delta_{applied}}{2b(a + |\Delta|_{av})} \quad (3\text{-}1)$$

where $|\Delta|_{av}$ is the averaged compliance constant, δ is the applied displacement, P is the reaction force at the crosshead and B is the specimen width. Rotation may occur at the crack front due to imperfections during the manufacture of the specimen. The averaged compliance constant accounts for this by treating the DCB as if it has a slighter longer crack. This was experimentally determined by generating a plot of the cube root of compliance $C^{1/3}$ as a function of crack length, a.

The Mode II strain energy release rate G_{II} was calculated using either modified beam theory method or compliance calibration method as shown in Equation (3-2) and (3-3) respectively.

$$G_{II} = \frac{9a^2 P\delta_{applied}}{2b(2L^3 + 3a^3)} \tag{3-2}$$

$$G_{II} = \frac{3ma^2P^2}{2b} \tag{3-3}$$

where L is the half span of the specimen and m is the slope of the compliance calibration curve. The compliance calibration curve is given as $C = C_0 + ma^3$. This was determined in a non-destructive experiment by changing the crack tip position along the half span L. A small displacement was then applied to generate a curve. The results of the compliance measurement curves for the bonded and composite ENF joints are shown in Figure 3-4. The compliance calibration factor is given as $m = 5.08 \times 10^{-8}$ and 3.42×10^{-8} for the bonded and composite specimens respectively. As a comparison of both methods, the calculated G_{II} were in good agreement and confirmed in reference [83]. Perhaps the compliance calibration method was more reflective of the specimen being tested as its variables were determined experimentally. The beam theory method yields a slightly more conservative result. To maintain consistency with the method used for Mode I, the beam theory method was used to calculate G_{II}. The measured compliance was still useful in monitoring the crack growth length.

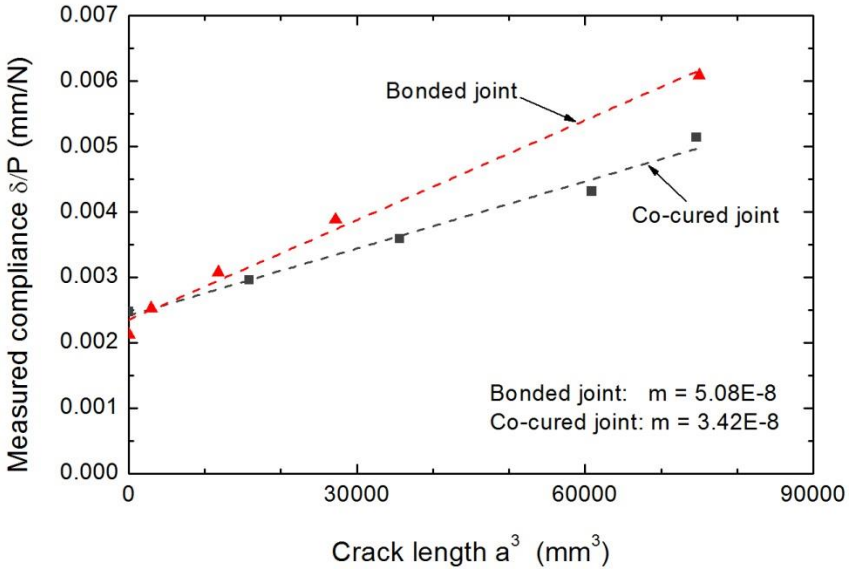

Figure 3-4: Measured compliance calibration curves of ENF specimens

To account for load ratio effects, different definitions of the correlating parameters were employed to analyse the influence of mean loads in the measured experimental data. The selection and derivation of the correlating parameters were presented in Chapter 2. The correlating parameters were defined as: -

- Maximum strain energy release rate, G_{max}
- Strain energy release rate range, $\Delta G = G_{max} - G_{min} = G_{max}(1 - R^2)$
- Equivalent strain energy release rate range, $\Delta G_{eq} = \left(\sqrt{G_{max}} - \sqrt{G_{min}}\right)^2 = G_{max}(1 - R)^2$

3.2.3 Test Procedure

All testing was carried out in ambient laboratory conditions (22 ± 2 ºC, 60 ± 5 %RH). The mode I fracture toughness tests were conducted on an Instron 10 kN tensile machine. The crosshead speed was controlled at 0.5 mm/min. The values of the fracture toughness G_{IC} were determined from the onset of a load drop experienced in the load-displacement curves.

Fatigue tests were done on a computer controlled servo-hydraulic testing system (Instron E3000, 3kN). Two types of fatigue tests; decreasing- G_{max} tests and constant-G_{max} tests, were conducted. In decreasing-load tests, the load was gradually reduced according to the instructions of ASTM standard E647 [25]. The initial highest load was chosen at approximately 60-70% of G_c. After the crack has grown approximately 1 to 1.25

mm, the number of cycles was then recorded and the loads reduced subsequently. This process was repeated until the threshold region was attained.

In the constant-G_{max} test, the applied load was varied to maintain the applied G_{max} after the crack had grown approximately 1 mm. The fatigue resistance behaviour was investigated with the increment of the crack length, similar to the R-curves under static loading. The test methodology was adopted from ASTM D6115 [86] which describes a test method of determining the onset of crack propagation in a composite DCB specimen. The procedure was as follows: 1) measure the initial crack length; 2) calculate the applied displacement and corresponding load for the pre-determined G_{max} value; 3) Start the test and monitor the change in compliance; 4) Stop the test if the compliance shows a change of 5%; 5) Measure the crack length. Continue the test with the same load if the crack growth is less than 1mm; 5) Otherwise calculate the new applied displacement for the corresponding G_{max} of the new crack length. In order to do this for the entire fatigue crack growth range, this method is time consuming and requires a larger number of specimens.

The mode I fatigue tests were conducted under displacement control at load-ratios of $R = 0.1, 0.3$ and 0.5. The mode II tests were tested under constant displacement amplitude at load-ratios of $R = 0$ and 0.45. An important aspect of operating in displacement control as opposed to load control is that G_{max} continuously decreases as the crack propagated. Consequently the crack growth will eventually be arrested as the G_{max} approaches the threshold level. The fatigue spectrum employed sinusoidal waveforms with a frequency of 10 Hz. The crack length was measured visually using optical microscopes at the magnification of 200. Alternatively the measurement of compliance calibration curves was also used to estimate the crack length. This was particularly useful for mode II tests as the crack tip could be difficult to detect. The da/dN was calculated with the secant method recommended in ASTM E647 [25]. The crack growth rate was estimated as the variation of crack length with respect to number cycles between two discrete, consecutive measurements (i and i+1). This is given as,

$$\frac{da}{dN} = \frac{a_{i+1} - a_i}{N_{i+1} - N_i} \tag{3-4}$$

Where i is the i th measurement performed during the test. The derived *da/dN* is the averaged value between increments.

3.3 Experimental Results

3.3.1 Failure Characterisation

For the bonded joints, the disbond growth was in a cohesive manner for both Modes I and II loading i.e. it grew within the adhesive. In the case of the bonded DCB specimen, the disbond growth occurred almost at the middle of the bondline thickness. For the ENF specimen, the disbond growth path occurred closer to adhesive-composite interface. In the composite specimens, the crack grew as a means of delamination i.e. between two composite plies.

3.3.2 Static Test

The relation between the loads and crack opening displacement for the mode I static tests under displacement control is illustrated in Figure 3-5. The load-displacement curves for both composite and bonded specimens were linear up to the maximum load point. Stick-slip behaviour was observed for both types of specimens. This behaviour was far more obvious for the bonded specimens as the failure is generally more unstable due to the crack tip experiencing higher loads.

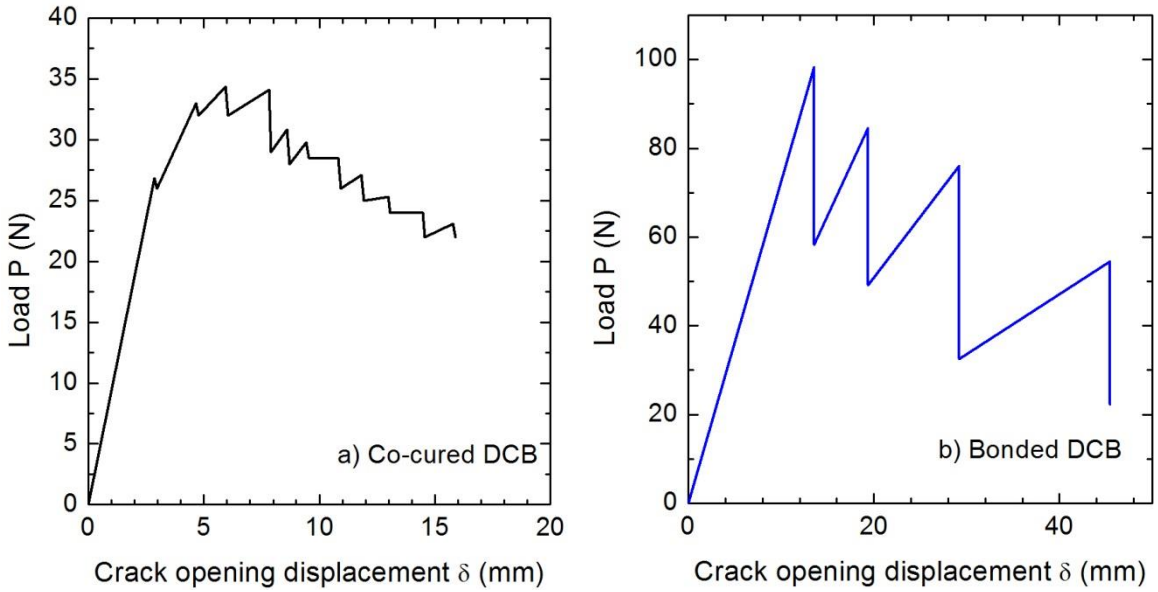

Figure 3-5: Relation between load and crack opening displacement for Mode I for a) composite and b) bonded DCB specimens

The relationship between the fracture toughness and the crack growth length (R-curve) is shown in Figure 3-6. The G_{IC} values of the composite DCB specimen gradually increased with the increment of crack length, Δa. The initial G_{IC} value (at $\Delta a = 0$ mm) was measured at 100 J/m^2. As the crack propagated, the strain energy release rate began to stabilise when the crack length $\Delta a = 23$ mm. The averaged G_{IC} ($\Delta a > 30$ mm) was measured at 240 J/m^2. This represents an increase of 140%. While the bonded joint has an initial G_{IC} value of 1520 J/m^2, the averaged G_{IC} (Δa > 10 mm) were slightly higher at 1660 J/m^2, an increase of 9.2%. It can be concluded that the fracture toughness of the bonded DCB was relatively independent of the crack length. The variation of the results is largely down to experimental scatter. The significant increase of G_{IC} in the R-curves of the composite DCB can be attributed to fibre bridging which was observed to occur extensively. From the R-curves, a fully developed bridging zone is approximately 23 mm.

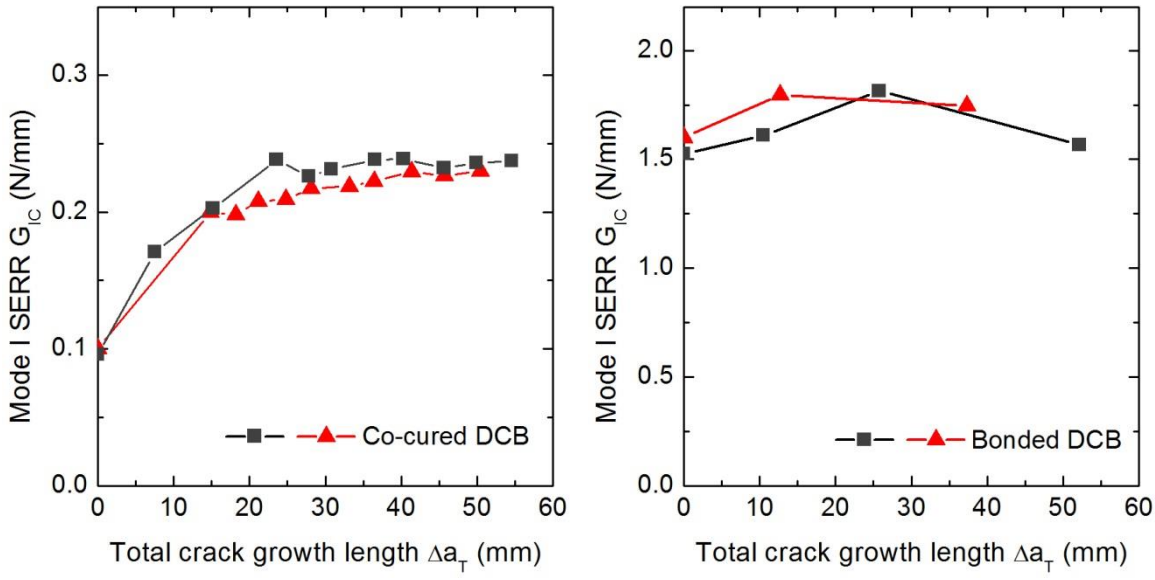

Figure 3-6: Relation between mode I energy release rate and increment of crack length for composite and bonded DCB specimens

Mode I and II static testing of the composite laminate and bonded DCB specimens were also independently conducted by the technicians at the CRC-ACS. The results are listed in the table below. However the results for bonded joints were not listed as failure was reported to have occurred at the adhesive-composite interface.

Table 3-1: Fracture properties of IM7/977-3 and FM300-2K adhesive

	Own Data		Other Sources	
	Laminate	Adhesive	Laminate	Adhesive
G_{IC} initial (J/m^2)	100	1520	219[1]	1330[2,3]
G_{IC} propagating (J/m^2)	240	1660		
G_{IIC} initial (J/m^2)	-	-	900[1]	6000[2]
G_{IIC} propagating (J/m^2)	-	-		

[1] Experimental data conducted by CRC-ACS, averaged value
[2] From reference [87]
[3] From reference [88]

3.3.3 Mode I Fatigue Loading

Mode I fatigue test were conducted at load ratios of 0.1, 0.3 and 0.5. The disbond growth rates were expressed as a function of the strain energy release rate. The question arises as to whether the independent variable should be based on the maximum strain energy release rate, $G_{I,max}$, strain energy release rate range or any other combination of G in order to account for the load ratio effects on the fatigue crack propagation in a composite laminate and bonded joint.

Figure 3-7 shows the relation of the measured fatigue crack growth rates and the maximum energy release rate $G_{I,max}$ for both DCB specimens. Although only two to three specimens were used for each DCB specimen under each load ratio, the measured crack growth rates were identical between the two specimens. This yields an overview of the fatigue behaviour under varying load ratios. The data point with the highest $G_{I,max}$ indicates the first data obtained after the test started (Δa = 0 mm). The exponents of the power were very high for both bonded DCB specimens (4.8 for $R = 0.1$, 4.9 for $R = 0.3$ and 5.4 for $R = 0.5$) and composite DCB specimens (9.9 for $R = 0.1$, 12.8 for $R = 0.3$ and 14.4 for $R = 0.5$). Again, this highlights the importance of selecting the correct fatigue design criterion as the crack growth rate can vary considerably over small changes in applied load. A dependence of the crack growth rates on load ratio was observed when $G_{I,max}$ was used as the correlating parameter. In keeping consistent with the fatigue behaviour of metals and adhesives discussed in the previous chapters, an increase in R leads to a slower crack growth rate. This behaviour is not unexpected as the load range experienced is decreased as R increases. Thus, this leads to a slower crack growth rate. The load range is not accounted for in the correlating parameter, G_{max}.

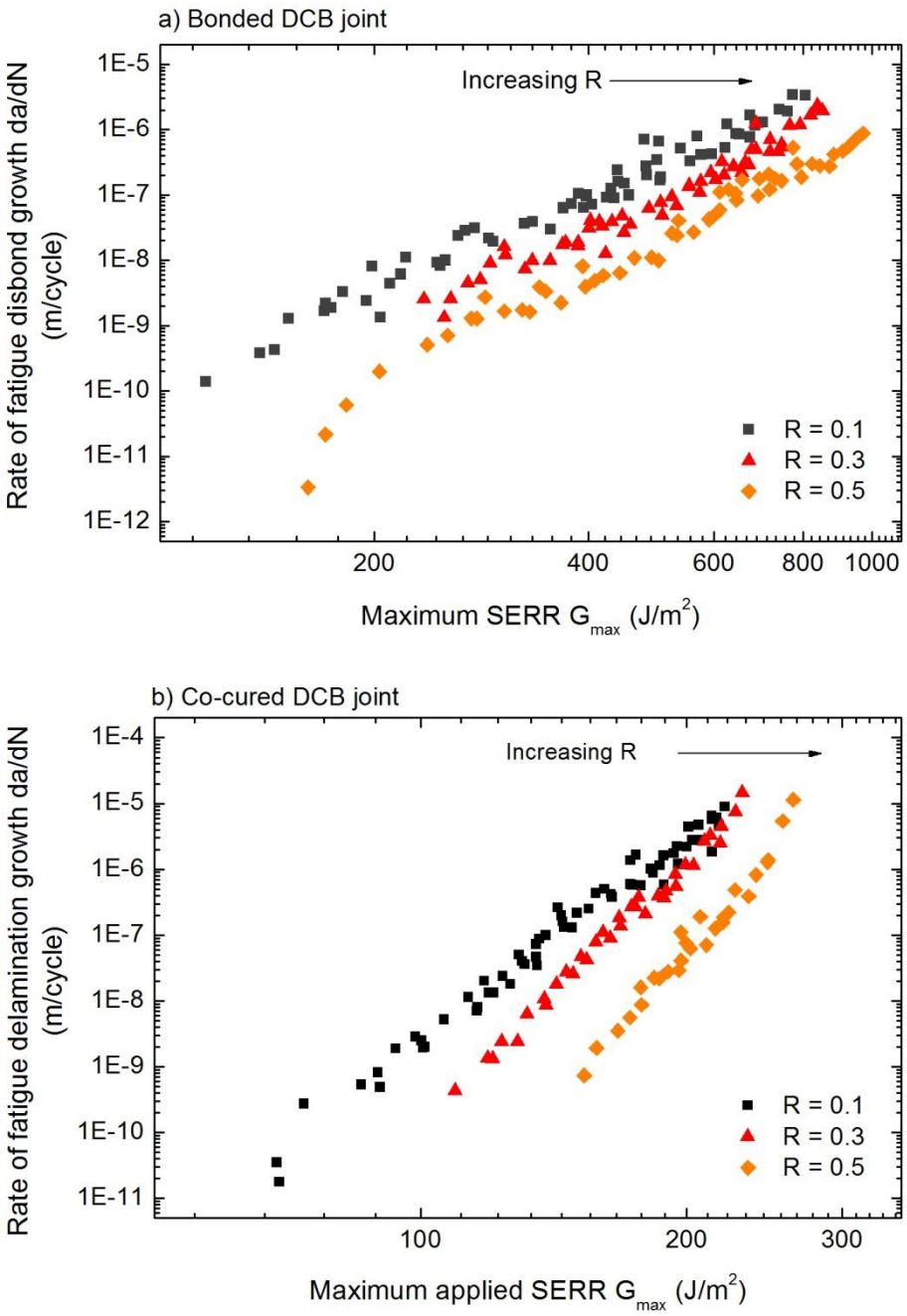

Figure 3-7: Relation between maximum applied strain energy release rates and crack growth rates at different load ratios for a) bonded and b) composite DCB specimens

Figure 3-8 illustrates the relation of the fatigue crack growth and the strain energy release rate range ΔG_I. On first inspection, the crack growth rates appear to have been collapsed into a narrow band especially at the higher ΔG_I values. However the load ratio dependency behaviour becomes more obvious as ΔG_I approaches the slow growth and threshold value. This behaviour has the same counter-intuitive behaviour (i.e. lower mean load = faster crack growth), previously reported in Chapter 2. This is particularly crucial as the fatigue criterion of composites and bonded joints is based on slow or no-growth. The

dependence of ΔG_I on load ratio meant that no unique value can be used as a no-growth design criterion.

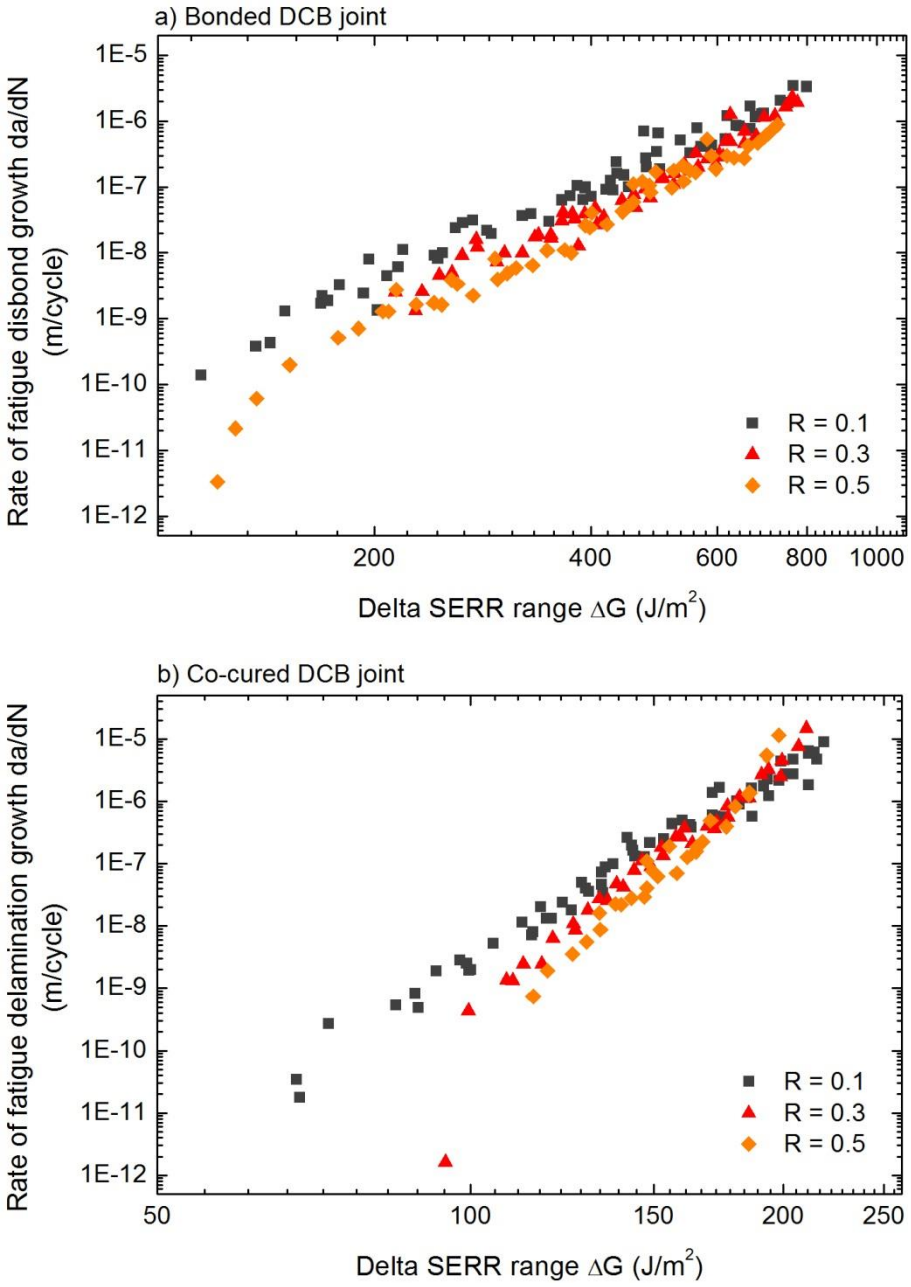

Figure 3-8: Relation between strain energy release rates range ΔG and crack growth rates at different load ratios for a) bonded and b) composite DCB specimens

The results of using the equivalent energy release rate $\Delta G_{I,eq}$ as the correlating parameter are shown in Figure 3-9. This term is equivalent to the cyclic J-integral range ΔJ used for fatigue crack growth in metals [46]. No improvement in the load ratio dependency fatigue behaviour can be observed in using $\Delta G_{I,eq}$. When compared with

ΔG_I, the load ratio effects are more significant in this case. However this behaviour is consistent with the metals' fatigue behaviour or when the crack propagation rate is plotted against ΔK [35]. Although ΔG_I is the best, among the three parameters examined, in correlating the fatigue crack growth rates, a better correlating parameter is still necessary to account for the load dependency behaviour at the threshold SERR regions. This will be further discussed in later chapters.

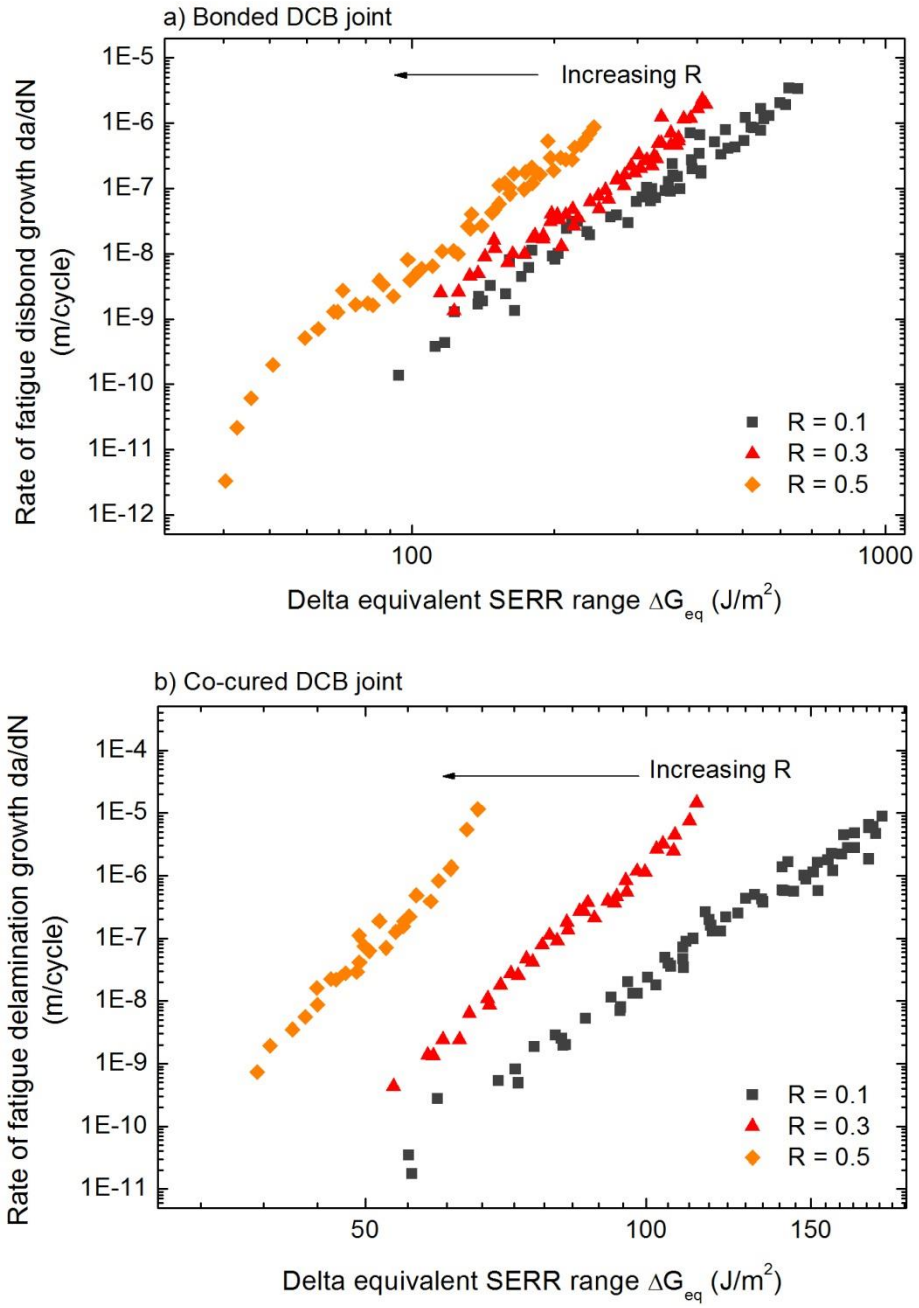

Figure 3-9: Relation between strain energy release rates range ΔG_{eq} and crack growth rates at different load ratios for a) bonded and b) composite DCB specimens

3.3.4 Mode II Loading

The same approach was taken in the assessment of a suitable correlating parameter for Mode II crack propagation. The measured crack growth rates were plotted against maximum energy release rate $G_{II,max}$, as shown in Figure 3-10.

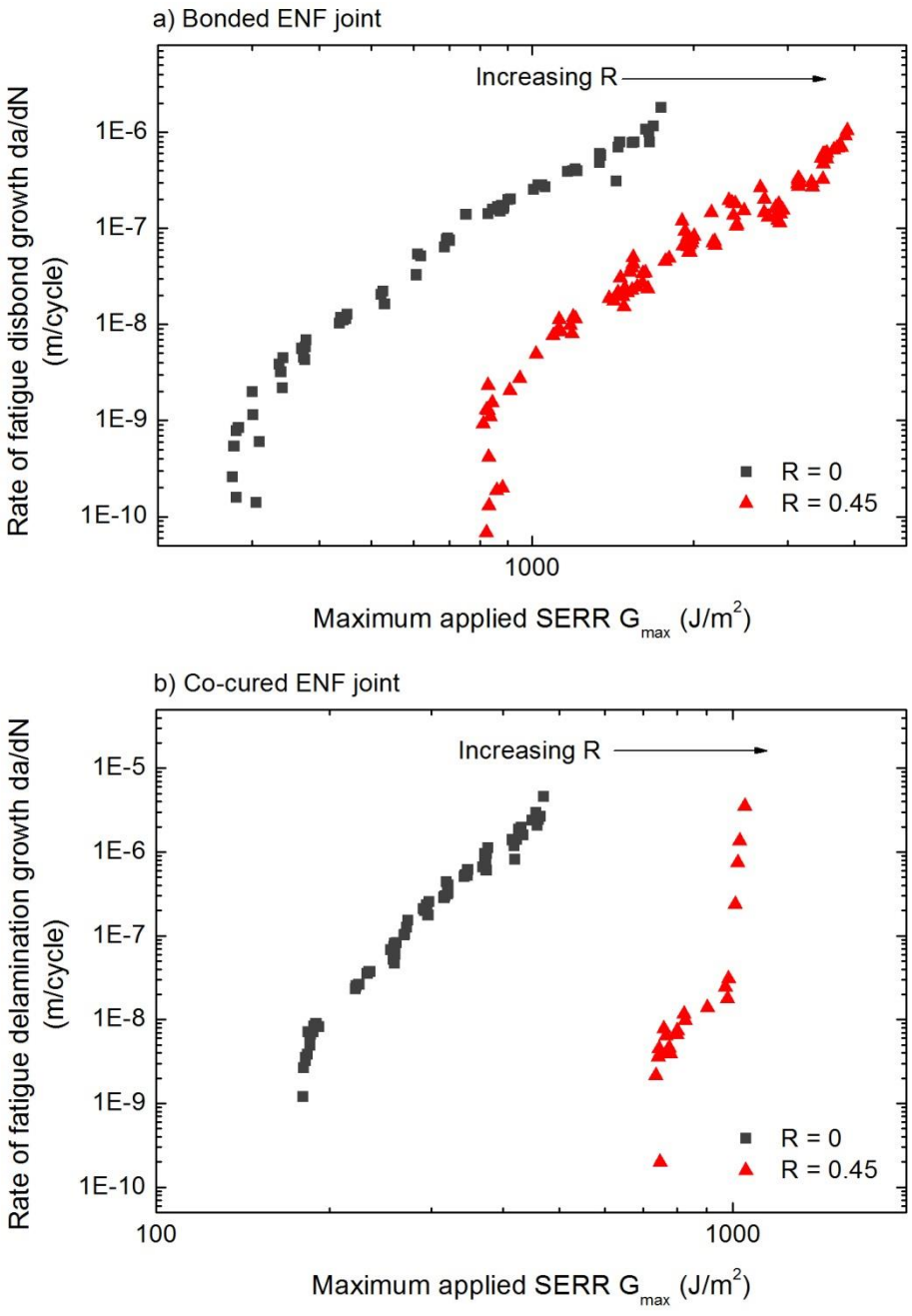

Figure 3-10: Relation between maximum applied strain energy release rates and crack growth rates at different load ratios for a) bonded and b) composite ENF specimens

A unique relation of the fatigue crack growth under different load ratios cannot be obtained for both types of DCB specimen. The degree of mean load effects appears to be

more significant when compared to Mode I. The stable crack growth region at R = 0.45 is rather small. Therefore the crack growth transition from no-crack to unstable crack growth occurs over small changes of applied load. Designing for stable crack growth would be impossible in this instance. Figure 3-11 shows the relation between the measured crack propagation rate and the energy release rate range ΔG_{II}. ΔG_{II} is unable to to correlate the Mode II crack growth rates for different load ratios in a unique relationship despite accounting for the strain energy release range. This load ratio dependency behaviour is counter-intuitive and as previously reported in Chapter 2.

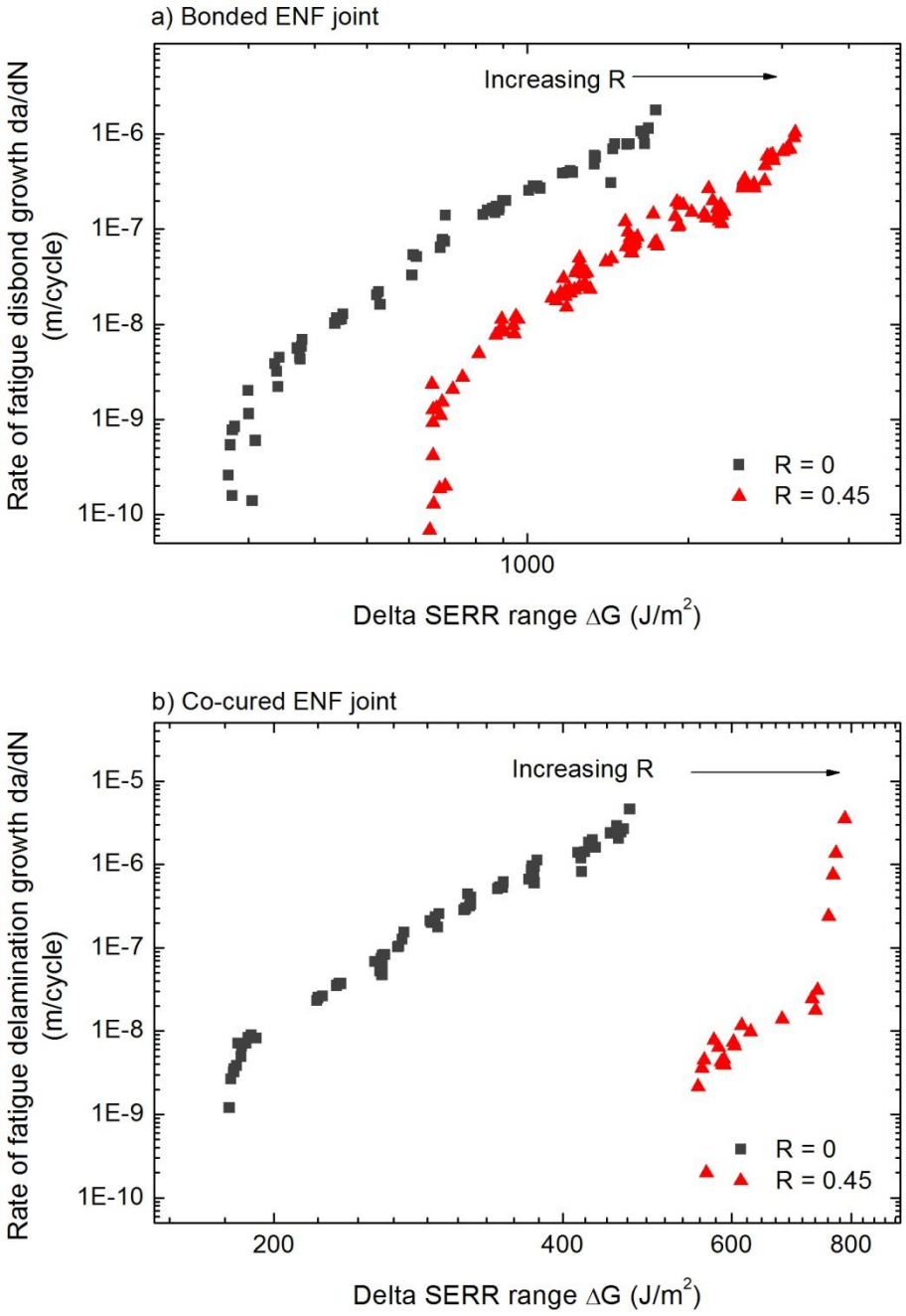

Figure 3-11: Relation between strain energy release rates range ΔG and crack growth rates at different load ratios for a) bonded and b) composite ENF specimens

Figure 3-12 shows the relation between the measured crack growth rate and the equivalent energy release rate $\Delta G_{II,eq}$. The load ratio dependency fatigue behaviour previously observed with the former two correlating parameters is now completely eliminated. Four data points of the crack growth rate for the composite specimens did not collapse into a narrow band because the values of $G_{II,max}$ were approaching the critical value. For the fatigue design of bonded joints and composite structures under pure Mode II cyclic loads, a unique threshold value can be obtained as the design criterion and is independent on the load ratio.

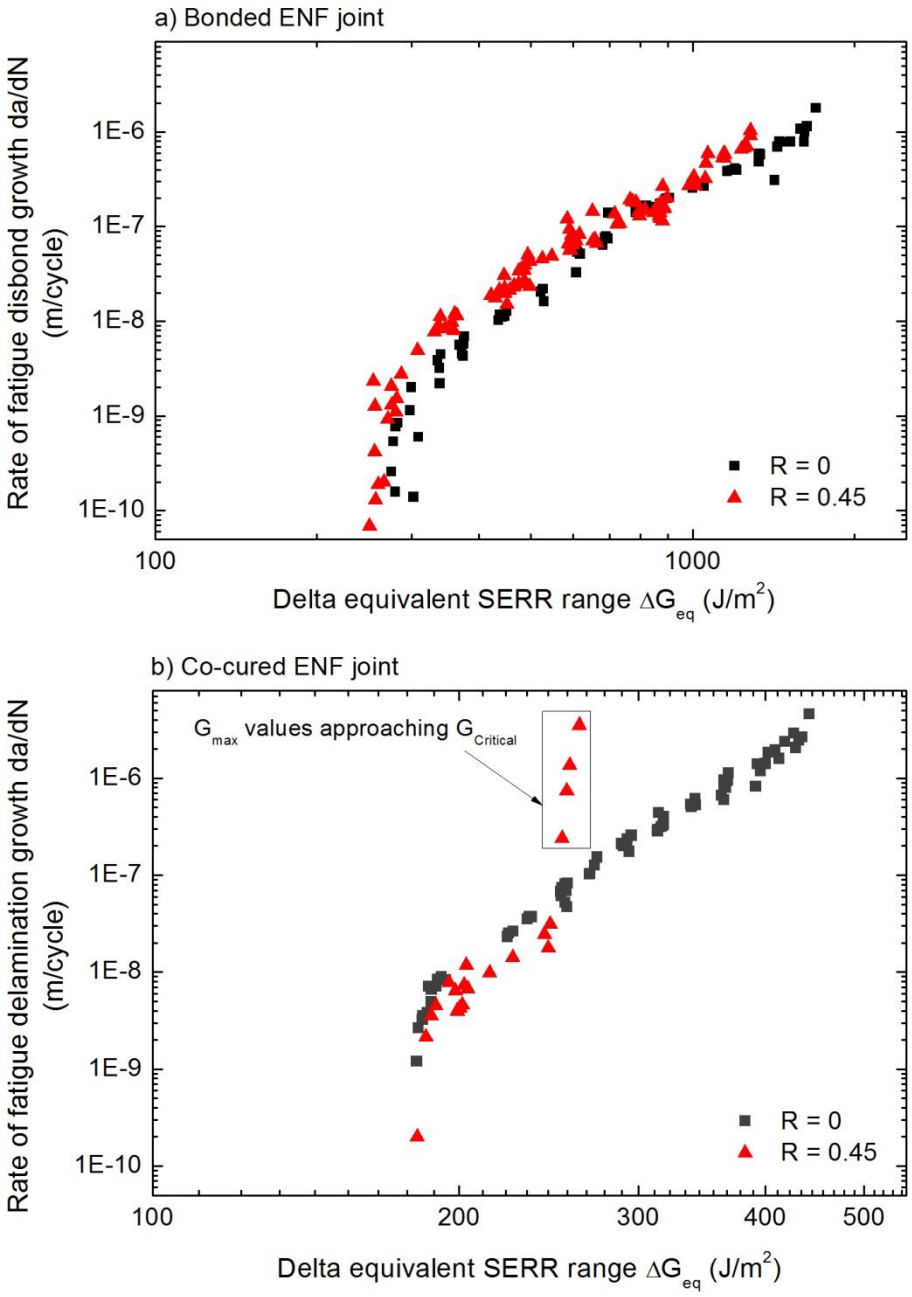

Figure 3-12: Relation between strain energy release rates range ΔG_{eq} and crack growth rates at different load ratios for a) bonded and b) composite ENF specimens

The experimental investigation of Mode I and II fatigue behaviour reinforces the findings of the case studies in Chapter 2. The finding poses a dilemma as to which correlating parameter ΔG or ΔG_{eq} to use for both Mode I and II. ΔG seemed to provide a better correlation for Mode I whereas a better correlation was obtained with ΔG_{eq} for Mode II. The definition of the correlating parameter should ideally not differ between crack propagation modes since it describes the same thing; the stress-strain field of the crack tip. In light of this findings from the experimental investigation and case studies material taken from literature, there is no parameter that is capable of unifying the fatigue crack growth rates of bonded joints and composite laminates under Mode I and II.

In the interim (unless proven otherwise), the ΔG_{eq} parameter is prefered because it maintains the theoretical requirement of similitude. Despite not being able to eliminate the load ratio effects under Mode I loading, a consistent fatigue behaviour was observed in a manner similar to metals' fatigue. Different hypothesis had been proposed to be the source of the mean load dependency behaviour observed in Mode I fatigue such as crack closure, fiber bridging and damage zones. Hence a qualitative analysis was then carried out to determine the presence of these mechanisms.

3.3.5 Constant G_{max} Mode I Loading

A significant toughening effect was observed in the R-curves of the composite DCB specimens whereas the R-curve of the bonded DCB specimens remained relatively constant. Mechanisms such as fibre bridging are responsible for providing shielding to the crack front and thereby increase the resistance to crack growth. The constant-$G_{I,max}$ was carried for the composite DCB specimen to investigate this behaviour under fatigue. A $G_{I,max}$ of 150 J/m^2 at R = 0.1 and 0.3 was applied. The applied $G_{I,max}$ was in the stable crack growth region.

The relationship of the measured delamination growth rate and total crack growth length is shown in Figure 3-13. An initial increase in the crack growth rates can be observed. This is likely due to the formation of a sharp crack tip from the resin rich region at the PTFE pre-crack. After which a steady decrease in the crack growth rate then occurs, indicating an increase in fatigue resistance. After a total crack growth length of 20~25 mm, the crack growth rates reach a steady state. In comparison with the static test, the strain energy release rate reaches steady state at Δa = 23 mm in the R-curves. From this, it can be said that a fully developed bridging zone is approximate 23 mm long, behind the crack tip. At Δa = 0 mm, the measured crack growth rate at this point will be devoid of any fibre bridging as the PTFE film is used to create the crack. However the

crack growth rate that is free from fibre bridging can be estimated by extrapolating from the slope of the crack growth curves.

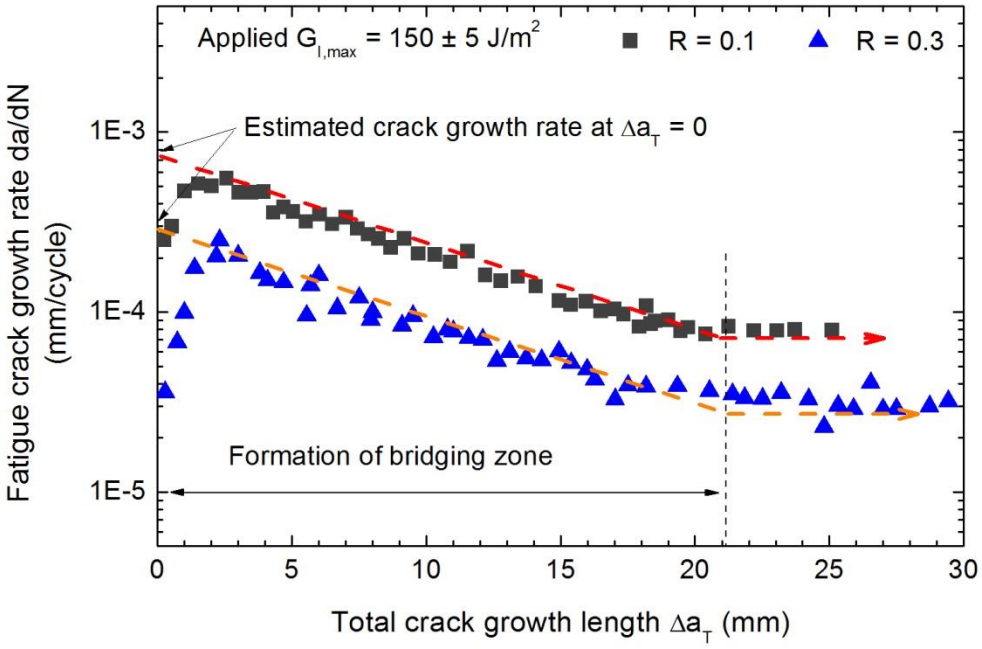

Figure 3-13: Variation in the fatigue crack growth rates with total crack growth length in a constant-$G_{I,max}$ test

3.4 Consideration of Load Ratio Dependency Mechanisms

3.4.1 Cohesive Failure

After the test was completed, the specimen was sectioned with the crack tip intact. In order to view the crack profile, a small pin was inserted to open the crack slightly. For observation with scanning electron microscopy (SEM), the specimen was coated with gold.

Figure 3-14 shows the side profile of the bonded DCB specimen taken under an optical microscope. The presence of plasticity can be observed within the adhesive, denoted by the de-colorised region. A plastic zone can be observed ahead of the crack tip as the crack undergoes cyclic loading. Plasticised material forms the plastic wake along the crack flanks as the crack propagates. This indicates the possibility of plasticity induced crack closure despite far field measurements of the compliance being unable to capture this phenomenon.

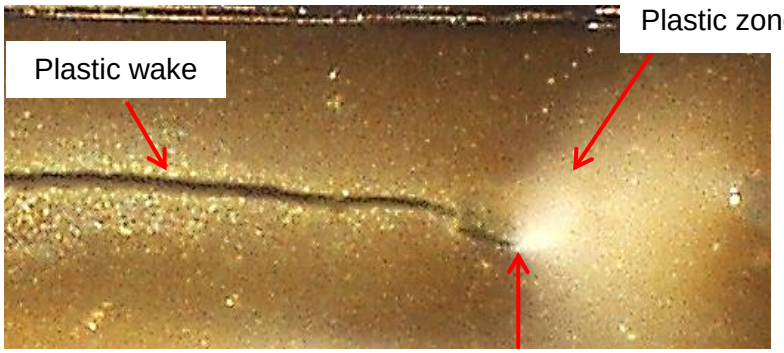

Figure 3-14: Plasticity in a cohesive crack at maximum cyclic Mode I load

3.4.2 Delamination Failure

Figure 3-15 shows the SEM images of the crack profile of the delaminated composite DCB specimens under Mode I loading. The image was taken at approximately 2 mm behind the crack tip. Fibre bridging can be observed along the crack propagation path. The zoomed-in images show the extensiveness of the bridging that occurred and is not simply limited to a few fibre tows. Increasing the intensity of the electron beam shows that bridging occurs along the entire width of the specimen and not just at the edge.

The SEM images of the fracture surfaces of the composite DCB specimen are shown below. The fracture surface plane was uneven (Figure 3-16a), suggesting that there is no defined crack propagation plane. Crack propagation is likely to occur at different layers of fibre tows, thereby causing fibre bridging to occur. A larger number of broken fibres can also be observed, pointing to the fatigue degradation of the bridging zone as the crack propagates. Fibre bridging phenomenon can be mitigated by offsetting the ply orientation at the delamination plane by a small angle [62]. This allows the crack a more defined propagation plane and, therefore, fibre bridging is less likely to occur. The morphology of the resin (Figure 3-16b) shows a brittle fracture. Plastic deformation of the matrix epoxy was likely to be absent or negligible due to the constraints provided by the fibres.

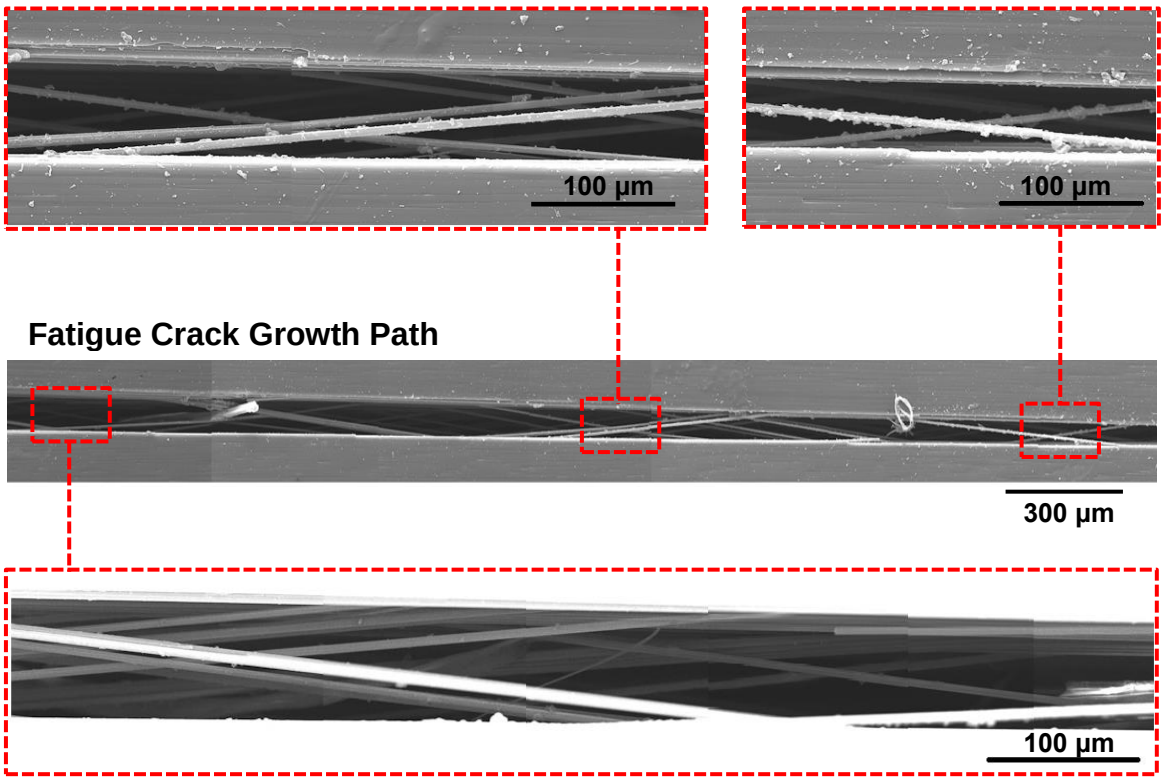

Figure 3-15: SEM evidence of fibre bridging along the fatigue crack path subjected to mode I loading

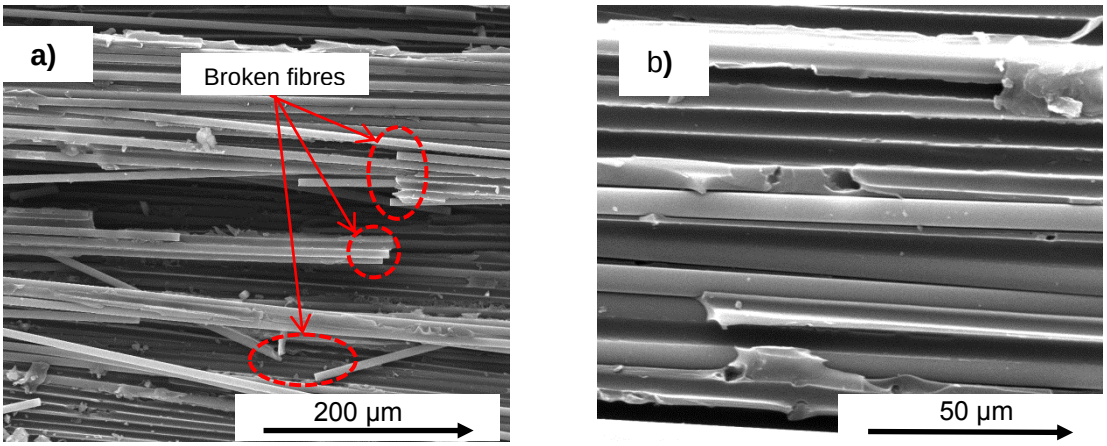

Figure 3-16: SEM images of the fracture surfaces under mode I fatigue loading

3.5 Concluding Remarks

Experimental investigations of the fatigue behaviour of a bonded joint and composite laminates were carried out under Mode I and II loadings. The experimental measured fatigue crack growth rates were then correlated to different parameters, G_{max}, ΔG and ΔG_{eq}. It was found that no single scaling parameter is capable of unifying the fatigue behaviour under varying load ratios for Mode I and II. The fatigue behaviour of the bonded joint and composite laminates is similar to the experimental data analysed from various literature.

Given the extensive research done on metal's fatigue, the ΔG_{eq} was preferred as it satisfies the fatigue similitude requirement. However the mean load effects in the Mode I fatigue behaviour indicated similitude was not met and nonlinear effects had been introduced. The crack closure phenomenon provides a physical basis to explain the mean load dependency behaviour in fatigue. Microscopy images showed the presence of the plasticity in the adhesive. However traditional methods of experimentally quantifying crack closure lack the required sensitivity and precision for a bonded composite DCB specimen. To this end, finite element modelling provides an alternative of quantifying crack closure where experimental measurement is difficult. This had been widely employed for metals. In the following chapter, numerical modelling was carried to quantify the mean load effects in bonded composite specimens.

For the composite DCB specimens, extensive fibre bridging could be observed behind the crack tip. Broken fibres and uneven fracture surfaces were further indications of fibre bridging. The morphology of the resin on the crack surfaces indicated a brittle fracture. Therefore it is highly plausible that fibre bridging was the main source of mean load dependency behaviour in composite laminates. Static and fatigue tests indicated that the full developed bridging zone is approximate 23 mm. Hence further analysis was carried out to investigate this further.

This page intentionally left blank

Chapter 4

Numerical Simulation of Plasticity Induced Crack Closure in Bonded Joints

4.1 Preamble

In metal fatigue, finite element (FE) analysis has proven to be an invaluable tool in the understanding of plasticity crack closure effects on the fatigue crack propagation behaviour. Newman was among the first to employ plane stress model to simulate and study the effect of plasticity induced crack closure (PICC) [89]. Fleck followed up the work with a plane strain model [55]. McClung and Sehitoglu provided a systematic overview of the assumptions involved in the modelling process, detailing the results obtained and the influence of each modelling assumption [58, 90].

Subsequently, the influence of PICC on fatigue crack growth rates had been greatly studied by means of FE simulation as a result of increased availability of computing power. Ellyin and Wu [91] and Rodrigues and Antunes [92] examined the influence of different material constitutive models which includes work hardening. Gonzalez-Herrera and Zapatero [93] and Solanki et al. [94] studied the crack tip mesh sensitivity on the crack closure results. Wei and James discussed the crack opening criteria definition, crack opening behaviour and compared their numerical results with the experimental results on a polycarbonate CT specimen [95]. Additional comprehensive reviews of previous work on FE simulation of PICC can also be found in reference [58, 90, 96-98]. These analyses were carried out on isotropic material, typically with the geometry of cracked body specimens as shown in Figure 4-1. This Chapter presents computational modelling PICC in bonded DCB joints.

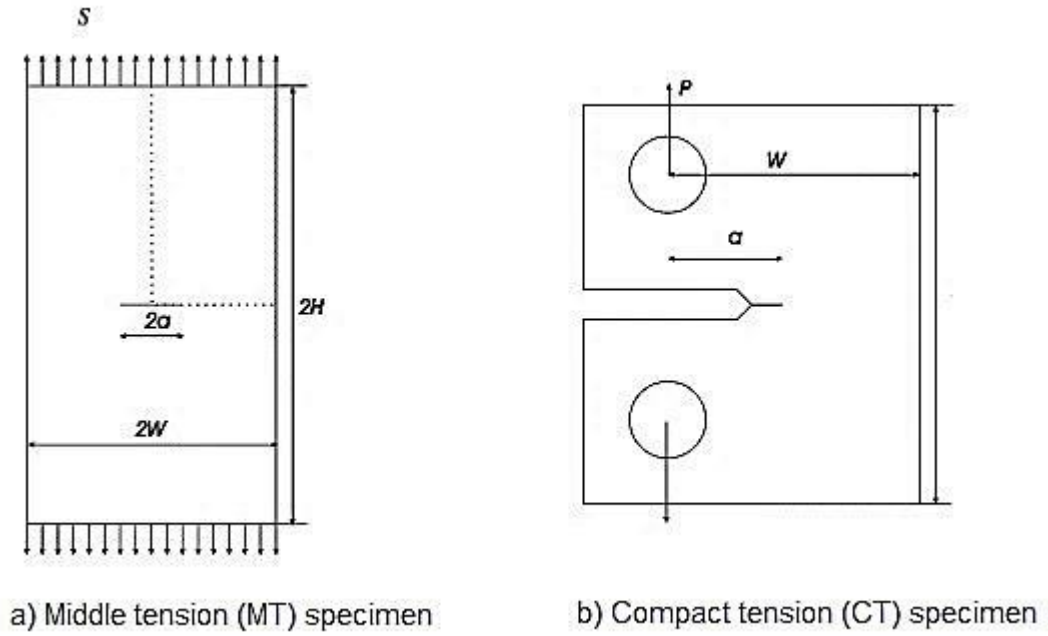

Figure 4-1: Typical geometry of a) Middle Tension and b) Compact Tension specimens used in PICC simulation in isotropic materials

4.2 Crack Closure Influence on Fatigue Crack Growth

The phenomenon of PICC was first proposed by Elber when he discovered non-linear behaviour in the material's compliance [38]. It is now a widely accepted explanation for the mean load effect on the fatigue behaviour of isotropic materials and has led to new concepts in fatigue crack growth modelling. In addition to PICC, several other crack closure mechanisms have also been identified such as oxide induced and roughness induced closure [99], schematically illustrated in Figure 4-2. However PICC has been considered the primary contributor to the mean load effect in the regimes I and II of fatigue crack growth. Crack closure is the phenomenon that occurs upon contact of the crack flanges for duration of the load cycle. This contact causes a decrease in the local stress and strain fields experienced at the crack tip. As a result, the crack propagation rate is less than if the crack remains fully open.

There are a number of methods used to detect crack closure. The most commonly used and direct approach to quantify crack closure is through compliance measurements where a variation in the load-displacement curves indicate the presence of this phenomenon. The measurement techniques include crack opening gauges, strain gauges along the crack propagation path, back-face strain measurements, electrical

potential, ultrasound and eddy current. Indirect observation includes striation counting and spacing, crack growth rate changes and high stress ratio tests to evaluate crack growth observations.

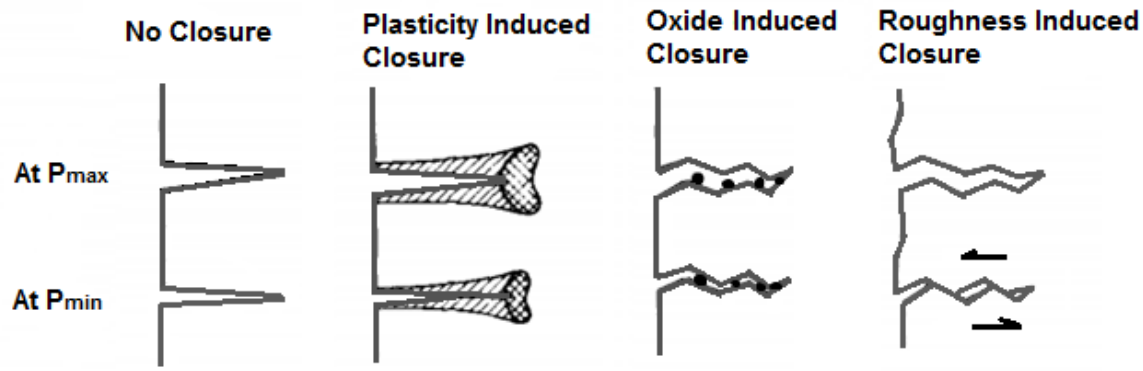

Figure 4-2: Schematic of different fatigue crack closure mechanisms

However the exact measurement of crack closure remains non-trivial. The sensitivity of the measuring technique is very much dependent on crack opening displacement (COD) measurement location. The onset of non-linearity in the load-displacement curve which denotes the start of crack closure will be higher if the measurement location taken close to the crack tip than those taken further away. The area of closure, over which the plastic wake comes into contact, is very much smaller under plane strain than under plane stress conditions. Hence crack closure detection of thick structures that closely resemble plane strain condition is much more difficult than in thin structures (plane stress). Fleck noted that crack mouth compliance measurement for crack closure detection in a thick CT specimen is only possible if special care is taken to eliminate electrical noise [57].

In a bonded joint, crack closure is difficult to measure because: -

1) The bending stiffness of the substrate in DCB geometry is low. Far field measurements using COD gauge must be extremely sensitive to be capable of capturing any sort of non-linearity behaviour.

2) The bondline thickness is typically between 0.1-0.2 mm. Consequently it is impossible to attach any strain gauges to take local measurements of the crack opening displacement.

Therefore the statements in the literature that crack closure is absent in bonded joints may be questionable, because there is lack of precision and sensitivity to detect closure in bonded joints. As presented in Chapters 2 and 3, significant load ratio effects can be observed in the experimental data for mode I fatigue debonding of the adhesive when the $\Delta G_{I,eq}$ parameter is used. For crack propagation in a cohesive manner, plasticised material can be observed in the wake of the crack and, hence, plasticity induced crack closure was postulated as the cause of this behaviour.

4.3 Analytical Description of the Plastic Zone

A plastic zone forms ahead of the crack tip during fatigue. As the crack propagates, the plastic material formed by the plastic zone is left behind. Hence the formation of this plastic zone is innately related to the crack closure behaviour. The mode I plastic zone is derived as a function of θ by applying the von Mises yield criterion. The boundary of the plane strain plastic zone is given as,

$$r_1(\theta) = \frac{K_{max}^2}{4\pi\sigma_y^2}\left[\frac{3}{2}\sin^2\theta + (1-2\upsilon)^2(1+\cos\theta)\right] \quad (4\text{-}1)$$

where σ_y and K_{max} denote the adhesive's yield strength and the maximum applied stress intensity factor.

In the case of a crack within a constrained layer [100, 101], the maximum stress intensity factor is related to the applied strain energy release rate via the usual relationship $K_{max} = \sqrt{G_{max}E_A}$, with E_A being the Young's modulus of the adhesive. The strain energy release rate of a DCB and ENF can be determined via beam theory as shown in Equation (4-2) and (4-3) respectively.

$$G_I = \frac{12P^2a^2}{E_{11}b^2h^3} \quad (4\text{-}2)$$

$$G_{II} = \frac{9P^2a^2}{16E_{11}b^2h^3} \quad (4\text{-}3)$$

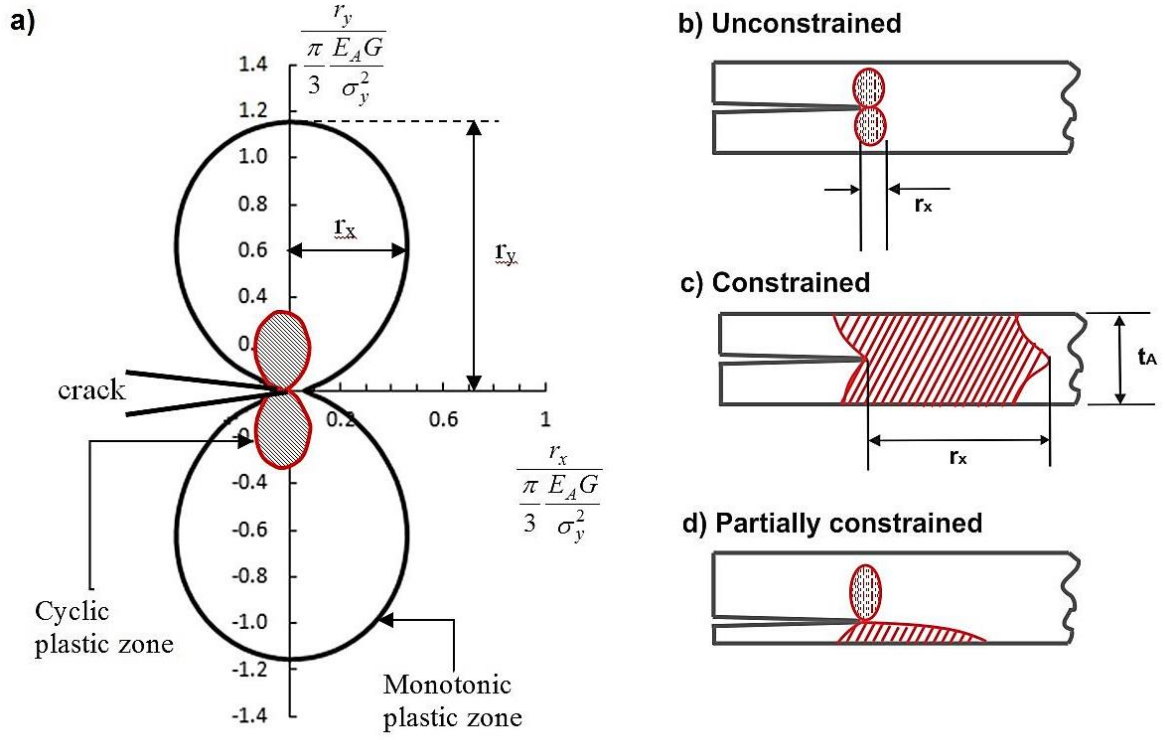

Figure 4-3: a) Analytical solution for an unconstrained plastic zone and scenarios which the plastic zone can form within a bondline; b) unconstrained, c) fully constrained; c) partially constrained

Therefore the plastic zone shape in a bonded joint under Mode I loading can be analytically using Equations (4-1) and (4-2). The shape of the unconstrained, plane strain plastic zone, derived from Equation (4-1) is shown in Figure 4-3a. The plastic zone height r_y, on either side of the crack tip is given in Equation (4-4). The forward plastic zone length r_x is approximately given when $\theta \approx \pi/4$.

$$r_y = r_1\left(\frac{\pi}{2}\right) = 1.15\left[\frac{1}{3\pi}\frac{E_A G_{max}}{\sigma_y^2}\right] \tag{4-4}$$

$$r_x \approx r_1\left(\frac{\pi}{4}\right) \approx 0.5\left[\frac{1}{3\pi}\frac{E_A G_{max}}{\sigma_y^2}\right] \tag{4-5}$$

Figure 4-3(b-d) shows the number of scenarios in which the plastic zone can form within the adhesive bondline. In the first scenario, the plastic zone is sufficiently small and is completely contained within the bondline thickness and the crack-tip singularity zone.

Consequently small scale yielding conditions are satisfied; hence this case is denoted as un-constrained plasticity. In the second scenario, the upper and lower plastic zone height extends to the composite substrates. Since the composite substrate remains elastic and is much stiffer than the adhesive, the plastic zone height is completely bounded by the bondline thickness and plasticity has to spread in the lateral direction. This condition is denoted as constrained plasticity. If the crack were to propagate close to the interface, the plastic zone is constrained only on one side and unconstrained on the other side. This shall be denoted as partially-constrained plastic zone.

4.4 Modelling Methodology

The FE analysis of PICC is based on discretising a continuous cracked body, propagating the crack under a cyclic load and measuring the closure level. Since the FE simulation is an approximate of the actual process, it is important to understand its limitations and idealisation, namely: -

- Discrete crack propagations as the crack is advanced per crack tip element at a single point of the load cycle. The actual crack propagation process is a continuous process occurring during the entire load cycle, provided that the crack flanks are open.

- A number of actual cycles are neglected in the simulation as the numerical crack advance per cycle is greater than the actual crack propagation rate.

- The numerical crack tip shape is typically modelled as a sharp crack. However real cracks have a very small radius at the tip which affects the local stress and strain fields.

- Numerical models only simulate PICC. All other mechanisms such as roughness induced closure are neglected.

Therefore the numerical aspects, which correlate with the above assumptions, must be carefully considered. The numerical processes must be optimised to ensure valid results are obtained. In this study, a bonded DCB specimen with a crack propagating in the middle of the bondline was investigated with the dimensions illustrated in Figure 4-4.

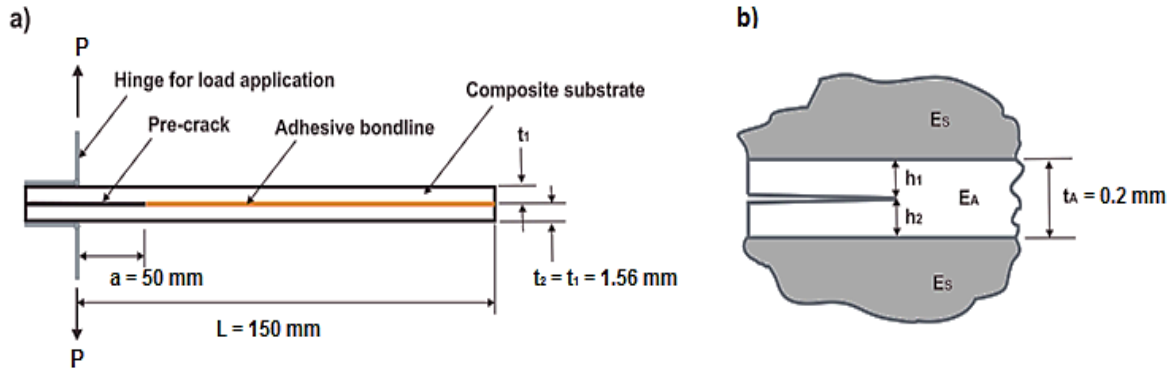

Figure 4-4: Double cantilever beam geometry

Computational simulations were performed under constant amplitude cyclic loading with Abaqus Standard solver in a multi-step analysis. A typical mesh and boundary conditions of a bonded DCB specimen are shown in Figure 4-5. The mesh size transits from a coarse mesh to a fine mesh at the crack tip vicinity. The composite substrates consisted of 12 unidirectional plies made of IM7/977-3 carbon epoxy prepregs, with ply thickness after cure being 0.13 mm. The fiber direction of the plies was along the x-axis. The substrate was assumed to remain elastic throughout the cyclic loading. The bondline was given the properties of FM300-2K adhesive. The von Mises yield criterion was employed to model the plastic yielding of the adhesive. The material input properties of the numerical simulation are given in Table 4-1. Crack propagation was achieved by liberating the crack tip node from its constraint by changing boundary conditions between successive analysis steps. The crack propagation scheme used in this work is discussed in Section 4.5.2. The contact of the crack flanks was simulated by placing a rigid body at the crack plane and employing a hard contact interaction to prevent the nodes from inter-penetrating in the event of closure. The most conventional method of determining the opening load P_{op} was by evaluating the contact status with the symmetry plane of the first node behind the current crack tip. This will be described in detail in Section 4.5.4 and different concepts of crack closure definition had also been considered and compared.

Table 4-1: Material properties used in the finite element model

Substrate : IM7/977-3				Adhesive : FM300-2K	
E_{11} =	159000 MPa	E_{33} =	9000 MPa	E =	2350 MPa
G_{13} =	7800 MPa	G_{23} =	4000 MPa	v =	0.4
v_{12} = v_{13} =	0.35	v_{23} =	0.3	σ_y =	83 MPa

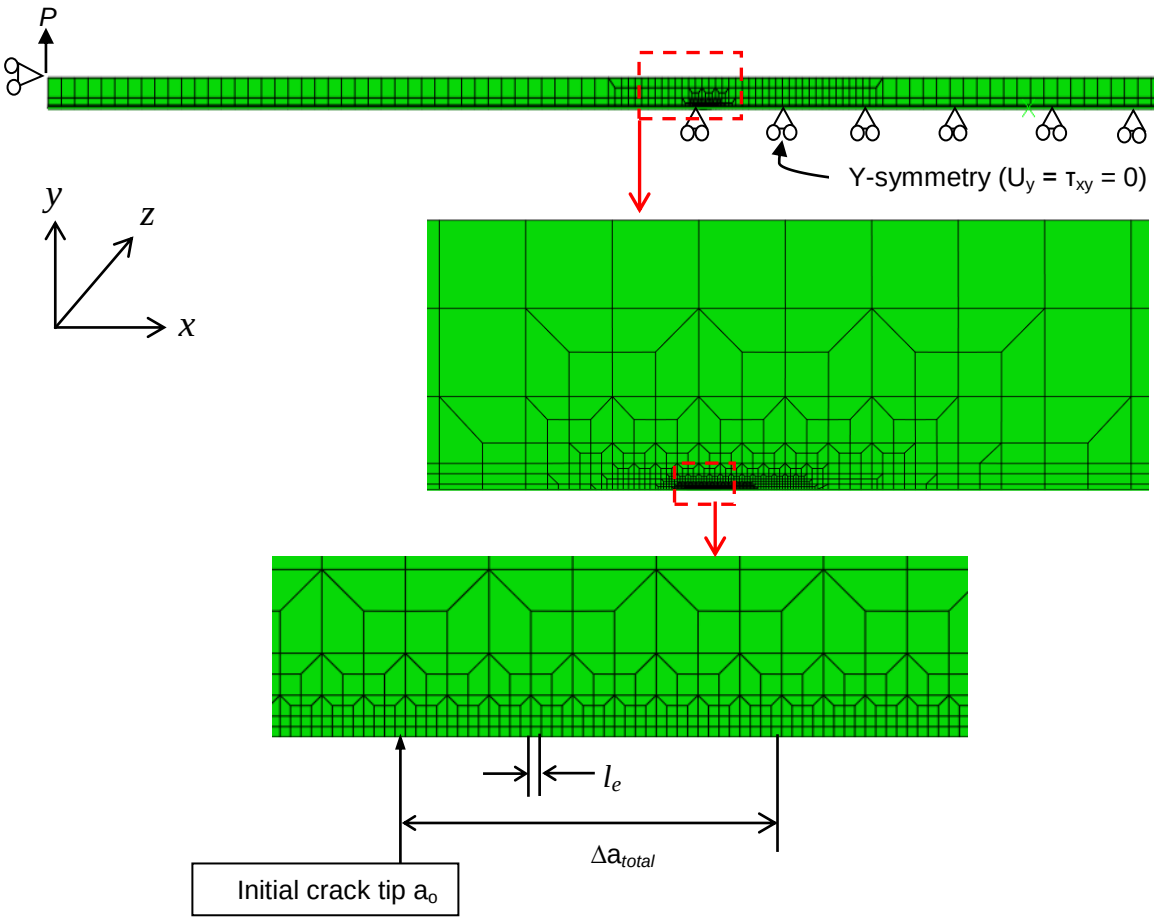

Figure 4-5: Finite element mesh and boundary conditions used for double cantilever bonded joint specimen

4.5 Consideration of Numerical Parameters

Based on the assumptions taken in the FE model, the numerical parameters identified as having potential influence on the crack closure results are the crack tip mesh size, crack propagation scheme, total crack extension and crack opening criterion.

4.5.1 Crack Tip Mesh Size

The crack tip element size is directly correlated to the numerical crack advance per cycle. The larger the numerical crack advance per cycle meant that a large number of the cycles that has occurred in reality are ignored. This can be avoided by decreasing the element size at the cost of severe computational burden. However, if the crack tip elements are too large, inaccurate results may be obtained due to the high strain gradient in this region. McClung et al. [58, 90] performed mesh sensitivity studies on a number of cracked specimen geometries and recommended that the mesh refinement must be

sufficient to represent the reversed plastic zone. In order to determine the minimum mesh refinement, an iterative approach was taken. The forward plastic zone r_p, shown in Equation (4-5), was used as a reference length to normalise the element length and the initial mesh was used to model the plastic zone with 3-4 elements. Each time the element size was reduced, the total crack growth length simulated was maintained. Consequently, this meant a higher number of load cycles were required as the mesh was refined. Only when a unique solution of the crack opening loads can be obtained, this result is then said to be independent of the finite element mesh size.

A secondary study was also done on the selection of element type. The selection of element types of PICC simulation is well established. Generally four-noded or higher order quadrilateral elements are used. However, under plane strain, these elements can be susceptible to plane-strain locking. When locking occurs, the stresses fluctuate wildly between two adjacent elements. Triangular elements in a “union-jack” configuration had been used to avoid this issue [55]. The model was meshed with four-noded, quadrilateral elements with different formulation, namely plane-stress (CPS4), plane-strain (CPE4), plane-strain with reduced integration (CPE4R) and generalised plane-strain (CPEG4).

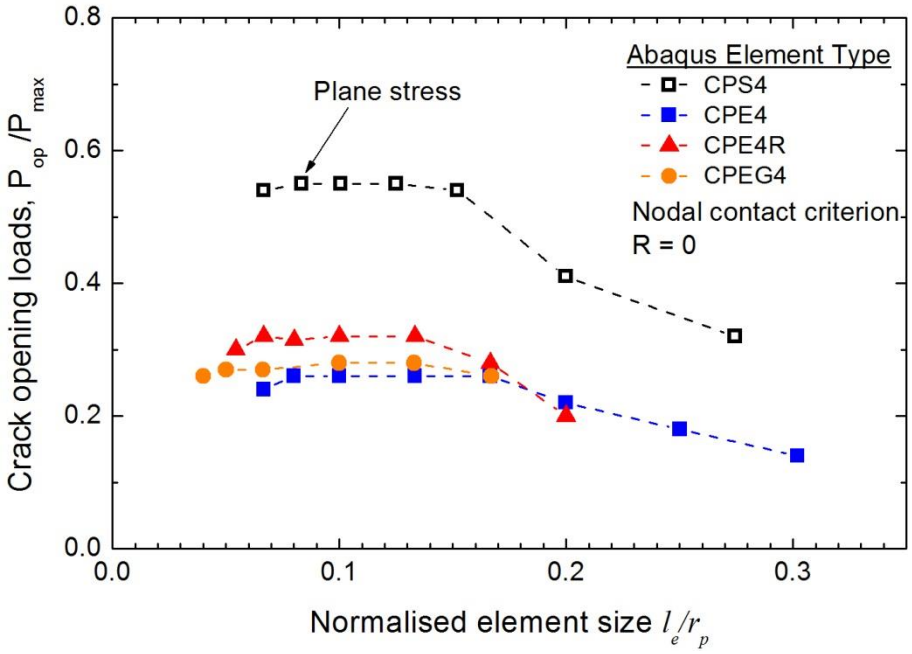

Figure 4-6: Crack tip mesh refinement study

The crack tip mesh was refined until a converged opening load was observed as shown in Figure 4-6. Under plane stress, the opening load converged at about 0.58 when $l_e/r_p < 0.16$. The plane strain opening load results showed convergence at $l_e/r_p < 0.14$. A higher opening load can be observed for the plane strain, reduced integration element.

This is due to the more “relaxed” stiffness nature of the element. The reduced integration scheme in Abaqus means that the integration scheme is one order less than the full integration and therefore decreases the number of internal constraints in the element such as incompressibility. The generalised plane strain elements allow a small amount of strain to occur in the out-of-plane direction. The opening load is almost identical to the opening load of the plane strain elements.

Further refinement of the mesh beyond $l_e/r_p < 0.07$ leads to a gradual decrease in the opening load values for both plane stress and plane strain. It is possible that the observed lack of convergence is an artefact of the crack growth algorithm as crack advance only occurs at a single point during the load cycle. This causes the crack tip element to experience excessive plastic deformation and strain locking occurs. Using a reduced integration formulation element did not improve convergence. This behaviour was also observed in PICC simulation in CT specimen [93, 94]. Therefore it is recommended to keep the mesh refinement range $0.07 < l_e/r_p < 0.16$ to avoid this issue.

4.5.2 Crack Propagation Scheme

The crack tip was incrementally propagated under the applied cyclic loading in order to develop the plastic wake. The numerical crack propagation was achieved by liberating the crack tip node from its constraint by changing boundary conditions between successive analysis steps. It should be noted that the modelling of the crack propagation was arbitrarily decided by the user and did not consider the stresses or strains of the crack tip node. There is no universal rule governing at what instance of the load cycle the crack tip node should be released. The crack tip node may be released at the minimum load, maximum load or during at any point in the loading/unloading cycle.

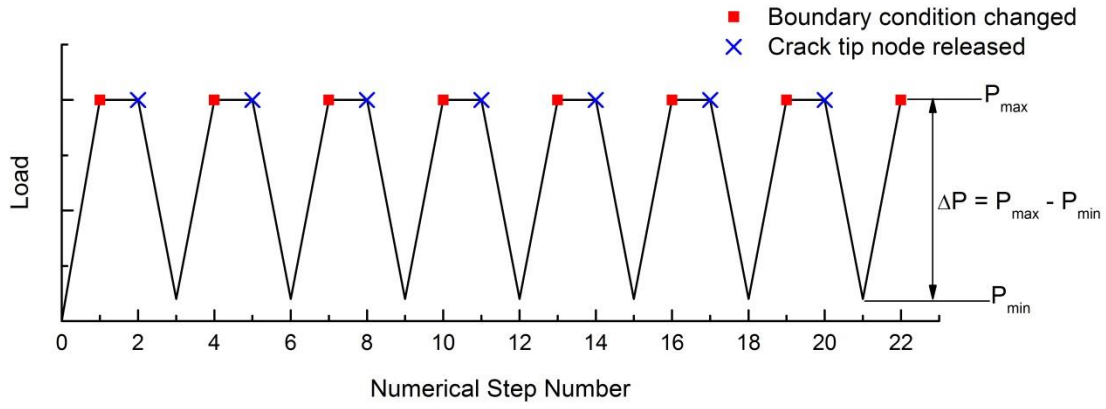

Figure 4-7: Crack propagation scheme used in this study

In this work, the crack propagation scheme was to advance the crack at P_{max} due to it having greater physical sense (the higher crack tip stresses, the more likelihood of crack growth). Since the actual unzipping and opening of the crack is a continuous process, a numerical stabilisation step was carried out to approximate this process, as shown in Figure 4-7. At the start of the step (e.g. step no. 2 in Figure 4-7), the boundary condition ($u_y = 0$) at the crack tip was removed. The released node would nonetheless remain closed and the boundary condition was replaced with a nodal force to maintain equilibrium. Therefore a constant, peak load was applied to the model. Subsequently, the released node opened as its nodal reaction forces equalled to zero prior to the unloading step.

4.5.3 Crack Extension for Stabilisation

From the initial crack tip position, the crack flanks are essentially free from any plastic deformation. Hence the results will not be representative of a growing crack. Under constant amplitude loading, the plastic wake develops from a transient state to a steady state as the crack propagates and, consequently, has a direct influence on the crack opening loads. Therefore the crack must be advanced for a determined amount of distance to allow the full development of the plastic wake.

Figure 4-8 shows that the crack opening values under plane strain condition is less sensitive to the total crack propagation length than plane stress. From the plane stress results, the crack opening results converges after it has propagate past the initial forward plastic zone, in agreement of the observation given by [90, 102]. Since the plane strain plastic zone is much smaller (approximately 1/3), the crack opening results quickly achieve a steady state.

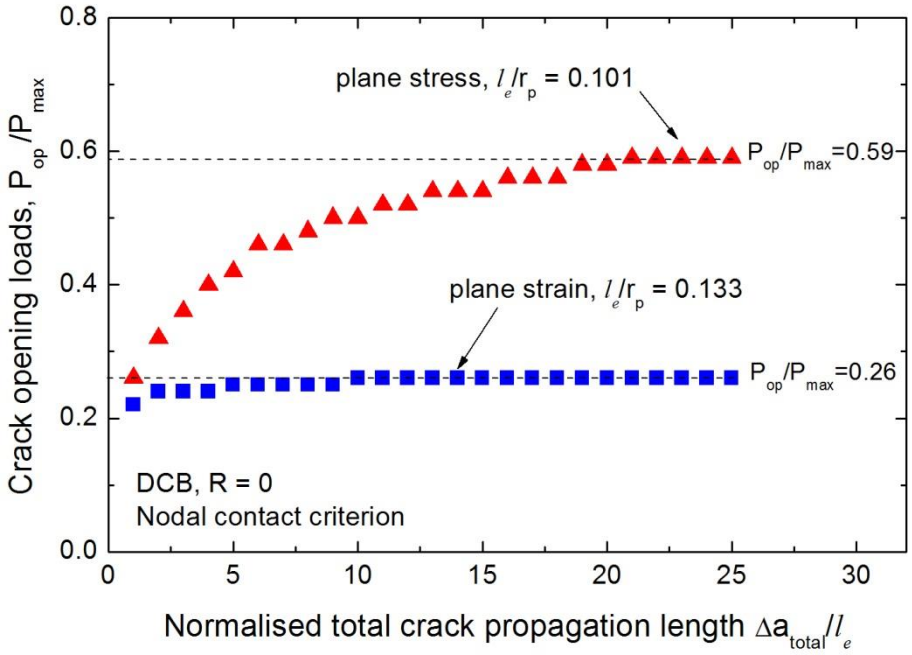

Figure 4-8: Stabilisation of crack opening results under plane stress and plane strain conditions

4.5.4 Crack Opening Assessment Criteria

Different crack opening assessment had been used to determine the crack opening loads and can be broadly categorised into a displacement [21, 55, 90, 92, 94, 95, 98, 102, 103] or stress [91, 104, 105] based criteria. The displacement based criteria is based on the nodal contact of the crack flank. The crack opening load is defined at the point which the assessment node is no longer in contact with a rigid surface along the crack plane during the loading phase. This criterion is typically used to determine the plane stress crack opening level. The assessment location, however, was varied between the works done. Most researchers used the first node behind the crack tip to assess the crack opening values due to observation that this node was the last to open. Others used the second node behind the crack tip [106]. Solanki et al. proposed a contact stress method which employs the entire crack surface nodal force distribution under minimum loading [106]. Since the contact stress criterion uses the entire crack surface, it is eliminates the need of deriving results from a particular node.

A stress based criterion, taken at the crack tip node, had been proposed by Sehitoglu and Sun [104] and Wu and Ellyin [91]. The crack opening load is defined when the crack tip nodal forces, perpendicular to the crack plane, overcome compressive stress during the loading segment of the load cycle. This criterion is based on the premise that crack propagation cannot occur under compressive stress fields behind and ahead of the

crack tip since the nucleation of micro-cracks is dependent on tensile stresses. From past works, both numerical and experimental measurements of crack closure indicated that the crack opening loads is dependent on the assessment location; the closer the assessment location to the crack tip the higher the crack opening loads. Hence Wu and Ellyin [91] argued that while the node behind the crack tip is open, the area between the crack tip and assessment node may not be fully open. This criterion had been used to determine crack closure under plane strain by [93, 95, 104, 105].

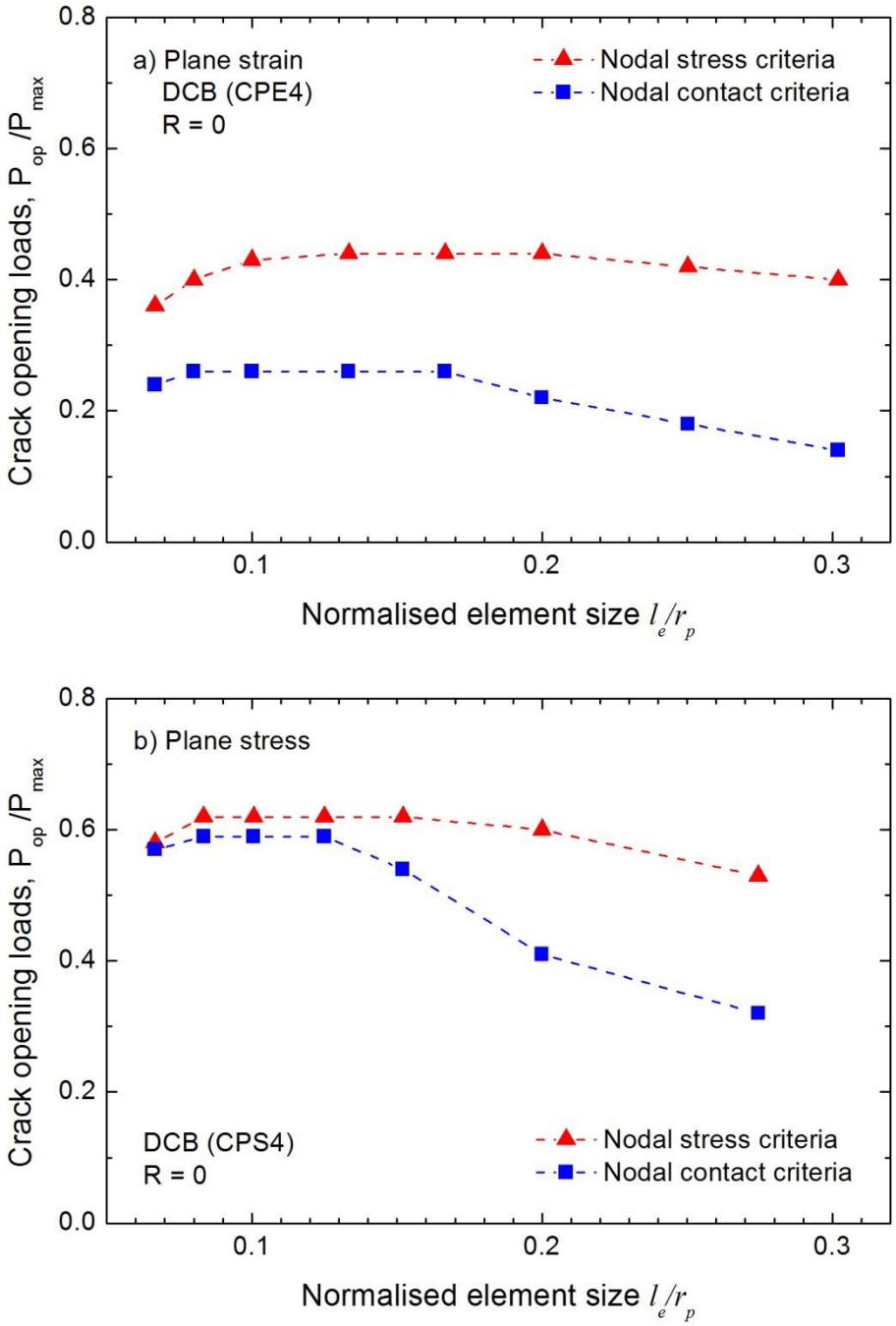

Figure 4-9: Comparison of predicted crack opening values using different crack opening criteria under a) plane strain and b) plane stress

A comparison of the two criteria was done and the results presented in Figure 4-9. Under plane strain idealisation, significant difference can be observed between the two criteria. This has also been reported in [104, 105]. When the criteria are use under plane stress, the crack opening value using either criterion converges. As the area which the crack wake closes under plane stress is large, it is less sensitive to either of the criteria used. This also validates the statement made by Wu and Ellyin. Since the plane strain crack closure area is very small, the results of the nodal contact criterion are more sensitive to the assessment location.

4.5.5 Summary of Numerical Parameters Selected

Steps were taken to analyse varying FE parameters which can potentially affect the results of the crack closure analysis in a bonded DCB joint. Each parameter was explored and the selected parameter rationalised. In summary,

- The crack tip mesh was selected to be $l_e/r_p = 0.133$ to ensure sufficient elements and to avoid excessive distortion as a result of overly small elements.
- Crack propagation occurred at P_{max} as it had a more physical meaning to it.
- The total crack length propagated simulated was $25l_e$ to ensure a converged opening load value was attained.
- Crack closure was first determined by the contact of the first node behind crack tip. When this condition was satisfied, the exact closure level was determined by the nodal stress criterion as this gave a more accurate representation of the closure level especially under plane strain.

4.6 Results

The results of elastic-plastic analysis of fatigue crack closure in a bonded joint are presented in the following section. In order to further our understanding, analyses on load ratios, bondline thickness, substrate to adhesive stiffness ratio, load history etc… were carried out.

4.6.1 Mechanism of Crack Closure

In order for PICC to occur, additional material volume must be transferred to the crack flanks as a result of plastic deformation. A 3-D analysis was carried out, taking the specimen width into consideration. Under plane stress idealisation, the mechanism of

material transfer to the Y-axis direction is the plastic contraction of the material in the out-of-plane (Z-axis) direction as it is not constrained ($\sigma_Z = 0$) as shown in Figure 4-10b below.

Figure 4-10a shows the additional material volume to form the plastic wake under plane strain is primarily contributed from plastic strain in the lateral (X-axis) direction. The plane strain assumption meant that no out-of-plane deformation can occur. The total residual strains in the x-direction are rather small from the crack tip due to the elastic constraint of the surrounding material. Hence the plastic zone under plane strain is much smaller than plane stress. It can also be seen that the forward plastic zone under plane strain is approximately a third of the plane stress plastic zone.

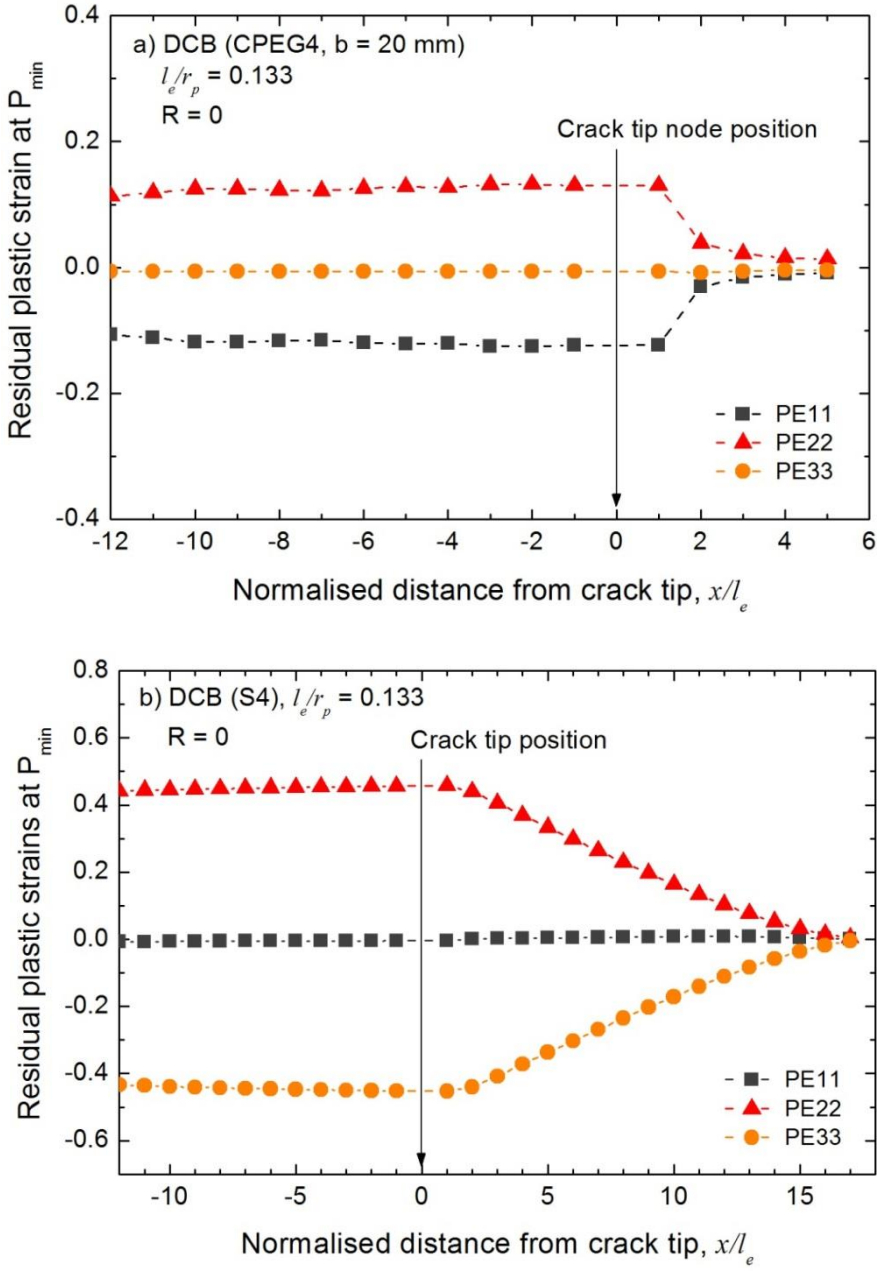

Figure 4-10: Residual plastic strain under a) plane strain and b) plane stress condition

4.6.2 Influence of Maximum Applied Strain Energy Release Rate G_{max}

The parameter G_{max} controls the size of the plastic zone. Therefore a range of maximum applied loads from G_{max} = 100 to 800 J/m^2 was applied to analyse its influence on the crack closure behaviour. The range of G_{max} analysed covers the range of maximum applied loads within the region of stable fatigue crack growth in bonded joints. For a nominal bondline thickness of 0.2 mm and a crack path at the mid-plane, the height of the plastic zone remained unconstrained. The crack tip mesh was varied in order to maintain a constant mesh density l_e/r_p. The results, in Figure 4-11, show that no variation in the crack opening loads with respect of the applied maximum loads. Therefore it can be concluded that the crack opening loads derived from a particular load is applicable to the entire load range in the fatigue experiment.

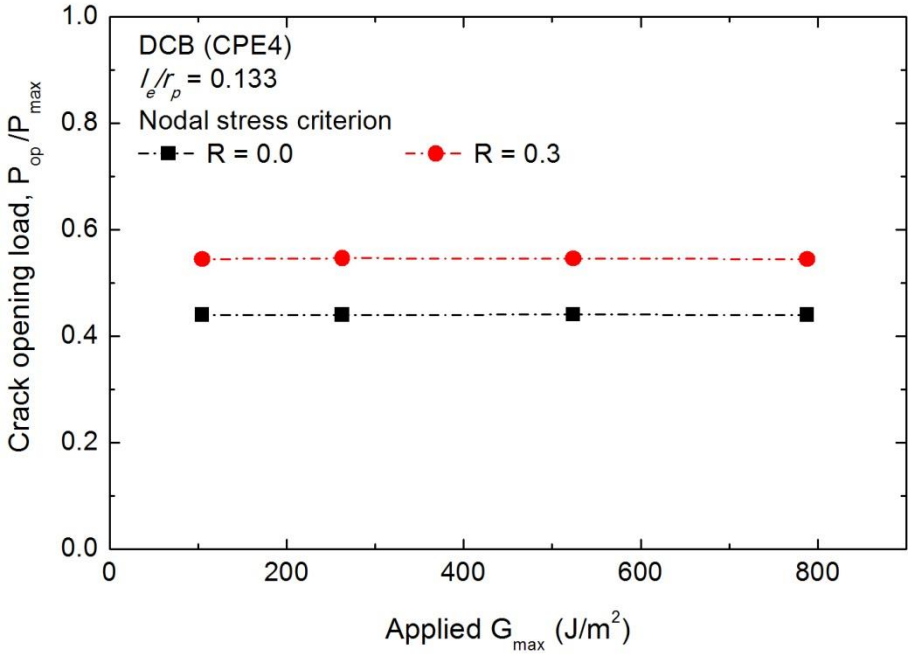

Figure 4-11: Influence of G_{max} on the plane strain crack closure behaviour in a DCB bonded joint

4.6.3 Ratio of Bondline and Substrate Stiffness

A comparison of the isotropic and bonded DCB joint was done by varying the substrate stiffness. The stiffer substrate may cause the plasticised adhesive material to undergo higher reverse yielding and possibly affect the crack opening value as it compresses the plasticised material. The maximum load was varied so that the number of elements in the forward plastic zone remains constant. In Figure 4-12, the crack opening load is observed

to be independent on the substrate stiffness. The plastic zone remained unconstrained at the applied load level. This also confirms that small scale yielding conditions are valid in bonded joints.

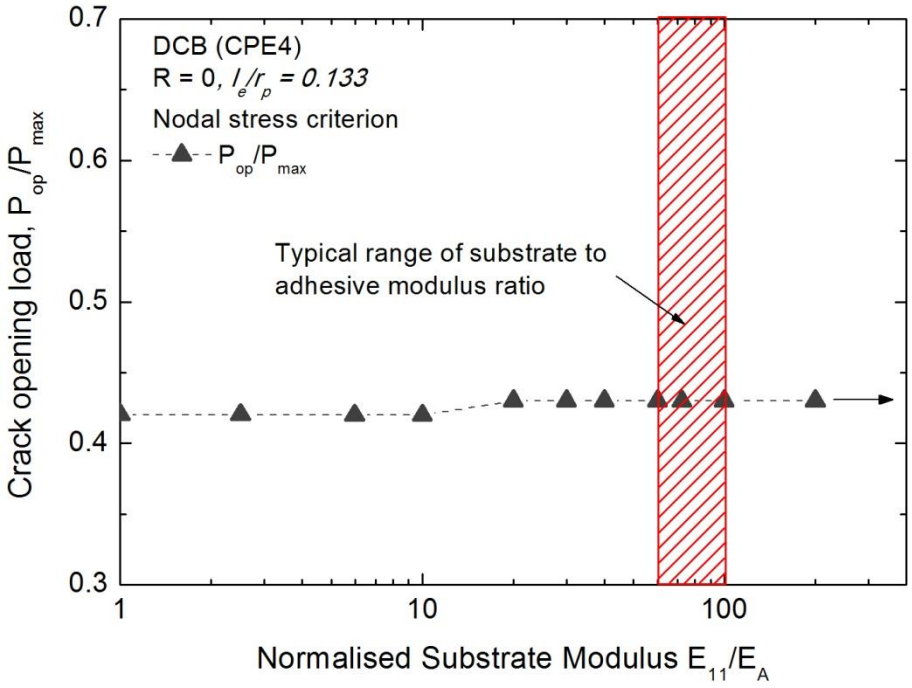

Figure 4-12: Influence of substrate stiffness on the crack opening behaviour

4.6.4 Load Ratio

The following analysis investigated the influence of load ratio on the crack closure behaviour in a bonded DCB joint. The load ratio is an important parameter as a result of the influence of the minimum load in the developing plastic wake. Several empirical closed form expressions had been proposed by different researchers to represent the load ratio effect on crack closure in the fatigue behaviour of metals. Newman's analytical estimate of crack opening stress was used to compare with the numerical results. The following equations were fitted to the crack opening stresses from the numerical simulation of a centre crack tension specimen,

$$\frac{\sigma_{op}}{\sigma_{max}} = \begin{cases} A_0 + A_1 R + A_2 R^2 + A_3 R^3 & for\ R \geq 0 \\ A_0 + A_1 R & for -1 \leq R \leq 0 \end{cases} \quad (4\text{-}6)$$

where

$$A_0 = 0.825 - 0.34\alpha + 0.05\alpha^2$$

$$A_1 = 0$$

$$A_2 = 1 - A_0 - A_1 - A_3$$

$$A_3 = 2A_0 + A_1 - 1$$

The numerical results of the crack opening load for a bonded joint and an isotropic DCB specimen, shown in Figure 4-13, are identical under positive *R* values. No further crack closure is observed for *R > 0.7* in both cases. Under negative *R*, the crack opening loads is lower for the bonded joints and remained constant for *R < -0.4*. The substrate, being stiffer than the adhesive, causes the plastic wake to experience a higher compressive strain. Consequently the crack opening load is lower. It is reasonable to conclude that the crack closure behaviour of *R < -0.4* is insensitive to the compressive stresses as a result of contact of the crack wake in this case. This analysis has shown that small scale yielding conditions are valid in the fatigue debonding of the DCB specimen.

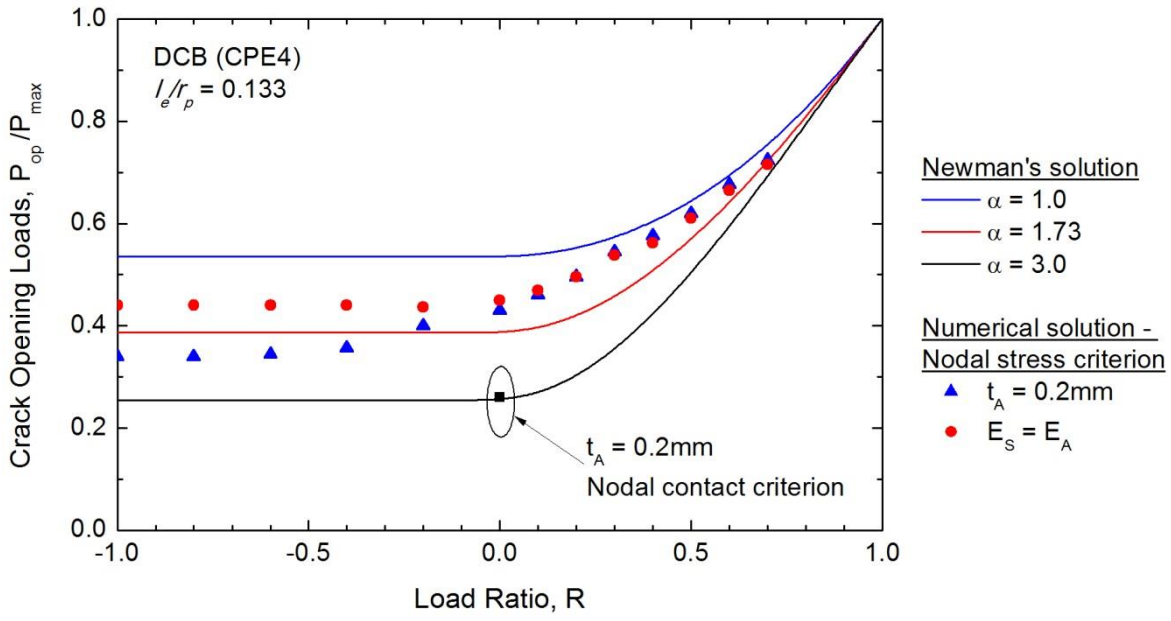

Figure 4-13: Influence of load ratio on the crack opening load value

The nodal contact criterion derives a crack opening load that coincides with Newman's analytical solution for *α = 3*. The crack opening loads given by the nodal contact criterion is lower than the crack tip stress criterion. Under plane-strain conditions, since the plastic wake extends to a small area, the use of displacement criterion can lead to large fluctuations in the crack opening loads. At higher load ratios, further mesh

refinement is needed to accurately evaluate the crack opening loads by the nodal contact criterion. However this leads to excessive deformation at the crack tip element and other issues mentioned earlier. Hence the nodal contact results may not be reliable. Moreover numerical studies done by Newman et al. showed that a constraint factor of 1.73 is more representative of an actual structure [107]. The crack opening loads obtained using the nodal stress criterion are closer to the analytical solution for $\alpha = 1.73$. The results from R = 0.3 to 0.5 is observed to be closer to $\alpha = 1$ of the Newman's approximation.

4.6.5 Vertical Positioning of Crack Tip

Crack propagation within a bondline is unlikely to occur in the middle of the bondline in a bonded joint. For example, the crack plane is more likely to be closer to one of the substrates for an ENF specimen. The non-symmetrical condition implies that the crack will not experience a purely Mode I or II condition. Hence this analysis investigated the vertical positioning of the crack tip effect on the crack opening loads. A full model was used in this analysis, shown in Figure 4-14, as symmetrical conditions were not maintained in the analyses. The bottom and top substrate were connected using Abaqus TIE constraint. Along the crack propagation path, zero thickness interface elements with a traction stiffness of 10^9 N/mm^3 were employed to "connect" the upper and lower surfaces. Advancing the crack was achieved by deleting the appropriate traction element. All other modelling aspects are as prescribed in the modelling methodology section.

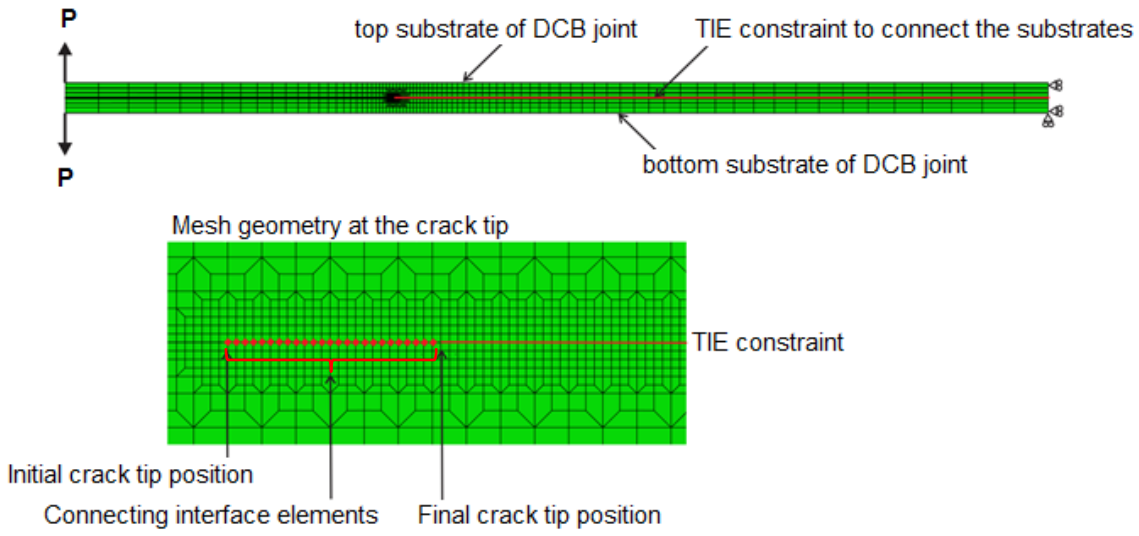

Figure 4-14: Schematic of a full finite element model of a bonded DCB joint

The result of the FE analysis is shown in Figure 4-15. The crack opening value based on the nodal stress criterion is observed to be relatively independent on the

vertical positioning of the crack. The crack opening value derived using the nodal contact criterion is also investigated. A gradual increase of the crack opening value can be observed with this criterion as the crack approaches the substrate-adhesive interface. This increase can be attributed to the increase in plastic deformation on the constrained side of the plastic zone, causing an increase in the crack opening load.

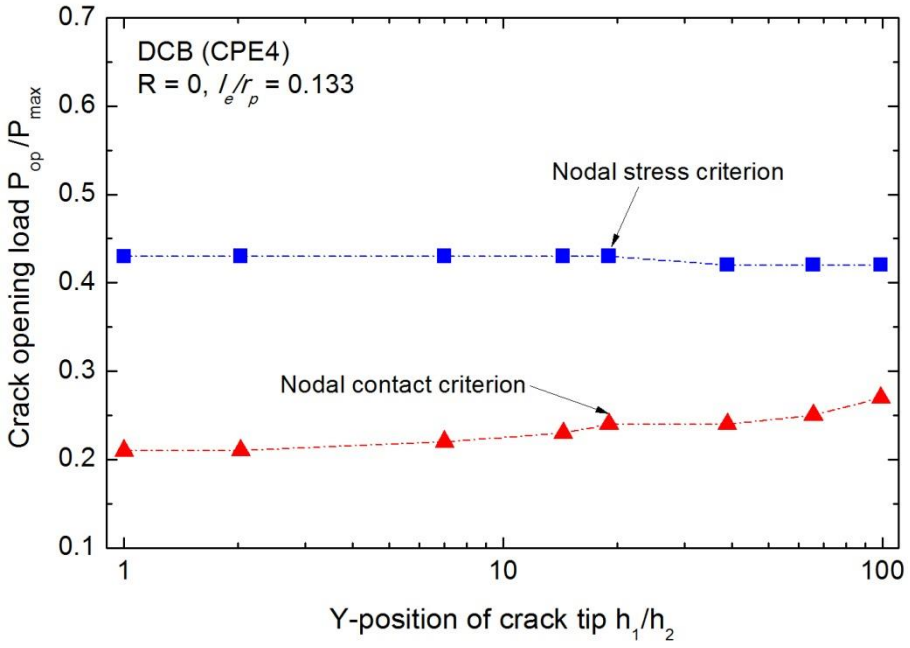

Figure 4-15: Influence of vertical position of crack tip on the crack opening load

It is important to note that the non-symmetrical condition of the crack position actually introduces a small amount of Mode II loading. However the Mode II component is very small. Therefore the crack propagation mode can still be considered to be under Mode I. The same can be applied to the ENF specimen. This finding is in agreement with the findings of Suo and Hutchinson [108].

4.6.6 Bondline Thickness

When the thickness of the adhesive is sufficiently small, the height of the plastic zone becomes constrained by the substrates. An analysis was undertaken to investigate the crack opening load behaviour when small scale yielding conditions may no longer be valid. The crack was assumed to propagate in the middle of the bondline and the substrate thickness was kept constant at 1.56 mm. Constrained plasticity was defined when the unconstrained plastic zone height is greater than the bondline thickness, given as $2r_y/t_A > 1$.

The results of the crack opening loads with respect to changes in the bondline thickness are presented in Figure 4-16. The results based on the nodal contact criterion shows a gradual increase in the crack opening values as the level of constraint increase. In using the nodal stress criterion, the crack opening loads is observed to be independent of the bondline thickness at R = 0 and 0.5

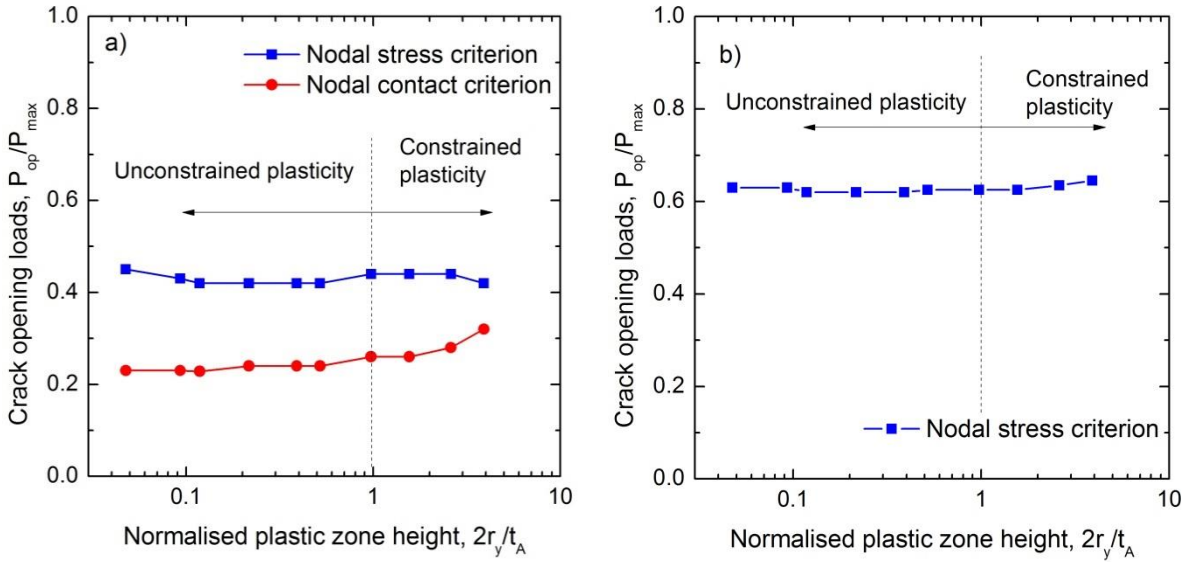

Figure 4-16: Influence of bondline thickness on the crack opening values

4.6.7 Influence of Load History

The primary interest of crack closure analysis is to consider the load interaction between load cycles under variable loading. Complex load histories are difficult to simulate with FE methods due to it being computationally intensive. Each cycle must be exactly simulated with the element size being the crack growth per cycle. However, efforts have been directed towards simple load histories (i.e. single overload) to provide a mechanistic explanation for crack growth retardation or acceleration [65, 109-111].

A single overload was applied at the 10th cycle and further followed by cycles of constant amplitude (equal in magnitude prior to the overload event). It is observed in Figure 4-15 that an abrupt decrease in the opening loads in the cycle immediately after the overload event. Similar behaviour was also been reported by Nakagaki et al. [65, 109] This decrease in the opening load is attributed to the increase in crack blunting due to the single overload. After this, the crack opening load increases to a peak value of P_{op}/P_{max} = *0.68* before it gradually decays back to the original value 28 cycles after the overload event. Therefore the effective SERR experiences a sudden jump immediately after the

overload and then decreases below its original value prior to the overload. This indicates the presence of crack growth retardation in this case. This behaviour is identical with the isotropic DCB. This paves the way of possibly using FASTRAN [39] to predict the crack growth of a bonded DCB under VA Mode I loading.

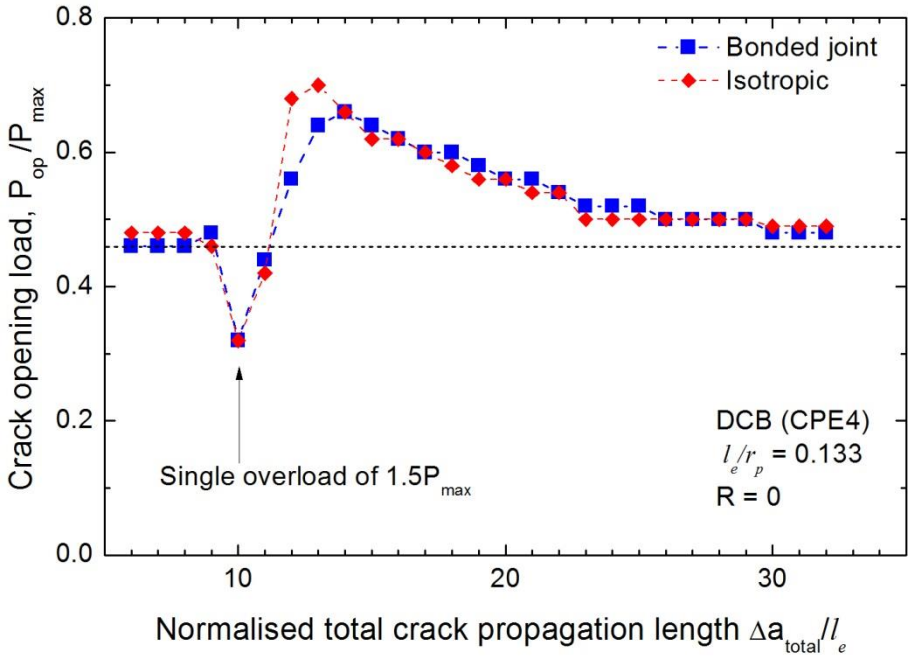

Figure 4-17: Crack closure behaviour after a single overload of 1.5 times P_{max}

4.6.8 Mode II Loading Conditions

The Mode II fatigue data obtained experimentally (Chapter 3.3.4) and from literature (Chapter 2.4.1) showed that the ΔG_{eq} parameter is able to successfully account for load ratios. Therefore crack closure is presumed to be absent under Mode II. FE simulation of the plastic wake under Mode II was carried out to confirm this hypothesis. A three point bend ENF specimen was used to carry out the FE simulation, as shown in Figure 4-18, to replicate the experimental work. The roller supports were modelled as rigid bodies. A friction coefficient of 0.3 was assigned to the contact surfaces between the roller supports and specimen surfaces. This was done to prevent the specimen from “floating away in space”. The crack was assumed to propagate in the middle of the bondline. A full model was employed and the modelling techniques are prescribed in Section 4.5 and 4.6.5.

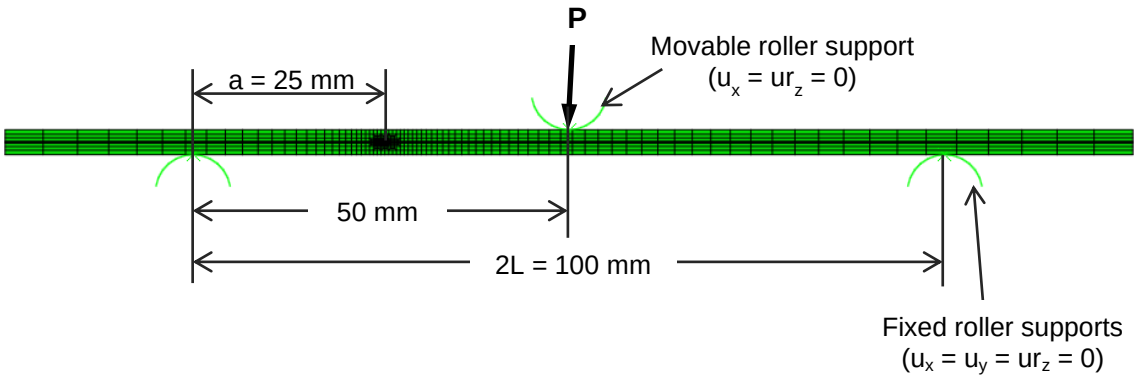

Figure 4-18: Schematic and boundary conditions of a three point ENF bonded joint

The computed shape and size of the plastic zone near the crack tip are shown in Figure 4-19. The shape of the plastic zone under Mode II is different to the Mode I plastic zone. The applied load was 8.4 N/mm and the resultant G_{II} was equal to 144 J/m^2. This was enough to ensure the plastic zone is discretised by at least 10 elements. The crack profile has an uneven surface due to the plastic wake. This will likely to result in roughness induced closure and hence its influence was analysed to determine if it was significant enough to affect Mode II crack growth rates.

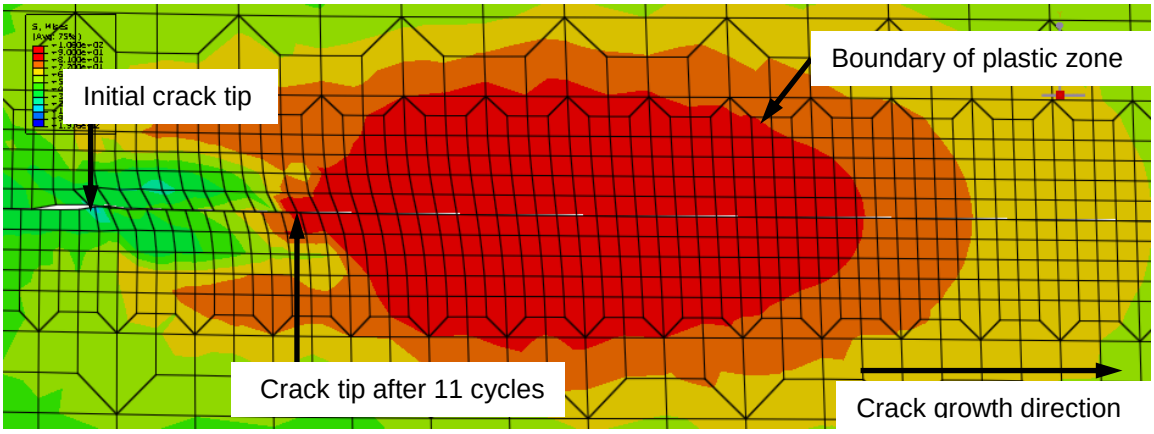

Figure 4-19: Crack profile and plastic zone under mode II loads after 11 cycles

In Figure 4-20, the crack opening displacements of the node immediately behind the crack tip is plotted. It was seen that after propagating the crack for 11 cycles, the normal displacement of the crack remained closed at all times during the load cycle. Therefore no plasticity induced crack closure was observed. This is in agreement with the Mode II crack propagation of isotropic materials [65].

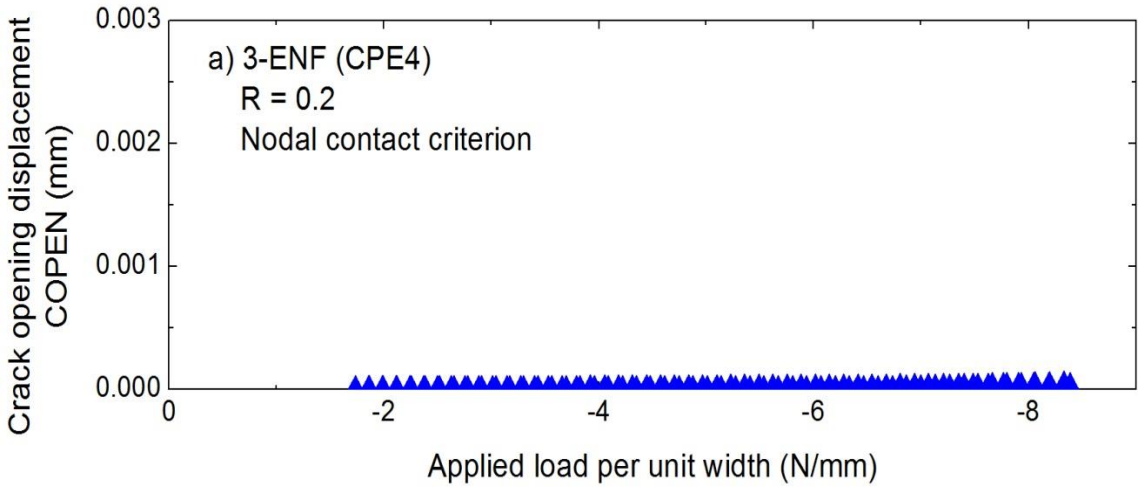

Figure 4-20: Crack opening displacement during a load cycle after 11 cycles

The crack faces are pressed together under Mode II loading in the ENF specimen. Consequently, friction effects will occur. Although the actual friction coefficient is difficult to assess in real-world situation, FE analysis can provide an insight of its influence on roughness induced closure under Mode II loading. A stationary crack length of 25 mm was analysed using the virtual crack closure technique (VCCT) [112]. VCCT assumes the energy required is equal to that required to close the crack back to its original length. The SERR is calculated based on the nodal forces and displacements as shown in the Equation (4-7) and (4-8) for a 2-D, four-noded element. The schematic of the nodal forces and displacement used in the calculation is shown in Figure 4-21.

$$G_I = \frac{1}{2\Delta a} Z_i (w_l - w_{l*}) \tag{4-7}$$

$$G_{II} = \frac{1}{2\Delta a} X_i (u_l - u_{l*}) \tag{4-8}$$

where Z_i and X_i is the nodal forces acting on node I in the x and z direction, w and u is the nodal displacement in the z and x direction respectively on the nodes denoted by the subscript and Δa is the element length.

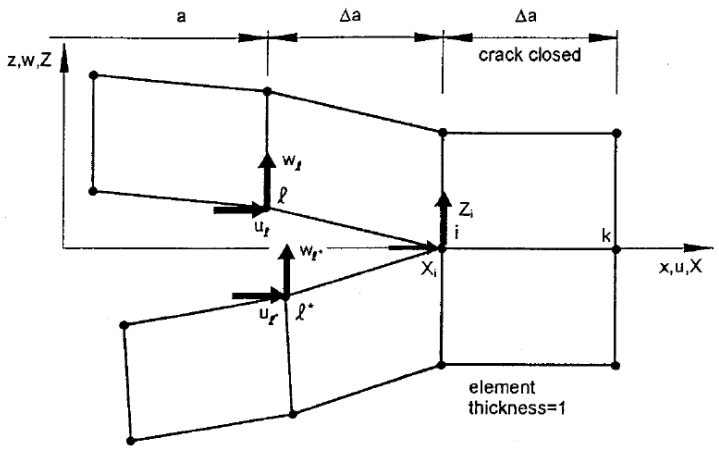

Figure 4-21: Schematic of the nodal forces and displacements for determining the SERR with a four-noded element using the VCCT approach [112]

The influence of the friction coefficient on the mode II strain energy release rate is presented in Figure 4-22. Friction reduces the stress experienced at the crack tip. Hence G_{II} is observed to gradually reduce as the friction coefficient increases. In the extreme case of $\mu = 0.8$, a reduction of 5% in the G_{II} is observed. Therefore it can be concluded that roughness induced closure and friction has minimum effect on the G_{II}. Mall et al. observed a pronounced effect for friction when the crack tip is in the vicinity of the support pins [64]. Therefore it is advisable to avoid obtaining fatigue crack propagation data at these regions.

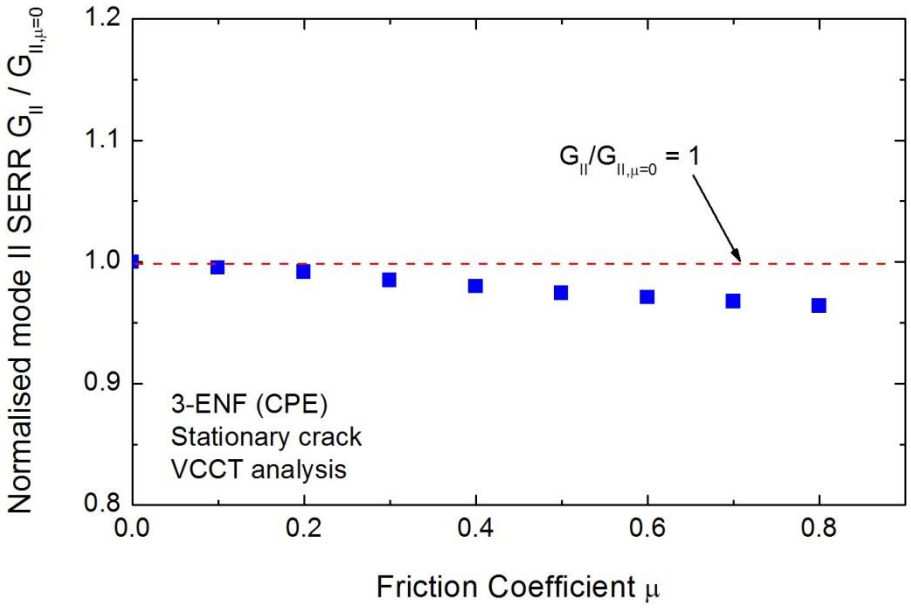

Figure 4-22: Influence of friction on the crack tip strain energy release rate under Mode II loading conditions

In summary, the phenomenon of crack closure was not observed in the numerical modelling of a 3-ENF bonded joint. Although the roughness of the crack profile may introduce roughness induced crack closure, the influence of friction on the fatigue crack growth is trivial. In the study of the more general problem of crack growth under mixed-mode loading which causes small scale yielding near the crack tip, crack-closure effects need only be considered for the Mode I component. It should be noted that dry friction may not completely model the effect of roughness or crack face asperities closure. Suresh and Ritchie [99] reported that roughness/asperities induced crack closure can affect the Mode II crack propagation of metallic alloys, particularly in the threshold region. Further investigation of the Mode II threshold behaviour can be conducted. If the effect of load ratio is found to be significant, the influence of roughness/asperities induced crack closure must be more thoroughly studied.

4.7 Correlation with Experimental Data

4.7.1 Load Ratio Effects in Mode I

The crack closure concept is used to characterise the load ratio dependency behaviour observed in Mode I fatigue disbond growth when similitude conditions are maintained in the definition of the correlating parameter. Based on the numerical results presented in the previous section, a new correlating parameter is defined as shown,

$$\Delta G_{eff} = \left(\sqrt{G_{max}} - \sqrt{G_o}\right)^2 = G_{max}\left(1 - \frac{P_{op}}{P_{max}}\right)^2 = \Delta G_{eq} U^2 \qquad (4\text{-}9)$$

where the parameter U denotes the effective load range ratio and is given as,

$$U = \frac{\Delta P_{eff}}{\Delta P} = \frac{P_{max} - P_{op}}{P_{max} - P_{min}} = \frac{1 - P_{op}/P_{max}}{1 - R}$$

It is worth noting that the relation given by Equation (4-9) is consistent with the definition of effective stress intensity range $\Delta K_{eff} = U\sqrt{\Delta G_{eq} E}$. Under Mode II, the numerical results show crack closure is absent. Therefore the effective load range ratio U_{II} is equal to 1 regardless of R and $\Delta G_{II,eff}$ is same as $\Delta G_{II,eq}$. The effective load range ratio U_I, under Mode I, is derived from the numerical results and is shown in Figure 4-23.

U_I is better correlated to the analytical solution of $\alpha = 1.73$ for $R \leq 0$. At increasing positive R, the numerical results of U_I is between the analytical solution of $\alpha = 1$ and 1.73. Although at load ratio between 0.3 and 0.6, the results are better correlated with $\alpha = 1$.

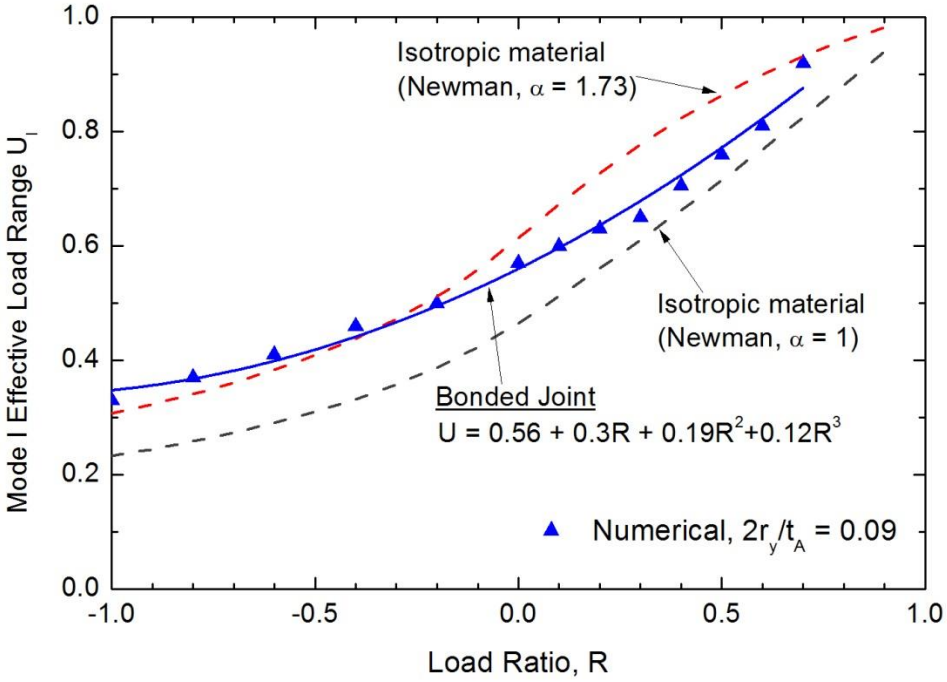

Figure 4-23: Effective load range ratio for a bonded DCB joint

To provide an approximate, closed form expression for the Mode I effective load range ratio U_I of a bonded joint, the numerical results in Figure 4-23 were curve-fitted using a cubic expression and is given below,

$$U_I = A_0 + A_1 R + A_2 R^2 + A_3 R^3 \qquad for -1 \geq R \geq 1 \tag{4-10}$$

where

$$A_0 = 0.56$$

$$A_1 = 0.3$$

$$A_2 = 0.19$$

$$A_3 = 0.12$$

This expression furnishes a convenient solution for bonded joints subjected to Mode I fatigue loading. The crack closure concept is employed to quantify the mean load

dependency of the mode I experimental results presented in Section 3.3.2 using ΔG_{eq} as the correlating parameter. As shown in Figure 4-24, the mean load dependency is now completely eliminated. If the plastic zone size is negligible with all dimensions including the bondline thickness, it is possible to use other analytical approaches besides Newman's method to evaluate the crack closure effect in bonded joints under small scale yielding [113-115]

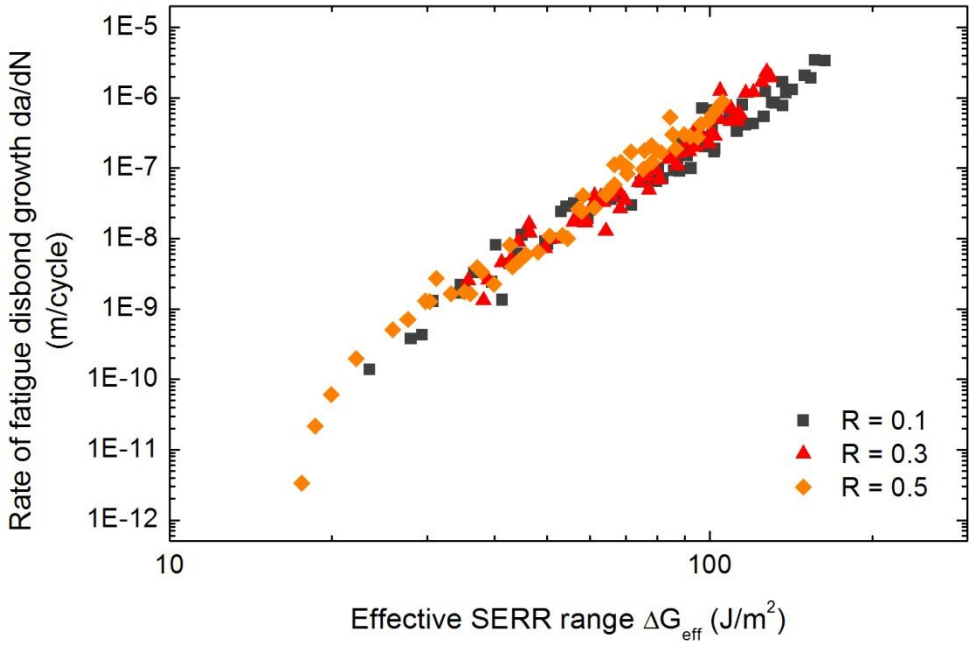

Figure 4-24: Experimental results of FM300-2K adhesive correlated with ΔG_{eff}

In order to verify the robustness of this correlating parameter, the crack closure model is also applied to the Mode I experimental results reviewed in Chapter 2. The results are plotted in Figure 4-25. The fatigue disbond growth data in Figure 4-25 (b, d) can be collapsed into a narrow band whereas Figure 4-25 (a, c) still display a substantial load ratio dependency.

Although the Paris law relationship took account of the effective load ratio induced by crack closure, it cannot account for the instability of the crack growth as the applied load approaches its critical fracture value. The Forman equation is extended to the crack closure concept and expressed as,

$$\frac{da}{dN} = \frac{C_F\left(\Delta G_{eff}\right)^{m_F}}{(1-R)\left(\sqrt{G_C} - \sqrt{G_{max}}\right)} \tag{4-11}$$

where G_C is the critical fracture toughness of the adhesive, C_F and m_F are the material constants from the Forman model. A unique value of C_F and m_F must be obtained in order for the Forman model to be valid.

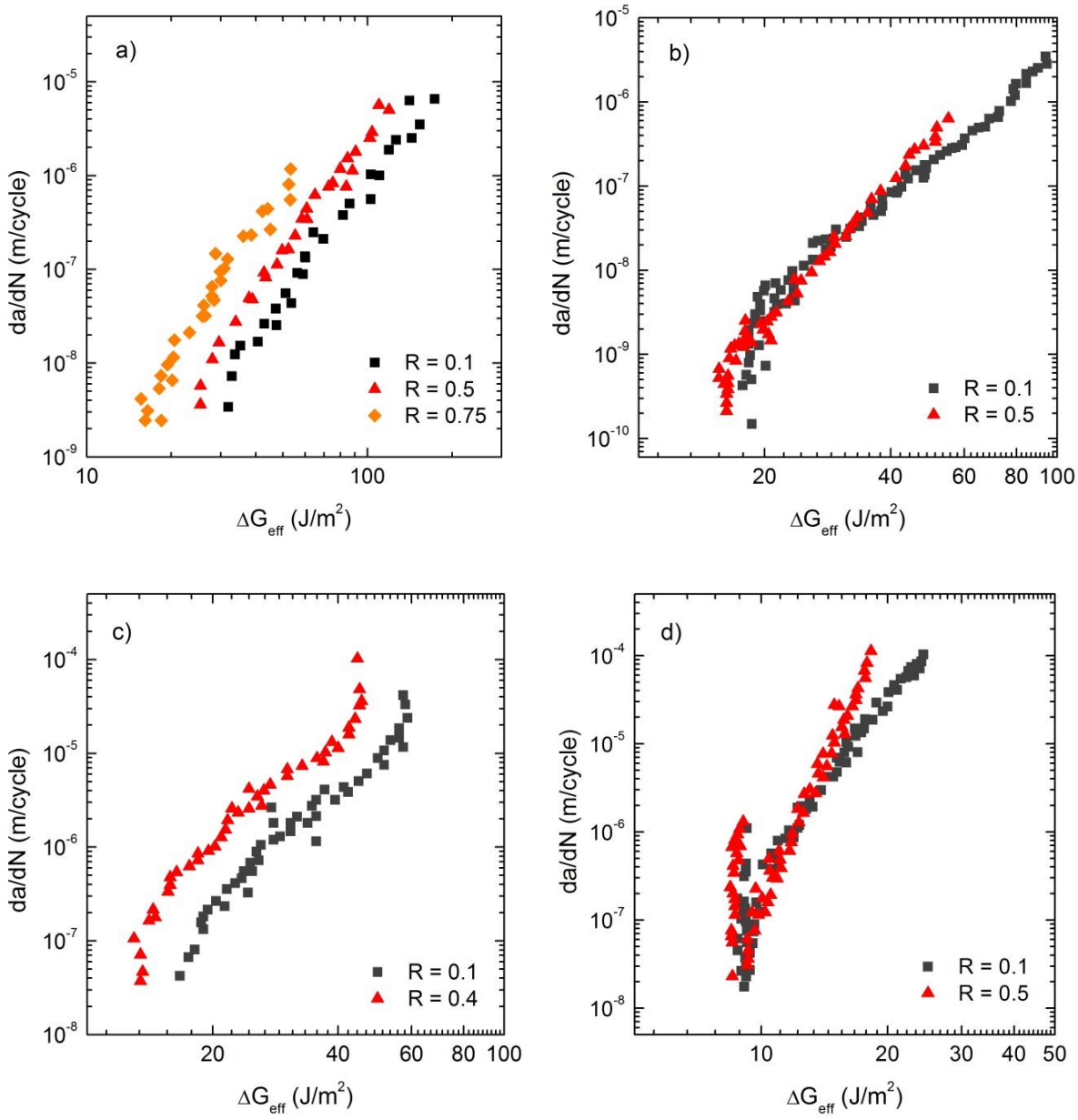

Figure 4-25: Experimental correlation with data from literature; a) EC-3445 [52], b) Cytec 4535A [28], c) Multibond 330 [53] and d) Toho 111 interleaved [54] adhesives

Figure 4-26 show the fatigue disbond growth data taken from literature plotted with the Forman model. The critical fracture toughness G_C of the adhesives are reported in [28, 54, 56, 116]. The Forman model is able to collapse the fatigue disbond growth trends into a narrow band. Therefore the Forman model is valid and a unique C_F and m_F

can be obtained across a range of *R*. Consequently a single threshold SERR range can be obtained for which a bonded joint or repair can be designed to satisfy the no- or slow-growth criterion.

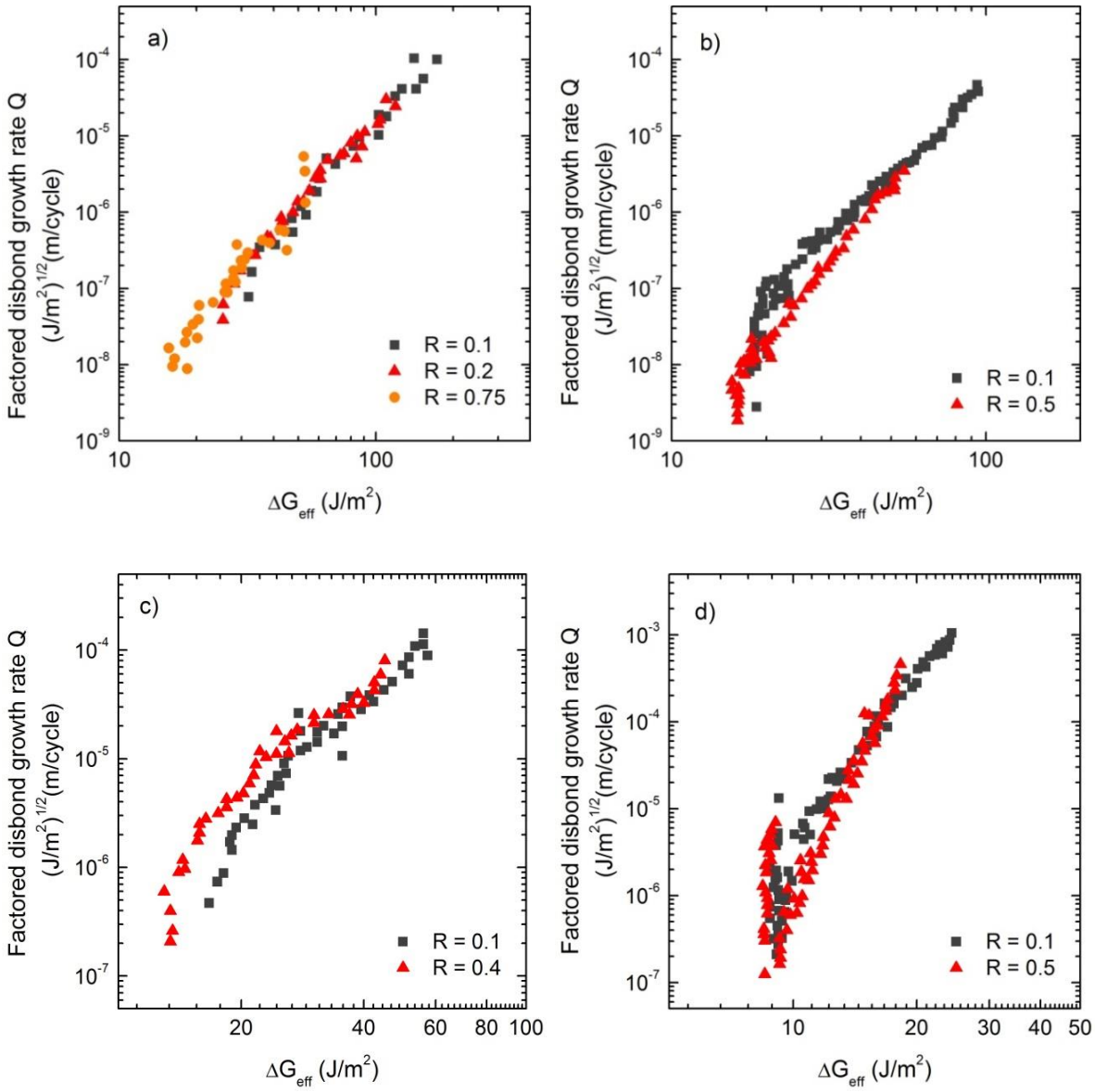

Figure 4-26: Experimental correlation with results of Mode I fatigue debonding of a) EC-3445 [52], b) Cytec 4535A [28], c) Multibond 330 [53] and d) Toho 111 interleaved [54] adhesives plotted with the Forman equation

It can now be concluded that the new correlating parameter, which accounts for load ratio effects using plasticity-induced crack closure model, is able to unify disbond growth rates under different load ratios for both Mode I and II crack propagation modes. This makes it possible to predict fatigue lives of bonded joints under variable amplitude or

spectrum loadings. This new finding paves the way for applying the plasticity-induced crack closure model, with appropriate treatment of the constraints imparted by the stiff substrates, to analyse the load interactions between load cycles and developing a predictive model for determining the disbond growth in bonded joints under spectrum loading.

4.7.2 Mode I and II

The experimental results of the Mode I and II fatigue crack growth rates are plotted in Figure 4-27 against the ΔG_{eq} parameter. It can be seen that ΔG_{eq} was unable to correlate the experimental data of the two mixed mode ratios. The fatigue resistance under Mode I loads is significantly lower than Mode II.

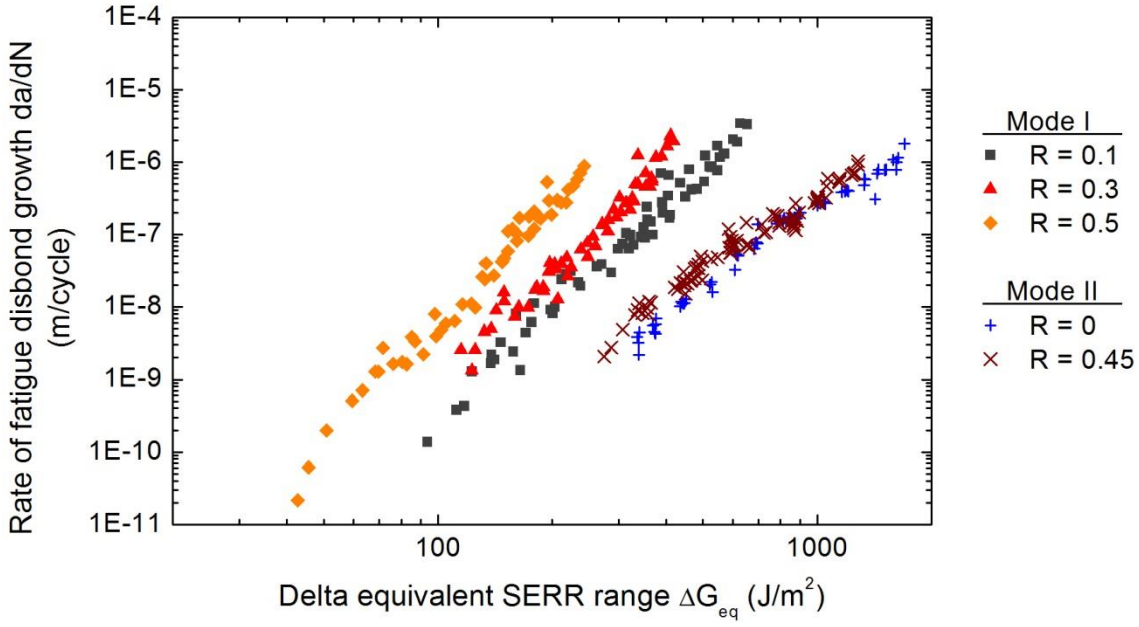

Figure 4-27: Mode I and II fatigue disbond growth rates of FM300-2K adhesive

In order to account for mode mixity, the following equivalent mixed mode strain energy release rate was proposed by Cheuk et al. [69] and is given as,

$$\Delta G_{m,eq} = \Delta G_{I,eq} + \left(\frac{G_{IC}}{G_{IIC}}\right)\Delta G_{II,eq} \tag{4-12}$$

where G_{IC} and G_{IIC} are the Mode I and II critical fracture energy. From Section 3.3.2, the respectively G_{IC} and G_{IIC} of the FM300-2K adhesive were given as 1660 J/m^2 and 6000 J/m^2.

It can be seen in Figure 4-28 that the Mode I and II data are still significantly influenced by the load ratio and mixed mode ratio when plotted against $\Delta G_{M,eq}$. The Mode II data is now shown to have lower fatigue crack growth resistance. This behaviour is not surprising as the Mode I debonding rates are affected by crack closure. Consequently this will result in an artificially higher Mode I fatigue resistance.

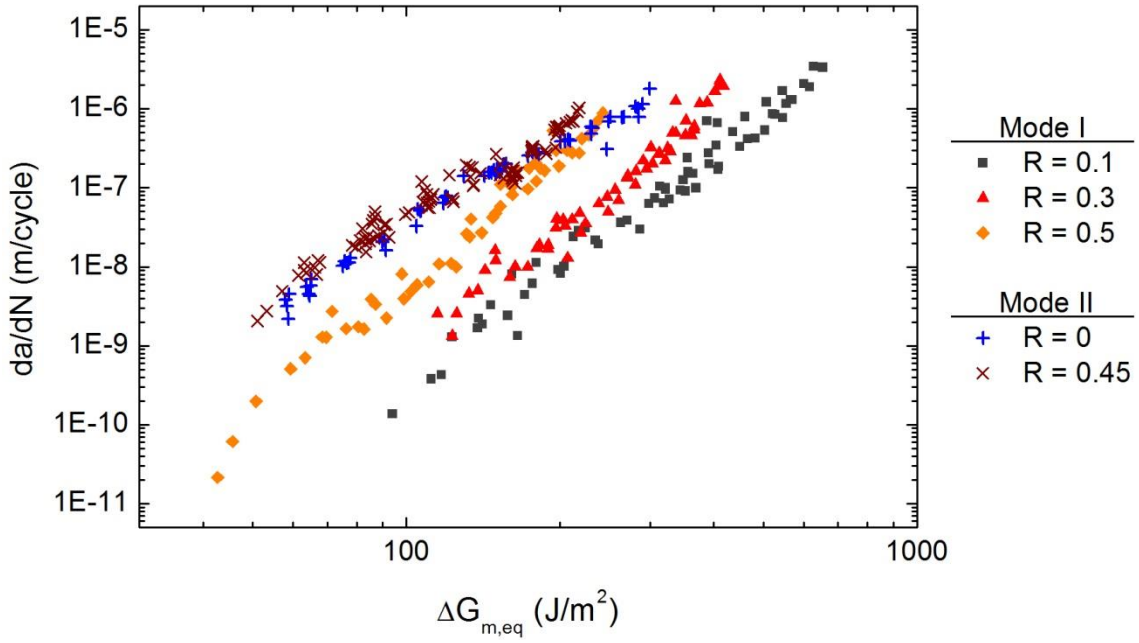

Figure 4-28: Mode I and II fatigue disbond growth rates of FM300-2K adhesive versus $\Delta G_{m,eq}$

Therefore Equation (4-12) was modified to account for crack closure and is expressed as,

$$\Delta G_{m,eff} = \Delta G_{I,eff} + \left(\frac{G_{IC}}{G_{IIC}}\right)\Delta G_{II,eq} \tag{4-13}$$

where $\Delta G_{I,eff}$ is the effective Mode I cyclic SERR range when the crack is fully open, given in Equation (4-9). Since crack closure does not affect the Mode II crack propagation, as shown in Section 4.6.8, the Mode II component $\Delta G_{II,eff}$ is simplified into $\Delta G_{II,eq}$. After accounting for the influence of crack closure with $\Delta G_{m,eff}$, the load ratio effects on the Mode I and II crack growth rates are eliminated as illustrated in Figure 4-29. Therefore the $\Delta G_{m,eff}$ parameter is capable of unifying the Mode I and II fatigue debonding growth rates.

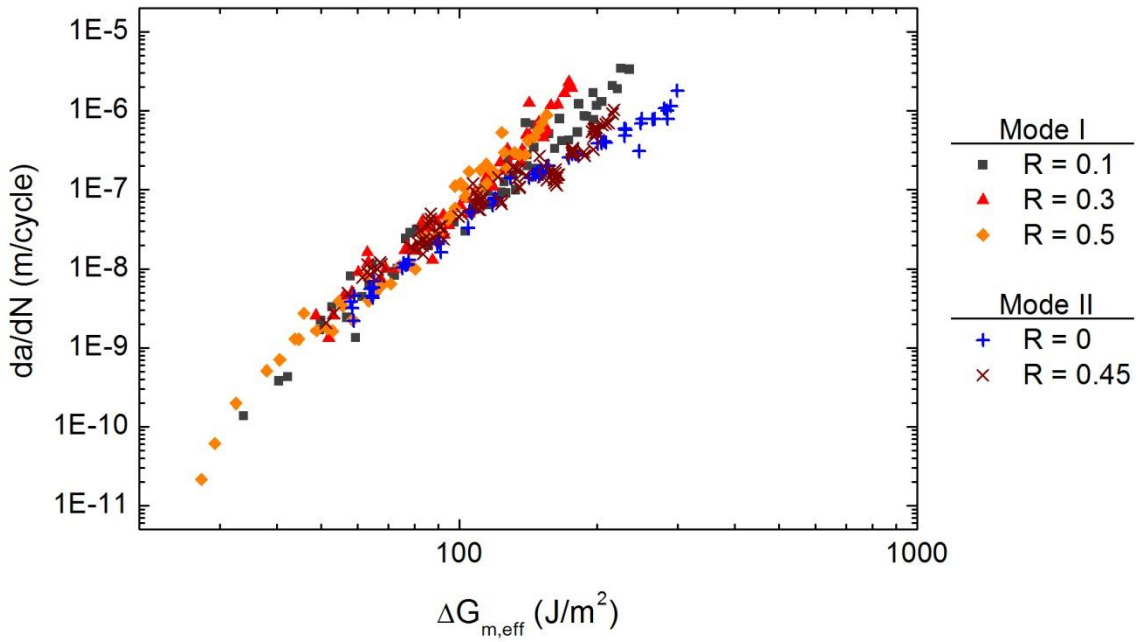

Figure 4-29: Mode I and II fatigue disbond growth rates of FM300-2K adhesive versus $\Delta G_{m,eff}$

4.8 Concluding Remarks

Detailed computational modelling of the plastic wake contact showed that fatigue crack growth in a bonded joint experiences significant level of plasticity-induced crack closure, contrary to the common belief that plasticity induced crack closure is absent in bonded structures. Parametric analysis of the plastic zone shape showed that the crack opening values is independent on the level of constraint acting on the plastic zone height if the nodal stress criterion is used. Therefore it is reasonable to assume the crack propagating in the middle of the bondline where small scale yielding conditions prevails, in order to simplify the modelling process and computation run time. The results of the present computational modelling showed that the level of plasticity-induced crack closure depends predominately on applied load ratios.

A preliminary analysis of VA loading was also conducted. A single overload event was modelled in the load cycle. An initial decrease of the crack opening values occurs immediately after the overload event due to crack blunting. Subsequent cycles then experience an increase in the crack opening load. This would suggest possibly crack growth retardation and more investigation are needed to confirm this. Investigation into plasticity induced crack closure under Mode II loading confirms the absence of closure.

Therefore crack closure effects only have to be considered for the Mode I component in mixed mode fatigue crack propagation.

A new correlating parameter, defined in terms of the effective cyclic load range, is able to unify the fatigue debonding behaviour for varying load ratios under Mode I and II loadings. An approximate solution of the effective load range was derived for Mode I crack propagation in a bonded joint. The crack closure model is able to merge the experimental data and data taken from literature into a narrow band for different load ratio. A mixed mode correlating parameter was also proposed. Together with the crack closure model, the correlating parameter is able to completely eliminate the influence of both load ratios and mixed mode ratios.

Chapter 5

Load Ratio Effects on the Fatigue Delamination Growth in Composites

5.1 Fatigue Behaviour of Composite Delamination

A manufacturing flaw within a bonded composite repair may exist in the form of delamination. Alternatively a low energy impact event can induce a network of delamination within the repair or the surrounding structure. Subsequently the delamination may grow under fatigue loading. Hence it is critical to analyse the composite laminate's delamination fatigue behaviour in a bonded composite repair as the laminate's resistance to crack growth is typically lower than that of an adhesive. A bonded composite repair design that accounts solely for crack propagation within the bondline may fail prematurely if crack initiate and propagate within the composite that has a lower fatigue resistance than adhesives.

The experimental results, presented in Figure 5-1, showed that the Mode I fatigue delamination growth rates depend strongly on the load ratio, *R*. Conversely the Mode II delamination growth rates are independent of R and a unique relation can be obtained using the cyclic strain energy release rate ΔG_{eq}. This behaviour is consistent with experimental data of several laminates under Mode I and II loadings summarised in Chapter 2. Another important observation is that the exponent *m* of Mode I fatigue crack in composite is significantly higher than those pertinent to cohesive debonding within the adhesive. It can be observed that, for the composite laminate, the Mode I exponent *m* was at least two times higher the Mode II exponent. This differs from the fatigue behaviour of cohesive debonding where the Mode I exponent, *m*, was comparable to Mode II. Extensive fibre bridging was observed in the wake of the crack. This could possibly explain some of the behaviour observed.

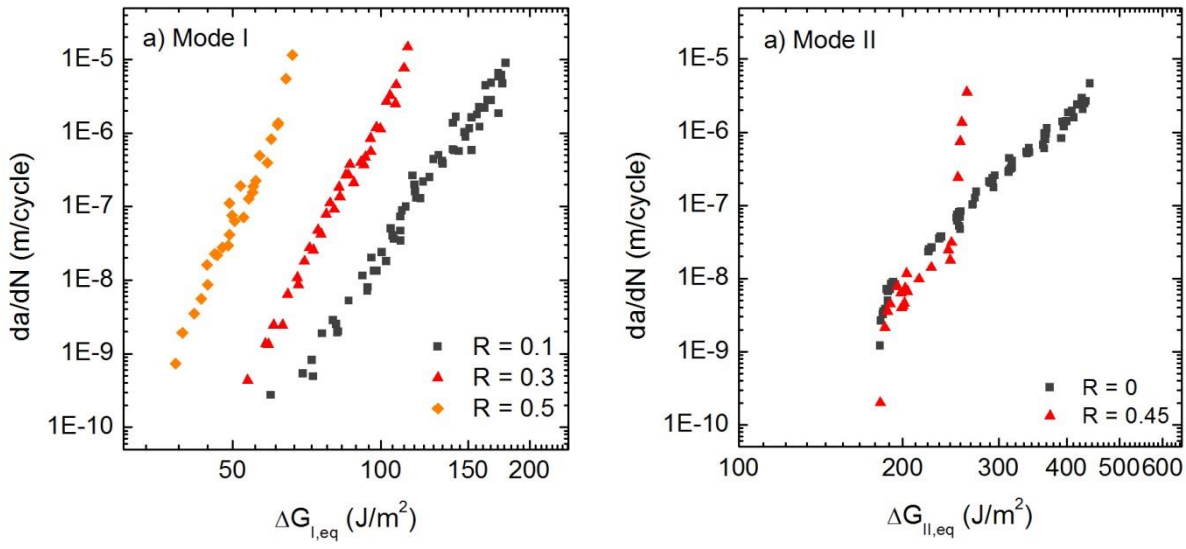

Figure 5-1: Experimental results of mode I and II fatigue delamination of IM7/977-3 composite laminates

Also highlighted in Chapter 2 is that none of the existing correlating parameters (i.e. G_{max}, ΔG or ΔG_{eq}) can satisfactorily eliminate the observed Mode I load ratio effects for a wide range of composite laminates. As a result, some modifications to the Paris law relation were proposed based on the observation of the delamination behaviour, rather than developing an understanding of the physical process. A satisfactory result by the semi-empirical approach can only be yielded from a broad dataset through extensive experimental testing and curve-fitting. Therefore the delamination growth driving force which correctly describes the underlying microscopic delamination behaviour is essential for the safe design of composite structures.

In previous works [36, 63], different hypotheses were formulated to provide a physical explanation of the load ratio dependency behaviour of composite laminates. The load ratio mechanisms proposed can be broadly categorised into intrinsic and extrinsic. Intrinsic mechanisms are inherent properties of the material and determine its resistance to crack growth (i.e. they control the driving forces to initiate cracking). It was hypothesised that G_{max} is a critical component as it introduces significant damage ahead of the crack tip, leading to a lower resistance [36]. On the other hand, extrinsic mechanisms act in the crack wake and decrease the crack growth rate by reliving the stresses at the crack tip. Fibre bridging was frequently reported in the Mode I delamination fracture. Under static loading, it is responsible for the development of a rising resistance-curve (R-curve) and thus plays a prominent role in the controlling the rate of crack propagation. Plasticity induced crack closure is another form of extrinsic shielding of the crack tip stress and its role was systematically described in Chapter 4.

However its role in composite laminates remains unclear. It is generally assumed to be absent, given that fibre composites, particularly carbon fibre composites, are generally very brittle. However this does not imply the absence of extensive plastic deformation before failure, as the matrix can undergo plastic deformation under shear loading. The objective of this Chapter is to investigate the role of plasticity induced crack closure, fibre bridging and damage zone on the delamination crack growth rates to identify the main mechanism responsible for the strong load ratio effects on Mode I disbond growth. Numerical methods are used to mechanistically simulate the effects of aforementioned mechanisms.

5.2 Cohesive Zone Model with Fatigue Degradation Law

In this section, a fatigue degradation law was implemented into a cohesive zone model (CZM) to simulate the progressive failure of a composite laminate under fatigue loading. Based on the model presented in references [22, 24, 117], the evolution of stiffness reduction damage variable, d, is expressed in Equation (5-1) as a function of the number of cycles lapsed. The entire derivation of the equation is described in Appendix A.

$$\frac{da}{dN} = \frac{1}{L_{CZ}} \frac{[\Delta^f (1-d) + d\Delta^0]}{\Delta^f \Delta^0} \frac{\partial a}{\partial N} \tag{5-1}$$

where Δ is the traction separation displacement and the superscript denotes the final and initial traction displacement. The rate of crack growth, $\partial a/\partial N$, is measured experimentally and L_{CZ} is the cohesive zone length. The definition of the cohesive zone length L_{CZ} varies among researchers. In this work, L_{CZ} is derived from the following analytical solution in order to keep it consistent with the model presented by Turon et al. [22].

$$L_{CZ} = \frac{9\pi}{32} \frac{E_{33} G_{max}}{(\sigma^0)^2} \tag{5-2}$$

where σ^0 is the maximum traction stress prior to damage and G_{max} is the maximum strain energy release rate experienced. The growth rate $\P a / \P N$ is represented by the Paris law given as,

$$\frac{\partial a}{\partial N} = C\left[\left(\sqrt{G_{I,max}} - \sqrt{G_{I,min}}\right)^2\right]^m \quad (5\text{-}3)$$

The strain energy release was determined by integrating the area under the traction-separation curve. For a bilinear traction-separation curve, the integral solution is given as,

$$G(\lambda) = \int_0^{\lambda} \sigma(\lambda) d\lambda = \frac{\sigma^0}{2}\left[\Delta^f - \frac{(\Delta^f - \lambda)^2}{\Delta^f - \Delta^0}\right] \quad (5\text{-}4)$$

where G(λ) is the crack driving force derived at the traction displacement λ. The load ratio *R* is defined as P_{min}/P_{max}. Therefore Equation (5-4) can be rewritten in terms of the cyclic strain energy release rate: -

$$\Delta G_{I,eq} = \frac{\sigma^0}{2}\left[\Delta^f - \frac{(\Delta^f - \lambda)^2}{\Delta^f - \Delta^0}\right](1 - R)^2 \quad (5\text{-}5)$$

The material properties of IM7/977-3 composite laminate and the cohesive zone model are given in Table 5-1. The Paris law constants were determined from the experimental results in Section 3.3.3 and schematically shown in Figure 5-2. The horizontal scale of the Paris plot was changed to mm/cycle to keep the units consistent with calculations in the fatigue law algorithm. The fatigue crack propagation thresholds were not accounted for in the algorithm. The governing equations presented in Equation (5-1) to (5-5), are then used to program the constitutive behaviour of a single cohesive element under tension-tension cyclic loads.

Table 5-1: Material properties of IM7/977-3 ply

Substrate : IM7/977-3					
E_{11} =	159000 MPa	E_{33} =	9000 MPa	$v_{12} = v_{13}$ =	0.35
G_{13} =	4800 MPa	G_{23} =	4000 MPa	v_{23} =	0.3
$v_{12} = v_{13}$ =	0.35	v_{23} =	0.3		
Constitutive response of cohesive zone					
K^0 =	10^6 N/mm^3	σ^0 =	40 MPa	G_{IC} =	0.24 N/mm

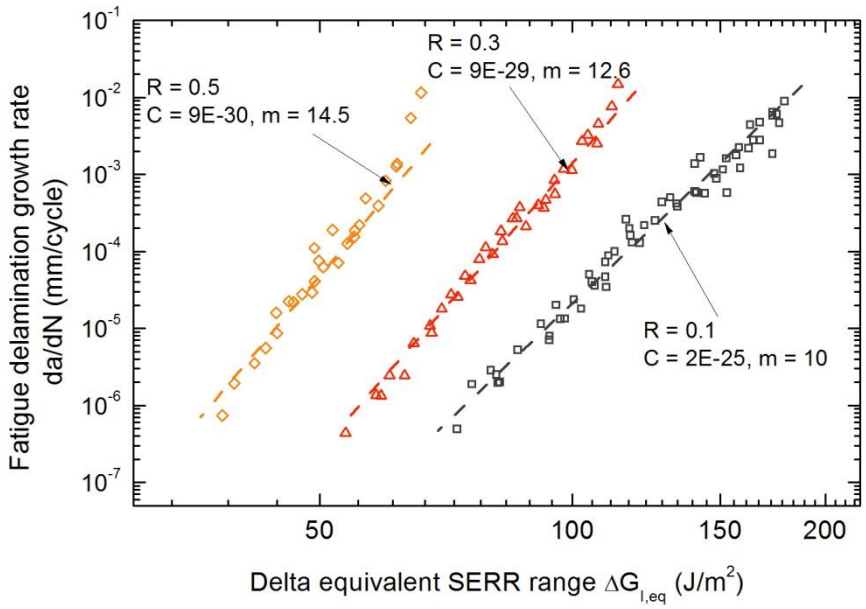

Figure 5-2: Mode I fatigue crack growth rates from experiments and the Paris law constants

The fatigue degradation law was implemented into the standard cohesive element in the Abaqus FE code with a user-subroutine UMAT. The modelling of the fatigue crack growth consisted of two stages as shown in Figure 5-3. In the first stage, the numerical model was quasi-statically loaded to the maximum cyclic displacement to firstly develop the process zone under the maximum displacement/load. The fatigue law was then activated in the second step and the applied displacement was held at the constant level. The cyclic load ΔP was represented by R in Equation (5-5) defined in the fatigue law algorithm. A load envelope strategy was employed to represent the each numerical "pseudo" time increment as an increment of loading cycles ΔN.

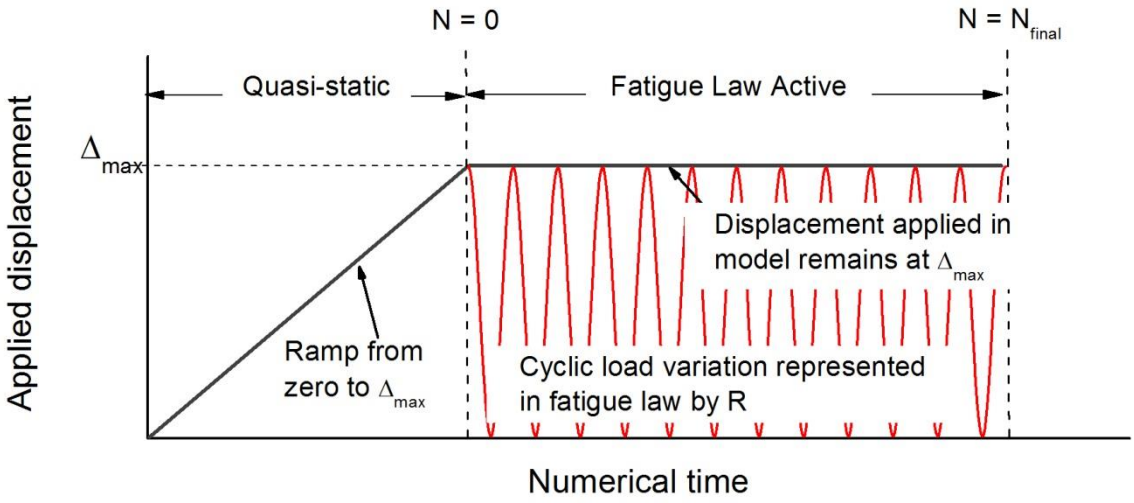

Figure 5-3: Numerical simulation of cyclic loading

A simple validation of the fatigue law algorithm was carried out using a composite DCB model and mode I fatigue data. Figure 5-4 shows the results of the simulated fatigue crack growth rates using the inputs for the experimental Paris law constants of its respective load ratio. The results are in close agreement with the experimental Paris law curve.

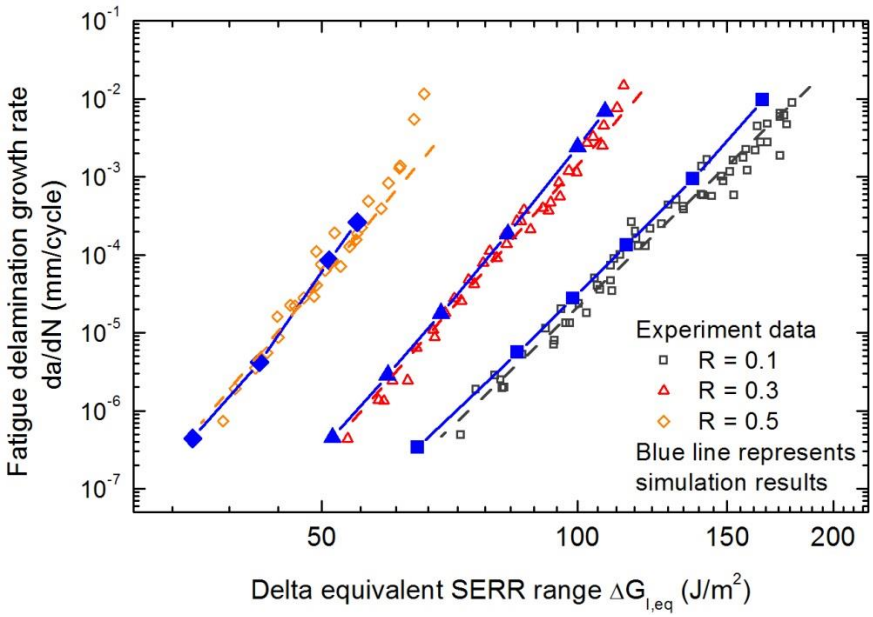

Figure 5-4: Comparison of the experimental data with the simulated crack growth rate from finite element analysis

The sensitivity of the CZM with fatigue degradation law to load ratio was then investigated. When plotted against ΔG_{eq}, the experimental data showed a strong dependence on load ratio. Using the Paris law constants from R = 0.1 as input, an analysis was carried out to predict the fatigue crack growth rates of R = 0.3 and R = 0.5. Figure 5-5 shows that the simulated results of R = 0.3 and 0.5 coincides with R = 0.1 (input Paris curve). Therefore the fatigue cohesive law was unable to predict the experimentally observed load ratio effects because the model assumes similitude conditions are maintained throughout during load cycle. In order for the currently model to correctly simulate the crack growth rates of any load ratio, the Paris law input must represent the effective load range experienced at the crack tip rather than the applied load range. This highlights the importance of maintaining the similitude conditions in the definition of the Paris law and non-linear mechanisms (i.e. crack closure and fibre bridging) need also be included in the numerical model in order to replicate the experimental data.

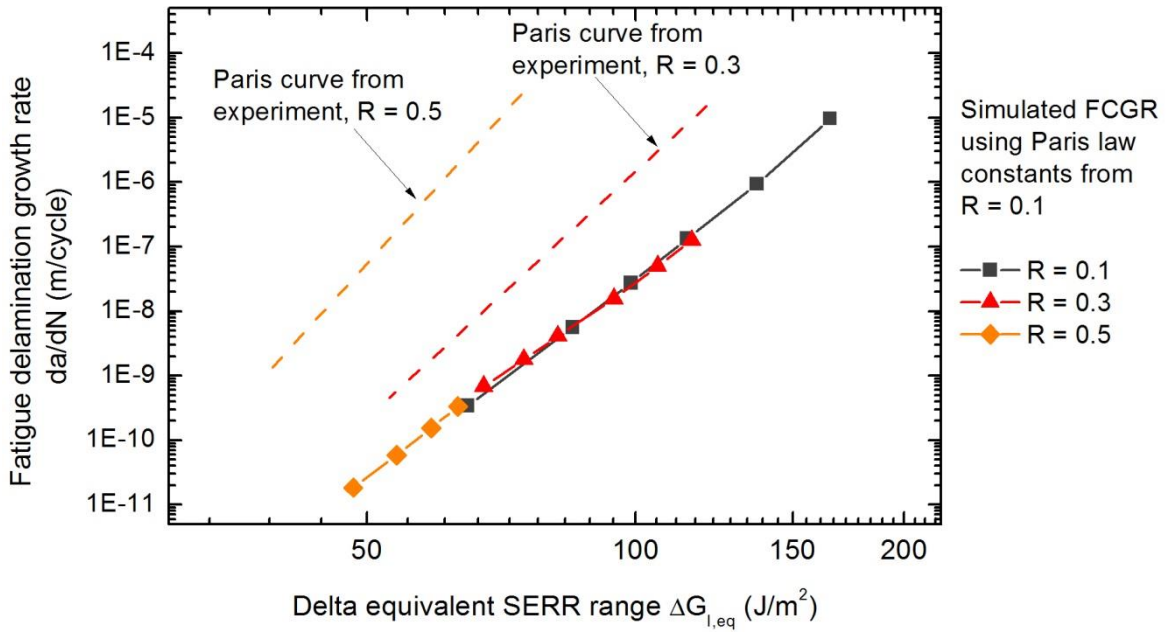

Figure 5-5: Comparison of predicted fatigue crack growth rates (with Paris law inputs from experimental R = 0.1) and actual fatigue crack growth rates of R = 0.3 and 0.5

Shown in Figure 5-5, the current model is unable to correctly predict crack growth rates for an arbitrary load ratio, except for load ratio from the Paris law constants defined by the user. In the author's opinion, this then limits the current model to being just a self-predictive model. A re-examination of the fatigue degradation law and its underlying assumptions is needed to further develop it as a more robust model. An independent approach of measuring the degradation of traction stress with respect to the number of cycles lapsed is needed. It is preferable that the test method will eliminate any non-linear mechanism influencing the fatigue crack growth rates. Then a fatigue law can then be developed to predict fatigue crack growth rates without being dependent on having *da/dN* as input.

5.3 Investigation of Laminate Plasticity

5.3.1 Overview

Chapter 2 re-examines the load ratio effects in the delamination behaviour of composite laminates and found no suitable correlating parameter for accounting for these effects. Fatigue simulation of delamination using the CZM approach was also found to be inadequate for predicting the load ratio effects. Therefore a suitable correlating parameter

of linking the observed load ratio effects with the resultant macroscopic behaviour is needed.

Plasticity induced crack closure is first investigated in composites' fatigue behaviour. Plasticity in fibre-reinforced epoxy composites is often considered an insignificant issue as SEM images of the fracture surfaces indicate a brittle fracture. However the mechanical response of fibre-reinforced composite laminates is known to exhibit nonlinear mechanical response under off-axis tension/compression loading. The nonlinear response is attributed to the inelastic behaviour of the matrix where plasticity occurs at relatively low stresses. In contrast to the matrix, the fibres generally maintain linear-elastic behaviour to the point of rupture. These non-linear behaviours of composite laminates had received significant attention in the literature. For example, Sun and Chen [118-120] and Yokozeki et al. [121] used anisotropic plasticity theory to model off-axis tension and compression experimental results. This approach is typically termed as the macromechanical model as it regards the composite lamina as a homogenous orthotropic elastic-plastic continuum.

Non-linear behaviour of composite laminate can also be modelled by the micromechanical approach. In the micro-mechanical model, the fibre and matrix are treated as individual constituents and then used to evaluate the effective macromechanical properties of the lamina [119, 122, 123]. An advantage of the micromechanical model over the macromechanical model is that the details of the stress- and strain-fields within the microstructure are determined, allowing a precise estimation of onset of damage. The constitutive model is dependent on the fibre and matrix properties, volume fraction, geometrical and spatial distribution of the fibre-matrix which may not be readily available. One possible method is to adjust the matrix properties to match experimental results of test coupons. This requires testing the composite for the purpose of comparison.

The concept of plasticity induced crack closure has previously not been considered a mechanism influencing the fatigue crack growth rates of composite laminates. However previous works indicate the presence of matrix plasticity within a laminate and hence plasticity induced crack closure is a plausible mechanism affecting the fatigue delamination propagation process. In the following section, a computational modelling of matrix plasticity in a composite laminates is presented using the Hill's yield plastic potential. To determine the yield properties ($\bar{\sigma}_{11}$, $\bar{\sigma}_{22}$ and $\bar{\sigma}_{12}$) of the laminate, a number of standard tensile tests were carried on three composite panels $[0]_8$, $[+45/-45]_8$

and $[90]_{16}$. Then anisotropic plastic behaviour is introduced to the DCB model to examine the presence of plasticity induced crack closure on fatigue delamination growth rates.

5.3.2 Hill's Yield Plastic Potential

The Hill's yield plastic potential had been successfully used in a number of works to analyse the non-linear response of composite laminates. The Hill's yield plastic potential is an extension of the von Mises yield criterion. It was originally developed to model the anisotropic yielding behaviour in metals. The yield criterion does not take into account the incompressibility of plastic deformation and hydrostatic stresses. Kinematic hardening and constraint hardening of the fibres are also not considered within the plasticity model. In using the Hill's plastic potential, Sun and Chen developed a one-parameter plasticity model to describe the non-linear behaviour of composite laminate under off-axis tension tests [119]. The method is simple and is able to collapse the experimental data into a master curve accurately. Since then, the one-parameter model had been used to model the non-linear behaviour of composite laminates for different studies [120, 121, 124, 125]. Given the success of using the Hill's yield criterion to model the yielding behaviour of composite laminates, this criterion will be used to model the anisotropic yielding of the composite laminate in the numerical model.

Expressed in terms of Cartesian stress component, the Hill's yield stress envelope is described in a homogeneous quadratic expression for the plastic potentials and is given as [126],

$$f(\sigma) = \sqrt{F(\sigma_{22}-\sigma_{33})^2 + G(\sigma_{33}-\sigma_{11})^2 + H(\sigma_{11}-\sigma_{22})^2 + L\sigma_{23}^2 + 2M\sigma_{31}^2 + N\sigma_{12}^2} = \sigma^0 \quad (5\text{-}6)$$

where *F, G, H, L, M* and *N* are constants characteristic of the state of anisotropy and can be obtained by tests of the material in different orientations. $\bar{\sigma}_{11}$, $\overline{\sigma}_{22}$ and $\bar{\sigma}_{33}$ are the tensile yield stresses in the principal anisotropic directions. Hence the terms F, G and H are defined as:

$$F = \frac{(\sigma^0)^2}{2}\left(\frac{1}{\bar{\sigma}_{22}^2} + \frac{1}{\bar{\sigma}_{33}^2} - \frac{1}{\bar{\sigma}_{11}^2}\right) = \frac{1}{2}\left(\frac{1}{R_{22}^2} + \frac{1}{R_{33}^2} - \frac{1}{R_{11}^2}\right) \quad (5\text{-}7)$$

$$G = \frac{(\sigma^0)^2}{2}\left(\frac{1}{\bar{\sigma}_{33}^2} + \frac{1}{\bar{\sigma}_{11}^2} - \frac{1}{\bar{\sigma}_{22}^2}\right) = \frac{1}{2}\left(\frac{1}{R_{33}^2} + \frac{1}{R_{11}^2} - \frac{1}{R_{22}^2}\right) \quad (5\text{-}8)$$

$$H = \frac{(\sigma^0)^2}{2}\left(\frac{1}{\bar{\sigma}_{11}^2} + \frac{1}{\bar{\sigma}_{22}^2} - \frac{1}{\bar{\sigma}_{33}^2}\right) = \frac{1}{2}\left(\frac{1}{R_{11}^2} + \frac{1}{R_{22}^2} - \frac{1}{R_{33}^2}\right) \quad (5\text{-}9)$$

where R_{11}, R_{22} and R_{33} are the ratio of the anisotropic yield stress and the user defined reference yield stress σ^0. Under shear, the reference shear yield stress is taken as $\tau^0 = \sigma^0/\sqrt{3}$ and $\bar{\sigma}_{12}$, $\bar{\sigma}_{13}$ and $\bar{\sigma}_{23}$ are the shear yield stress with respect to the principal axes of anisotropy, then

$$L = \frac{3}{2}\left(\frac{\tau^0}{\bar{\sigma}_{23}^2}\right) = \frac{3}{2R_{23}^2} \quad (5\text{-}10)$$

$$M = \frac{3}{2}\left(\frac{\tau^0}{\bar{\sigma}_{13}^2}\right) = \frac{3}{2R_{13}^2} \quad (5\text{-}11)$$

$$N = \frac{3}{2}\left(\frac{\tau^0}{\bar{\sigma}_{12}^2}\right) = \frac{3}{2R_{12}^2} \quad (5\text{-}12)$$

In order to fully describe the anisotropic yield behaviour, the six independent yield stresses need to be determined. For the purpose of simulating the elastic-plastic response of the DCB laminate under plane strain conditions, the requirements of the yield stresses of the unidirectional laminate can be simplify to just and $\bar{\sigma}_{11}$, $\bar{\sigma}_{22}$, $\bar{\sigma}_{33}$ and $\bar{\sigma}_{12}$.

5.3.3 Experimental Results

Four material characterisation tests were carried out to measure and determine the yield stresses of the IM7/977-3 carbon/epoxy laminates. The specimen geometry and test configurations are designed based on various ASTM test standards and are summarised in Table 5-2. The experiment was done under displacement control at a rate of 0.5 mm/min. End tabs were bonded to the specimens using epoxy adhesive to prevent failure at the grips. The strain of the specimen was measured using a clip gauge, placed in the middle of the specimen.

Table 5-2: Material characterisation test matrix

Test Standard	Specimen configuration	Loading	Measurement
ASTM D3039 [127]	$[0]_8$, 15x120 mm	Tension	$\bar{\sigma}_{11}$
ASTM D3518 [128]	$[+45/-45]_8$, 25x120 mm	Tension	$\bar{\sigma}_{12}$
ASTM D3039 [127]	$[90]_{16}$, 25x120 mm	Tension	$\bar{\sigma}_{22}$
NASA Short Block	$[90]_{16}$, 25 x 50 mm	Compression	$\bar{\sigma}_{22}$

Experimental longitudinal stress-strain curves of the $[0]_8$ composite specimens are presented in Figure 5-6(a). It can be seen that the $[0]_8$ laminates remained nearly perfectly linear elastic until an applied axial strain of 1.6%. A slight load drop was observed at this point. This was caused by matrix shear cracking which was characterised by audible cracking sounds. Shortly after, the $[0]_{12}$ laminates failed catastrophically at an axial strain of 1.9%. Since the axial direction of the laminate display little non-linearity, the yield stress $\bar{\sigma}_{11}$ is taken as the ultimate strength of the axial fibre tows.

The measured stress-strain curves of the angle-ply $[+45/-45]_8$ laminates under tensile loading are presented in Figure 5-6(b). The shear stress-strain behaviour which is matrix dominated, displayed extensive non-linear deformation of the laminate. Therefore this demonstrates the inelastic behaviour of the matrix system. A deviation from linearity first occurred at a stress of 45 MPa. The rate of change in the stress with respect to the applied strain begins to plateau at approximately 80 MPa. The gradual increase in the stress after the yielding of the matrix is possibly due to the subsequent change in alignment of the fibre upon further loading. There is no distinct yield point which can be easily defined from the shape of the stress-strain curves. Therefore the shear yield point is taken at an offset of 0.2% which gives a yield stress of 64 MPa.

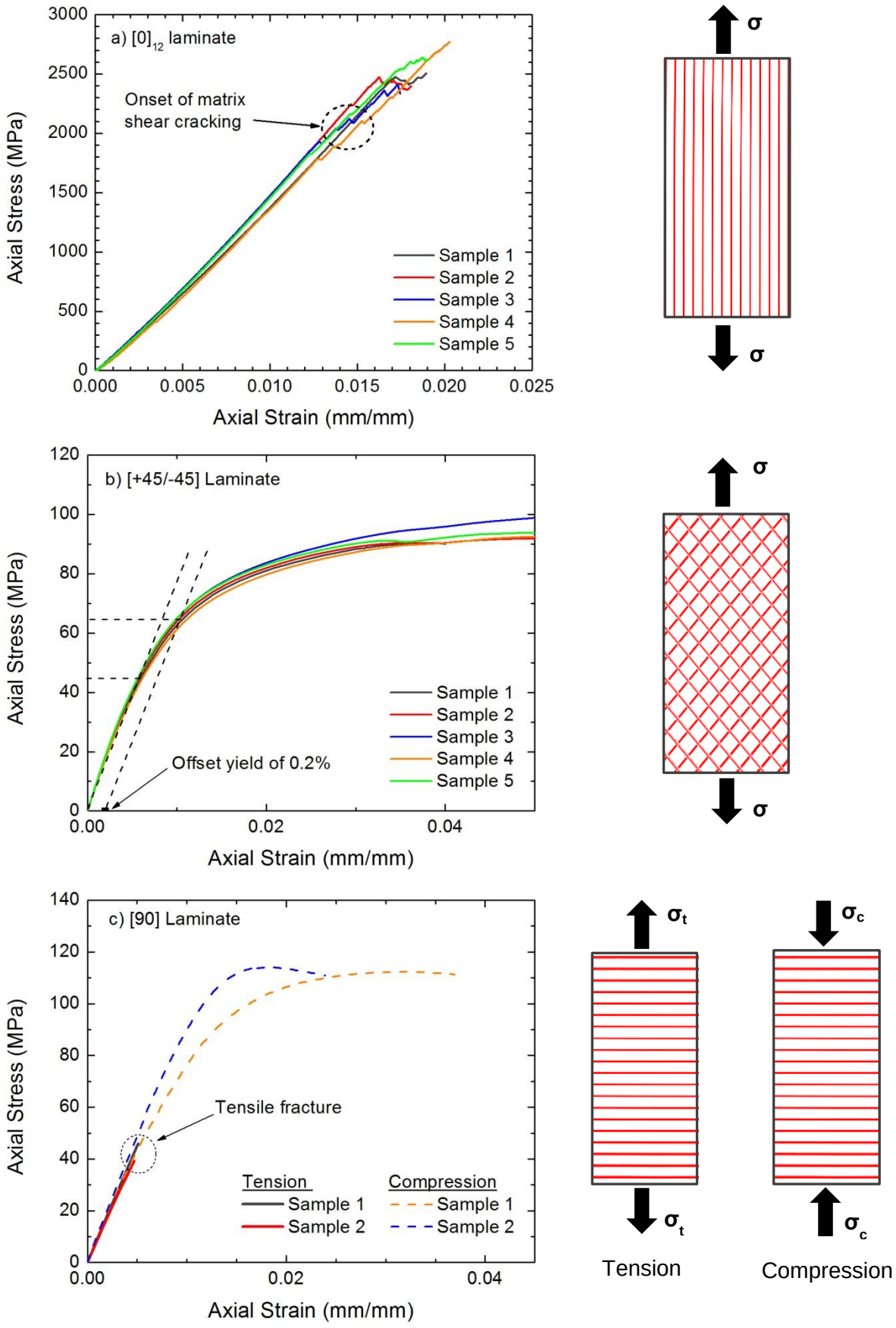

Figure 5-6: Experimental stress-strain curves of the $[0]_8$, $[+45/-45]_8$ and $[90]_{16}$ IM7/977-3 laminates

The stress-strain curves of the $[90]_{16}$ laminates under tensile and compressive loading are shown in Figure 5-6(c). The tensile behaviour of the $[90]_{16}$ laminates was linear-elastic till the point of failure. Previous works using the micromechanical model of modelling the fibres and matrix had shown the matrix region between the fibres experiences high local stress and strains even at low applied stresses. This is due to stress concentration induced by the fibres. The localisation of the matrix plastic strain along the shear bands is a dominant factor on the failure strength of the laminate. Due to the constraint of the fibres, the matrix is unable to dissipate the strain energy and, hence, fracture occurs very quickly. The compressive behaviour exhibits a higher failure stress and strain as compared to the tensile results. Prior to failure, non-linear deformation can be observed and the onset of this behaviour occurs at an applied strain of 1.4%.

The compressive yield stress is approximately 110 MPa. This corresponds to $\sqrt{3}\tau_{y,0.2\%}$ which corresponds to the von Mises yield stress. The experimental evidence showed that the $[90]_{16}$ composite laminate failed at an angle along planes parallel to the fibres. The angle formed between the failure plane and the through thickness loading (or perpendicular to the loading direction) is approximately 50-56°. This is indicative of the direction of the shear bands and fracture occurs in a direction perpendicular to this. The yield stress of the [90] laminate was taken to be 40 MPa. To summarise, the properties of the laminate and its respective yield stresses are listed in Table 5-3.

Table 5-3: Elastic properties and yield stress of IM7/977-3 laminate

Elastic properties					
E_{11} =	159000 MPa	E_{33} =	9000 MPa	v_{12} = v_{13} =	0.35
G_{13} =	4800 MPa	G_{23} =	4000 MPa	v_{23} =	0.3
v_{12} = v_{13} =	0.35	v_{23} =	0.3		
Yield stress					
σ^0 =	40 MPa				
$\bar{\sigma}_{11}$ =	2800 MPa	$\bar{\sigma}_{22}$ =	40 MPa	$\bar{\sigma}_{33}$ =	40 MPa
$\bar{\sigma}_{23}$ =	64 MPa	$\bar{\sigma}_{12}$ =	47 MPa	$\bar{\sigma}_{13}$ =	47 MPa

5.3.4 Plasticity Induced Crack Closure in Composite Laminates

PICC is simulated in the DCB laminate by incorporating the Hill's yield potential into the laminate elastic properties. The geometrical details and mesh of the DCB specimen were as previously described in Section 4.4. A mesh sensitivity study was first performed to

ensure the crack tip stresses were represented by sufficient number of elements. Since the plastic zone length is difficult to determine analytically for anisotropic yielding, the plastic zone length was determined numerically. Shown in Figure 5-7 is the shape of the plastic zone within the composite laminate which is defined by the boundary of the area that the Hill's yield criterion is satisfied. The Hill's stress from Equation (5-6) was implemented into the numerical code via the user subroutine UVARM in order to visually display the stress field. The anisotropic plastic zone shape in a unidirectional DCB laminate is different from the plastic zone in an isotropic material. The length of the plastic zone was measured from the crack tip to the end of the forward plastic zone.

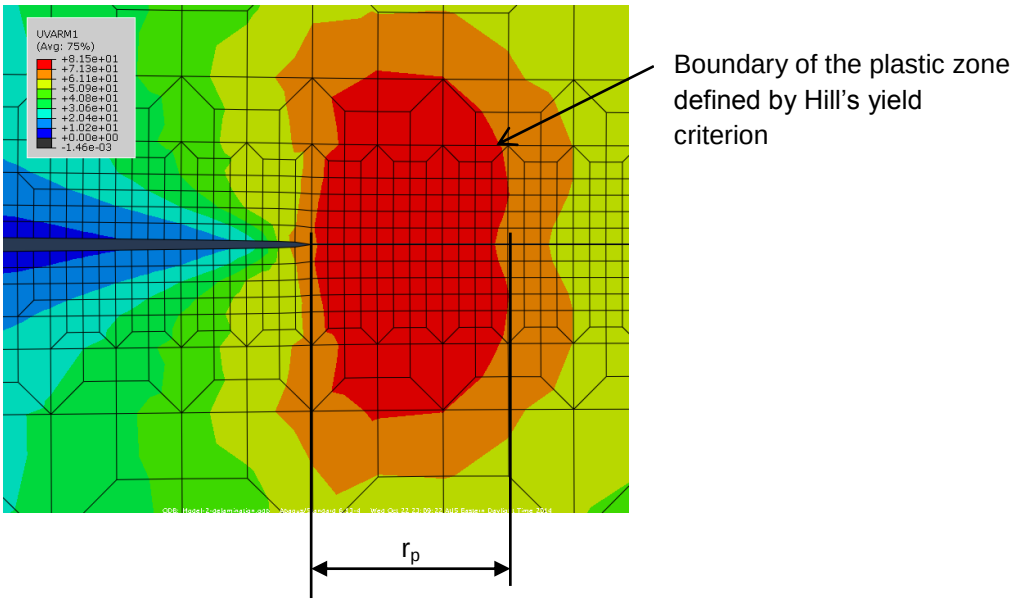

Figure 5-7: Plastic zone shape from Hill's yield criterion in a $[0]_{24}$ DCB specimen under an applied G of 71.4 J/m2 and the approximation of the plastic zone length

Mesh sensitivity studies were done for three DCB configuration; the composite ply adjacent to the crack was varied from 0°//0°, 0°//45° and 0°//90° while the rest plies within the DCB specimen remains aligned in 0°. The results of the mesh sensitivity investigation on crack closure in composite laminate DCB specimen are presented in Figure 5-8. In the case of crack propagation at the 0°//0° interface, the crack opening loads do not exhibit convergence for both crack opening criteria used as further mesh refinement is carried out. This would indicate either that no unique crack opening value can be obtained which can be interpreted as the absence of plasticity induced crack closure; or the crack closure would be negligible upon further interpolation of the results. It is likely to be the former.

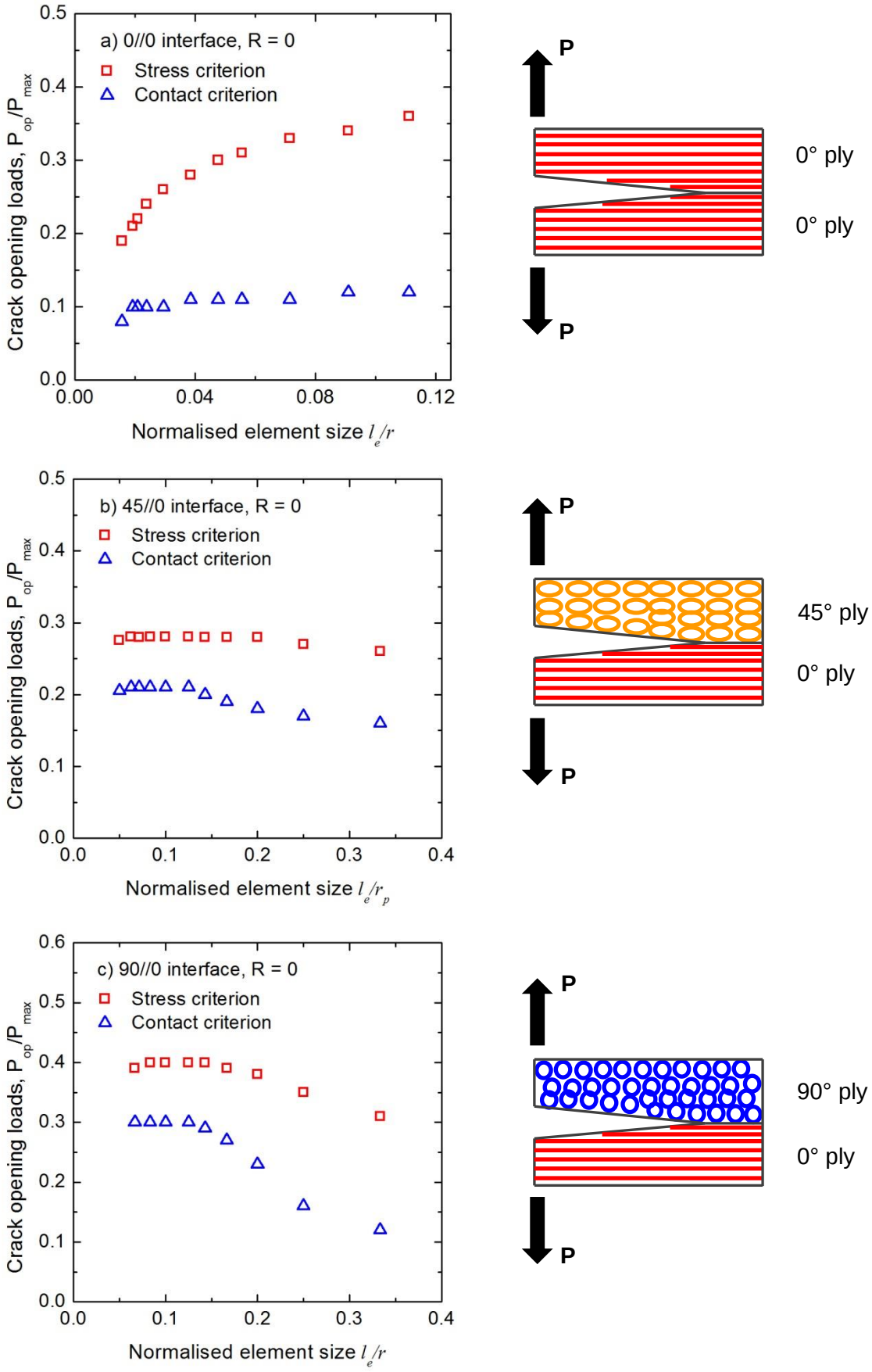

Figure 5-8: Mesh refinement study for delamination growth along a) 0//0, b) 45//0 and c) 90//0 interface under mode I loading

According to plastic flow theory, the volume change of the material associated with plastic strain is zero. Consider a growing crack under plane strain conditions, plasticised material must be transferred from the lateral direction (i.e. crack growth direction) to the crack flanks (i.e. normal to the crack path). Then only plane strain crack closure can occur and the crack closure mechanism under plane strain was discussed in Section 4.6.1. Due to the constraint provided by the fibres, very little plasticity can occur along the fibre direction. Consequently, no or very little crack closure can occur in the 0°//0° interface. In order to investigate the above point further, mesh sensitivity studies were also conducted for 45°//0° and 90°//0° ply interfaces. In both cases, a convergence of the crack opening loads can be observed in Figure 5-8(b) and Figure 5-8(c). Therefore this goes to show that it is possible for crack closure to occur in composite laminate if the material transfer associated with plasticity can occur.

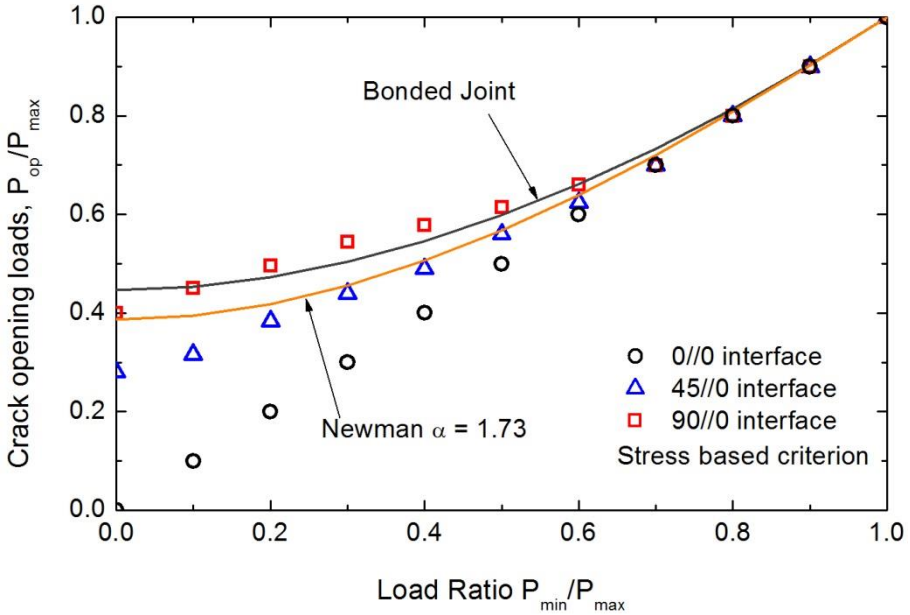

Figure 5-9: Influence of load ratio on the crack opening loads for fatigue delamination along 45//0 and 90//0 interface

It is clear that plasticity-induced crack closure does exist for delamination cracks between 45 and 0 degree plies, and between 90 and 0 degree plies. The influence of load ratio on crack closure between the two ply interface configurations is shown in Figure 5-9. It can be observed that the crack opening loads for 90°//0° is higher than 45°//0°. This is due to the lower stiffness of the 90° ply in the X-direction and thereby more plasticised material can be displaced. No further crack closure was observed for R ≥ 0.7. Comparing the crack closure results with the bonded joint results, the crack opening level of the 90°//0° is similar to the bonded joint. For the 45°//0° interface laminate, the crack

opening values are similar to Newman's approximation for $\alpha = 1.73$ when $R \geq 0.3$. For $R < 0.3$, the crack opening values of the 45°//0° interface is lower than the Newman's approximation.

A number of researches had previously shown that composite laminates exhibit non-linear stress-strain curves due to the inelastic behaviour of the matrix system. Using the Hill's yield criterion, it is shown that PICC can occur if an off-axis ply is adjacent to the delamination. However it is also demonstrated that plasticity induced crack closure was not a contributing factor to the load ratio effects observed in the crack growth rates of 0° unidirectional DCB specimen. This is due to the constraint along the width of the DCB under plane strain assumption and elastic constraint of the fibres in the lateral direction. Therefore the mean load dependency behaviour observed in the Mode I experimental data of the composite laminates, in Section 3.3.3, was not due to crack closure.

5.4 Investigation of Fibre Bridging

5.4.1 Fibre Bridging Overview

As presented in Section 3.4.2, it was observed that the delamination fracture of the composite laminates was accompanied by a zone which the fibres remained connected across in the wake of the crack faces. The bridging mechanism is thought to be the primary cause in increasing the delamination growth resistance under static loading [62, 129]. This is evident in the rising R-curve as the critical strain energy release rate raises monotonically from the initial value to a steady state value usually corresponds to a fully developed bridging zone. The bridging zone then attains a steady state i.e. the crack now maintains a self-similar opening profile with a constant bridging zone length translating in the DCB specimen, when the applied strain energy release rate is constant. This behaviour is more apparent in the delamination fracture of nested plies (having the same orientation) as fibre bridging becomes more substantial. In the absence of plasticity induced crack closure as previously indicated by numerical simulations in Section 5.3.4, fibre bridging was also assumed to affect the delamination behaviour under fatigue. Past works also provided evidence of influence of fibre bridging on the fatigue behaviour [130-134]. The fatigue model typically involves normalising $G_{I,max}$ with $G_{I,R}$(a) from the derived R-curve that is dependent on crack growth length.

A comprehensive characterisation of the fibre bridging is needed to account for its influence on the delamination growth for damage tolerant design and reliability

assessment. However the experimental measurement of the bridging properties and the extent at which it may influence the measured toughness is difficult to assess. A micromechanical model where the bridging fibres were modelled as beams subjected to shear and bending were used to describe the experimental data [135, 136]. However this requires making an assumption on the ligaments stiffness, length and density. Stutz et al. employed an inverse-numerical procedure by comparing the measured strain to determine the bridging law parameters [137, 138]. The longitudinal strain field along the crack flanks and tip were experimentally measured from a novel technique using a fibre Bragg grating embedded sensor. The parameters of the bridging traction distribution were then optimised using a numerical approach to match the measured strains. In this section, the influence of fibre bridging on fatigue delamination was analysed and taken into consideration in the development of the fatigue prediction model.

5.4.2 Determination of Bridging Law Parameters

Figure 5-10 shows the schematic of fibre bridging in the delamination crack path in a DCB laminate and the bridging traction distribution over the bridging zone. Based on physical considerations and models proposed in the literature, the bridging traction distribution was observed to decrease monotonically from a maximum σ_{br} at the crack tip to zero at the end of the bridging zone. The bridging fibres will hold the crack flanks and effectively reduce the stress field at the crack front and thereby results in an increase in fracture toughness.

The bridging traction and its parameters can be determined by the J-integral approach [129, 139]. Consider a bridging traction law, the fibre bridging zone is represented by fibres crossing across the crack plane which could be represented by position dependent, equivalent traction stress. Accordingly the bridging traction stresses are defined as a function of the crack opening displacement (COD) δ,

$$\sigma_{br} = \sigma_{br}(\delta) \tag{5-13}$$

This function is specific to the damage and assumed to be the same for every point in the bridging zone. Shown in Figure 5-10, the traction stress is assumed to be the peak at the crack tip and eventually decays to zero when δ reaches the maximum separation limit, δ_f, so that $\sigma_{br}(\delta_f) = 0$.

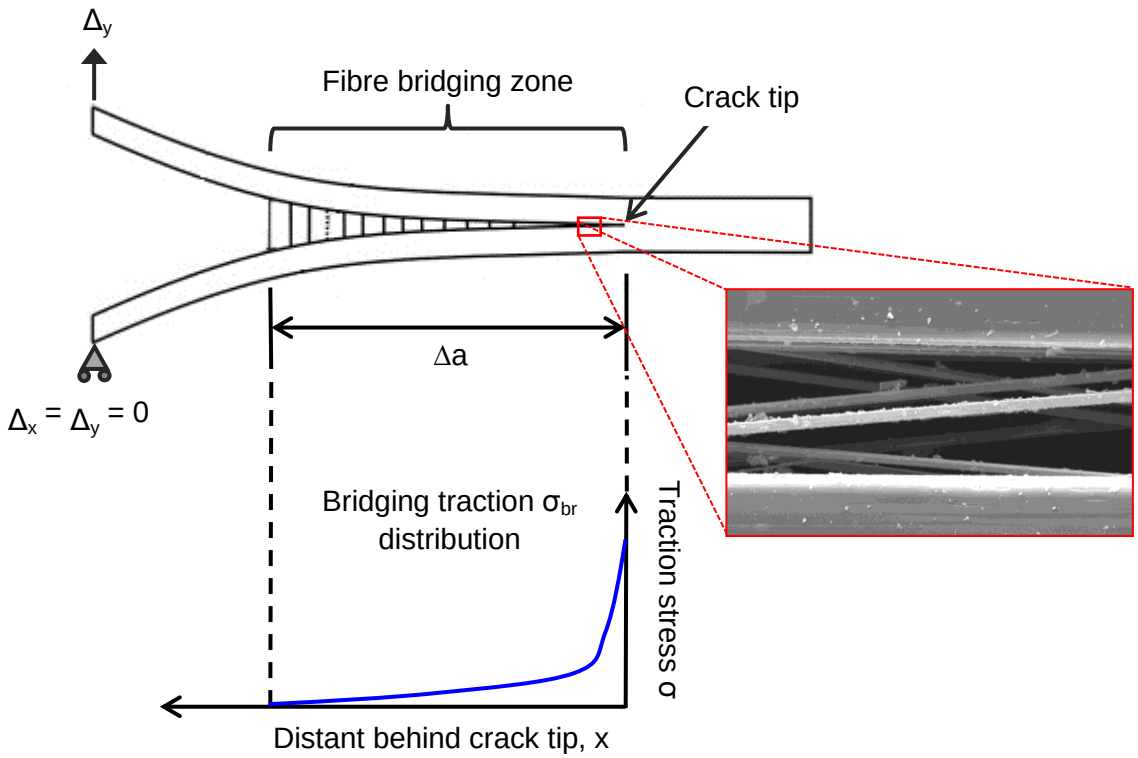

Figure 5-10: Schematic of fibre bridging in the wake of the delamination crack in a DCB specimen after crack propagated for a distance of Δa and the distribution of the bridging stress over the bridging zone

From the initial position, the strain energy release rate (SERR) obtained would be free from any influence of bridging since the pre-crack was created from a Teflon film. Although a resin rich pocket can be observed at the crack tip, it was noted that this will have little effect on the results if the thickness of the Teflon film is less than 13 µm [140]. Therefore any increase in the SERR is attributed to fibre bridging and the energy balance due to the J-integral conservation can be summarised as: -

$$G_p = G_i + G_{br} = G_i + \int_0^{\delta_{max}} \sigma_{br}(\delta)\, d\delta \tag{5-14}$$

where the subscripts *p, i* and *br* represent the fracture energy dissipated during the propagation phase, initiation phase and contribution by fibre bridging, respectively. The contribution of G_{br} can be determined by integrating the bridging traction stress over the crack opening displacement where δ_{max} is COD at the end of the bridging zone. Equation (5-14) is schematically represented in Figure 5-11.

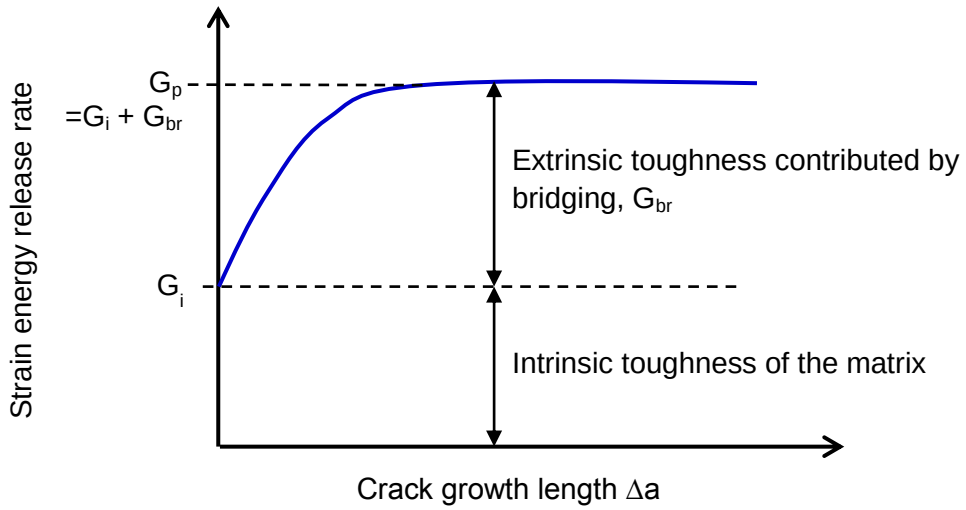

Figure 5-11: Schematic of the fracture energy contribution by fibre bridging to the intrinsic toughness of the matrix system

During the measurement of the R-curve, the initial crack tip coincides with the end of bridging zone. Once the SERR plateaus in the R-curve, it was assumed that the fibre bridging zone had fully developed and, hence, there would be no increase in toughening for further crack propagation. The corresponding crack growth length at which the plateau occurs is the full bridging zone length. Equation (5-14) suggests an experimental procedure of determining the fibre bridging response. In this work, this experimental method is coined as the SERR-COD approach. By measuring the COD δ and the R-curve, the bridging law can be experimentally obtained by differentiating Equation (5-14).

$$\sigma_{br} = \frac{\partial G_{br}}{\partial \delta_{max}} \tag{5-15}$$

To evaluate the distribution of the the traction stress, the SERR G_p was calculated using the modified beam theory, prescribed in the ASTM standards [85]. This is referred to as the global parameter as the SERR is determined by the response of the DCB specimen. G_i and G_{br} are referred at the local SERR experienced at the crack tip. The measurement of δ was done using the optical microscope with 200x zoom. Measurements close to the crack tip require very high resolution to eliminate errors which can be experimentally difficult to implement. The COD δ was measured from the initial crack tip position. The measurements were taken at different points in a displacement hold position after the crack had arrested in a stick-slip manner under static loads. Experimental plots of G versus δ are shown in Figure 5-12a. The results were then curve-

fitted. The bridging traction law was then calculated by differentiating the *G-δ* curves and the results are shown in Figure 5-12b. The bridging traction law is observed to behave in an exponential function. These curves were found to be similar to other investigations of large scale bridging [129, 137, 138].

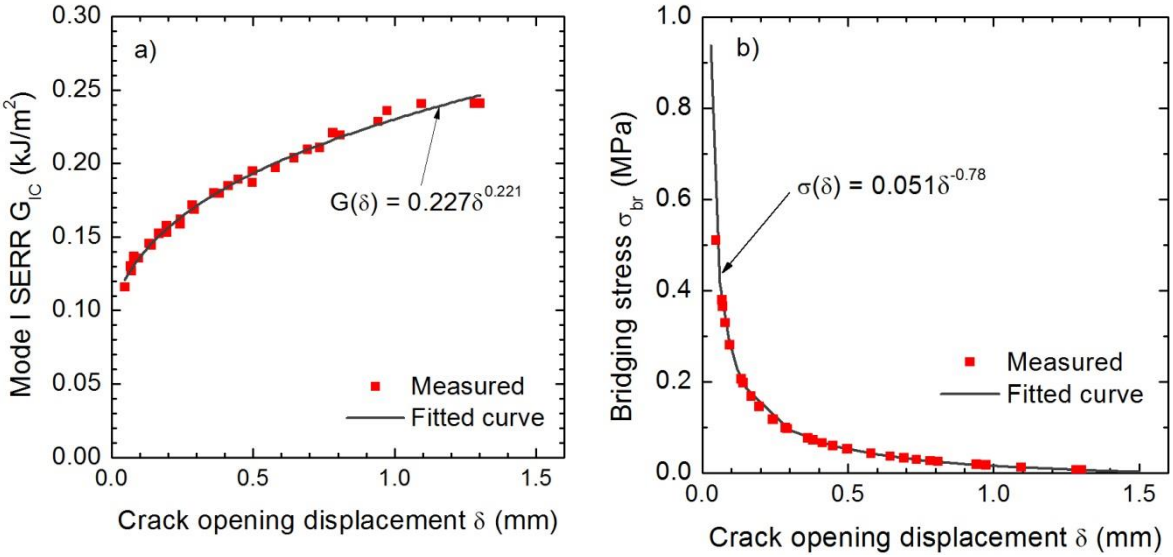

Figure 5-12: a) Measured G_{IC} versus crack opening displacement and b) calculated bridging traction law

It can be seen that there is some limitation in using the SERR-COD method of determining the bridging traction law. The stress distribution is significantly influenced by the fit of the SERR-COD curve, especially near the crack tip. No measurement data are available for very small δ due to the current limitations measurement equipment. As the value of δ approaches zero, the fit function approaches an asymptote as σ_{br} will approach infinity. Secondly, the exact value of δ_f is also difficult to determine due to the asymptotic nature of the function. Therefore the full description of the bridging law can only be resolved by making certain assumptions. From the R-curves, the contribution of the SERR due to fibre bridging is assumed to be approximately 140 J/m^2, given by the difference between the steady state SERR in the propagation phase and the initial SERR in Equation (5-14). The total crack growth length taken for the SERR to plateau is approximate 20 to 25 mm. This length is taken as the bridging zone length l_{br} where the bridging stresses vanish as δ reaches its maximum separation limit δ_f, as schematically shown in Figure 5-10. Therefore the values of the $\sigma_{br,max}$ and δ_f were selected to best fit the traction law derived from the SERR-COD approach while satisfying the criteria of G_{br} = 140 J/m2 and l_{br} = 20 mm. In an iterative method, the values of $\sigma_{br,max}$ and δ_f were

selected to be 0.73 MPa and 1.32 mm respectively, as shown in Figure 5-13 to satisfy the two requirements.

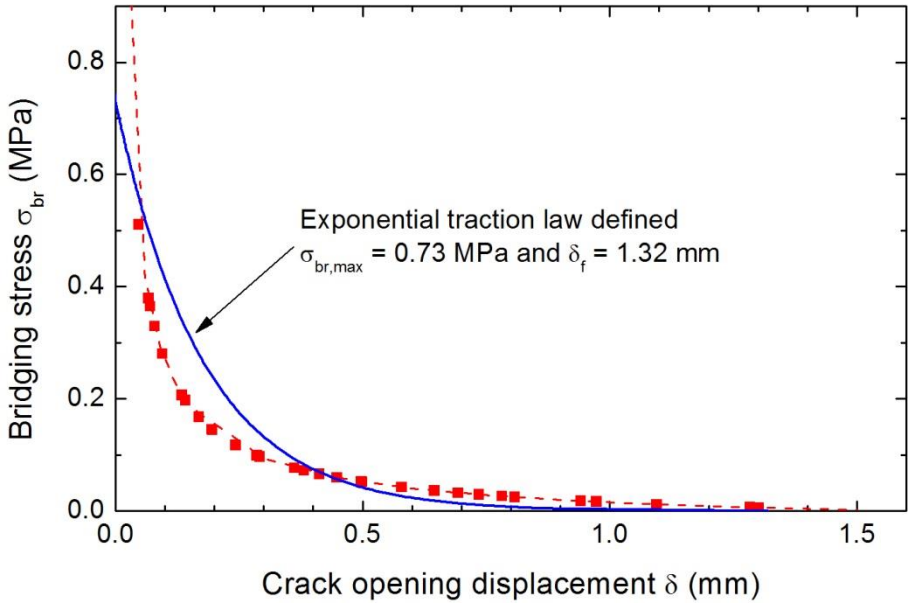

Figure 5-13: Definition of the traction-separation laws (fibre bridging) for static loading

5.4.3 Finite Element Modelling of Fibre Bridging

Cohesive elements are commonly employed to simulate progressive delamination within a composite laminate in a pre-defined path. In this work, the constitutive response of the cohesive elements encompasses of both the conventional atomic decohesion of the polymer matrix and fibre bridging along the delaminated crack plane. The underlying traction-separation behaviour is illustrated in Figure 5-14. The cohesive elements first behave linear-elastically until the damage initiation criterion is satisfied. Once damage has occurred, the traction stiffness is reduced following a degradation law. In Figure 5-14, it can be seen that the degradation law consisted of two processes; 1) the fracture of the matrix and creation of new crack surfaces which corresponds to the intrinsic toughness of the material G_i, and 2) the degradation of the bridging fibres defined by G_{br} which corresponds the extrinsic toughening provided by the bridging mechanism. In the first part of the degradation process associated with the matrix fracture, a linear stiffness reduction was modelled until the maximum stress of the fibre bridging traction σ_{br}. The identified bridging law (see Figure 5-13) was then appended to the traction-seperation law to complete the cohesive zone model which accounts for fibre bridging during the crack growth progression.

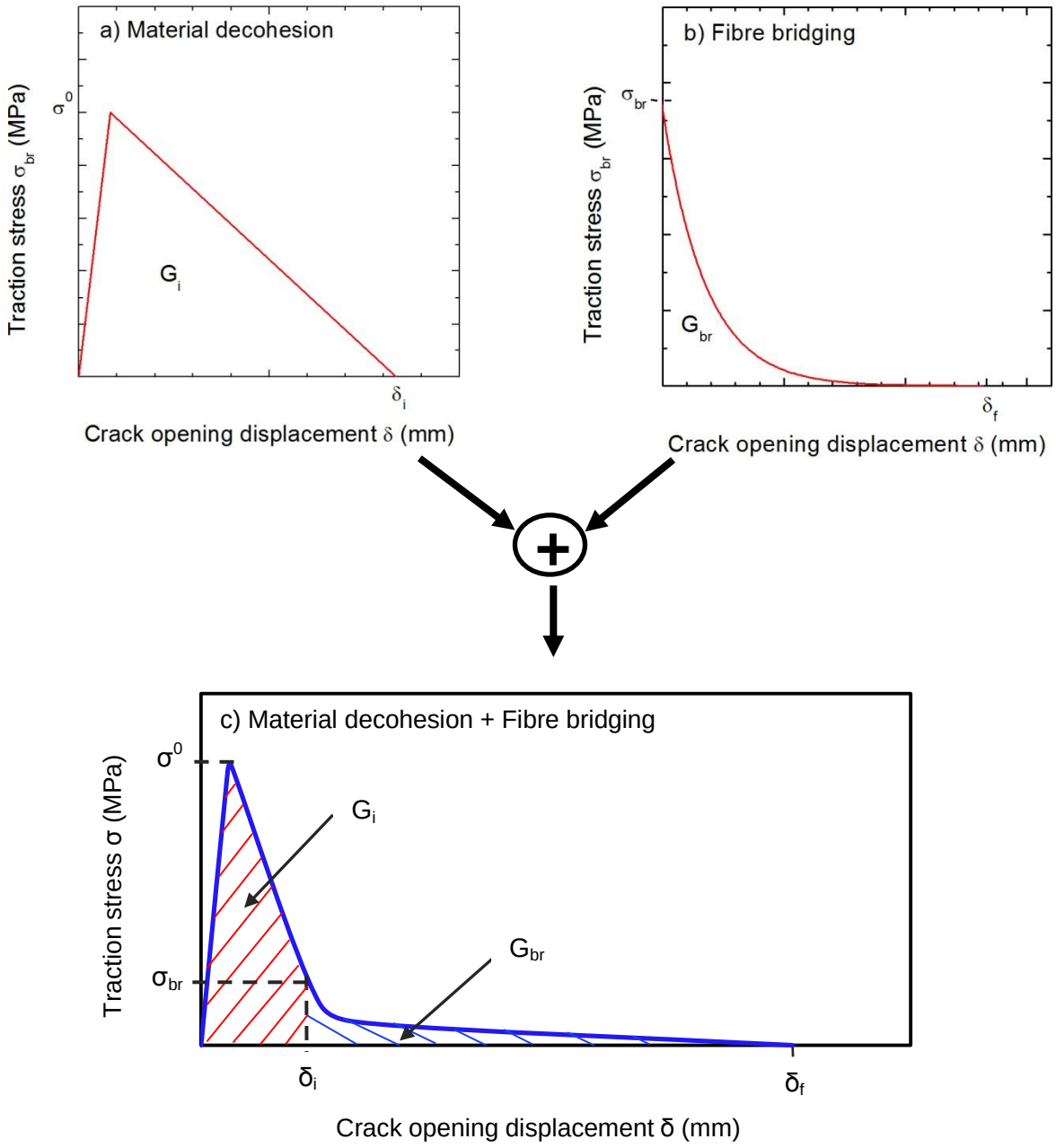

Figure 5-14: Traction-separation law of the cohesive zone model by appending the fibre bridging component to the material decohesion component

The damage initiation stress was taken to be 40 MPa which was the failure stress of the 90º laminates in tension. The initial stiffness was selected at 10^6 N/mm^3 to minimise its effect on the global compliance of the specimen prior to damage while maintaining numerical stability. The degradation law was implemented into the cohesive elements in Abaqus Standard v6.12 in tabular form using a displacement controlled damage evolution. Approximately 500 points (referring to Figure 5-14c) were used in the tabular inputs to avoid round-off and avoid sudden drop in the stiffness. The opening

displacement δ_i was determined such that the area under the curve for the first section of the degradation corresponds to G_i.

The substrate of the DCB specimen was modelled using four noded plane strain (CPE4R) elements. The substrates were connected by the cohesive zone which was discretised by 1000 zero thickness cohesive (COH2D4) elements. The surface-based TIE constraint was used to link cohesive layer and the continuum elements together. A feature of the TIE constraint is that it allows mismatch mesh to be constrained together. The model was loaded under displacement control and the boundary conditions are shown in Figure 5-10. Simulating the fracture process without fibre bridging can be done by omitting the second portion of the traction separation law in the cohesive zone model as shown in Figure 5-14a. The parameters of the cohesive law used are summarised in the Table 5-4.

Table 5-4: Traction law parameters of different cohesive law used in simulations

Traction law	Traction description	σ^0 (MPa)	G_i (kJ/m^2)	σ_{br} (MPa)	δ_f (mm)
1	Without bridging – bilinear (see Figure 5-14a)	40	0.1	-	-
2	With bridging – bilinear (see Figure 5-14a)	40	0.24	-	-
3	With bridging – bilinear-exponential (see Figure 5-14c)	40	0.1	0.73	1.32

The cohesive zone model (CZM) was validated by comparing the simulated load-displacement curve with the experimental results. A sample of the load-displacement curve from the static DCB experimental tests is shown in Figure 5-15. The onset of nonlinearity symbolises the start of crack propagation. Three cohesive law as detailed in Table 5-4 were used to simulate the crack propagation process in the DCB specimen. It can be observed that the cohesive law which ignores fibre bridging (traction law 1) was able to predict the onset of nonlinearity in the experimental load-displacement curve but grossly under-predicts the crack propagation phase. In traction law 2, the SERR contribution by the fibre bridging was included in the bilinear traction law parameter. In this instance, the crack initiation from the pre-crack was over-estimated. However the subsequent reduction in the applied load closely corresponds to the experimental data as the crack propagates. Hence the constitutive behaviour of the large scale fibre bridging must be correctly modelled into the traction law to accurately simulate the crack initiation and propagation phase. Implementing the measured bridging traction into the cohesive

law (traction law 3), it was able to replicate the experimental load-displacement response of the DCB specimens and, thereby, validating the parameters used for fibre bridging.

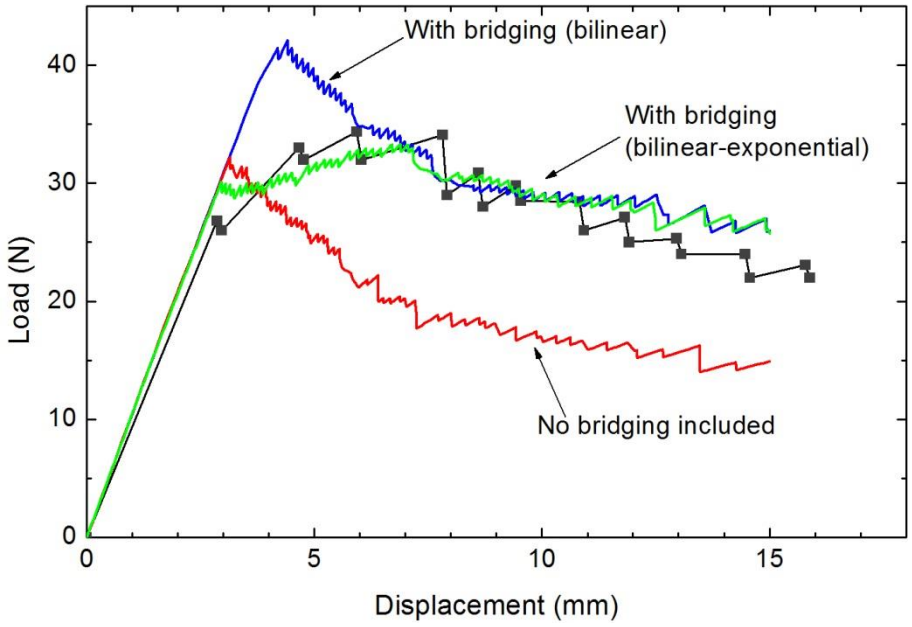

Figure 5-15: Comparison of load-displacement curves of DCB from experiment (lines with symbols) and simulation (lines). The red lines are cohesive model without bridging. The blue and green lines are cohesive model with bridging.

Shown in Figure 5-16 is the R-curve of the DCB specimen. The SERR were determined using the modified beam theory from the load-displacement curves derived experimentally and numerical simulations. The SERR from the numerical simulation corresponds well to the results obtained from experiments. The propagation plateau of the numerical G_{IC} was reached after a crack advancement of 15 mm which was 5 mm shorter than the experimental results. As a convention, the numerical crack tip is demarcated as the start of the bridging zone. For fibre cross-over bridging and brittle fracture, the crack tip is observed to be at the start of the bridging zone. However this definition may result in some ambiguity for ductile fracture due to the large process zone and softening of the material prior to failure. Hence care must be taken in the crack tip definition to correctly reflect the experimental observation for ductile materials.

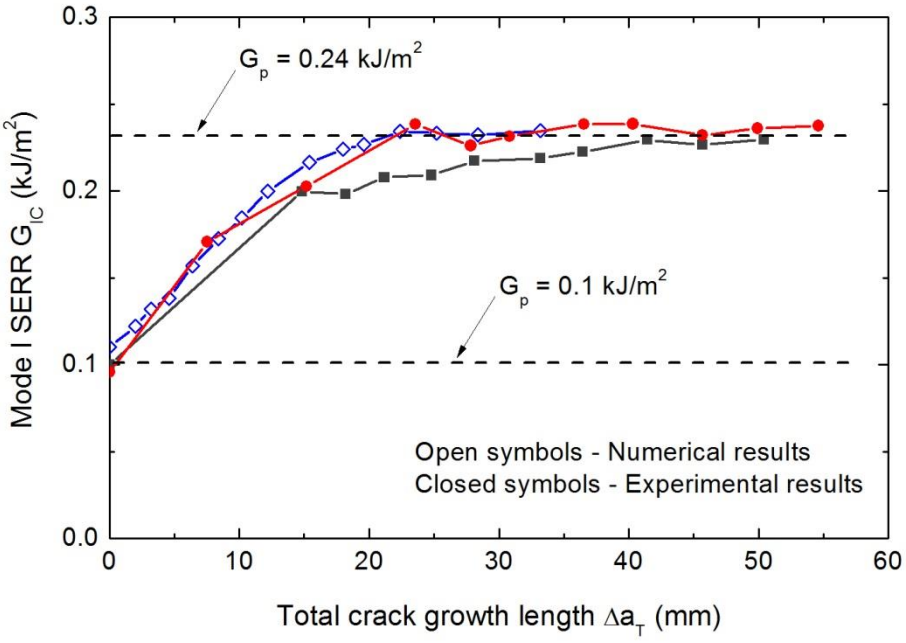

Figure 5-16: Strain energy release rate versus the total crack growth length obtained experimentally and numerically

Shown in Figure 5-17 is the measured crack opening displacement of the DCB specimen that underwent static fracture. It can be observed that the crack opening displacement of the crack is higher than the measured values if large scale fibre bridging was not correctly modelled using the bilinear bridging law. With the measured bridging traction law implemented, the crack opening displacement closely corresponds with the experimental measurements. Therefore the parameters of the bridging law, shown in Figure 5-13, are validated in these analyses.

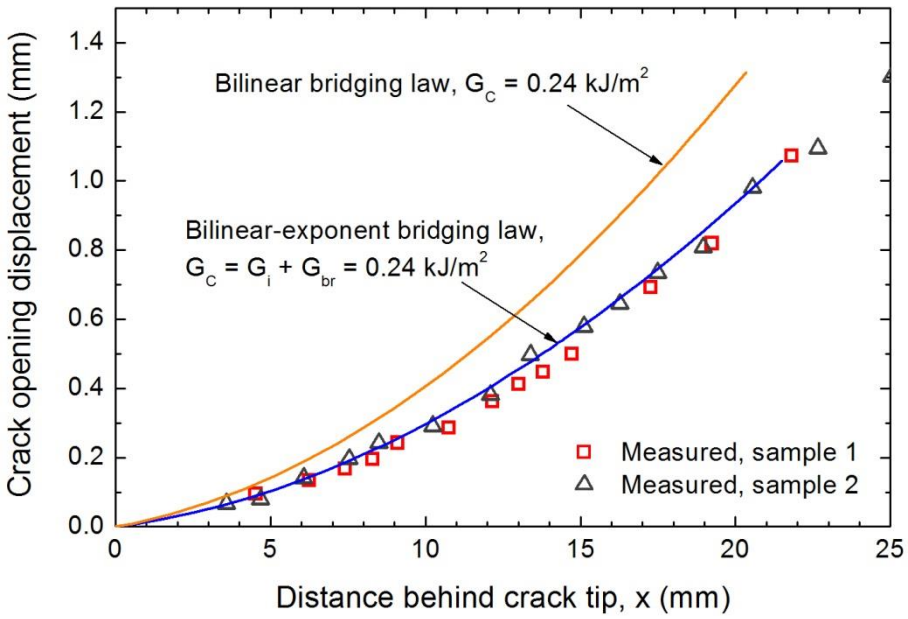

Figure 5-17: Crack opening displacement of DCB specimen under static loading

For sub-critical loads, the crack opening displacement is smaller than the ones under static fracture. Having characterised the static bridging law based on the SERR-COD approach, this then raises the question of how will the fatigue bridging law differ from the static bridging law. Previous attempts to characterise fibre bridging phenomenon under fatigue were performed by normalising the Paris equation with the R-curve [130, 131, 133]. This would require an assumption that the static and fatigue bridging traction laws are identical. However Yao et al. reported that two distinct fatigue resistance curves were obtained for two identical laminates with a bridging zone length of 10 mm [132]. In one specimen, the bridging zone was formed under cyclic loads of R = 0.5 and the bridging zone in the other specimen was produced under static loads. After which, the fatigue test commences and the delamination growth rates were recorded. This has led to them to speculate the damage state and fatigue bridging law is different from the static one. Stutz et al. also found the parameters of the fatigue bridging law to be different from the static bridging law using the inverse numerical procedure [138].

In the following work, a numerical analysis of the influence of large scale bridging on the SERR experienced at the crack tip was carried out. Virtual Crack Closure Technique (VCCT) was used to calculate the crack tip SERR of a non-propagating crack front. The schematic of the DCB model is shown in Figure 5-18. The crack consisted of a region of 50 mm from the load application point that is free from fibre bridging and a region of 20 mm fibre bridging zone. The fibre bridging is represented by cohesive elements. Its properties consist of the only the measured bridging traction properties and

is summarised in Table 5-5. The remaining length of the upper and lower substrate was bonded together by VCCT using the *DEBOND keyword in Abaqus Standard.

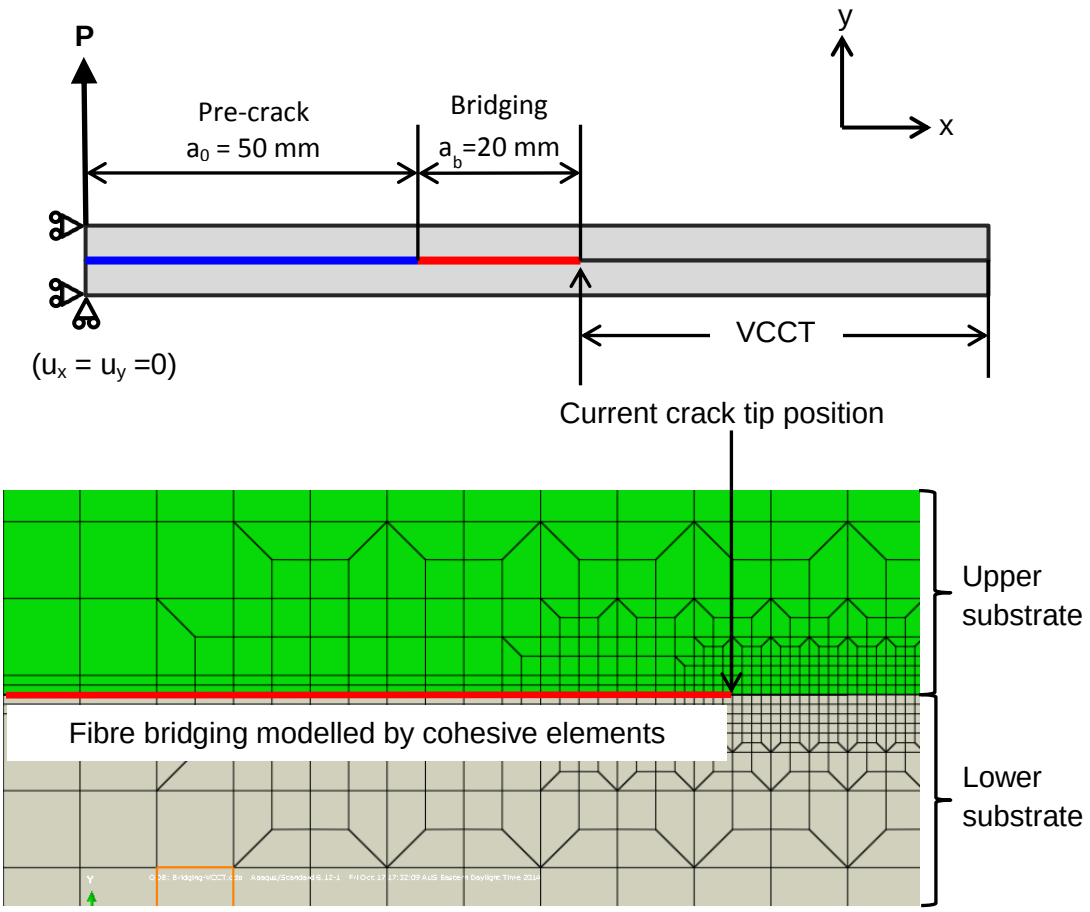

Figure 5-18: Schematic of the DCB model with fibre bridging of a non-propagating crack

Table 5-5: Traction properties to simulate fibre bridging only in VCCT analysis

Traction law behaviour	Elastic stiffness K_b	Maximum traction stress σ_0	Maximum traction separation δ_{max}	Rate of damage evolution α
Exponent damage evolution	120 N/mm^3	0.73 MPa	1.319 mm	7.5

The steady state fatigue bridging law would be different from the static bridging law from the evidence given by Yao et al. [132] and Stutz et al. [138]. This is due to the different damage state of the bridging zone under sub-critical loadings. Figure 5-19 illustrates the static bridging law and the steady state fatigue bridging law. Once self-similar crack growth is achieved, the fatigue bridging law was assumed to have lower δ_{max}

as the additional fatigue damage induced to the bridging zone by cyclic loadings reaches steady state.

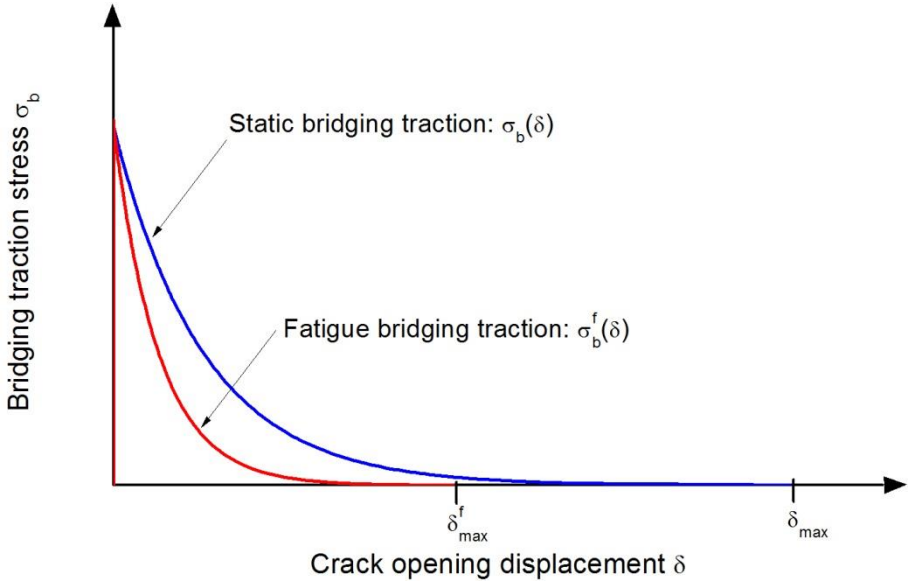

Figure 5-19: Bridging traction law for the static and fatigue case

Shown in Figure 5-20 is the effect crack tip shielding as a result of fibre bridging. The crack tip SERR was determined by VCCT from the numerical analysis while the global SERR was calculated from the load-displacement response of the model with beam theory analytical solution. It can be seen the crack tip and the global SERR is the same when fibre bridging is ignored. The static bridging law, denoted by the red line in Figure 5-20 provide considerable shielding at the crack tip by holding the crack faces together and redistributing the crack tip stresses. Only once the applied SERR overcomes the bridging SERR G_b^f, the SERR at crack tip begins to increase and is equal to $G_{tip} = G_{global} - G_b^f$. Assuming the maximum traction separation of the fatigue traction law is $\delta_{max}^f = 0.5\delta_{max}$, it can be seen that the bridging SERR G_b^{f2} is approximately reduced by 43%. Under fatigue loading, the crack shielding characterised by G_b^{f2} should be much less than G_b^{f1}. Otherwise no crack growth will occur for $G_{global} < G_b^{f1}$.

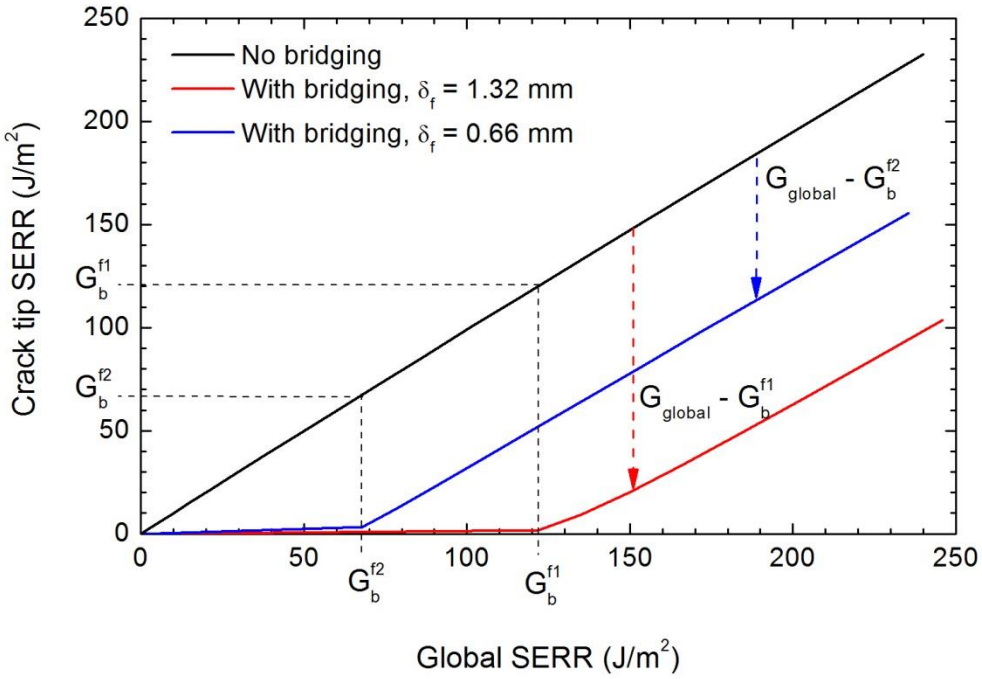

Figure 5-20: Influence of fibre bridging on the crack tip strain energy release rate

5.5 Correlation with Fatigue Crack Growth Rates

The role of plasticity induced crack closure and fibre bridging was investigated in this Chapter. While plasticity induced crack closure is found in off-axis ply interfaces, crack closure is assumed to be negligible in zero degree laminates due to the constraints provided by the fibres and plane strain conditions. Therefore fibre bridging was postulated to be the primary cause of the load ratio effects observed in the experimental results presented in Chapter 2.

Large scale fibre bridging, developed in the wake of the crack, is critically dependent on the crack size and is responsible for the rising R-curve toughness behaviour. The constitutive response of the fibre bridging under static loads was measured using the SERR-COD approach. Fibre bridging introduces a traction stress distributed over a large area on the crack faces and this, in turn, reduces the effective SERR experienced at the crack tip. Accordingly, the fatigue crack growth rates can be correlated to the SERR experienced at the crack tip, given as,

$$\frac{da}{dN} = C\left[\Delta G_{eff}\right]^m = C\left[\left(G_{max} - G_b^f\right)(1-R)^2\right]^m \tag{5-16}$$

where G_{max} is the SERR determined by the global response of the DCB specimen and G_b^f is the amount of crack shielding provided by the fatigue bridging law. G_b^f should be approximately less than or equal to the fatigue threshold SERR as no crack growth will occur due to the crack tip SERR being close to zero. Therefore a self-consistency analysis was carried out to determine if a unique value of G_b^f can be obtained which is capable of eliminating the load ratio dependency behaviour in the experimental data. The threshold SERR $\Delta G_{eq,th}$ was taken at da/dN = 1E-9 m/cycle. By adjusting G_b^f, $\Delta G_{eq,th}$ reaches a crossover point where its value for all three load ratio are approximately the same. Further increases in G_b^f causes the $\Delta G_{eq,th}$ to be over compensated. Based on this analysis, the value of G_b^f was selected to be 61 J/m^2. This value was used to determine the fibre bridging correlating parameter capability of converging the fatigue crack growth rates into a narrow band.

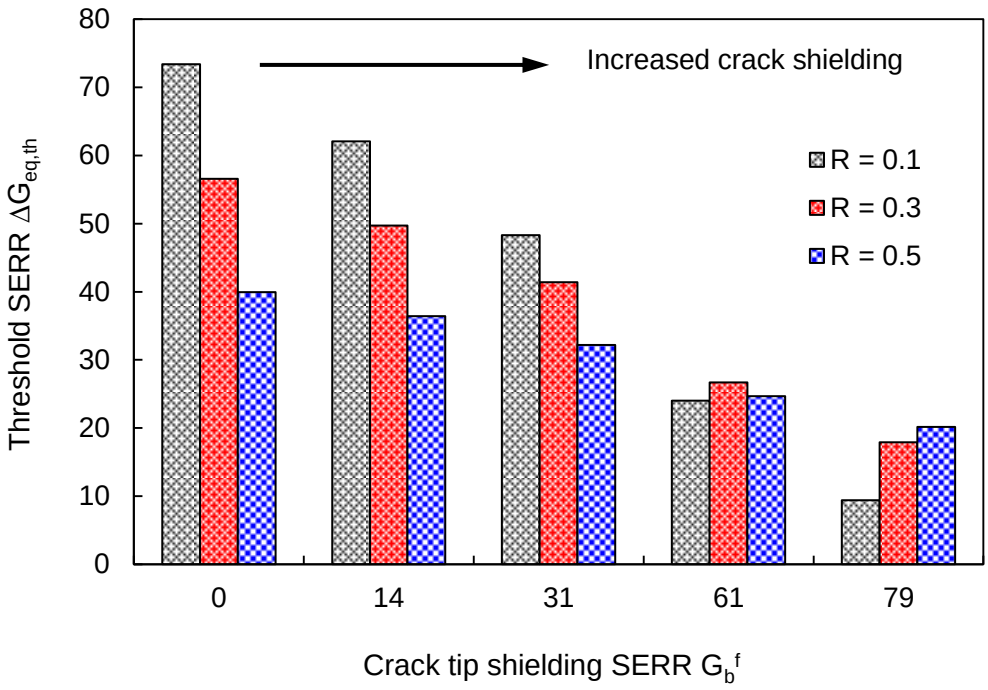

Figure 5-21: Self-consistency check to determine the crack tip shielding strain energy release rate G_b^f for a fatigue bridging traction law

The Mode I fatigue crack growth rates of the IM7/977-3 laminates are correlated against the controlling parameter ΔG_{eff} defined in Equation (5-16). Using this definition, the load ratio effects in the threshold region are eliminated. However significant load ratio effects can still be observed in the mid-high SERR region. This can be due to the material's sensitivity to G_{max} as its approach G_C at higher load ratios. The Forman

equation can provide an alternative in expressing the fatigue crack growth rate to eliminate the influence of high values of G_{max}.

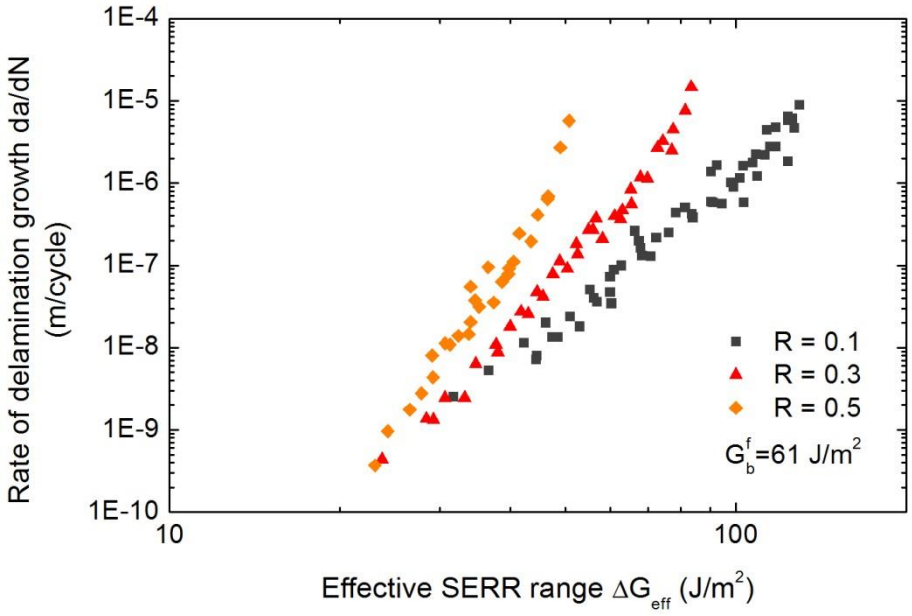

Figure 5-22: Experimental Paris plot of IM7/977-3 carbon/epoxy laminate correlated with ΔG_{eff}, accounting for the effects of fibre bridging

The Forman model is modified to account for fibre bridging in composite delamination and is expressed as: -

$$\frac{da}{dN} = \frac{C_F\left(\Delta G_{eff}\right)^{m_F}}{(1-R)\left(\sqrt{G_C^f} - \sqrt{G_{max}^f}\right)} \tag{5-17}$$

where $G_C^f = G_C - G_b^f$ and $G_{max}^f = G_{max} - G_b^f$.

A unique solution for the Forman parameters C_F and m_F must be established for all the load ratios in order for the Forman model to be applicable. The critical fracture toughness G_C is taken as 240 J/m^2 from the result of the static tests. The Mode I experimental results of the IM7/977-3 are plotted with the Forman model as shown in Figure 5-23. It can be seen that the correlation of the different load ratios was greatly improved. Consequently C_F and m_F is derived to be 4E-16 and 5.04 respectively. It can be seen that the slope of the Forman plot (m_F = *5.04*) is now significantly lower as compared to data before fibre bridging was taken into account (m = 10 for R = 0.1, m =

12.8 for R = 0.3 and m = 15.7 for R = 0.5). Although the slope is still considered high as compared to conventional materials such as aluminium, the delamination crack growth rate may not be as sensitive to small changes to load applied as initially thought. This may enable designers to permit for very slow growth while still maintaining the benefits of a safe life design.

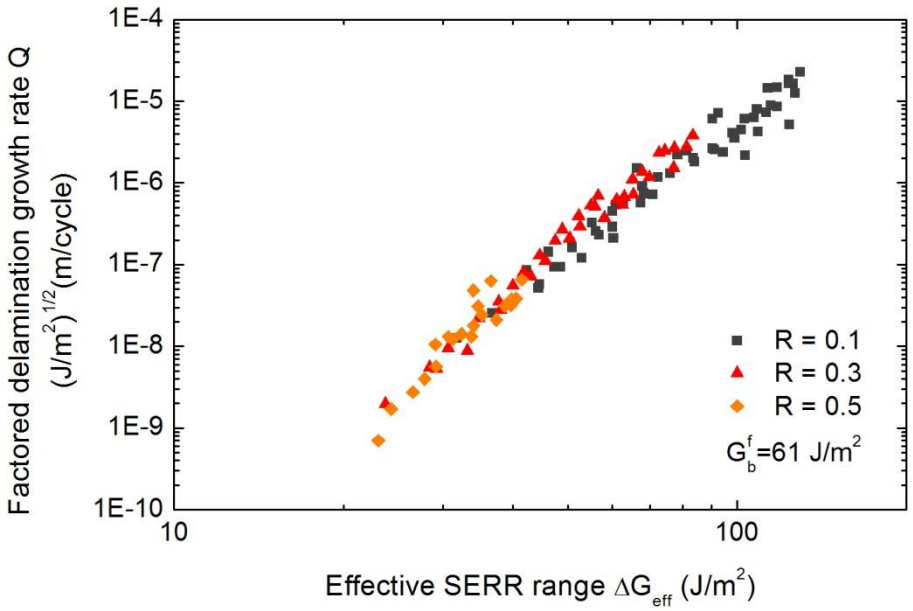

Figure 5-23: Forman plot of IM7/977-3 carbon/epoxy laminate correlated with ΔG_{eff}

The fibre bridging model was also applied to the Mode I experimental data of various 0º unidirectional carbon/epoxy laminate surveyed from literature. It should be noted that the authors did not make any indication of fibre bridging affecting the results. However plasticity induced crack closure was deemed to be absent in 0º unidirectional laminates. Consequently fibre bridging remains the only plausible explanation for observed load ratio effects. By doing a self-consistency analysis, the value of G_b^f each of the composite materials was determined. Figure 5-24 shows the Paris plot of the composite laminates analysed using the fibre bridging model. Although the correlation was improved as compared to ΔG_{eq}, The Paris plot of the fatigue delamination growth data still show considerable dependency on the load ratios.

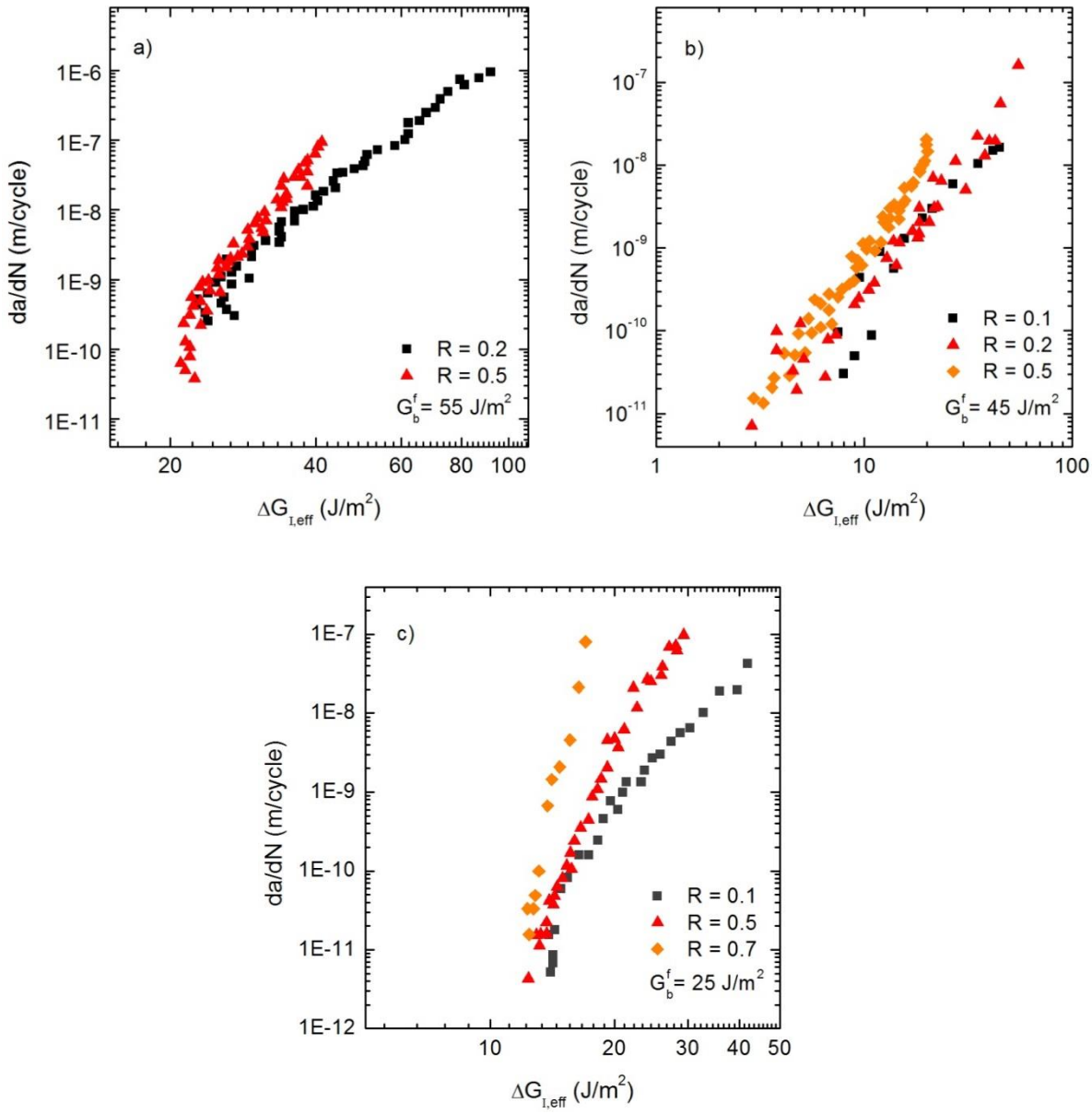

Figure 5-24: Paris plot of mode I delamination data from literature; a) AS4/8552 [28], b) T300/914C [35] and c) T300/P305 [35]

The Forman model was used to replot the fatigue delamination data as shown in Figure 5-25. The critical SERR G_C of the AS4/8552, T300/914C and T300/P305 is given as 350 J/m^2 [28], 160 J/m^2 [35] and 250 J/m^2 [35] respectively. It can now be observed that the correlation has improved further and the delamination growth of different load ratios is collapsed into a narrow band. Hence it can be concluded that the fibre bridging model is able to eliminate the load ratio effects observed in composite fatigue behaviour. Unlike previous models, this correlating parameter uses the physical basis of fibre bridging of explaining the load ratio dependency behaviour.

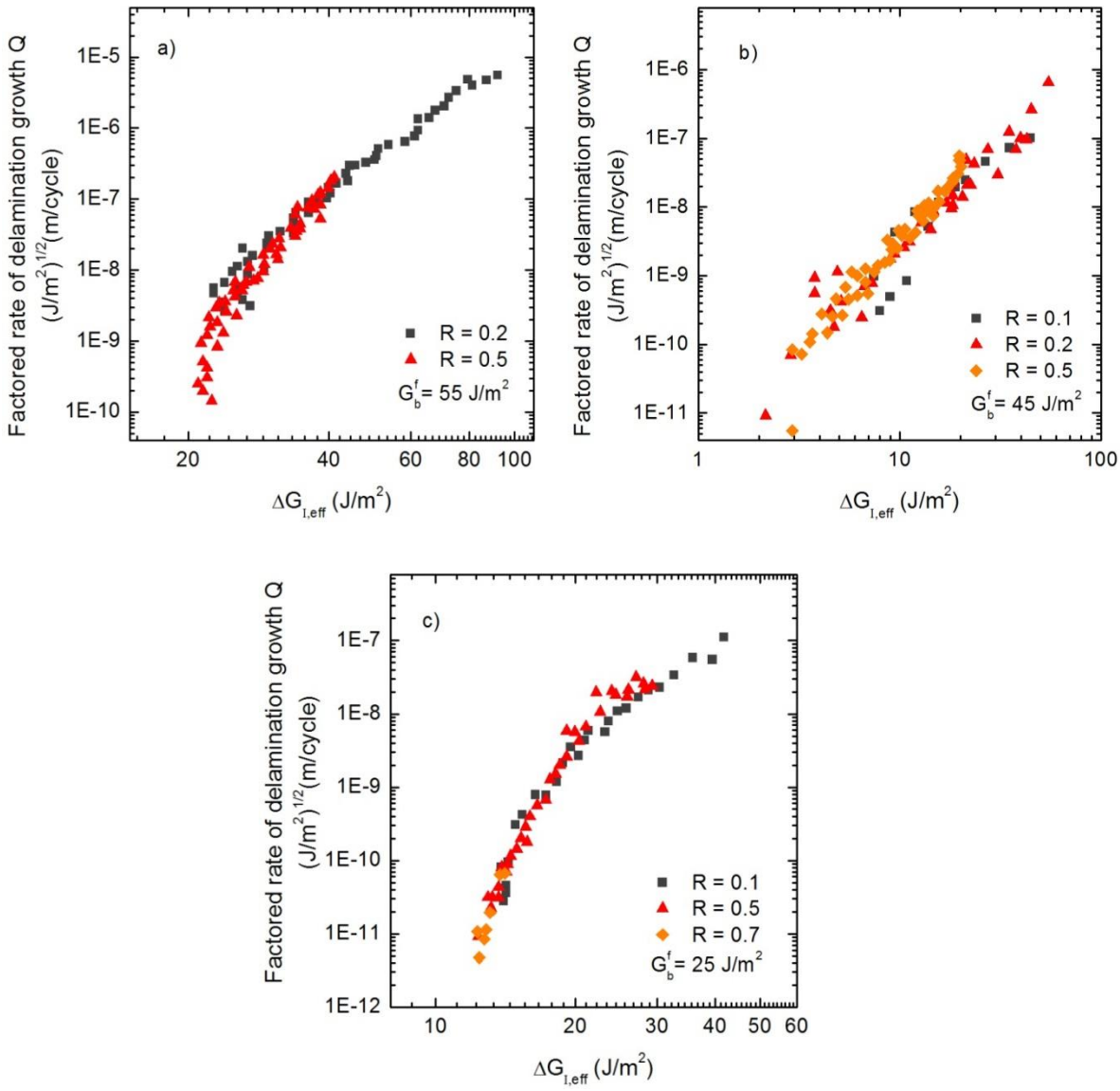

Figure 5-25: Forman plot of mode I delamination data from literature; a) AS4/8552 [28], b) T300/914C [35] and c) T300/P305 [35]

5.6 Concluding Remarks

A phenomenological approach had conventionally been employed to model the observed strong dependence of delamination growth rates on load ratio. A fatigue degradation algorithm implemented into cohesive elements has been found unable to predict the observed load ratio dependency behaviour of the composite laminates. Therefore computational modelling has been performed to examine two possible mechanisms, plasticity induced crack closure and fibre bridging, responsible for the phenomenon of load ratio effects.

Plasticity in composite laminates is typically ignored due to the assumed brittle nature of the matrix. However extensive plasticity can occur within the matrix prior to failure as presented in the stress-strain fields of the micromechanical model. The Hill's plastic potential was used to model the anisotropic yielding of the laminate. The numerical results confirmed the absence of crack closure in the delamination growth along a 0°//0° ply interface, but strong closure for cracks growing along 45°//0° and 90°//0° ply interfaces, due to the matrix plastic deformation.

Having established that plasticity induced crack closure was not responsible for the observed load ratio effects in the experimental results of laminates made of zero degree plies, fibre bridging is left as the primary cause. Significant fibre bridging was observed in the wake of the crack. The static bridging traction law was determined by the SERR-COD method. Fibre bridging was found to significantly shield the crack tip by reducing and redistributing the stresses. The fatigue bridging traction law was postulated to differ from the static one due to its damage state as it undergoes fatigue damage. The fatigue crack shielding SERR was determined using a self-consistency method. A new correlating parameter accounting for fibre bridging was proposed. In conjunction with the Forman model, good correlation was obtained for the fatigue data generated in the laboratory and taken from literature.

Chapter 6

Mixed Mode Crack Propagation in a Cracked Lap Shear Specimen

6.1 Adhesive Bonded Repairs

Adhesively bonded repairs are designed for either very slow or no crack growth to ensure safe operation because the rate of crack growth is highly sensitive to changes in the applied load compared to metals. Consequently bonded repairs are often designed to operate below the fatigue threshold loads or not to grow to critical size to prevent catastrophic failure from the growth of an existing flaw. The fatigue crack growth behaviour of composite laminates and bonded joints under pure Mode I and Mode II has been investigated in earlier chapters. However, fatigue cracks in typical repair configurations, such as a patch repair and a step-lap or scarf repair for a flush surface, may occur under a mixture of Modes I and II due to load path eccentricity. The Mode III contribution is not considered as it is generally insignificant due to the constraints of adjacent plies [141, 142].

It is costly to test all mixed mode and loading ratio combinations. Consequently it is important to define the design threshold criterion that correctly characterise the threshold and subcritical strain energy release rate (SERR) at varying mixed mode combinations. Suitable inspection intervals could then be predicted with higher accuracy. Therefore it is important to quantify the effect of mixed mode loading on fatigue crack growth in bonded and composite structures.

As compared to fatigue crack growth in homogeneous materials, fatigue crack growth in bonded joints and composite laminates exhibit a strong dependence on the SERR and are very sensitive to the mixed mode ratio [143]. Cui et al. reported poor prediction of the onset of delamination under mixed mode using a stress criterion that was based on only either peel or shear component [144]. Relation between Mode I and II SERR had been proposed to account for the dependence of the fracture energy on mixed

mode. For example, the power law [145] and B-K law [72] are established failure criteria to model this dependence under static loading. These criteria are largely empirical requiring some fitting parameters to be obtained over a range of experimental data. The equivalent correlating parameter under mixed mode fatigue loads was typically derived from the static mixed mode criteria such as the power law and B-K law.

This Chapter presents an investigation of the mixed mode fatigue crack propagation behaviour. Three different cracked lap-shear (CLS) specimens, representative of a bonded patch repair with an existing flaw, were tested. These geometrical configurations provided different mode ratios of G_I and $\underline{G_{II}}$. The virtual crack closure technique (VCCT) was employed to determine the SERR for CLS specimens. A correlating parameter was then proposed to account for the influence of mixed mode on the fatigue crack growth.

6.2 Experimental Setup

6.2.1 Materials and Specimen Geometry

The CLS specimen, as shown in Figure 6-1, was used to study the behaviour of fatigue crack growth under mixed mode because it represents a simple bonded patch repair subjected to in-plane loading. Both shear and peel stresses are present in the bondline as a result of the change in joint stiffness in the overlap region. The ratio of mode mixity can be adjusted by changing the relative thickness of the doubler substrate. The parent substrate consisted of a quasi-isotropic layup configuration of $[+45/0/0/-45/90]_{3S}$ with +45 degree ply at the substrate-adhesive interface. The averaged thickness of a cured ply was approximately 0.13 mm. The 0^o ply was orientated along the x-axis, which coincides with the main loading direction. The current work employs geometry of a doubler thickness, consisting of 1/3, 2/3 and 1 times the number of plies of the parent substrate. The 1/3, 2/3 and 1 doubler thickness is denoted as specimen Type I, II and III. Although the terminus of a patch repair is likely to be tapered to reduce the magnitude of peel stresses, the CLS specimen has a block end configuration to maintain a constant SERR that is dependent only on the applied loads. The lengths of doubler and parent substrates were 350 and 240 mm respectively; the grip support was set at 120 mm on both ends. The width of the CLS specimen was 20 mm.

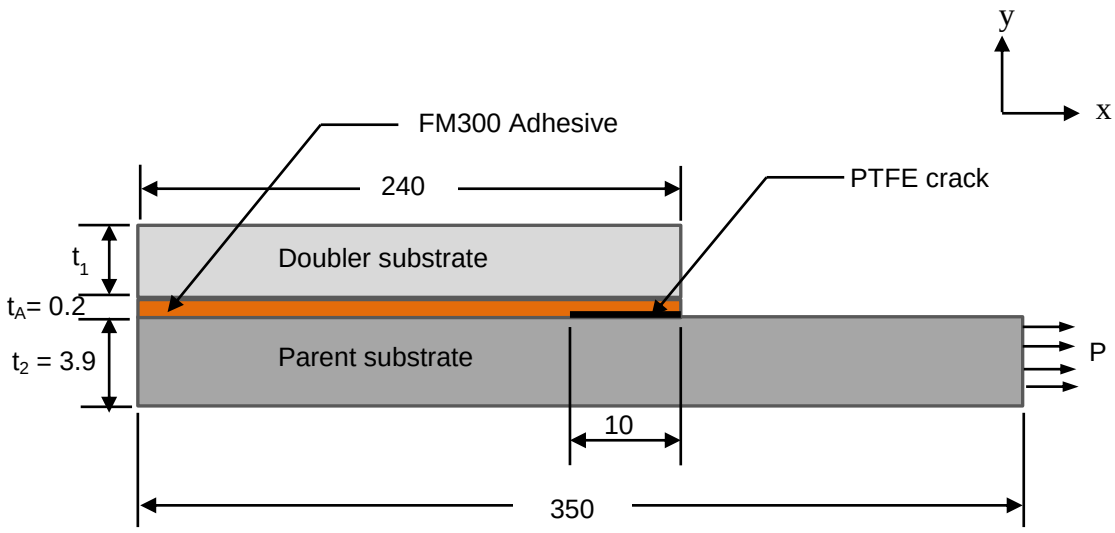

Figure 6-1: Geometry and dimensions of the cracked lap-shear specimen (all dimensions are in mm. Not to scale)

The bonded system consisted of carbon/epoxy (IM7/977-3) substrates, secondarily bonded with FM300-2K adhesive. The FM300-2K adhesive is an epoxy film adhesive supported by a carrier fabric and has a curing temperature of 120 ºC. The composite substrates were lightly grit blasted. Specimens were fabricated by conventional secondary bonding procedure in a vacuum bag under atmospheric pressure in an oven. This process was to simulate the bonding process of a bonded patch repair. The average bondline thickness was approximately 0.2 mm. A 10 mm pre-crack was produced by inserting a poly-tetrafluoroethylene (PTFE) film of 13 µm thickness at the interface of the adhesive and parent substrate. Tabs of the same doubler thickness and width, 60 mm long were bonded using Araldite epoxy adhesive on the parent substrate. To perform finite element (FE) analysis, the average values of all dimensions were used as shown in Figure 6-1.

6.2.2 Fatigue Test Procedure

The objective of the test program was to measure the fatigue crack growth rates under mixed modes. The fatigue tests of all specimens were carried out in a servo-hydraulic MTS 100 kN machine at a cyclic frequency of 10 Hz. Constant amplitude tension-tension loads were applied at a stress ratio of 0.1, 0.3 and 0.5. The maximum sinusoidal load ranged from 6 to 15 kN. The fatigue cycles were monitored throughout the test and fatigue crack growth was visually inspected and measured via a 200x optical traveling microscope. The measured crack growth length and fatigue cycles provide the fatigue

crack growth rates, da/dN. The SERR is used to characterise da/dN. The SERR of a CLS joint, derived from beam theory, is expressed as such

$$G = \frac{P^3}{2B^2}\frac{E_1 t_1}{E_2 t_2 (E_1 t_1 + E_2 t_2)} \tag{6-1}$$

where the subscript 1 and 2 denotes the doubler and parent substrate respectively. *P, B E* and *t* stand for the applied load, specimen width, Young's modulus and thickness respectively.

However the beam theory solution does not take into account for the bending deflection of the single CLS specimen. This will lead to either an overestimate or underestimate of the SERR and its individual mode components. The CLS specimen undergoes geometrically nonlinear deformation which may decrease the local peel stress at the crack tip, hence leads to lower mode I fracture component. Moreover the analytical solution does not separate the SERR into its individual mode components. Therefore a numerical analysis of the SERR in a CLS specimen was carried out to determine the individual mode I and II SERR components under representative experimental boundary conditions. The finite element analysis methodology is described in Section 6.3. It is interesting to note that, unlike the double-cantilever beam (DCB) or end-notched flexure (ENF) specimens, the beam theory solution for the CLS specimen (Equation 6-1) indicates that the SERR is independent of crack length. Therefore the constant thickness CLS specimen offers a convenient method in determining the mixed mode SERR as the precise location of the crack tip is not important.

6.2.3 Results and Discussion

Crack propagation was measured using travelling microscope throughout the tests. The crack growth rate was computed after the crack had propagated for approximately 1 mm to ensure the crack has propagated through the plastic zone of the previous load cycle. The possible failure modes that can occur in a bonded composite CLS specimen are cohesive, delamination, substrate failure or a combination of these. From the experimental investigations, it was observed that all the CLS specimens failed in the same consistent manner: a combination of intra-ply failure and delamination. The crack would firstly initiate from the PTFE pre-crack into the 45° interface ply of the parent substrate. A typical crack propagation path is schematically shown in Figure 6-2(a). The crack continued to propagate in this manner until it approached the 45°/0° ply interface.

Subsequently the crack path kinked and propagated along this interface in the form of delamination.

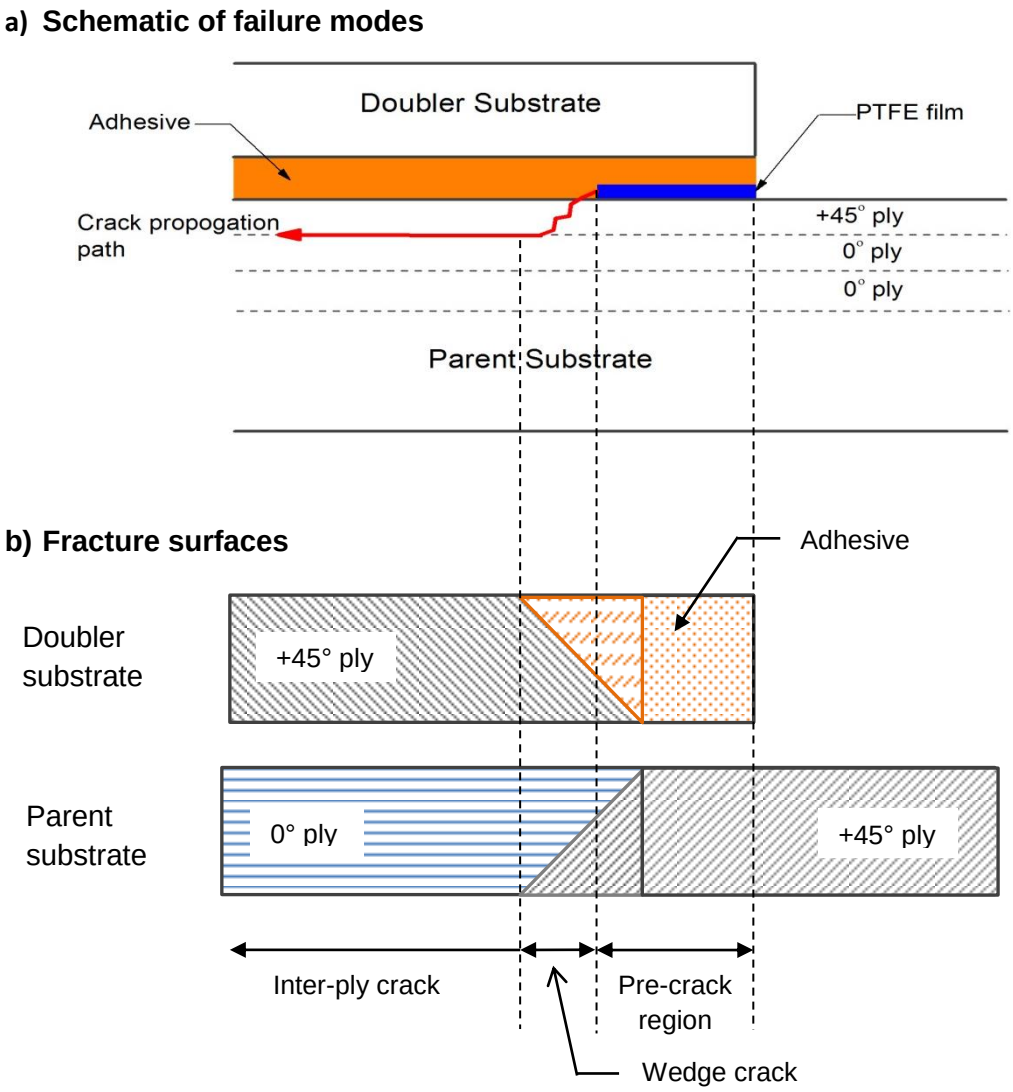

Figure 6-2: Failures modes in a CLS specimen subjected to cyclic loading

Figure 6-2(b) shows the schematic of the typical fracture surface of a specimen. The fracture area can be divided into three regions; the pre-cracked surface, a wedge-shaped crack surface and an interlayer crack surface. The pre-cracked surface is the interface of the adhesive and parent substrate where the PTFE film was placed. When crack initiated from the pre-cracked region, the crack path deviated from the initial crack plane and propagated into the interface ply in the form of a wedge-shaped area. The wedge-shaped crack formed approximately at the angle equal to orientation of the adjacent ply. The crack initiated at about mid-width of the CLS specimen into the interface ply. The crack then propagated width-wise along the direction of the ply angle.

After the crack had propagated past this area, delamination along the 45º and 0º ply interfaces now characterised majority of the crack propagation during the experimental testing.

Figure 6-3(a) shows a scanning electron microscopy (SEM) image of the side crack profile tip, of the CLS specimen Type I, taken approximately 1 mm behind the crack. The SEM micrograph clearly shows the crack propagated close to the interface of the 0° and 45° plies adjacent to the adhesive layer. Moreover, unlike the crack propagation in a 0° unidirectional DCB composite laminate reported in Chapter 3, no fibre bridging could be observed along the crack propagation path. The SEM micrographs of a typical fracture surface are also depicted in Figure 6-3(b) and Figure 6-3(c). Zero degree fibres and hackles between the fibres can be observed on the fracture surfaces of the parent substrate. Hackles are the resin material which is parabola shaped, pointing “upwards” and elongated along the loading direction. The loading direction is also the direction of crack propagation. This is an indication that the local stresses were acting in the out-of-plane direction as a result of mode mixity. The hackles possibly developed under plastic strains in the direction of the local principal stress. This is a resultant of the presence of peel stress at the crack tip that is the tensile Mode I. The crack propagation was believed to be stable. The tip of the hackles is noticeably blunt which can be associated to the variation in cyclic stress levels and crack growth and arrest. The propagation of crack under mixed mode along the delamination plane progresses by coalescing of the micro-cracks formed ahead of the main crack tip under the local tensile mode, as evident by the hackle pattern. The imprints of the zero degree fibres can be observed on the corresponding fracture surface of the doubler. As no fibre bridging occurred, the fracture surfaces were relatively “clean” and broken fibres were not evident.

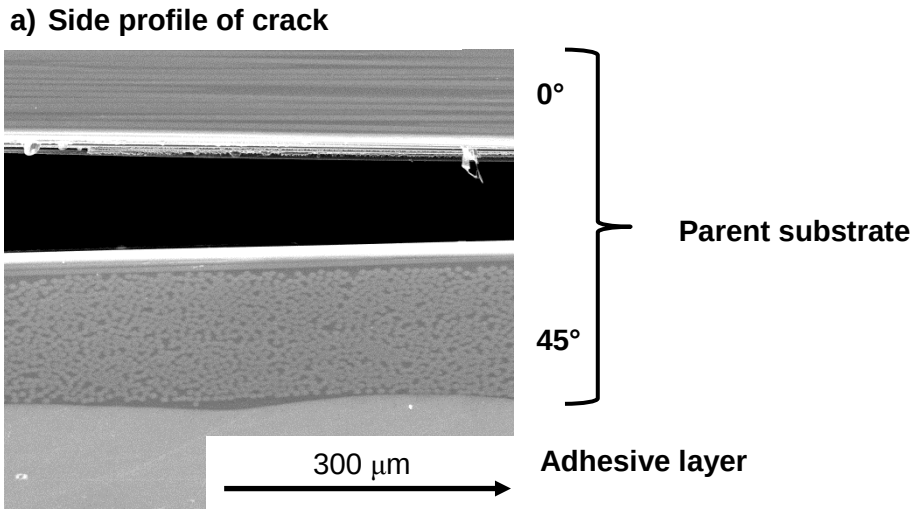

Figure 6-3: Scanning electron micrographs of cracked lap shear specimen a) crack profile, b) fracture surface on parent substrate and b) fracture surface on doubler substrate

Similar crack propagation behaviour was reported for bonded composite joints of varying mixed mode ratios and interface ply orientations [27, 29, 143, 146]. Intra-ply failure will always occur whenever the fibre orientations of the adjacent ply are not parallel to the crack growth direction. As a direct comparison, Johnson and Mall reported that the crack propagation mode was also a combination of intra-ply and delamination failure for the 45º interface ply in the parent substrate [146]. They also indicated that the crack initiation stress is similar with a 0º or 45º interface ply as the crack will have to first initiate within the adhesive from the PTFE pre-crack. In the case of the 0º interface ply, the crack will continue to propagate in a cohesive manner, with the crack path being

closer to the parent substrate (which carries the load) than the patch substrate (the end is unloaded).

6.3 Finite Element Analysis

A bonded composite repair's response to an applied load is dependent on a number of geometric and material parameters. In this investigation, the CLS specimens were firstly analysed with Abaqus Standard solver to accurately determine the individual fracture mode components. The two-dimensional FE analysis accounts for the geometric nonlinearity associated with the large rotation in a CLS specimen where out-of-plane bending is not constraint at the end of the overlap region. Secondly, a simple parametric analysis of the CLS specimen was also conducted to better understand the crack growth behaviour under mixed mode. The effects of varying the substrates dimensions and boundary conditions are discussed. Finally the FE results were then used to correlate with the experimental results.

6.3.1 Modelling Methodology

A typical FE model of a cracked lap-shear specimen is shown in Figure 6-4. Only the gauge section between the machine grips was modelled. One end of the model was fixed in the X and Y translation and the other end was fixed only in the Y translation with an applied load. The first five plies adjacent to the bondline were modelled individually and subsequent layers were homogenised as an orthotropic laminate. The 0º ply was aligned along the X axis. Plane strain conditions were assumed. Unless stated otherwise, a sharp crack of 10 mm was embedded in the interface of the 45º and 0º ply layers. The placement of the crack was based on the experimental observation of the fracture path. The mesh consisted of quadrilateral elements. Fine mesh was used in the vicinity of the crack tip and had an aspect ratio of one as shown in Figure 6-4. The material properties of the composite laminate and adhesive are listed in Table 6-1.

Table 6-1: Material properties of IM7/977-3 ply and FM300 adhesive

Substrate : IM7/977-3				Adhesive : FM300-2K	
E_{11} =	159000 MPa	E_{33} =	9000 MPa	E =	2350 MPa
G_{13} =	4800 MPa	G_{23} =	4000 MPa	v =	0.4
v_{12} = v_{13} =	0.35	v_{23} =	0.3	σ_y =	83 MPa

The individual SERR components, G_I and G_{II}, were determined using VCCT. The displacements and nodal forces in the vicinity of the crack tip are used to compute G_I and G_{II}, based on the premise that the energy needed to lengthen a crack by a small increment is equal to the energy needed to close the crack back to its previous position. The details of the VCCT calculations are given in Section 4.5.3 and also in references [112, 147].

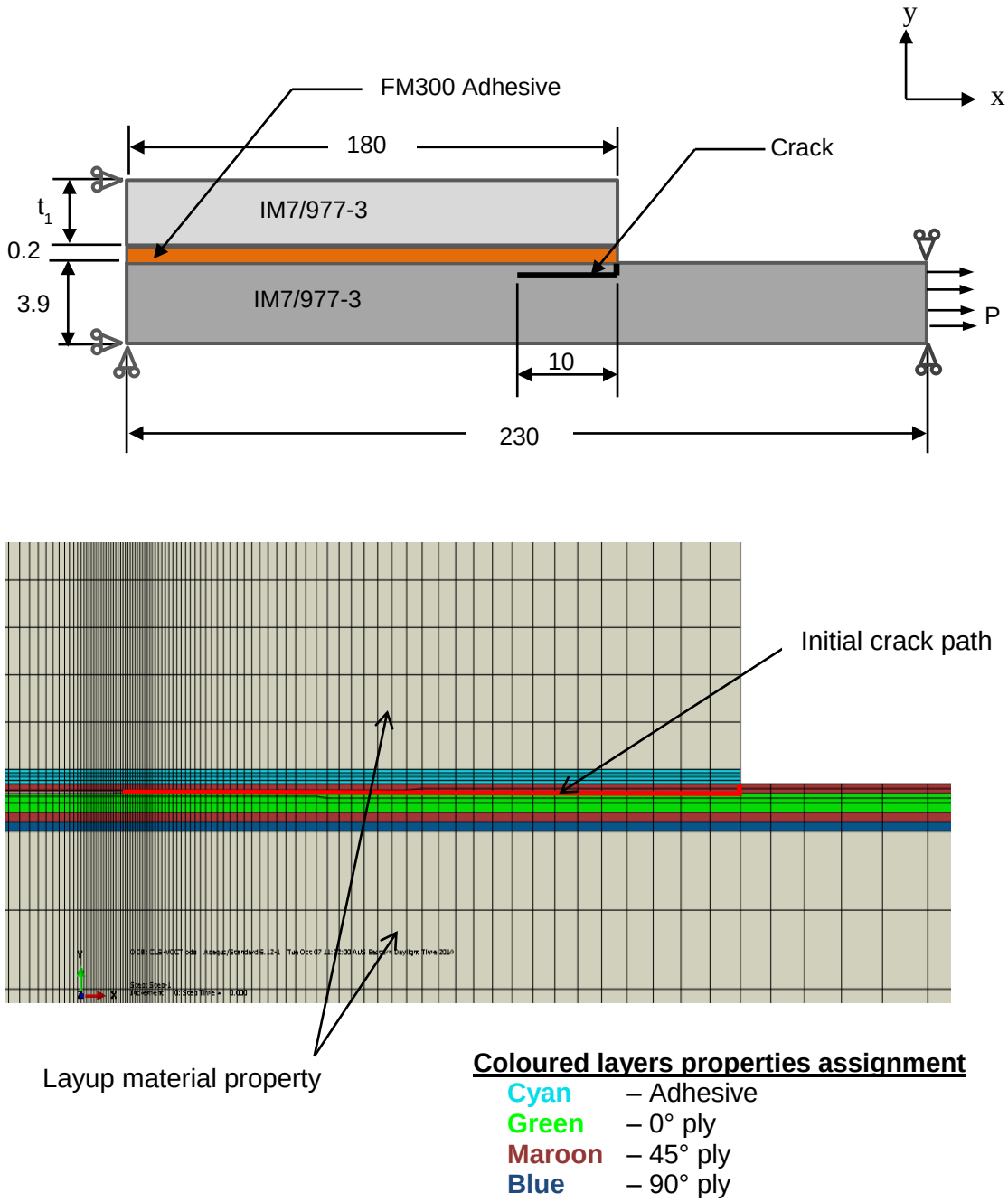

Figure 6-4: Geometry and boundary conditions of finite element model

6.3.2 Results and Discussion

Figure 6-5 shows the total, Mode I and II components of the SERR versus the crack length measured from the terminus of the doubler substrate. It can be seen that the total SERR G_T increases monotonically with crack length. The initial value of G_I is significantly higher for shorter cracks and gradually declines to a steady state value as the delamination crack increases. The G_I value in the short crack region was approximately twice the steady state value. The value of G_I is shown to decrease to zero as the crack length approaches zero [69]. It must be noted here at the total, Mode I, and Mode II strain energy release rates are all equal to zero when the crack size is zero. Previous studies have found that the G_I value increases to a peak value when the crack length is approximately the adhesive thickness [148]. This behaviour is similar to the distribution of the peel stress at the terminus in a bondline prior to the formation of cracks. The G_{II} value is initially much lower and gradually increases as the crack length increases. Therefore it is contended that Mode I is the dominant fracture mode when the crack is short (less than 2 mm). Once the crack length exceeds 2 mm, G_I and G_{II} are essentially constant for this given CLS geometry. Hence this simplifies the correlation of strain energy release rates with the fatigue crack growth data. The computed G_I and G_{II} at a crack length of 10 mm can be used to correlate with the experimental data of any crack length.

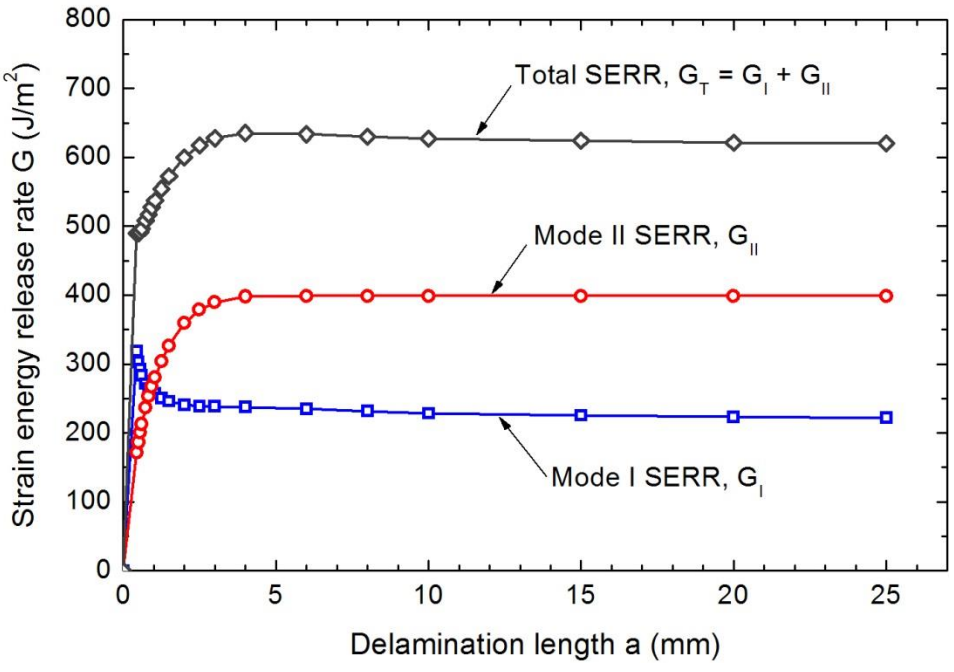

Figure 6-5: Variation of strain energy release rates with crack length. The applied load P = 750 N/mm.

The relations of the Mode I and II SERR components G_I and G_{II} with the applied load for the CLS specimens are shown in Figure 6-6. A decrease in the Mode I and II SERR can be observed with a decrease in the doubler substrate thickness. It can be seen that the magnitude of G_{II} is approximately proportional to the thickness of the doubler substrate. The Type I CLS specimen experiences about 1/3 of the G_{II} of the Type III CLS specimen, given that its doubler thickness is also 1/3 of the Type III CLS specimen. The redistribution of stress from the parent substrate to the doubler overlap region ensues by the shear lag mechanism and therefore G_{II} is directly related with the doubler thickness. The thicker the doubler, the higher the shear stresses needed to transfer the loads across the joint.

The presence of G_I is attributed to the out-of-plane bending of the specimens induced by the load path eccentricity. As seen in Figure 6-6a, the variation of the G_I with respect to the doubler substrate thickness is less than G_{II}. As all the CLS specimens were allowed to deflect without any constraint, the value G_I does not varied much. As a result, the mixed mode ratio $G_I/(G_I + G_{II})$ of Type I, II and III CLS specimen is given as 0.5, 0.41 and 0.36 respectively. Given that the SERR is independent of the crack length if it is sufficiently long, the experimental G_I and G_{II} can be determined from Figure 6-6 by means of regression analysis.

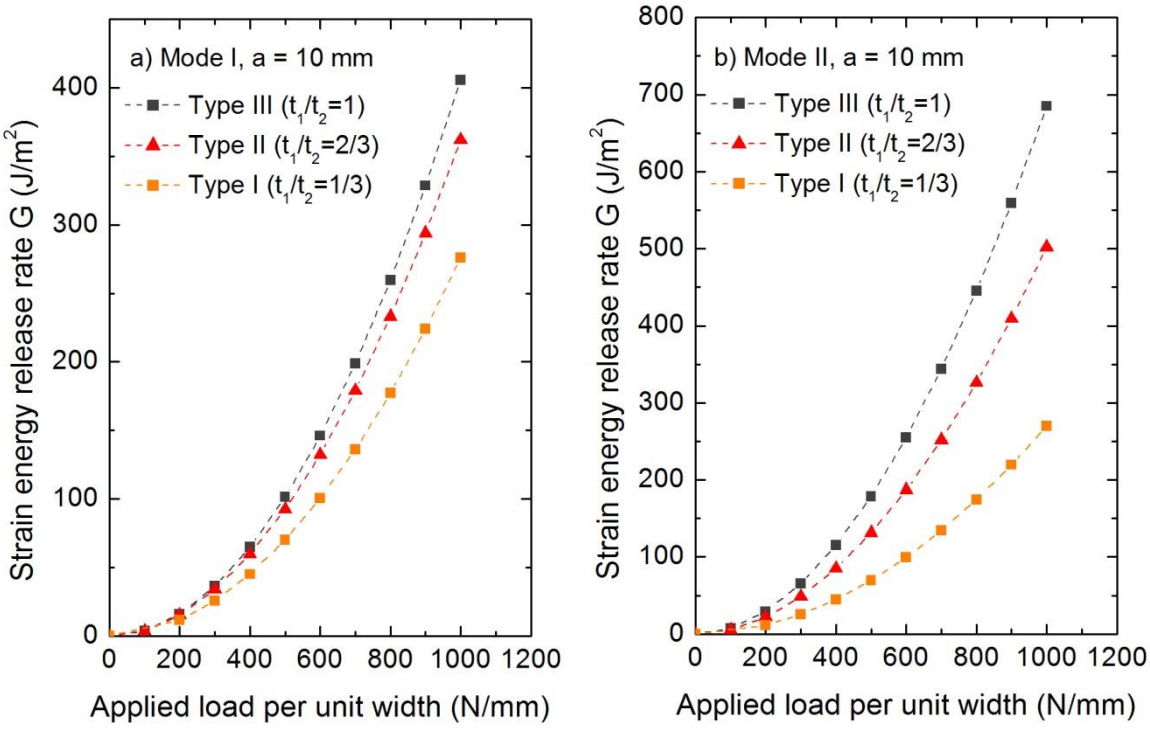

Figure 6-6: G_I and G_{II} versus the applied for Type I, II and III CLS geometry

An investigation was carried out to analyse the effect of the global bending of the CLS specimen. A CLS geometric configuration was analysed where the bottom of the CLS specimen was fixed in the Y-displacement. Hence the boundary conditions are akin to a double CLS joint where symmetry conditions are applied. The boundary conditions for both specimen configurations are schematically shown in Figure 6-7. The thickness of the repair substrate was also varied relative to the parent substrate in order to change the mode mixed ratio $G_I/(G_I + G_{II})$. The results in Figure 6-7 show that a range of mixed mode ratios can be achieved by changing the geometrical parameters and specimen configuration (i.e. single or double CLS specimen by apply Y-symmetry boundary conditions).

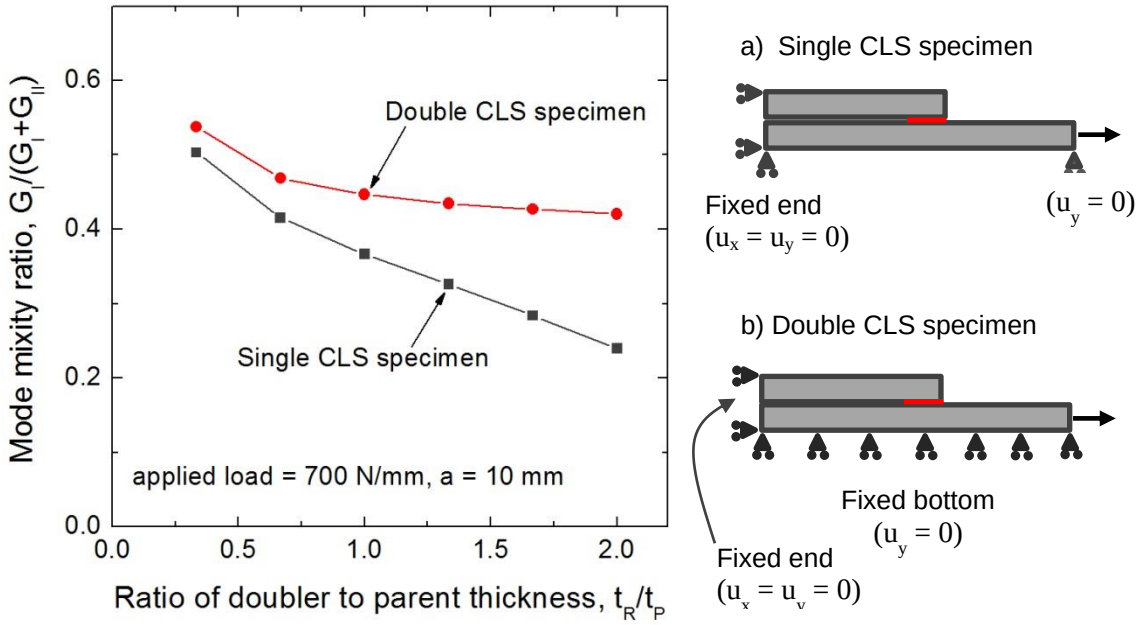

Figure 6-7: Variation of mixed mode ratio with boundary conditions (single and double CLS) and doubler substrate thickness

Assuming the crack growth is symmetrical on both side of the double CLS specimen, the bonded joint as a whole does not rotate. Only the overhang region of the doubler substrate, where the crack has propagated past, was allowed to deflect freely. As a result, the double CLS specimen has a higher $G_I/(G_I + G_{II})$ ratio than the single CLS specimen, as shown in Figure 6-7. When the repair substrate is thin, the overall bending deflection of the single CLS specimen is small. Therefore the mode mixed ratio is almost the same as the double CLS specimen. As the thickness of repair substrate increases, the bending deflection of the single CLS specimen increases due to greater load path eccentricity. This alleviates the peel stresses at the crack tip and $G_I/(G_I + G_{II})$ decreases

as a result. In the double CLS, the parent substrate is unable to deflect. Consequently, the Mode I and II SERR components are approximately proportional to the increase in repair substrate thickness, leading to an almost constant mixed mode ratio.

Lastly, a numerical investigation was conducted to study the behaviour of crack initiation under mixed mode. A number of studies had been done to investigate the crack growth behaviour under mixed mode. It was shown that fracture would generally occur in the direction perpendicular to the maximum principal stress [149, 150]. A vector plot of the maximum principal stress (denoted by red lines) and minimum principal stress (denoted by blue lines) directions acting in the vicinity of the crack in a Type III (t_1/t_2 = 1) CLS specimen is shown in Figure 6-8. It is shown that the crack will initiate and propagate at approximately 70° from the pre-cracked plane into the 45° adjacent ply. This corresponds to the experimental observation of the crack path propagation. Similar analyses were also conducted for Type I and II CLS specimens and the acting principal stress directions were similar. In the 0° ply, the fibres carry bulk of the tensile loads. The stress in the matrix is relatively low, making it difficult for fibre fracture or intra-ply matrix failure to occur in the 0° ply. Therefore the crack kinks and propagated in the matrix along the 0° ply interface. The acting maximum principal stress direction is also evident in the angle which the hackles occur along the delaminated surfaces. This would suggest that the crack propagates under a local Mode I fashion in the mixed-mode joints.

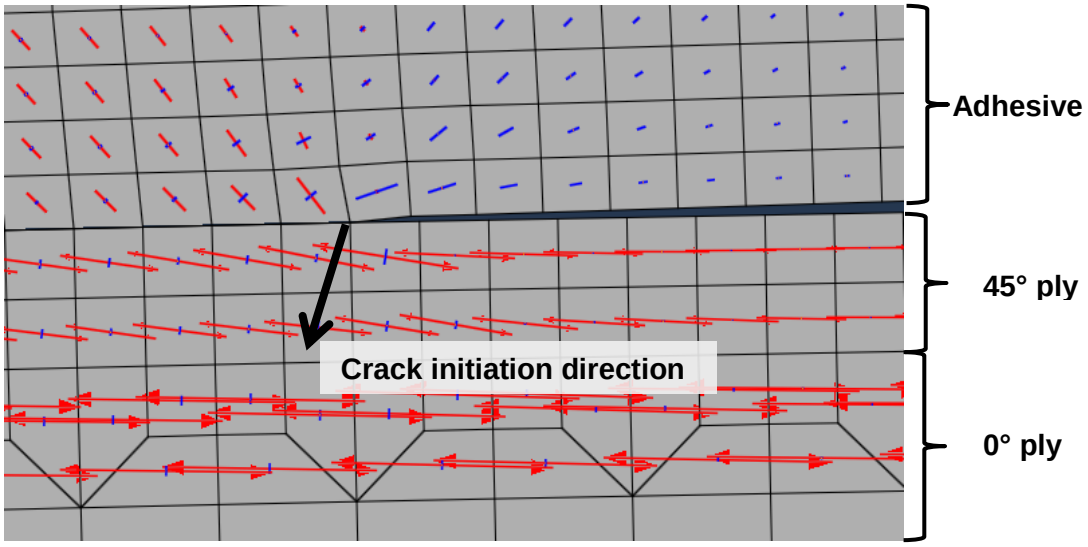

Figure 6-8: Vector plot of the direction of the maximum and minimum principal stress in the vicinity of the crack tip in the CLS specimen with an applied load of 700 N/mm.

The FE analyses provide an insight of the behaviour of a crack in a CLS specimen under a tensile load. An increase in the doubler substrate thickness will lead to increase in G_{II} in a proportionate manner. The magnitude of G_I component is related to the amount of bending displacement in the CLS joint. Factors influencing this include the boundary conditions and doubler substrate thickness. Next the fatigue crack growth rates measured experimentally are analysed with the individual SERR components to derive a suitable correlating parameter for mixed mode loading.

6.4 Fatigue Crack Growth Analysis

The SERR components determined numerically were employed to correlate with the experimental fatigue crack growth rates measured. Since the prevailing crack propagation mode is delamination, only datum points corresponding to this failure mode were included in the da/dN plot; the initial datum points associated intra-ply crack growth were omitted. The intra-ply crack propagation path initially yielded a much slower crack propagation rate due to the complex crack path and first initiating within the adhesive. Firstly, the influence of mode mixity on fatigue behaviour was investigated with the objective of developing a correlating parameter that can correlate crack growth rates under varying mode ratios. The effect of load ratio on mixed mode crack propagation was then investigated.

6.4.1 Effect of Mixed Mode Ratios

As previously stated, the objective of the present work is to investigate the influence of the individual components of SERR on crack propagation under in-plane mixed mode loading conditions. Therefore the measured fatigue crack growth rates of the CLS specimens were correlated to G_I, G_{II} and other definitions of equivalent mixed-mode G, previously discussed in Chapter 2. For the current set of CLS specimens, the mixed mode ratio, $G_I/(G_I + G_{II})$ was 0.5, 0.41 and 0.36 for Type I, II and III specimens respectively. If one component of the fracture energy has a dominant influence over the other, it would correlate the fatigue crack growth rates significantly better than others when comparing the crack growth data from specimens with different mixed mode ratios.

Firstly, the measured crack growth rates from the three CLS specimen configurations were correlated with only the Mode I SERR component $\Delta G_{I,eq}$. The definition of $\Delta G_{I,eq}$ is given as,

$$\Delta G_{I,eq} = \left(\sqrt{G_{I,max}} - \sqrt{G_{I,min}}\right)^2 \quad (6\text{-}2)$$

Figure 6-9 shows the relation between $\Delta G_{I,eq}$ and crack growth rates from the three CLS geometries. The experiment data from the Mode I delamination tests were also included to compare the crack growth behaviour under Mode I and mixed mode. From the Figure 6-9(a, b and c), $\Delta G_{I,eq}$ was able to provide a relative good correlation for the crack growth rates of the CLS specimens with different doubler thickness. However the Mode I crack growth data did not correlate well the mixed mode data. This would likely suggest that G_I and G_{II} both contributed to the mixed-mode fatigue and fracture processes.

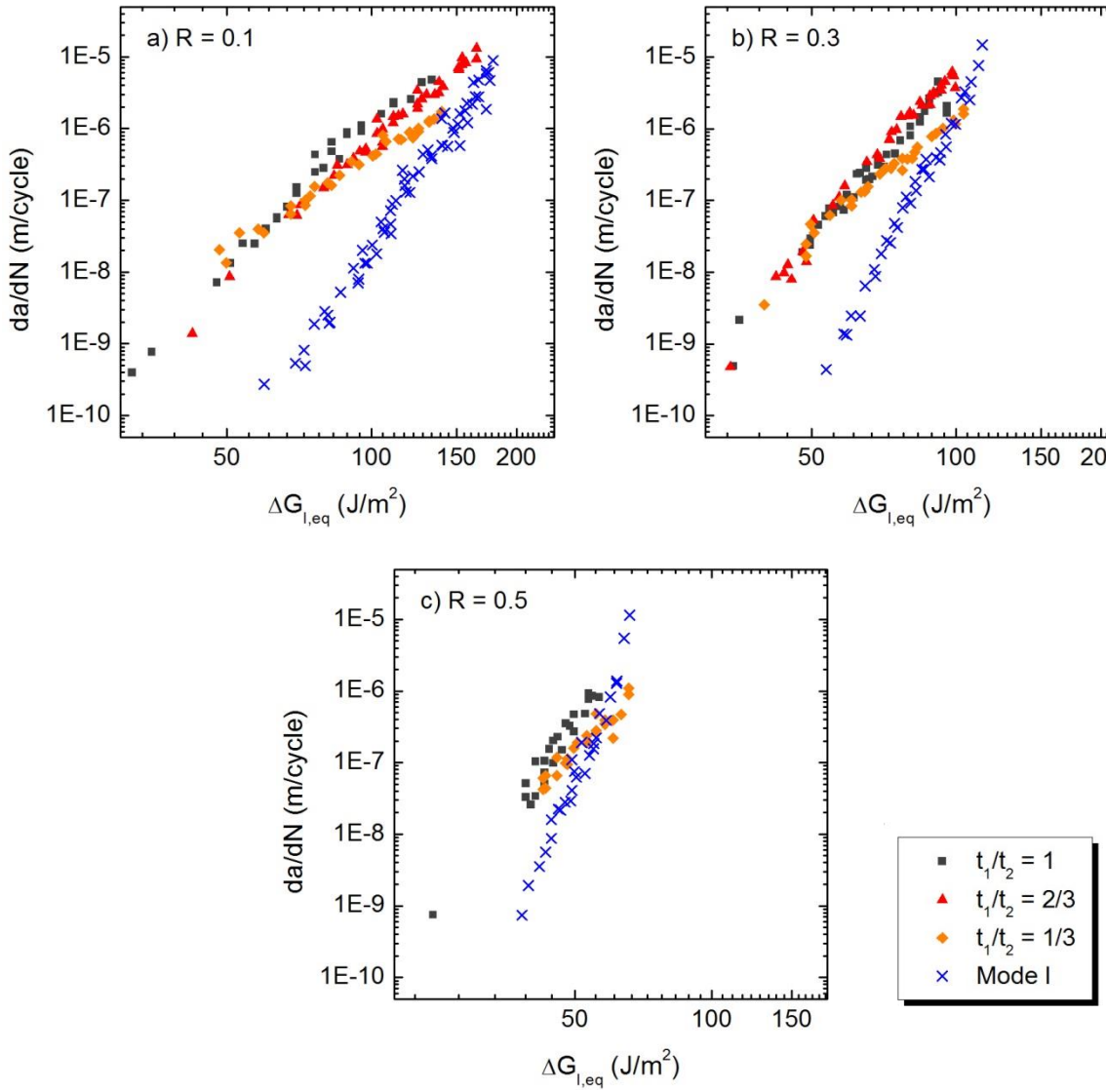

Figure 6-9: Relation between Mode I strain energy release rate and crack growth rates from CLS and DCB specimens

Figure 6-10 shows the CLS specimens' fatigue crack growth rates correlated with the Mode II component of the SERR range $\Delta G_{II,eq}$, defined as,

$$\Delta G_{II,eq} = \left(\sqrt{G_{II,max}} - \sqrt{G_{II,min}}\right)^2 \quad (6\text{-}3)$$

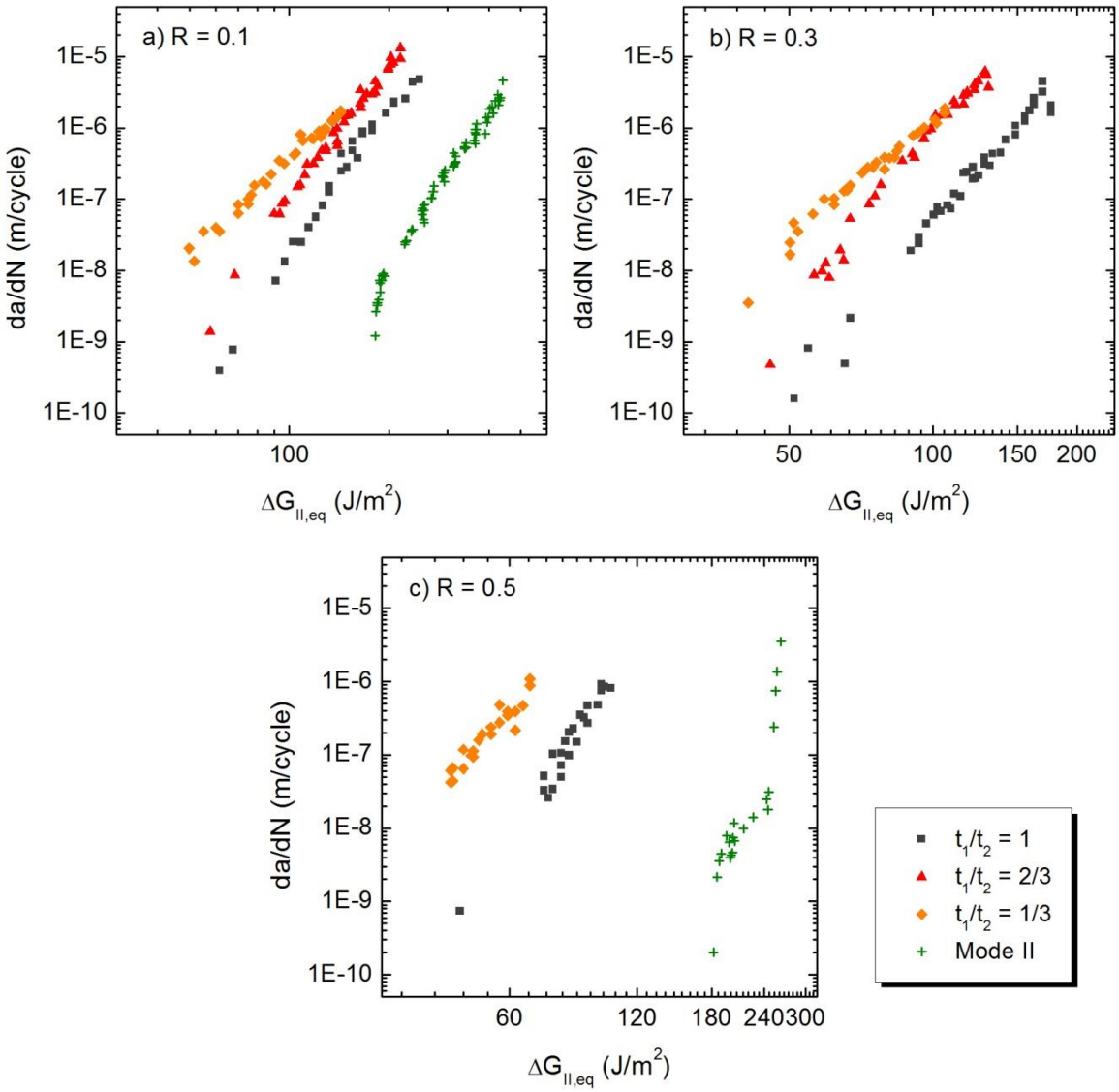

Figure 6-10: Relation between Mode II strain energy release rate and crack growth rates from CLS and DCB specimens

Although the Mode II component was the dominant fracture mode for Type II and III (e.g. t_1/t_2 = 1/3 and 2/3) CLS specimens, as their Mode II SERR contribution accounts for more than 50% of the total SERR, $\Delta G_{II,eq}$ was unable to correlate with the crack growth data of different mixed mode ratios. The single Mode II experimental data

generated from the 3-ENF specimens showed that a much greater SERR value was needed to generate fatigue delamination crack growth than mixed mode loadings. Hence it is likely that both Mode I and II components contribute to crack growth under mixed mode conditions. Therefore any correlating parameter for mixed mode loading conditions needs to account for the interaction between the two modes.

From the works of Mall, Johnson and colleagues [52, 68], the total strain energy release rate, given as $\Delta G_T = \Delta G_I + \Delta G_{II}$, was reported to collapse crack growth rates into a master curve for cohesive debonding of CLS specimens with different load ratios and mixed mode ratios. The simple superposition of the ΔG components assumes that the stresses correspond to its respective fracture modes do not interact. Any corresponding mixed mode definition of the strain energy release rates should reflect the contributions of both G_I and G_{II} and at the two extremes (i.e. $G_I = 0$ or $G_{II} = 0$). In this work, the definition of $\Delta G_{T,eq}$ differs from Mall et al. [52, 68], such that the similitude conditions were maintained. Therefore the parameter $\Delta G_{T,eq}$ is given as,

$$\Delta G_{T,eq} = \Delta G_{I,eq} + \Delta G_{II,eq} \tag{6-4}$$

where the definition of $\Delta G_{I,eq}$ and $\Delta G_{I,eq}$ is given in Equation (6-2) and (6-3) respectively.

For either pure Mode I or II crack propagation, $\Delta G_{T,eq}$ simplifies to either $\Delta G_{I,eq}$ or $\Delta G_{II,eq}$. Figure 6-11 shows that it is impossible to collapse the fatigue crack growth data into a narrow band using $\Delta G_{T,eq}$. The mixed mode crack growth rates are approximately in between Mode I and II crack growth rates. This suggests a range of threshold values for different mixed mode ratios that is bounded by the pure Mode I and II threshold. Therefore this has excluded ΔG_T as the unifying parameter for fatigue crack growth rates for different mixed mode ratios.

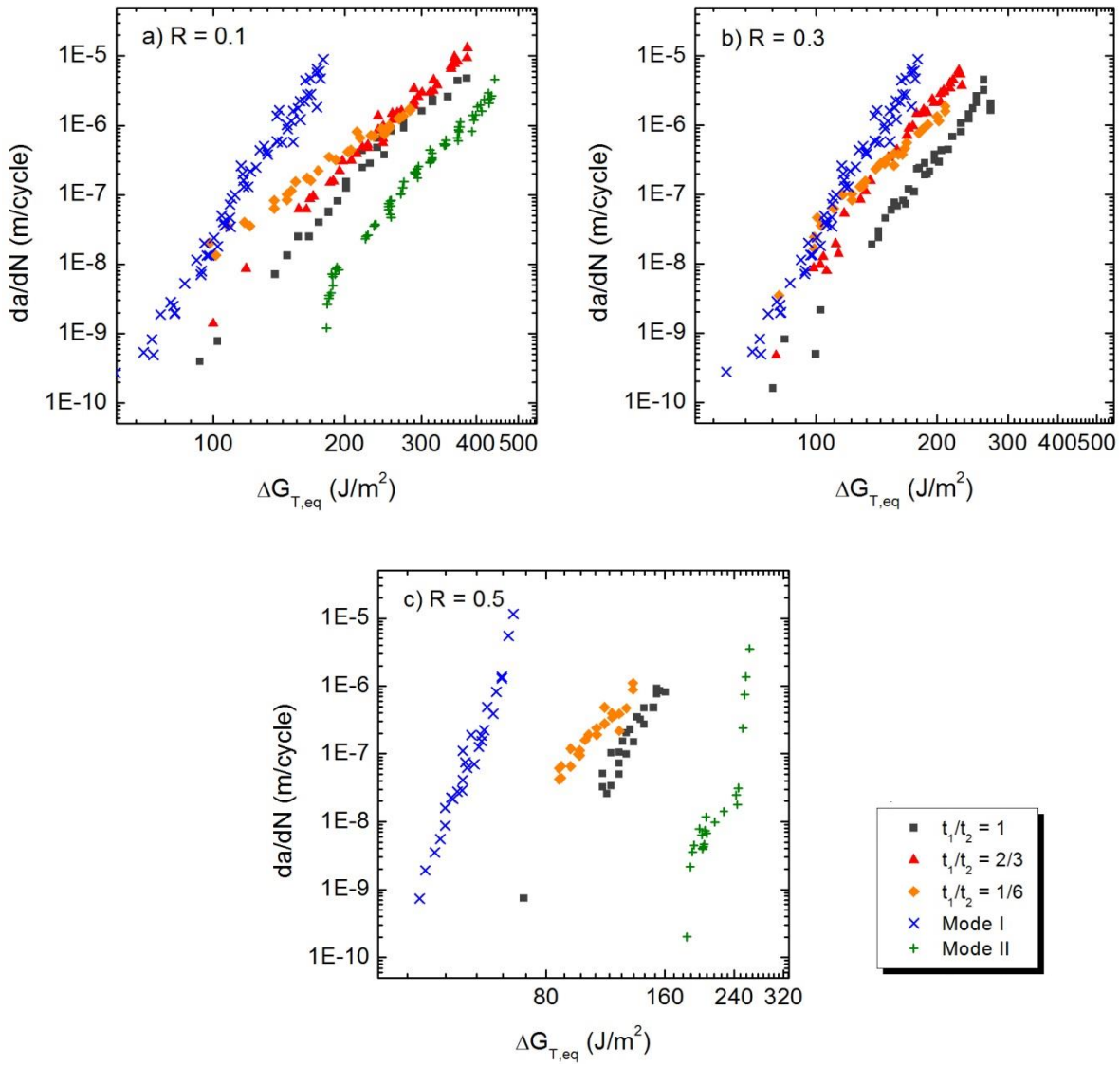

Figure 6-11: Relation between total strain energy release rate and mixed-mode crack growth rates

A comparison of the three controlling parameters previously introduced, $\Delta G_{I,eq}$, $\Delta G_{II,eq}$ and $\Delta G_{T,eq}$, shows that a better correlation can be obtained with $\Delta G_{I,eq}$ for the three CLS geometries tested. This observation suggests that the Mode I component is a more dominant parameter for mixed mode crack propagation than Mode II. It can also be seen in Figure 6-11 that the mixed mode ratio dependency increases as the Mode II component increases. SEM images showed the presence of hackles in the direction of delamination growth. This indicates the formation micro-cracks under local tensile loads (i.e. perpendicular to the maximum principal stress) and subsequent coalescing of the formed micro-cracks allows the onset of crack propagation. Therefore the local Mode I tensile stress acting on the material just ahead of the crack tip is an important factor to account for. It also provide an explanation on the increase in fracture toughness of pure

Mode II or mixed modes is due to the result of the off-axis orientation of the micro-cracks formation ahead of the crack tip in relation to the crack growth plane. Due to the constraint by the fibres, the crack is unable to propagate normal to the maximum principal stress ahead of the crack tip. Hence it leads to an increase in the fracture toughness of the material.

The mixed mode failure criterion, proposed by Benzeggagh and Kenane [71-73] or otherwise known as the B-K law, is commonly used to account for variation of fracture toughness as a function of mode ratio in the static fracture of composite laminates. The B-K law failure envelope is accepted in ASTM D6671 for the characterisation of composite delamination under mixed mode loadings [151]. The B-K law relation was also developed by the authors to predict the threshold SERR under mixed mode loading. The equation was modified to account for the cyclic Mode I and II SERR under fatigue loading and expressed according to Equation (6-5).

$$\Delta G_{BK,eq} = \Delta G_{I,eq} + \left(\Delta G_{II,eq} - \Delta G_{I,eq}\right)\left(\frac{G_{II}}{G_I + G_{II}}\right)^{\eta} \quad (6\text{-}5)$$

where $\Delta G_{I,eq}$ and $\Delta G_{II,eq}$ represents the cyclic Mode I and II SERR defined in Equation (6-2) and (6-3) respectively. $G_{II}/(G_I + G_{II})$ is the mixed mode ratio of Mode II to the total fracture energy. The exponent parameter η is a correction factor which accounts for the interaction between different modes of loading. Therefore this parameter can be adjusted so that the influence of the Mode I can be increased accordingly. The η parameter needs to be obtained by curve fitting into the experimental results of different mixed mode ratios. For the IM7/977-2 carbon/epoxy laminate, the parameter η was determined to be 1.39 [145]. Since the IM7/977-2 and IM7/977-3 laminates consisted of the same carbon fibre with very similar matrix system, the η value of 1.39 was assumed to be reasonable to be used in Equation (6-5) for IM7/977-3 carbon epoxy laminates.

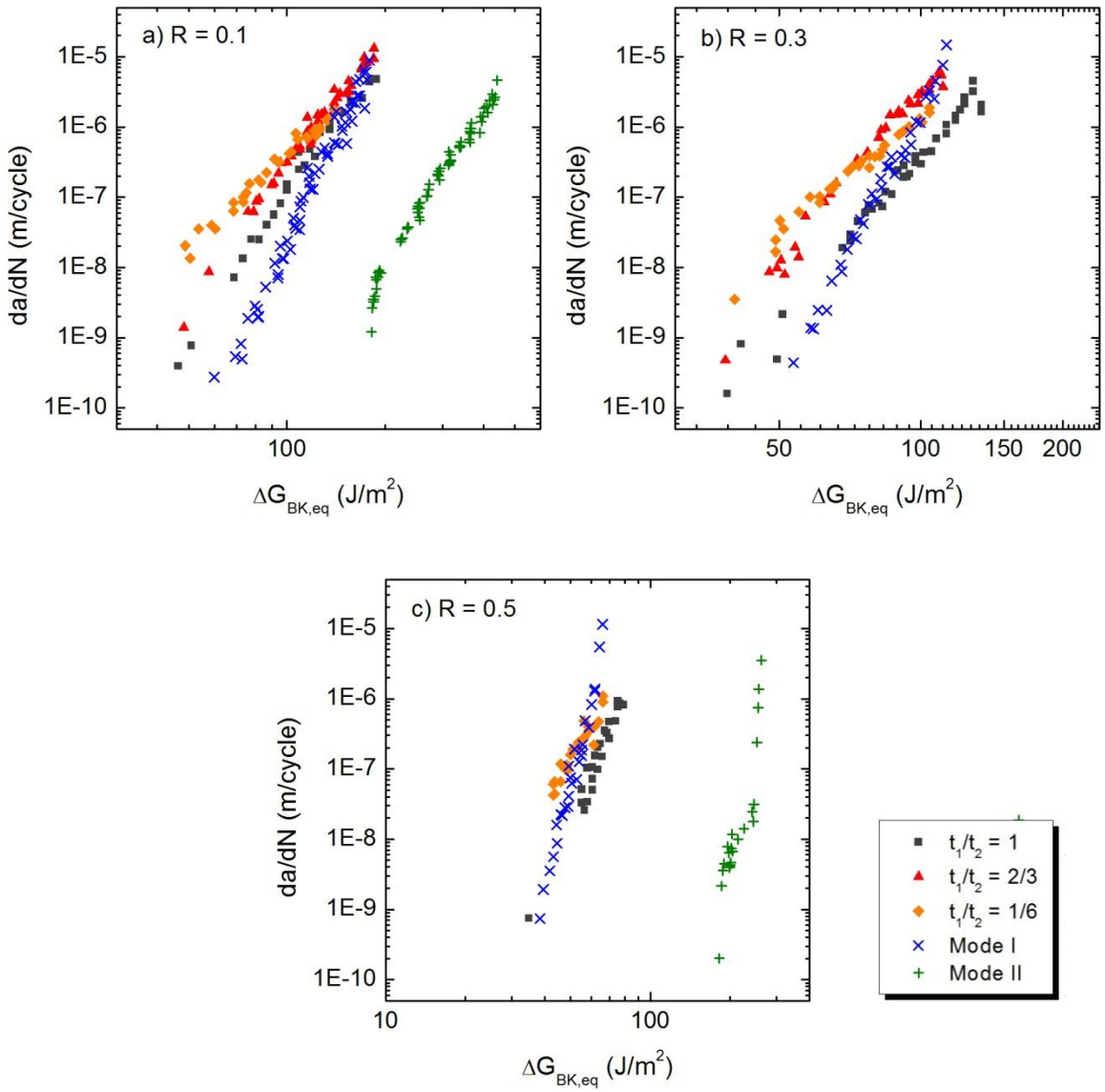

Figure 6-12: Relation between B-K strain energy release rate and mixed-mode crack growth rates

Figure 6-12 shows the fatigue crack growth rates of the CLS specimen correlated with ΔG_{BK}. The ΔG_{BK} correlating parameter appears to give a stronger preference to the Mode I SERR component than ΔG_T as the fatigue crack growth rates of the CLS specimens are shifted closer to the mode I data. It is clear that ΔG_{BK} does not unify the Mode I and II data into a single relationship. This result suggests that the fatigue crack growth rates and threshold ΔG_{BK} of arbitrary mixed mode ratios will not be unique and has to be determined experimentally for each case. Consequently Kenane and Benzeggagh [73] proposed an semi-empirical method of predicting the Paris law constants, *m* and *D*;

$$\log D_m = \log D_{II} + (\log D_I - \log D_{II}) \left(1 - \frac{G_{II}}{G_I + G_{II}}\right)^{\alpha} \quad (6\text{-}6)$$

$$m_m = m_I + (m_{II} - m_I) \left(1 - \frac{G_{II}}{G_I + G_{II}}\right)^{\beta} \quad (6\text{-}7)$$

where the subscripts I, II and m denotes Mode I, II and mixed mode respectively. The parameters α and β are curve-fitting parameters determined experimentally.

In a similar approach, they also have proposed a semi-empirical formulation of predicting the threshold SERR, given that the threshold SERR is used to design composite structures against fatigue. The equation is given as,

$$\Delta G_{eq}^{th} = \Delta G_{I,eq}^{th} + \left(\Delta G_{II,eq}^{th} - \Delta G_{I,eq}^{th}\right) \left(\frac{G_{II}}{G_I + G_{II}}\right)^{d} \quad (6\text{-}8)$$

In this work, the term ΔG_{eq}^{th} was modified to be equal to $\left(\sqrt{G_{\max}^{th}} - \sqrt{G_{\min}^{th}}\right)^2$ from the original definition of $G_{max}^{th} - G_{min}^{th}$. Again, the term d is to be determined by the curve-fitting process. Although the methodology proposed by Kenane and Benzeggagh allows engineers a means of predicting the mixed mode fatigue behaviour and threshold, multiple experimental testings of different mixed mode ratio must still be carried out. It can be observed that the Mode I fatigue crack growth behaviour is dependent on the load ratio when correlated against ΔG_{eq} term. Therefore it is highly unlikely that the curve-fitting parameters in Equation (6-6), (6-7) and (6-8) are independent on the load ratio, further complicating the design process.

In Section 4.7.2, the correlating parameter proposed by Cheuk et al. [69] was used to correlate the Mode I and II fatigue debonding rates of the bonded DCB specimens. The mixed mode correlating parameter, $\Delta G_{m,eq}$, is defined as: -

$$\Delta G_{m,eq} = \Delta G_{I,eq} + \left(\frac{G_{IC}}{G_{IIC}}\right) \Delta G_{II,eq} \quad (6\text{-}9)$$

where G_{IC} and G_{IIC} are the critical strain energy release rate under Mode I and II loading respectively.

$\Delta G_{m,eq}$ is similar to the linear Power law type failure criterion used for static fracture. The equation is simple to implement. Moreover it does not require the use of a curve fitting parameter. For the IM7/977-3 carbon epoxy laminates, the critical strain energy release rates are G_{IC} = 240 J/m^2 and G_{IIC} = 1000 J/m^2, determined experimentally in Section 3.3.2. This gives a ratio G_{IC}/G_{IIC} = 0.24.

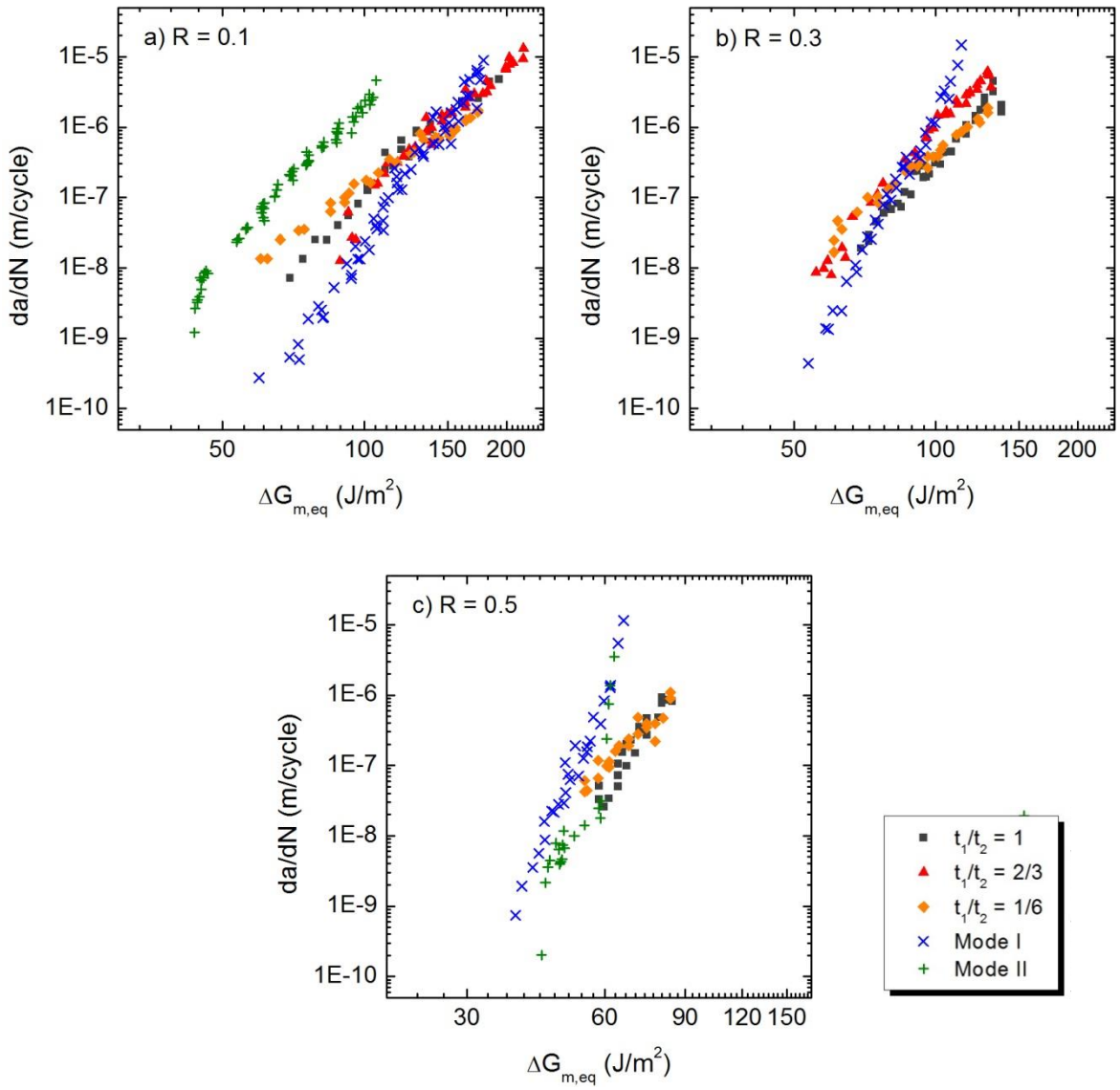

Figure 6-13: Single mode and mixed mode fatigue crack growth rates plotted against $\Delta G_{M,eq}$

Figure 6-13 shows the fatigue delamination growth behaviour of the three CLS specimen characterised by $\Delta G_{m,eq}$. An improvement in the correlation was obtained for the fatigue crack growth rates of the three CLS geometries. However the Mode II fatigue crack growth rates appears to be over-compensated as it is now on the left hand side of the mixed mode crack growth rates. This will then indicate that the Mode II fatigue

resistance is much lower than mixed mode or mode I based on this definition of the correlating parameter. This behaviour was also observed in the Mode I and II fatigue debonding of the bonded DCB specimens in Section 4.7.2. In the case of the bonded joint, plasticity induced crack closure was successfully used to explain the observed higher Mode I fatigue resistance when the correlating parameter $\Delta G_{m,eq}$ was used. Therefore it was postulated that some form of non-linear mechanism is present affecting the mixed mode fatigue behaviour. In so doing, it causes the similitude conditions not to be maintained. This effect can be more clearly observed when the fatigue crack growth rates of different load ratios are compared.

6.4.2 Effect of Load Ratios

In the previous Section, it was postulated that the mixed mode crack growth experiences some form of crack closure which affects its crack growth. As a result, this causes the Mode II fatigue crack growth rates to be over compensated when correlate with $\Delta G_{m,eq}$. The same fatigue behaviour in bonded joint, as reported in Section 4.7.2 and this can be eliminated when $\Delta G_{m,eq}$ was corrected to account for plasticity induced crack closure.

Figure 6-14 shows the fatigue crack growth rates of the CLS specimen of different load ratios when correlated with $\Delta G_{m,eq}$. It can be seen that significant load ratio effects are observed in the mixed mode delamination growth of all three CLS specimen geometries. The influence of load ratios on fatigue crack growth is similar to the observation made in the mode I delamination data in Section 3.3.3.

The SEM images, in Section 6.2.3, of the fracture surfaces of all the CLS geometries show a relatively “clean” surface. No debris of broken fibres was observed along the delamination path. The SEM images also indicate a clear delamination propagation plane. Hence, unlike the Mode I fracture surfaces, the fracture surfaces of the CLS specimens showed no indication of fibre bridging. This was also confirmed when an image of the side profile of the crack in the CLS specimen showed no fibre bridging at all. Since fibre bridging cannot be accountable for the observed load ratio effects, another probable mechanism is plasticity induced crack closure. Plasticity induced crack closure was simulated in composite laminates under mode I delamination growth. The presence of crack closure was established for crack growth along the 45//0 and 90//0 ply interface. Given that the crack propagated along the interface of the 45º and 0º plies, the crack closure mechanism shall be further investigated in the CLS specimens.

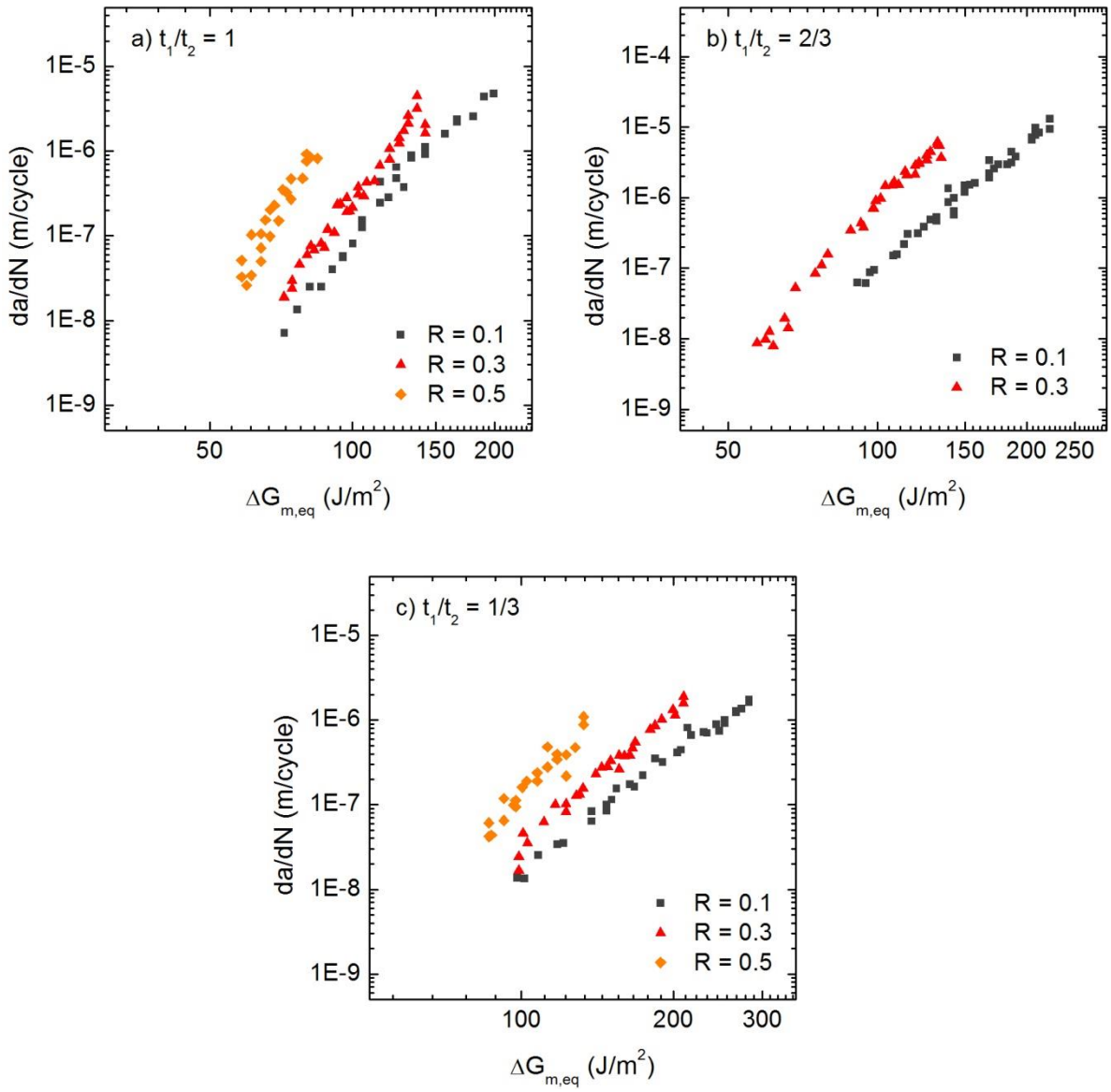

Figure 6-14: Influence of load ratios on the mixed mode delamination growth rates

6.4.3 Effects of Crack Closure

No fibre bridging in the crack wake was observed for the tested specimen. Previously in Section 5.3, numerical analysis of plasticity induced crack closure in an elastic-plastic lamina demonstrates the presence of crack closure in the 45 and 0 degree ply. Therefore modelling approach described in Section 4.4 and 5.3 was applied to the CLS specimen to determine if crack closure is a contributing factor for the experimental mean load dependency behaviour.

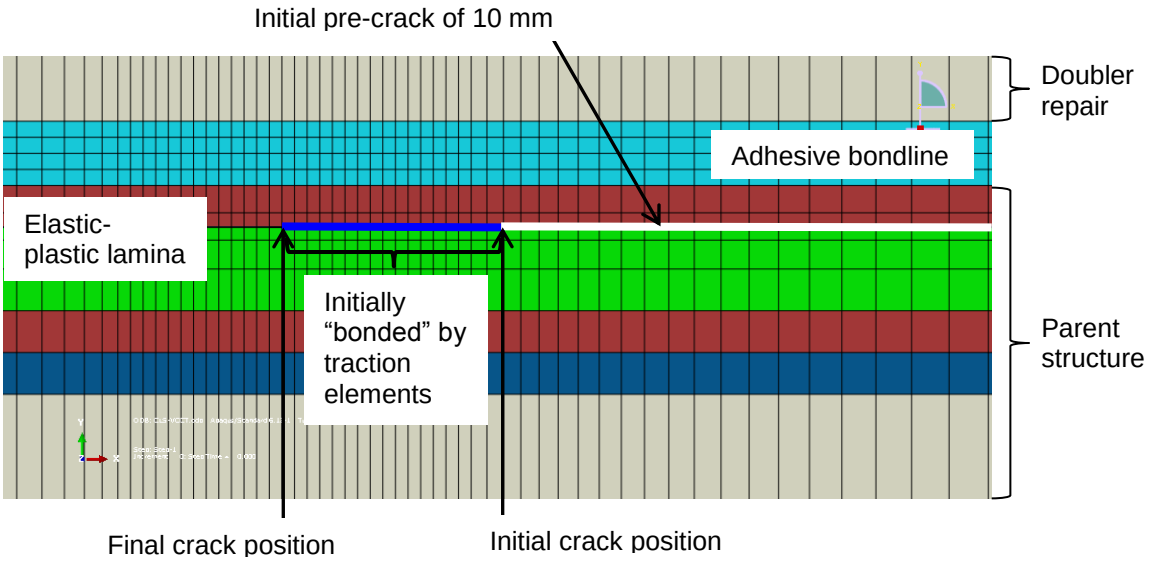

Figure 6-15: Finite element mesh at the crack tip

Plasticity induced crack closure was simulated in CLS specimens of all three geometries under constant amplitude cyclic loading. The geometry and boundary conditions of the FE model is shown in Figure 6-4. The details of the mesh at the vicinity of the crack tip are shown in Figure 6-15. Only the first five plies adjacent to the bondline were modelled individually and the rest of the model was homogenised as an orthotropic laminate. The Hill's plastic potential was used to simulate anisotropic yielding of the 45º and 0º ply adjacent to the crack. The crack faces was initially connected via traction elements and subsequently the traction elements were deleted one by one at P_{max} to advance the crack. Hard contact surface properties were assigned to the crack flanks to prevent the nodes from inter-penetrating in the event of closure. The crack tip nodal stress criterion was used to determine the crack opening loads. The properties of the laminate and adhesive are given in Table 6-1 and the yield stresses of the lamina in Table 5-3.

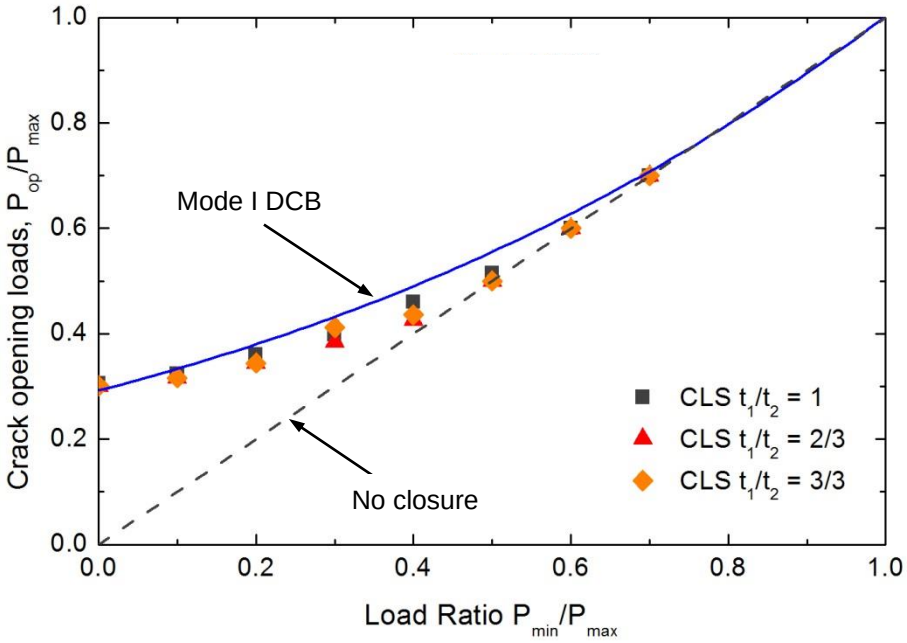

Figure 6-16: Crack closure along the 45//0 interface plies in the DCB and CLS specimens

Shown in Figure 6-16 are the crack closure results along the interface of 45 and 0 degrees plies in both DCB and different CLS specimens. The closure levels of all three CLS geometries are approximately are the same and no closure was observed for $R \geq 0.5$. Secondly it can be observed that the closure levels of the CLS specimen are approximately similar. Therefore the Mode I crack closure analysis can be used to correlate the load ratio effects observed in the CLS specimen.

6.4.4 A New Correlating Parameter for Mixed Mode Crack Propagation

From the analysis presented earlier in the Thesis, it was established that crack closure affects primarily the Mode I component. Mode II crack propagation is generally not affected by crack closure as the crack faces moves in the direction parallel to the fracture plane under cyclic loads. Therefore the following effective mixed mode correlating parameter is proposed to account for crack closure.

$$\Delta G_{m,eff} = \Delta G_{I,eff} + \left(\frac{G_{IC}}{G_{IIC}}\right)\Delta G_{II,eq} \tag{6-10}$$

where the Mode I parameter $\Delta G_{I,eff} = \left(G_{I,max} - G_b^f\right)\left(1 - P_{op}/P_{max}\right)^2$. In the absence of fibre bridging or plasticity induced crack closure, the term G_b^f and P_{op} will be simplified to zero and P_{min} respectively.

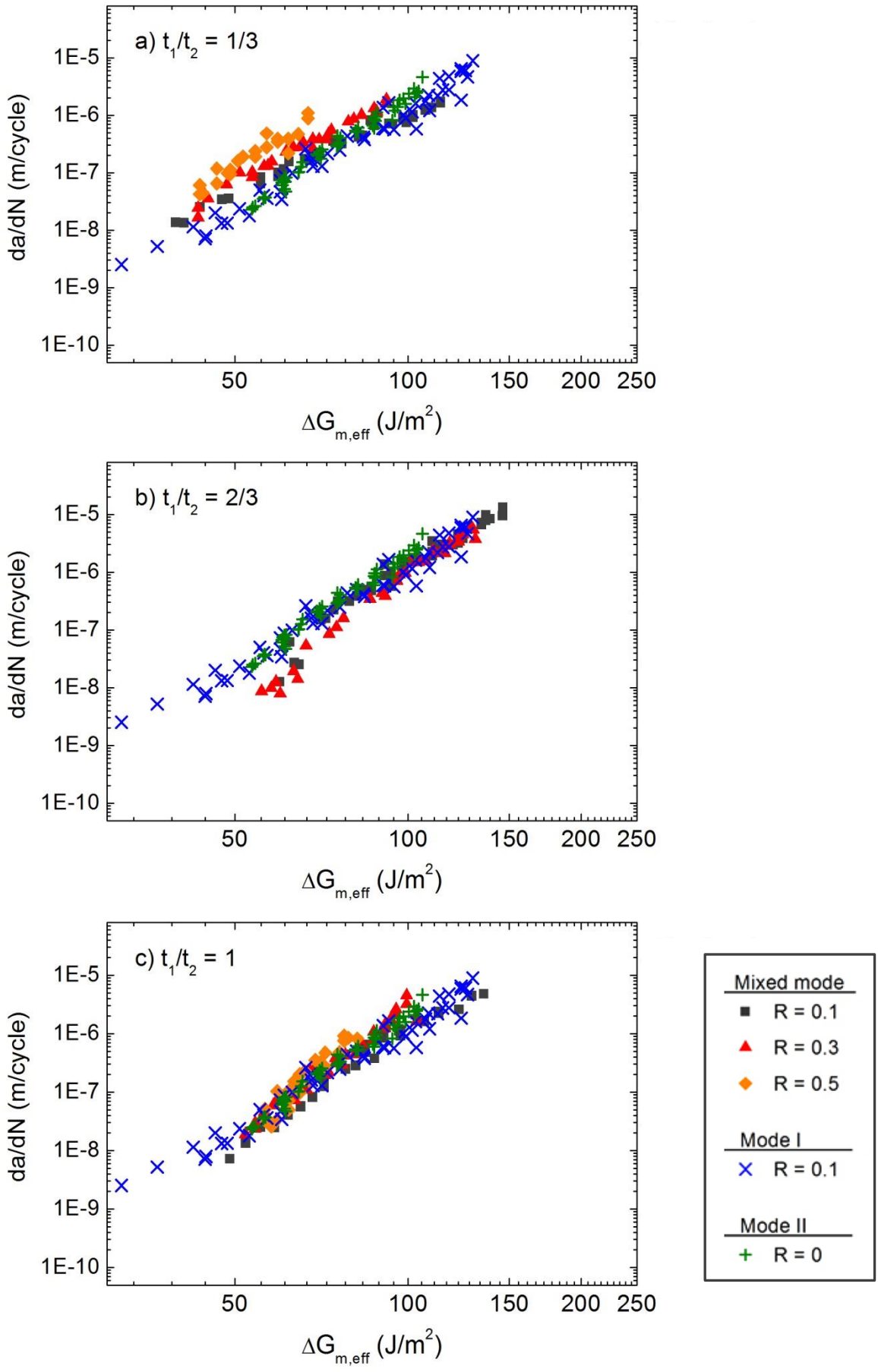

Figure 6-17: Fatigue delamination growth rates of varying mode mixity versus $\Delta G_{m,eff}$

Since crack closure does not affect the Mode II component, the Mode II parameter can be represented by $\Delta G_{II,eq}$. Therefore the crack closure model is only applied to the Mode I component. Shown in Figure 6-17 is the fatigue delamination growth rates of mixed and single modes correlated with the $\Delta G_{m,eff}$ parameter. In the CLS specimen, the crack propagated along 45º//0º interface within the parent substrate. No fibre bridging was observed. Therefore $G_b^f = 0$ for the CLS specimen. On the other hand, the Mode I crack growth data was generated from a unidirectional DCB laminate and the crack is propagated along the 0º//0º interface. In this instance, fibre bridging was the main cause of load ratio effects. Hence G_b^f was determined to be 61 J/m^2 from Section 5.5. The values of the parameters used in $\Delta G_{m,eff}$ for the different joints is summarised in Table 6-2. It can be seen that the $\Delta G_{m,eff}$ parameter is able to unify delamination growth for both load ratio and mixed mode ratio. Therefore a unique value of the delamination threshold can be obtained for design purposes.

Table 6-2: Summary of fibre bridging and crack closure parameters for experimental data presented in Figure 6-17

Specimen configuration	Crack propagation mode	Closure mechanism	P_{op}/P_{max}	G_b^f
DCB	I	Fibre bridging	0.1 for R = 0.1	61
CLS (t_1/t_2 = 0.33)	Mixed	Plasticity induced closure	0.1 for R 0.1 0.38 for R=0.3 0.5 for R=0.5	0
CLS (t_1/t_2 = 0.66)	Mixed	Plasticity induced closure	0.1 for R 0.1 0.38 for R=0.3 0.5 for R=0.5	0
CLS (t_1/t_2 = 1)	Mixed	Plasticity induced closure	0.1 for R 0.1 0.38 for R=0.3 0.5 for R=0.5	0
ENF	II	-	0 for R = 0	0

The proposed correlating parameter $\Delta G_{m,eff}$ provides a convenient means of providing a fatigue design parameter for bonded repairs that is independent of load ratio and as well as mixed mode ratio. Therefore the threshold value can determined from a single Mode I experiment and accounting for any mechanism affecting the crack growth. Using the ratio of the Mode I and II critical strain energy release rate, the repair strength which no further crack propagation will occur can then be predicted.

6.5 Bonded Patch Repair Design Considerations

The results presented in this Chapter are based on the patch repair configuration. Changes in the substrate properties, thickness or geometry will result in a change of the strain energy release rate and mode mix ratio for a same applied load. Hence the fatigue strength of the repair is dependent on a number of geometrical parameters. Consequently a design parameter that is able to account for these factors is desirable without the need of extensive experimental testing. To this end, the proposed correlating parameter $\Delta G_{m,eff}$ is able to characterise the crack tip conditions independent of the load ratio and mixed mode ratio. Consequently, by obtaining the static and fatigue behaviour of the material system from simple coupon test, it is possible to predict the threshold and crack growth rates of arbitrary mixed modes.

From the definition of $\Delta G_{m,eff,}$ it can be seen that the peel stresses or Mode I SERR component plays a dominant role in the mixed mode fatigue crack growth behaviour. A faster crack growth rate was observed as the mode I SERR component increases. This is in agreement with works of Hart-Smith [76, 77] which a recommendation was made to reduce the peel stress within a joint in order to maximise the bonded repair strength. Increasing the repair's strength can be achieved by tapering or a different repair configuration (i.e. scarf repair).

A second consideration point is the failure mode of the bonded composite repair as failure can occur in the composite laminate or within the adhesive. A pre-existing flaw is typically assumed to be in the adhesive for damage tolerant design. However the crack may progress within the adhesive or between composite plies. For example, a repair was designed for the adhesive threshold based on the assumption of the initial flaw to be cohesive. If the crack were to propagated into the composite due to extreme severe overloads or operational damage, a rapid increase in the crack length can occur as the fatigue threshold of the adhesive may be much higher than that of the composite. Therefore the failure mechanisms and criticality of the crack propagation path needs to be understood so that an appropriate decision can be made on the design parameter. Subsequently knowledge of the failure mode, crack path and the exact envelope of the fatigue threshold criterion will allow engineers to correctly size the repair that is designed to be cyclically loaded indefinitely under normal operating conditions.

6.6 Summary and Conclusions

A combined experimental and numerical investigation of composite bonded CLS joints was undertaken to characterise the influence of components of SERR on fatigue crack propagation under mixed mode loading. The CLS joint consisted of IM7/977-3 carbon composite substrates bonded with FM300-3K adhesive. The doubler substrate tested had different thickness to generate different mixed mode ratios. This study has led to the following conclusions:

- The crack propagation path is dependent on the adjacent ply orientation and the direction normal to the principal stress.
- The Mode I SERR component plays a dominant role in the crack propagation behaviour under mixed mode and it should be minimised to increase the fatigue strength of the repair.
- Fibre bridging was not observed in the fatigue delamination growth along the 45//0 ply interface in the CLS specimens. However the fatigue crack growth rates were dependent on load ratio and the cause of such behaviour is due to plasticity induced crack closure in the adjacent 45º ply.
- Elastic-plastic analysis of the adjacent plies to the crack was done to determine level of crack closure in the CLS specimen and it was found to be similar to the results from the DCB specimen. Therefore the closure results obtained from the DCB can be used to correlate the closure in mixed mode experimental data.
- A new correlating parameter was proposed that is capable of unifying the crack growth rates of varying load ratios and mixed mode ratio.

Chapter 7

Concluding Remarks

7.1 Summary of Research Findings

Fatigue is a major design consideration in bonded composite joints where cracks are likely to initiate and propagate either in the adhesive bondline or between composite plies. Despite the recent research effort in this area, predictive methodologies are largely empirical and phenomenological, needing many fitting parameters. This research project aims to develop new correlating parameters for disbond growth in bonded structures and delamination in composites under fatigue loading of varying load ratios.

A critical review of the literature reveals that existing correlating parameters, mostly proposed as a means of curve fitting, do not correctly account for the effects of mean loads. By considering the similitude principle in fatigue, a correlating parameter ΔG_{eq} has been proposed and is given as,

$$\Delta G_{eq} = \left(\sqrt{G_{max}} - \sqrt{G_{min}}\right)^2 \tag{7-1}$$

In the absence of crack closure or fibre bridging, the similitude condition is maintained; this scaling parameter will be independent of the specimen size and can be applied from coupons to large-scale structures.

To investigate the effects of crack closure and fibre bridging, experimental tests and numerical simulations have been carried out on two major fatigue mechanisms: cohesive debonding of bonded structures and delamination cracking of composites, under two crack propagation modes, Mode I and II. A summary of the research findings are presented below.

7.1.1 Mode I Crack Propagation in Bonded Joint

Mode I crack growth data, obtained in this project and from the literature, have been plotted in terms of ΔG_{eq}, revealing that is parameter alone is unable to account for the effects of mean loads. Experimental evidence showed a distinct plastic zone ahead of the crack tip and plasticised material was left behind in the crack flanks. This suggests that plasticity induced crack closure was the key mechanism responsible for the load ratio effects in the Mode I fatigue crack growth behaviour in bonded joints.

Numerical simulation has been carried out to quantify the plasticity-induced crack closure level in bonded joints. The results showed that bonded joints experience significant level of plasticity induced crack closure. A new correlating parameter, accounting for crack closure, has been proposed,

$$\Delta G_{eff} = \left(\sqrt{G_{max}} - \sqrt{G_{op}}\right)^2 = G_{max}\left(1 - \frac{P_{op}}{P_{max}}\right)^2 \quad (7\text{-}2)$$

Comparison with experimental results has shown that this new parameter can unify the fatigue disbond growth rates under varying load ratios.

7.1.2 Mode II Crack Propagation in Bonded Joint

Unlike mode I fatigue, the experimental results from mode II tests and data reported in the literature under different load ratios can be successfully correlated by the equivalent strain energy release rate ΔG_{eq}. This has removed the mean load dependency behaviour reported in literature.

To investigate the underlying mechanism, plasticity simulation has been carried out to quantify crack closure under mode II loading. Although extensive plasticity was present in the wake of the crack, the normal displacement of the crack flanks equal to zero during the loading cycle. Therefore plasticity induced crack closure does not affect Mode II crack propagation since the cyclic deformation occurs parallel to the fracture plane rather than perpendicular to it. Therefore ΔG_{eq} is able to give good correlation.

7.1.3 Forman Model for Strong Influence of G_{max}

Past work has hypothesised that G_{max} can significantly affect the rate of crack growth by introducing damage ahead of the crack tip. The formation of this damage (i.e. voids,

micro-cracks and shear yielding) results in a reduction of the material's intrinsic resistance to crack propagation. Some researchers had proposed a phenomenological two-parameter (G_{max} and ΔG_{eq}) correlating parameter. In this Thesis, the Forman model has been modified to account for the effects of G_{max}. The modified Forman equation in this Thesis is given as

$$\frac{da}{dN} = \frac{C_F\left(\Delta G_{eff}\right)^{m_F}}{(1-R)\left(\sqrt{G_C} - \sqrt{G_{max}}\right)} \tag{7-3}$$

where ΔG_{eff} is the effective cyclic strain energy release rate given by equation (7-1), accounting for plasticity induced crack closure and/or fibre bridging. The correlation of the experimental data for composite laminates and bonded joints have been significantly improved with the Forman model, as shown in Section 4.7 and 5.5.

7.1.4 Composite Delamination along 0º//0º Interface

From the Mode I and II tests of delamination growth between 0° plies, it has been found that the load ratio has a strong effect when the crack growth rates are correlated with ΔG_{eq} where no load ratio effects have been observed under Mode II loading. This phenomenon has been attributed to extensive fibre bridging in the wake of the crack for the DCB specimens.

Elastic-plastic simulation of the lamina was done by using Hill's anisotropic yield criterion but it was established that plasticity induced closure was not responsible for the effects of mean loads. Therefore large scale fibre bridging was assumed to be the prevailing cause. The parameters of the bridging zone were determined using the SERR-COD approach. The bridging zone under static and fatigue loads is hypothesised to be different as the bridging zone will have undergone further damage under fatigue loading. Consequently the following correlating parameter is proposed,

$$\Delta G_{eff} = \left(G_{max} - G_b^f\right)(1-R)^2 \tag{7-4}$$

Assuming self-similar crack growth is attained; a self-consistency analysis is done to determine G_b^f which represents the amount of crack tip shielding provided by fibre bridging and is found to be independent on load ratios. In conjunction with the Forman

model, a good correlation can be obtained for the generated experimental data and also data from literature.

7.1.5 Composite Delamination along 45º//0º and 90º//0º Interfaces

Elastic-plastic analysis of the composite lamina was carried out for delamination along 45º//0º and 90º//0º interfaces indicated significant crack closure can be found in these interfaces. The level of crack closure is higher in the 90°//0° interface than 45°//0° interface. This is because more plasticised material can be displaced to the crack flanks in the 90° ply.

7.1.6 Composite Delamination under Mixed Mode

Despite having the pre-crack in the bondline, experimental findings showed the crack propagated along the interface of 45º and 0º plies of the parent substrate adjacent to the bondline. The numerical analysis showed that the Mode I component of the strain energy release rate is a dominant driving force in the mixed mode crack propagation. Therefore a correlating parameter, shown in Equation (7-5) was proposed to account for mixed mode ratios.

$$\Delta G_{m,eff} = \Delta G_{I,eff} + \left(\frac{G_{IC}}{G_{IIC}}\right)\Delta G_{II,eq} \tag{7-5}$$

Since load ratio was also found to significantly affect the mixed mode crack growth rates, the $\Delta G_{I,eff}$ is defined as the following by combining Equation (7-2) and (7-4) to account for both crack closure and fibre bridging.

$$\Delta G_{eff} = \left(G_{max} - G_b^f\right)\left(1 - \frac{P_{op}}{P_{max}}\right)^2 \tag{7-6}$$

A good correlation can be obtained for different mixed mode ratios and load ratios. Therefore Equation (7-5) is able to unify the crack growth rates of varying load ratios and mixed mode ratios.

7.2 Future Research Area

This Thesis has provided an explanation of the mean load dependency fatigue behaviour found in bonded joints and composite laminates. Correlating parameters were developed to account for non-linear mechanism affecting the crack growth. Further validations of the proposed predictive methodology can be carried out on more representative bonded repairs such as a scarf repair to improve confidence. Ultimately, the work in the Thesis can be expanded to investigate variable amplitude loading and new numerical predictive methodologies.

7.2.1 Variable Amplitude Loading

In this Thesis, the fatigue behaviour under constant amplitude loading was investigated. In a real structure, constant amplitude loading rarely does occur and it is more likely that the bonded composite joint experiences a range of loads. Hence it is proposed that the load interactions under spectrum loading be examined for both delamination and cohesive disbond failure modes.

At the point of writing this thesis, limited work had been conducted on the spectrum loading. So far, the Palmgren-Miner rule is typically used to characterise the life of the joint using the S-N curve. Its limitations includes: 1) damage accumulation is assumed to be linear; 2) No load history effects is taken into account and; 3) No information regarding the crack tip conditions are provided and hence the approach is geometry dependent. Using plasticity induced crack closure as a basis, it is possible to investigate the behaviour of bonded joints under spectrum loads and understand the mechanism for load acceleration or retardation. Consequently a predictive model can then be developed and a design approach can be adopted for the damage tolerant principles.

7.2.2 Constitutive Model for Fatigue Degradation in Cohesive Elements

The implementation of a fatigue degradation law into the cohesive zone model is an attractive approach of modelling the onset and propagation of crack growth. However, in the author's opinion, some of the assumptions in the fatigue model can be contentious. Firstly damage is correlated to an equivalent crack length within the element. Damage is conventionally link to the deterioration in stiffness of the material due to plasticity, voids and micro-cracks. Secondly, the resultant crack growth per cycle is "smeared" across the process zone. The onset of crack growth should be applied to the crack tip element. As an example, when the crack tip element is full degraded, the crack then advanced by one

element length. Lastly the use of da/dN in the fatigue degradation law is a self-predicating model, given that the model is predicting the crack growth rates.

Given the potential capabilities of the cohesive zone mode, it is worthwhile to re-examine the fatigue law and rigorous validate the model. Firstly the assumptions taken in the model need to be re-examined to determine its validity. Secondly an independent experimental test should be designed to measure the material's degradation with the respect to the cycles lapsed.

Bibliography

[1] plusComposites. *Carbon reinforced composites - User sectors (continued)*. [Webpage] 2013 29/06/2013; Available from: http://www.pluscomposites.eu/content/6-carbon-reinforced-composites-user-sectors-continued.

[2] Composites, H.-P. *Growth Opportunities: Materials innovation will drive composites usage to new heights* [Webpage] 2012 5/1/2012; Available from: http://www.compositesworld.com/columns/growth-opportunities-materials-innovation-will-drive-composites-usage-to-new-heights.

[3] FAA, *Composite Aircraft Structure: Advisory Circular (AC) 20-107B*, in *Change 1*2010, FAA.

[4] Baker, A., *A Proposed Approach for Certification of Bonded Composite Repairs to Flight-Critical Airframe Structure.* Applied Composite Materials, 2011. **18**(4): p. 337-369.

[5] Schön, J., et al., *A numerical and experimental investigation of delamination behaviour in the DCB specimen.* Composites Science and Technology, 2000. **60**(2): p. 173-184.

[6] Ashcroft, I.A., *Fatigue Load Conditions*, in *Handbook of adhesion technology*, L.F.M. Da Silva, Editor. 2011, Springer: Berlin. p. 846-873.

[7] Erpolat, S., et al., *A study of adhesively bonded joints subjected to constant and variable amplitude fatigue.* International Journal of Fatigue, 2004. **26**(11): p. 1189-1196.

[8] Kinloch, A. and S. Shaw, *The fracture resistance of a toughened epoxy adhesive.* The Journal of Adhesion, 1981. **12**(1): p. 59-77.

[9] Adams, R.D., et al., *The effect of temperature on the strength of adhesive joints.* International Journal of Adhesion and Adhesives, 1992. **12**(3): p. 185-190.

[10] Kanchanomai, C. and A. Thammaruechuc, *Effects of stress ratio on fatigue crack growth of thermoset epoxy resin.* Polymer Degradation and Stability, 2009. **94**(10): p. 1772-1778.

[11] Ashcroft, I.A. and S.J. Shaw, *Mode I fracture of epoxy bonded composite joints 2. Fatigue loading.* International Journal of Adhesion and Adhesives, 2002. **22**(2): p. 151-167.

[12] Renton, J.W. and J.R. Vinson, *On the behavior of bonded joints in composite material structures.* Engineering Fracture Mechanics, 1975. **7**(1): p. 41-60.

[13] Crocombe, A.D. and G. Richardson, *Assessing stress state and mean load effects on the fatigue response of adhesively bonded joints.* International Journal of Adhesion and Adhesives, 1999. **19**(1): p. 19-27.

[14] Paris, P. and F. Erdogan, *A critical analysis of crack propagation laws.* Journal of Basic Engineering, 1963. **85**(4): p. 528-33.

[15] Pascoe, J.A., R.C. Alderliesten, and R. Benedictus, *Methods for the prediction of fatigue delamination growth in composites and adhesive bonds – A critical review.* Engineering Fracture Mechanics, 2013. **112–113**(0): p. 72-96.

[16] Quaresimin, M. and M. Ricotta, *Fatigue behaviour and damage evolution of single lap bonded joints in composite material.* Composites Science and Technology, 2006. **66**(2): p. 176-187.

[17] Quaresimin, M. and M. Ricotta, *Stress intensity factors and strain energy release rates in single lap bonded joints in composite materials.* Composites Science and Technology, 2006. **66**(5): p. 647-656.

[18] Quaresimin, M. and M. Ricotta, *Life prediction of bonded joints in composite materials.* International Journal of Fatigue, 2006. **28**(10): p. 1166-1176.

[19] Dugdale, D.S., *Yielding of steel sheets containing slits.* Journal of the Mechanics and Physics of Solids, 1960. **8**(2): p. 100-104.

[20] Barenblatt, G.I., *The mathematical theory of equilibrium cracks in brittle fracture*, in *Advances in applied mechanics*, H. Dryden, et al., Editors. 1962, Elsevier. p. 55-129.

[21] Robinson, P., et al., *Numerical simulation of fatigue-driven delamination using interface elements.* International Journal for Numerical Methods in Engineering, 2005. **63**(13): p. 1824-1848.

[22] Turon, A., et al., *Simulation of delamination in composites under high-cycle fatigue.* Composites Part A: Applied Science and Manufacturing, 2007. **38**(11): p. 2270-2282.

[23] Khoramishad, H., et al., *Predicting fatigue damage in adhesively bonded joints using a cohesive zone model.* International Journal of Fatigue, 2010. **32**(7): p. 1146-1158.

[24] Harper, P.W. and S.R. Hallett, *A fatigue degradation law for cohesive interface elements – Development and application to composite materials.* International Journal of Fatigue, 2010. **32**(11): p. 1774-1787.

[25] ASTM Standard D5573, "*Standard Practice for Classifying Failure Modes in fibre-Reinforced-Plastic Joints"*, 1999(2005), ASTM International, West Conshohocken, PA, 2005, DOI: 10.1520/C0033-03, www.astm.org

[26] Campilho, R.D.S.G., et al., *Modelling the tensile fracture behaviour of CFRP scarf repairs.* Composites Part B: Engineering, 2009. **40**(2): p. 149-157.

[27] Meneghetti, G., M. Quaresimin, and M. Ricotta, *Damage mechanisms in composite bonded joints under fatigue loading.* Composites Part B: Engineering, 2012. **43**(2): p. 210-220.

[28] Erpolat, S., et al., *Fatigue crack growth acceleration due to intermittent overstressing in adhesively bonded CFRP joints.* Composites Part A: Applied Science and Manufacturing, 2004. **35**(10): p. 1175-1183.

[29] Renton, W.J. and J.R. Vinson, *Fatigue Behavior of Bonded Joints in Composite Material Structures.* Journal of Aircraft, 1975. **12**(5): p. 442-447.

[30] Rans, C., R. Alderliesten, and R. Benedictus, *Misinterpreting the results: How similitude can improve our understanding of fatigue delamination growth.* Composites Science and Technology, 2011. **71**(2): p. 230-238.

[31] Andersons, J., M. Hojo, and S. Ochiai, *Empirical model for stress ratio effect on fatigue delamination growth rate in composite laminates.* International Journal of Fatigue, 2004. **26**(6): p. 597-604.

[32] Allegri, G., et al., *A new semi-empirical model for stress ratio effect on mode II fatigue delamination growth.* Composites Part A: Applied Science and Manufacturing, 2011. **42**(7): p. 733-740.

[33] Arad, S., J.C. Radon, and L.E. Culver, *Fatigue crack propagation in Polymethylmethacrylate; the effect of the mean value of stress intensity factor.* Journal of Mechanical Engineering Science, 1971. **13**(2): p. 75-81.

[34] Arad, S., J.C. Radon, and L.E. Culver, *Design against fatigue failure in thermoplastic.* Engineering Fracture Mechanics, 1972. **4**(3): p. 511-522.

[35] Hojo, M., et al., *Effect of stress ratio on near-threshold propagation of delimination fatigue cracks in unidirectional CFRP.* Composites Science and Technology, 1987. **29**(4): p. 273-292.

[36] Hojo, M., et al., *Effect of matrix resin on delamination fatigue crack growth in CFRP laminates.* Engineering Fracture Mechanics, 1994. **49**(1): p. 35-47.

[37] Filis, P.A., I.R. Farrow, and I.P. Bond, *Classical fatigue analysis and load cycle mix-event damage accumulation in fibre reinforced laminates.* International Journal of Fatigue, 2004. **26**(6): p. 565-573.

[38] Elber, W., *Fatigue crack closure under cyclic tension.* Engineering Fracture Mechanics, 1970. **2**(1): p. 37-45.

[39] Newman, J.C.J., *FASTRAN-II: a fatigue crack growth structural analysis program*, 1982, NASA Technical Memorandum 104159,Langley Research Centre, Hampton, Virginia, USA.

[40] Anderson, T.L., *Fracture Mechanics: Fundamentals and Applications*. 3rd ed. 2005, Boca Raton: CRC Press.

[41] Nakamura, T., *Three-Dimensional Stress Fields of Elastic Interface Cracks.* Journal of Applied Mechanics, 1991. **58**(4): p. 939-946.

[42] Hutchinson, J.W., M.E. Mear, and J.R. Rice, *Crack Paralleling an Interface Between Dissimilar Materials.* Journal of Applied Mechanics, 1987. **54**(4): p. 828-832.

[43] Shih, C.F. and R.J. Asaro, *Elastic-Plastic Analysis of Cracks on Bimaterial Interfaces: Part I—Small Scale Yielding.* Journal of Applied Mechanics, 1988. **55**(2): p. 299-316.

[44] Jablonski, D.A., *Fatigue Crack Growth in Structural Adhesives.* The Journal of Adhesion, 1980. **11**(2): p. 125-143.

[45] Matsubara, G., H. Ono, and K. Tanaka, *Mode II fatigue crack growth from delamination in unidirectional tape and satin-woven fabric laminates of high strength GFRP.* International Journal of Fatigue, 2006. **28**(10): p. 1177-1186.

[46] Tanaka, K., Y. Akiniwa, and H. Nakamura, *J-Intergral approach to mode III fatigue crack propagation in steel under torsional loading.* Fatigue & Fracture of Engineering Materials & Structures, 1996. **19**(5): p. 571-579.

[47] Kotousov, A. and C.H. Wang, *Three-dimensional stress constraint in an elastic plate with a notch.* International Journal of Solids and Structures, 2002. **39**(16): p. 4311-4326.

[48] Kotousov, A., et al., *Effect of the thickness on elastic deformation and quasi-brittle fracture of plate components.* Engineering Fracture Mechanics, 2010. **77**(11): p. 1665-1681.

[49] Kotousov, A., et al., *Three-dimensional stress states at crack tip induced by shear and anti-plane loading.* Engineering Fracture Mechanics, 2013. **108**(0): p. 65-74.

[50] Lazzarin, P. and M. Zappalorto, *A three-dimensional stress field solution for pointed and sharply radiused V-notches in plates of finite thickness.* Fatigue & Fracture of Engineering Materials & Structures, 2012. **35**(12): p. 1105-1119.

[51] Nakamura, T. and D.M. Parks, *Three-Dimensional Stress Field Near the Crack Front of a Thin Elastic Plate.* Journal of Applied Mechanics, 1988. **55**(4): p. 805-813.

[52] Mall, S., G. Ramamurthy, and M.A. Rezaizdeh, *Stress ratio effect on cyclic debonding in adhesively bonded composite joints.* Composite Structures, 1987. **8**(1): p. 31-45.

[53] Pirondi, A. and G. Nicoletto, *Fatigue crack growth in bonded DCB specimens.* Engineering Fracture Mechanics, 2004. **71**(4–6): p. 859-871.

[54] Hojo, M., et al., *Modes I and II interlaminar fracture toughness and fatigue delamination of CF/epoxy laminates with self-same epoxy interleaf.* International Journal of Fatigue, 2006. **28**(10): p. 1154-1165.

[55] Fleck, N.A., *Finite element analysis of plasticity-induced crack closure under plane strain conditions.* Engineering Fracture Mechanics, 1986. **25**(4): p. 441-449.

[56] Mall, S. and G. Ramamurthy, *Effect of bond thickness on fracture and fatigue strength of adhesively bonded composite joints.* International Journal of Adhesion and Adhesives, 1989. **9**(1): p. 33-37.

[57] Fleck, N.A. and R.A. Smith, *Crack closure - is it just a surface phenomenon?* International Journal of Fatigue, 1982. **4**(3): p. 157-160.

[58] McClung, R.C. and H. Sehitoglu, *On the finite element analysis of fatigue crack closure—1. Basic modeling issues.* Engineering Fracture Mechanics, 1989. **33**(2): p. 237-252.

[59] Kujawski, D., *A fatigue crack driving force parameter with load ratio effects.* International Journal of Fatigue, 2001. **23**(1): p. 239-246.

[60] Noroozi, A.H., G. Glinka, and S. Lambert, *A two parameter driving force for fatigue crack growth analysis.* International Journal of Fatigue, 2005. **27**(10–12): p. 1277-1296.

[61] Kwofie, S. and N. Rahbar, *An equivalent driving force model for crack growth prediction under different stress ratios.* International Journal of Fatigue, 2011. **33**(9): p. 1199-1204.

[62] Johnson, W.S. and P.D. Mangalgiri, *Investigation of Fiber Bridging in Double Cantilever Beam Specimens*, 1986, NASA. p. 22.

[63] Khan, R., C. Rans, and R. Benedictus. *Effect of stress ratio on delamination growth behaviour in unidirectional carbon/epoxy under mode I fatigue loading*. in *ICCM*. 2009. Edinburgh, UK.

[64] Mall, S. and N.K. Kochhar, *Characterization of debond growth mechanism in adhesively bonded composites under mode II static and fatigue loadings.* Engineering Fracture Mechanics, 1988. **31**(5): p. 747-758.

[65] Nakagaki, M. and S.N. Atluri, *Elastic-plastic Analysis of Fatigue Crack Closure in Modes I and II.* AIAA Journal, 1980. **18**(9): p. 1110-1117.

[66] Chester, R.J., K.F. Walker, and P.D. Chalkley, *Adhesively bonded repairs to primary aircraft structure.* International Journal of Adhesion and Adhesives, 1999. **19**(1): p. 1-8.

[67] Kawashita, L.F., et al. *Static and fatigue delamination from discontinuous plies - Experimental and numerical investigations*. in *ICCM*. 2009. Edinburgh, UK.

[68] Johnson, W.S. and S. Mall, *A Fracture Mechanics Approach for Designing Adhesively Bonded Joints*, in *Delamination and debonding of materials*, W.S. Johnson, Editor. 1985, ASTM International: Pittsburgh, Pa. p. 189-199.

[69] Cheuk, P.T., et al., *Fatigue crack growth in adhesively bonded composite-metal double-lap joints.* Composite Structures, 2002. **57**(1–4): p. 109-115.

[70] Russell, A.J. and K.N. Street, *Predicting interlaminar fatigue crack growth rates in compressively loaded laminates*, in *Composite Materials: Fatigue and Fracture*, P.A. Lagace, Editor. 1989, ASTM International: Philadephia. p. 162-178.

[71] Kenane, M., et al., *Experimental development of fatigue delamination threshold criterion.* Composites Part B: Engineering, 2011. **42**(3): p. 367-375.

[72] Benzeggagh, M.L. and M. Kenane, *Measurement of mixed-mode delamination fracture toughness of unidirectional glass/epoxy composites with mixed-mode bending apparatus.* Composites Science and Technology, 1996. **56**(4): p. 439-449.

[73] Kenane, M. and M.L. Benzeggagh, *Mixed-mode delamination fracture toughness of unidirectional glass/epoxy composites under fatigue loading.* Composites Science and Technology, 1997. **57**(5): p. 597-605.

[74] Blanco, N., et al., *Mixed-mode delamination growth in carbon–fibre composite laminates under cyclic loading.* International Journal of Solids and Structures, 2004. **41**(15): p. 4219-4235.

[75] Gustafson, C.-G. and M. Hojo, *Delamination Fatigue Crack Growth in Unidirectional Graphite/Epoxy Laminates.* Journal of Reinforced Plastics and Composites, 1987. **6**(1): p. 36-52.

[76] Hart-Smith, L., *Designing to minimize peel stresses in adhesive-bonded joints.* Astm Stp, 1985. **876**: p. 238-266.

[77] Hart-Smith, L.J., *Adhesive-bonded single-lap joints*. 1973: Langley Research Center Hampton, VA.

[78] Everett, R.A., Jr., *The role of peel stresses in cyclic debonding*, 1982, NASA Langley Research Centre: Hampton, VA, United States. p. 26.

[79] Xu, X.X., A.D. Crocombe, and P.A. Smith, *Mixed-mode fatigue and fracture behaviour of joints bonded with either filled or filled and toughened adhesive.* International Journal of Fatigue, 1995. **17**(4): p. 279-286.

[80] Allegri, G., M.R. Wisnom, and S.R. Hallett, *A new semi-empirical law for variable stress-ratio and mixed-mode fatigue delamination growth.* Composites Part A: Applied Science and Manufacturing, 2013. **48**(0): p. 192-200.

[81] Carlsson, L.A., J.W. Gillespie, and R.B. Pipes, *On the Analysis and Design of the End Notched Flexure (ENF) Specimen for Mode II Testing.* Journal of Composite Materials, 1986. **20**(6): p. 594-604.

[82] Fernández, M.V., et al., *Characterization of composite bonded joints under pure mode II fatigue loading.* Composite Structures, 2013. **95**(0): p. 222-226.

[83] de Moura, M.F.S.F., R.D.S.G. Campilho, and J.P.M. Gonçalves, *Pure mode II fracture characterization of composite bonded joints.* International Journal of Solids and Structures, 2009. **46**(6): p. 1589-1595.

[84] De Moura, M.F.S.F., et al., *Numerical analysis of the ENF and ELS tests applied to mode II fracture characterization of cortical bone tissue.* Fatigue & Fracture of Engineering Materials & Structures, 2011. **34**(3): p. 149-158.

[85] Standard test method for mode I interlaminar fracture toughness of unidirectional fiber-reinforced polymer matrix composites, "*D5528"*, 2001(2013), ASTM International, West Conshohocken, PA, 2013, DOI: 10.1520/D5528, www.astm.org

[86] ASTM Standard D6115, "*Standard test method for mode I fatigue delamination growth onset of unidirectional fiber-reinforced polymer matrix composites"*, 1997(2011), ASTM International, West Conshohocken, PA, 2011, DOI: 10.1520/D6115-97R11, www.astm.org

[87] Tenchev, R.T. and B.G. Falzon. *Experimental and numerical study of debonding in composite adhesive joints*. in *16th International Conference on Composite Materials*. 2007. Kyoto, Japan.

[88] Kim, M.K., et al., *Interaction of laminate damage and adhesive disbonding in composite scarf joints subjected to combined in-plane loading and impact.* Composite Structures, 2012. **94**(3): p. 945-953.

[89] Newman Jr, J.C., *A finite-element analysis of fatigue crack closure.* ASTM STP, 1976. **590**: p. 281-301.

[90] McClung, R.C. and H. Sehitoglu, *On the finite element analysis of fatigue crack closure—2. Numerical results.* Engineering Fracture Mechanics, 1989. **33**(2): p. 253-272.

[91] Wu, J. and F. Ellyin, *A study of fatigue crack closure by elastic-plastic finite element analysis for constant-amplitude loading.* International Journal of Fracture, 1990. **82**(1): p. 43-65.

[92] Antunes, F.V. and D.M. Rodrigues, *Numerical simulation of plasticity induced crack closure: Identification and discussion of parameters.* Engineering Fracture Mechanics, 2008. **75**(10): p. 3101-3120.

[93] González-Herrera, A. and J. Zapatero, *Influence of minimum element size to determine crack closure stress by the finite element method.* Engineering Fracture Mechanics, 2005. **72**(3): p. 337-355.

[94] Solanki, K., S.R. Daniewicz, and J.C. Newman Jr, *Finite element modeling of plasticity-induced crack closure with emphasis on geometry and mesh refinement effects.* Engineering Fracture Mechanics, 2003. **70**(12): p. 1475-1489.

[95] Wei, L.W. and M.N. James, *A study of fatigue crack closure in polycarbonate CT specimens.* Engineering Fracture Mechanics, 2000. **66**(3): p. 223-242.

[96] Solanki, K., S.R. Daniewicz, and J.C. Newman Jr, *Finite element analysis of plasticity-induced fatigue crack closure: an overview.* Engineering Fracture Mechanics, 2004. **71**(2): p. 149-171.

[97] Dougherty, J.D., J. Padovan, and T.S. Srivatsan, *Fatigue crack propagation and closure behavior of modified 1070 steel: Finite element study.* Engineering Fracture Mechanics, 1997. **56**(2): p. 189-212.

[98] de Matos, P.F.P. and D. Nowell, *Numerical simulation of plasticity-induced fatigue crack closure with emphasis on the crack growth scheme: 2D and 3D analyses.* Engineering Fracture Mechanics, 2008. **75**(8): p. 2087-2114.

[99] Suresh, S. and R.O. Ritchie, *A geometric model for fatigue crack closure induced by fracture surface roughness.* Metallurgical Transactions A, 1982. **13**(9): p. 1627-1631.

[100] Wang, C.H., *On the fracture of constrained layers.* International Journal of Fracture, 1998. **93**(1-4): p. 227-246.

[101] Wang, C.H., *Analysis of cracks in constrained layers.* International Journal of Fracture, 1997. **83**(1): p. 1-17.

[102] Lee, H.J. and J.H. Song, *Finite-element analysis of fatigue crack closure under plane strain conditions: stabilization behaviour and mesh size effect.* Fatigue & Fracture of Engineering Materials & Structures, 2005. **28**(3): p. 333-342.

[103] Park, S.J., Y.Y. Earmme, and J.H. Song, *Determination of the Most Appropriate Mesh Size For a 2-D Finite Element Analysis of Fatigue Crack Closure Behaviour.* Fatigue & Fracture of Engineering Materials & Structures, 1997. **20**(4): p. 533-545.

[104] Sehitoglu, H. and W. Sun, *Modeling of Plane Strain Fatigue Crack Closure.* Journal of Engineering Materials and Technology, 1991. **113**(1): p. 31-40.

[105] Zapatero, J., B. Moreno, and A. González-Herrera, *Fatigue crack closure determination by means of finite element analysis.* Engineering Fracture Mechanics, 2008. **75**(1): p. 41-57.

[106] Solanki, K., S.R. Daniewicz, and J.C. Newman Jr, *A new methodology for computing crack opening values from finite element analyses.* Engineering Fracture Mechanics, 2004. **71**(7–8): p. 1165-1175.

[107] Wang, C.H., L.R.F. Rose, and J.C. Newman, *Closure of plane-strain cracks under large-scale yielding conditions.* Fatigue & Fracture of Engineering Materials & Structures, 2002. **25**(2): p. 127-139.

[108] Suo, Z. and J.W. Hutchinson, *Sandwich test specimens for measuring interface crack toughness.* Materials Science and Engineering: A, 1989. **107**(0): p. 135-143.

[109] Nakagaki, M. and S.N. Atluri, *Fatigue Crack Closure and Delay Effects Under Mode I Spectrun Loading.* Fatigue & Fracture of Engineering Materials & Structures, 1979. **1**(4): p. 421-429.

[110] Pommier, S., *Plane strain crack closure and cyclic hardening.* Engineering Fracture Mechanics, 2002. **69**(1): p. 25-44.

[111] Shercliff, H.R. and N.A. Fleck, *Effect of Specimen Geometry on Fatigue Crack Growth in Plane Strain—II Overload Response.* Fatigue & Fracture of Engineering Materials & Structures, 1990. **13**(3): p. 297-310.

[112] Krueger, R., *The Virtual Crack Closure Technique: History, Approach and Applications*, 2002, NASA: Hampton, VA. p. 64.

[113] Codrington, J. and A. Kotousov, *The distributed dislocation technique for calculating plasticity-induced crack closure in plates of finite thickness.* International Journal of Fracture, 2007. **144**(4): p. 285-295.

[114] Codrington, J. and A. Kotousov, *A crack closure model of fatigue crack growth in plates of finite thickness under small-scale yielding conditions.* Mechanics of Materials, 2009. **41**(2): p. 165-173.

[115] Rose, L.R.F. and C.H. Wang, *Self-similar analysis of plasticity-induced closure of small fatigue cracks.* Journal of the Mechanics and Physics of Solids, 2001. **49**(2): p. 401-429.

[116] Pirondi, A. and G. Nicoletto, *Mixed Mode I/II fracture toughness of bonded joints.* International Journal of Adhesion and Adhesives, 2002. **22**(2): p. 109-117.

[117] Landry, B. and G. LaPlante, *Modeling delamination growth in composites under fatigue loadings of varying amplitudes.* Composites Part B: Engineering, 2012. **43**(2): p. 533-541.

[118] Sun, C.T. and J.L. Chen, *A Simple Flow Rule for Characterizing Nonlinear Behavior of Fiber Composites.* Journal of Composite Materials, 1989. **23**(10): p. 1009-1020.

[119] Sun, C.T. and J.L. Chen, *A micromechanical model for plastic behavior of fibrous composites.* Composites Science and Technology, 1991. **40**(2): p. 115-129.

[120] Sun, C.T. and C. Zhu, *The effect of deformation-induced change of fiber orientation on the non-linear behavior of polymeric composite laminates.* Composites Science and Technology, 2000. **60**(12–13): p. 2337-2345.

[121] Yokozeki, T., et al., *Simple constitutive model for nonlinear response of fiber-reinforced composites with loading-directional dependence.* Composites Science and Technology, 2007. **67**(1): p. 111-118.

[122] Hsu, S.Y., T.J. Vogler, and S. Kyriakides, *Inelastic behavior of an AS4/PEEK composite under combined transverse compressionand shear.Part II: modeling.* International Journal of Plasticity, 1999. **15**(8): p. 807-836.

[123] González, C. and J. Llorca, *Mechanical behavior of unidirectional fiber-reinforced polymers under transverse compression: Microscopic mechanisms and modeling.* Composites Science and Technology, 2007. **67**(13): p. 2795-2806.

[124] Dvorak, G.J. and Y. Bahei-El-Din, *Plasticity analysis of fibrous composites.* Journal of Applied Mechanics, 1982. **49**(2): p. 327-335.

[125] Sun, C. and J. Tao, *Prediction of failure envelopes and stress/strain behaviour of composite laminates.* Composites Science and Technology, 1998. **58**(7): p. 1125-1136.

[126] Hill, R., *The Mathematical Theory of Plasticity, The Oxford Engineering Science Series*. 1950: Oxford.

[127] ASTM Standard D3039, "*Standard test method for Tensile Properties of Polymer Matrix Composite Materials"*, 2014, ASTM International, West Conshohocken, PA, 2013, DOI: 10.1520/D5528, www.astm.org

[128] ASTM Standard D3518, "*Standard test method for In-Plane Shear Response of Polymer Matrix Composite Materials by Tensile Test of a ±45° Laminate"*, 2001, ASTM International, West Conshohocken, PA, 2013, DOI: 10.1520/D5528, www.astm.org

[129] Sorensen, L., et al., *Bridging tractions in mode I delamination: Measurements and simulations.* Composites Science and Technology, 2008. **68**(12): p. 2350-2358.

[130] Peng, L., et al., *Mixed mode delamination growth of multidirectional composite laminates under fatigue loading.* Engineering Fracture Mechanics, 2012. **96**(0): p. 676-686.

[131] Peng, L., et al., *Mode I delamination growth of multidirectional composite laminates under fatigue loading.* Journal of Composite Materials, 2011. **45**(10): p. 1077-1090.

[132] Yao, L., et al., *Bridging effect on mode I fatigue delamination behavior in composite laminates.* Composites Part A: Applied Science and Manufacturing, 2014. **63**(0): p. 103-109.

[133] Zhang, J., et al., *Fatigue delamination growth rates and thresholds of composite laminates under mixed mode loading.* International Journal of Fatigue, 2012. **40**(0): p. 7-15.

[134] Murri, G.B., *Effect of data reduction and fiber-bridging on Mode I delamination characterization of unidirectional composites.* Journal of Composite Materials, 2014. **48**(19): p. 2413-2424.

[135] Spearing, S.M. and A.G. Evans, *The role of fiber bridging in the delamination resistance of fiber-reinforced composites.* Acta Metallurgica et Materialia, 1992. **40**(9): p. 2191-2199.

[136] Sørensen, B.F., et al., *Micromechanical model of cross-over fibre bridging – Prediction of mixed mode bridging laws.* Mechanics of Materials, 2008. **40**(4–5): p. 220-234.

[137] Stutz, S., J. Cugnoni, and J. Botsis, *Crack – fiber sensor interaction and characterization of the bridging tractions in mode I delamination.* Engineering Fracture Mechanics, 2011. **78**(6): p. 890-900.

[138] Stutz, S., J. Cugnoni, and J. Botsis, *Studies of mode I delamination in monotonic and fatigue loading using FBG wavelength multiplexing and numerical analysis.* Composites Science and Technology, 2011. **71**(4): p. 443-449.

[139] Suo, Z., G. Bao, and B. Fan, *Delamination R-curve phenomena due to damage.* Journal of the Mechanics and Physics of Solids, 1992. **40**(1): p. 1-16.

[140] Murri, G.B. and R.H. Martin, *Effect of initial delamination on mode I and mode II interlaminar fracture toughness and fatigue fracture threshold.* ASTM SPECIAL TECHNICAL PUBLICATION, 1993. **1156**: p. 239-239.

[141] Jensen, H. and I. Sheinman, *Straight-sided, buckling-driven delamination of thin films at high stress levels.* International Journal of Fracture, 2001. **110**(4): p. 371-385.

[142] Glaessgen, E.H., I.S. Raju, and C.C. Poe, *Analytical and Experimental Studies of the Debonding of Stitched and Unstitched Composite Joints.* Journal of Composite Materials, 2002. **36**(23): p. 2599-2622.

[143] Kim, B.W. and A.H. Mayer, *Influence of fiber direction and mixed-mode ratio on delamination fracture toughness of carbon/epoxy laminates.* Composites Science and Technology, 2003. **63**(5): p. 695-713.

[144] Cui, W. and M.R. Wisnom, *A combined stress-based and fracture-mechanics-based model for predicting delamination in composites.* Composites, 1993. **24**(6): p. 467-474.

[145] Reeder, J.R., *An evaluation of mixed-mode delamination failure criteria*, 1992, NASA: Hampton, VA.

[146] Johnson, W.S. and S. Mall, *Influence of interface ply orientation on fatigue damage of adhesively bonded composite joints*, in *NASA technical memorandum ; 86443*1985, National Aeronautics and Space Administration, Langley Research Center: Hampton, Va.

[147] Rybicki, E.F. and M.F. Kanninen, *A finite element calculation of stress intensity factors by a modified crack closure integral.* Engineering Fracture Mechanics, 1977. **9**(4): p. 931-938.

[148] Wang, C., *Analysis of cracks in constrained layers.* International Journal of Fracture, 1998. **94**: p. 199-200.

[149] Harris, J.A. and R.A. Adams, *Strength prediction of bonded single lap joints by non-linear finite element methods.* International Journal of Adhesion and Adhesives, 1984. **4**(2): p. 65-78.

[150] Erdogan, F. and G.C. Sih, *On the Crack Extension in Plates Under Plane Loading and Transverse Shear.* Journal of Fluids Engineering, 1963. **85**(4): p. 519-525.

[151] ASTM Standard D6671, "*Standard test method for mixed mode I-mode II interlaminar fracture toughness of unidirectional fiber reinforced polymer matrix composites"*, 2001(2013), ASTM International, West Conshohocken, PA, 2013, DOI: 10.1520/D5528, www.astm.org

[152] May, M. and S.R. Hallett, *A combined model for initiation and propagation of damage under fatigue loading for cohesive interface elements.* Composites Part A: Applied Science and Manufacturing, 2010. **41**(12): p. 1787-1796.

[153] May, M. and S.R. Hallett, *An advanced model for initiation and propagation of damage under fatigue loading – part I: Model formulation.* Composite Structures, 2011. **93**(9): p. 2340-2349.

Appendix

A.1 Cohesive zone model with fatigue degradation law

In the numerical simulation using the cohesive zone model (CZM) approach, cohesive elements are positioned between continuum elements along a potential crack propagation path. The benefit of cohesive elements is its ability of simulating crack initiation and propagation. The implementation of a fatigue degradation law was discussed references [21-24, 117, 152, 153]. The fatigue degradation law was implemented in some analyses of the Thesis and the description of the model is given in this Section.

The constitutive response of the cohesive element can be separated into the continuum regions described by the bulk material properties and the fracture properties captured by the cohesive elements. Shown in Figure A-1 is a typical traction-separation response of a cohesive element under static load using a bilinear relationship.

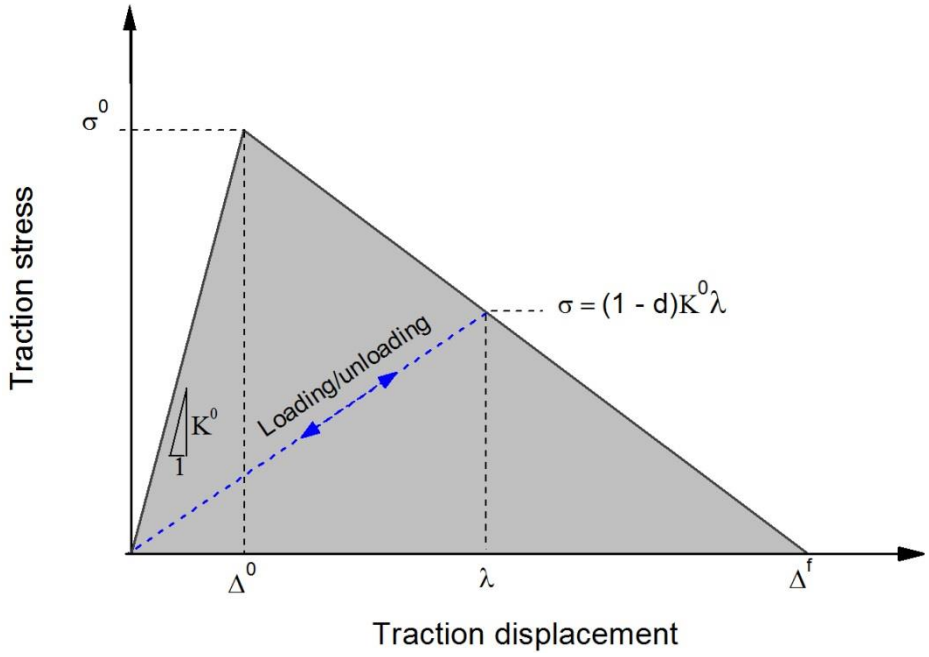

Figure A-1: Bilinear traction-separation relation. Prior to damage, the interface is characterised by K^0. Upon damage initiation, the stiffness of the cohesive element is reduced by a damage index, d.

It consists of a linear elastic region followed by a linear softening region. The onset of damage is determined by the interfacial strength σ° at a traction displacement of

Δ°. Upon further loading, the traction stiffness undergoes a linear softening until the critical traction displacement Δ^f is attained. The area under the traction-separation curve is equal to the critical fracture energy G_C. In order to correctly simulate the progression of delamination, 1) the cohesive elements must be sufficiently stiff to avoid introducing a fictitious compliance to the global compliance of the model prior to softening and 2) the cohesive zone length must be greater than one element length.

The stiffness softening of the interface after the onset of damage is characterised by a damage parameter, d, defined as

$$d\left(\lambda\right)=\begin{cases} 0 & for\ \lambda \le \Delta^0 \\ \dfrac{\Delta^f}{\lambda}\left(\dfrac{\lambda-\Delta^0}{\Delta^f-\Delta^0}\right) & for\ \Delta^0 < \lambda < \Delta^f \\ 1 & for\ \lambda \ge \Delta^f \end{cases} \tag{A-1}$$

where λ is the traction displacement that occurred at the point of interest. The traction stress is given as

$$\sigma = (1-d)K^0\lambda \tag{A-2}$$

where K^0 is the initial traction stiffness prior to damage occurring. For subcritical loads under fatigue, the local traction during subsequent unloading and loading follows the blue dashed line shown in Figure A-1. Under the current definition of the cohesive element, no further damage will occur since the traction displacement does not exceed λ. Therefore the evolution of the damage under cyclic loads needs to be modelled into the quasi-static cohesive element behaviour.

The fatigue damage model further degrades the material strength under sub-critical cyclic load cycles and its formulation is based on the model presented by Turon et al [22] and Harper and Hallet [24]. The total loss of traction strength $\overline{d}_T$ is the sum of the reduction in traction strength due to static and fatigue component, $\overline{d}_s$ and $\overline{d}_f$ respectively. Therefore the relation is given in Equation (A-3) and also depicted in Figure A-2.

$$\sigma = \sigma^0\left(1-\overline{d}_T\right) = \sigma^0\left[1-\left(\overline{d}_s+\overline{d}_f\right)\right] \tag{A-3}$$

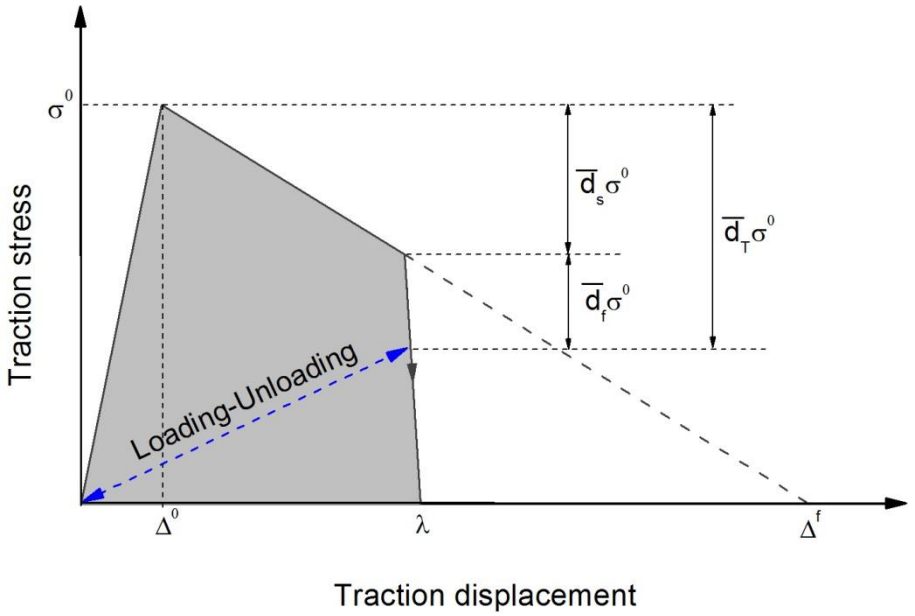

Figure A-2: Representation of fatigue damage evolution law implemented in a cohesive element. A fatigue damage $\overline{d}_f$ is compounded to the quasi-static damage $\overline{d}_s$.

Considering for a 2-D cohesive element, the accumulation of damage within the element is linked to the formation of new cracks surfaces within the element (i.e. when d = 1, the crack has propagated by 1 element length) [22, 24]. By combing Equation (A-2) and (A-3), the ratio of damaged length with respect to the element length is given as such

$$\overline{d}_s + \overline{d}_f = \frac{L_d}{L_e} = 1 - \frac{\lambda}{\Delta^0}(1-d) \tag{A-4}$$

where L_e is the characteristic element length and L_d is the damaged length. By substituting Equation (A-1), the damaged length ratio within an element becomes

$$\frac{L_d}{L_e} = \frac{d\Delta^0}{\Delta^f(1-d) + d\Delta^0} \tag{A-5}$$

The evolution of the stiffness reduction damage variable, d, with respect to the number of cycles can be expressed as follows

$$\frac{\partial d}{\partial N} = \frac{\partial d}{\partial L_d}\frac{\partial L_d}{\partial N} \tag{A-6}$$

where the term $\frac{\partial L_d}{\partial N}$ is the rate of increase of the damaged length. The term $\frac{\partial d}{\partial L_d}$ can be obtained by differentiating Equation (A-5).

$$\frac{\partial d}{\partial L_d} = \frac{1}{L_e}\frac{\left[\Delta^f(1-d)+d\Delta^0\right]}{\Delta^f\Delta^0} \tag{A-7}$$

The increased in the delamination length is equal to the total damaged length in all the elements ahead of the crack tip. Therefore the crack growth rate is assumed to be the sum of the damaged length growth rates in all the elements in the cohesive zone.

$$\frac{\partial a}{\partial N} = \sum_{e\in L_{cz}}\frac{\partial L_d}{\partial N} \tag{A-8}$$

where L_{CZ} is the cohesive zone length. Assuming that $\frac{\partial L_d}{\partial N}$ is constant throughout the cohesive zone length, the rate of crack growth can be estimated as,

$$\frac{\partial a}{\partial N} = \sum_{e\in L_{cz}}\frac{\partial L_d}{\partial N} = \frac{L_{cz}}{L_e}\frac{\partial L_d}{\partial N} \tag{A-9}$$

where $\frac{L_{cz}}{L_e}$ is the number of elements within the cohesive zone length. From Equation (A-9), it is assumed that the resultant crack growth Δa is *"smeared"* across the cohesive elements within the process zone. By substituting Equation (A-7) and (A-9) into Equation (A-6), the damage index is then expressed as a function of the number of cycles lapsed.

$$\frac{\partial d}{\partial N} = \frac{1}{L_{CZ}}\frac{\left[\Delta^f(1-d)+d\Delta^0\right]}{\Delta^f\Delta^0}\frac{\partial a}{\partial N} \tag{A-10}$$

The derivation of the cohesive zone length L_{CZ} varied from papers to papers. Harper and Hallet [24] assumed the effective cohesive zone length is 50% of the static cohesive zone length which needs to be determined first numerically. Landry and LaPlante [117] applied the fatigue damage evolution law only to the crack tip element. Therefore the effective cohesive zone length is the remaining undamaged cohesive element length. On the other hand, Turon et al. [22] derived this term analytical using Rice's approximation, given as such

$$L_{CZ} = \frac{9\pi}{32}\frac{E_{33}G_{\max}}{\left(\sigma^0\right)^2} \tag{A-11}$$

In this work, we shall base our assumptions on the process zone length to be the same as Turon et al.'s model, given that only a single mode is analysed. The stable crack growth of typical composite fatigue behaviour can be represented by the Paris law when plotted on a log-log scale, as shown below.

$$\frac{\partial a}{\partial N} = C\left[\Delta G_{I,eq}\right]^m \tag{A-12}$$

where C and m are material constants determined by curve-fitting to the experimental data and $\Delta G_{I,eq}$ is the cyclic delamination driving force given as $\Delta G_{I,eq} = \left(\sqrt{G_{I,max}} - \sqrt{G_{I,min}}\right)^2$. The term $\Delta G_{I,eq}$ was used to keep it consistent with the correlating parameter used in this Thesis. Since the area under the traction-separation curve is characterised by the critical fracture energy and, hence, G_I can be obtained via integration. The integral solution for a bilinear traction-separation curve is given as,

$$\Delta G(\lambda) = \int_0^{\lambda} \sigma(\lambda) d\lambda = \frac{\sigma^0}{2}\left[\Delta^f - \frac{\left(\Delta^f - \lambda\right)^2}{\Delta^f - \Delta^0}\right](1-R)^2 \tag{A-13}$$

where G(λ) is the crack driving force derived at the traction displacement λ. The cyclic load is by the load ratio R is defined as P_{min}/P_{max}.